AD-A182 451 STRENGTH DESIGN OF REINFORCED CONCRETE HYDRAULIC 1/3
STRUCTURES REPORT 5 EXPE (U) ARMY ENGINEER WATERWAYS
EXPERIMENT STATION VICKSBURG MS STRUC
UNCLASSIFIED R S WRIGHT ET AL APR 87 WES/TR/SL-80-4/5 F/G 13/3 NL

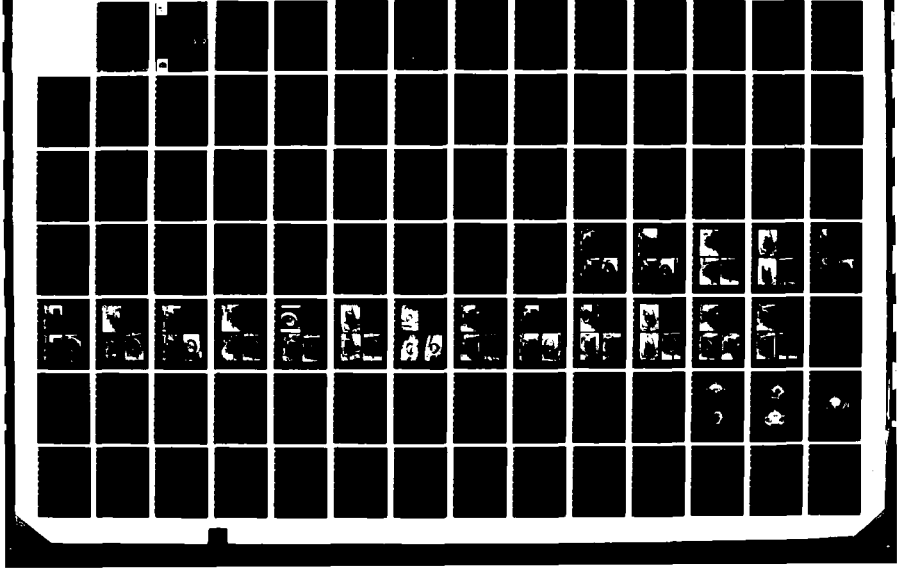

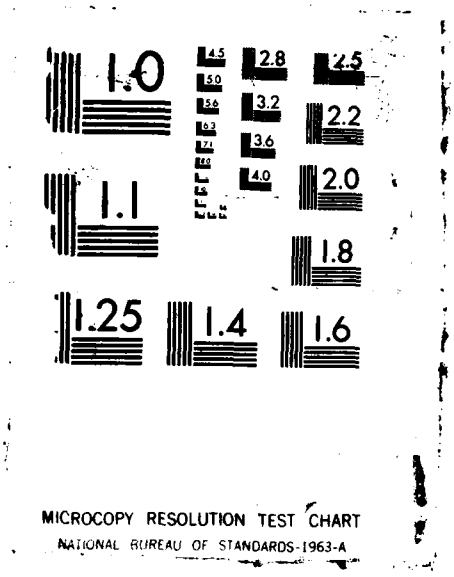
1.0
1.1
1.25
1.4
1.6
1.8
2.0
2.2
2.5
2.8
3.2
3.6
4.0
4.5
5.0
5.6
6.3
7.1
8.0
MICROCOPY RESOLUTION TEST CHART
NATIONAL BUREAU OF STANDARDS-1963-A

TECHNICAL REPORT SL-80-4

STRENGTH DESIGN OF REINFORCED CONCRETE HYDRAULIC STRUCTURES

Report 5

EXPERIMENTAL STUDY ON THE ULTIMATE BEHAVIOR OF MODEL REINFORCED CONCRETE CIRCULAR CONDUITS

by

R. Stephen Wright, Vincent P. Chiarito

Structures Laboratory

DEPARTMENT OF THE ARMY
Waterways Experiment Station, Corps of Engineers
PO Box 631, Vicksburg, Mississippi 39180-0631

April 1987

Report 5 of a Series

Prepared for DEPARTMENT OF THE ARMY
US Army Corps of Engineers
Washington, DC 20314-1000

US Army Corps of Engineers

STRUCTURES LABORATORY

Destroy this report when no longer needed. Do not return it to the originator.

The findings in this report are not to be construed as an official Department of the Army position unless so designated by other authorized documents.

The contents of this report are not to be used for advertising, publication, or promotional purposes. Citation of trade names does not constitute an official endorsement or approval of the use of such commercial products.

Unclassified
SECURITY CLASSIFICATION OF THIS PAGE

REPORT DOCUMENTATION PAGE

Form Approved
OMB No 0704-0188
Exp Date Jun 30 1986

AD-A182 457

1a REPORT SECURITY CLASSIFICATION Unclassified	1b RESTRICTIVE MARKINGS
2a SECURITY CLASSIFICATION AUTHORITY	3 DISTRIBUTION/AVAILABILITY OF REPORT Approved for public release; distribution unlimited
2b DECLASSIFICATION/DOWNGRADING SCHEDULE	
4 PERFORMING ORGANIZATION REPORT NUMBER(S) Technical Report SL-80-4	5 MONITORING ORGANIZATION REPORT NUMBER(S)
6a NAME OF PERFORMING ORGANIZATION USAEWES Structures Laboratory 6b OFFICE SYMBOL (If applicable) WESSS	7a NAME OF MONITORING ORGANIZATION
6c ADDRESS (City, State, and ZIP Code) PO Box 631 Vicksburg, MS 39180-0631	7b ADDRESS (City, State, and ZIP Code)
8a NAME OF FUNDING/SPONSORING ORGANIZATION US Army Corps of Engineers 8b OFFICE SYMBOL (If applicable)	9 PROCUREMENT INSTRUMENT IDENTIFICATION NUMBER
8c ADDRESS (City, State, and ZIP Code) Washington, DC 20314-1000	10 SOURCE OF FUNDING NUMBERS PROGRAM ELEMENT NO / PROJECT NO / TASK NO / WORK UNIT ACCESSION NO

11 TITLE (Include Security Classification)
Strength Design of Reinforced Concrete Hydraulic Structures; Report 5, Experimental Study on the Ultimate Behavior of Model Reinforced Concrete Cellular Conduits

12 PERSONAL AUTHOR(S)
Wright, R. Stephen and Chiarito, Vincent P.

13a TYPE OF REPORT	13b TIME COVERED	14 DATE OF REPORT (Year, Month, Day)	15 PAGE COUNT
Report 5 of a series	FROM _____ TO _____	April 1987	196

16 SUPPLEMENTARY NOTATION
Available from National Technical Information Service, 5285 Port Royal Road, Springfield, VA 22161.

17 COSATI CODES			18 SUBJECT TERMS (Continue on reverse if necessary and identify by block number)
FIELD	GROUP	SUB-GROUP	Aqueducts (LC) Reinforced concrete (LC) Hydraulic models (LC) Hydraulic structures (LC)

19 ABSTRACT (Continue on reverse if necessary and identify by block number)

A test program was initiated to investigate the two-dimensional failure response of reinforced concrete (R/C) circular conduits under a known 16-point loading. This was achieved by testing 18 R/C models to failure. The test specimens were instrumented to obtain concrete and steel strains and intrados deflections at the crown and springing line. Steel percentage ratios, loading distribution, and curvature were varied for each test. All models failed primarily in flexure; ductile and brittle failure modes were observed. In a later test program, models which were exposed to 2-point and 4-point loadings and the three-edge-bearing method failed in diagonal or radial tension.

20 DISTRIBUTION/AVAILABILITY OF ABSTRACT	21 ABSTRACT SECURITY CLASSIFICATION
☒ UNCLASSIFIED/UNLIMITED ☐ SAME AS RPT ☐ DTIC USERS	Unclassified
22a NAME OF RESPONSIBLE INDIVIDUAL	22b TELEPHONE (Include Area Code) / 22c OFFICE SYMBOL

DD FORM 1473, 84 MAR 83 APR edition may be used until exhausted
All other editions are obsolete

SECURITY CLASSIFICATION OF THIS PAGE
Unclassified

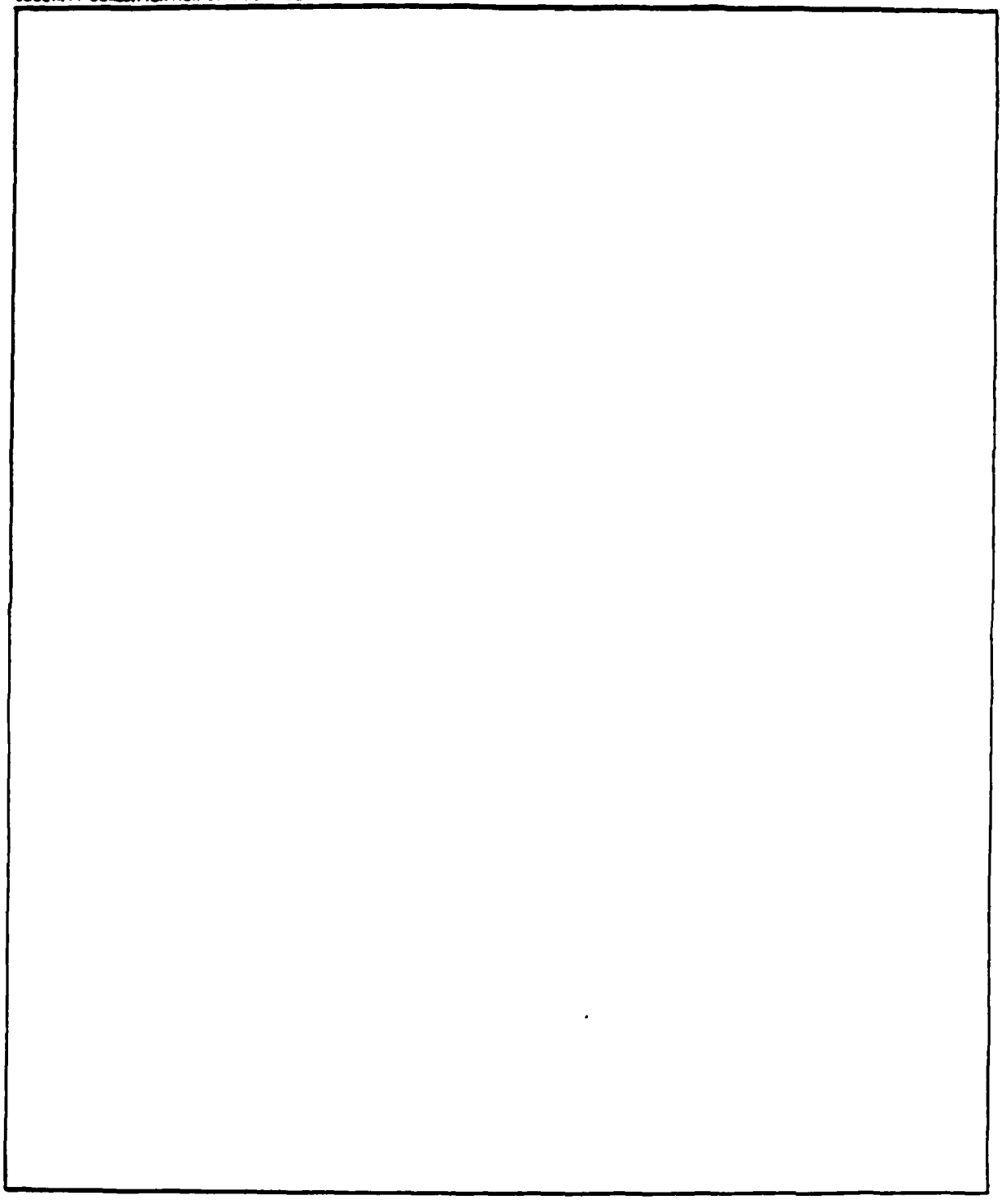

PREFACE

This study was conducted during the period April 1983 through December 1984 by the US Army Engineer Waterways Experiment Station (WES) under the sponsorship of the Office, Chief of Engineers (OCE), US Army. The Technical Monitor was Mr. Don Dressler, OCE.

This work was accomplished by the Structures Laboratory (SL), WES, under the general supervision of Messrs. Bryant Mather, Chief, SL, James. T. Ballard, Assistant Chief, SL, and under the direct supervision of Dr. Jimmy P. Balsara, Chief, Structural Mechanics Division (SMD), SL. Dr. Paul F. Mlakar, formerly of SMD, was involved in planning and directing different phases of work. Acknowledgment is made to the Instrumentation Services Division for instrumentation support and to the Concrete Technology Division for testing support. Messrs. Robert E. Walker, Robert A. Cole, C. Dean Norman and Robert L. Hall, SMD, reviewed this report. Mr. William L. Boyt, SMD, prepared the test data for processing, and the Engineering and Construction Services Division fabricated the unusual testing system. This report was prepared by Messrs. R. Stephen Wright and Vincent P. Chiarito, SMD, and edited by Ms. Gilda Miller, Information Products Division, Information Technology Laboratory, WES.

COL Allen F. Grum, USA, was the previous Director of WES. COL Dwayne G. Lee, CE, is the present Commander and Director. Dr. Robert W. Whalin is Technical Director.

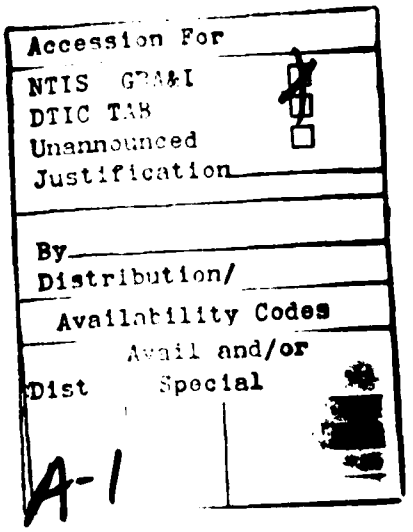

CONTENTS

CONVERSION FACTORS, NON-SI TO SI (METRIC)
UNITS OF MEASUREMENT

Non-SI units of measurement used in this report can be converted to SI (metric) units as follows:

Multiply	By	To Obtain
Fahrenheit degrees	5/9	Celsius degrees or kelvins*
feet	0.3048	metres
foot-pounds (force)	1.355818	joules
inches	25.4	millimetres
kips (force)	4.448222	kilonewtons
kips (force) per square inch	6.894757	megapascals
pounds (force)	4.448222	newtons
pounds (force) per square inch	6.894757	kilopascals
square inches	6.4516	square centimetres

* To obtain Celsius (C) temperature readings from Fahrenheit (F) readings, use the following formula: C = (5/9) (F - 32). To obtain kelvin (K) readings, use K = (5/9) (F - 32) + 273.15.

EXPERIMENTAL STUDY ON THE ULTIMATE BEHAVIOR OF MODEL REINFORCED CONCRETE CIRCULAR CONDUITS

PART I: INTRODUCTION

1. The objective of this project was to test various circular reinforced concrete (R/C) conduit models to observe and analyze the failure modes. These models represent possible Corps of Engineers designs. The results of this study will be used to develop a proposed strength design criteria for R/C circular conduits.

2. Twenty-one circular conduits were fabricated, eighteen being reinforced, and three being unreinforced. The three unreinforced models served as rehearsal test specimens. Three variables were analyzed in this testing procedure: the curvature, steel percentage, and loading conditions. Constants were: f'_c* , f_y , E_c , E_s , and γ_c where

f'_c = 28-day uniaxial compressive strength of concrete
f_y = yield strength of steel
E_c = initial elastic concrete modulus
E_s = modulus of elasticity of steel
γ_c = unit weight of concrete

The test specimens were instrumented at the crown and springing line sections to measure strains on the concrete and steel reinforcement and deflections. Figure 1 shows a typical test section. Table 1 summarizes the models and Table 2 lists the order of testing.

3. These models were tested in a loading apparatus that simulated a design pressure loading, as discussed in Report 4 of this series (Chiarito and Mlakar 1986). Each of the 18 reinforced circular conduit models failed primarily in flexure. All of the failures were ductile (the steel yielded

---

* For convenience, symbols are listed and defined in the Notation (Appendix H).

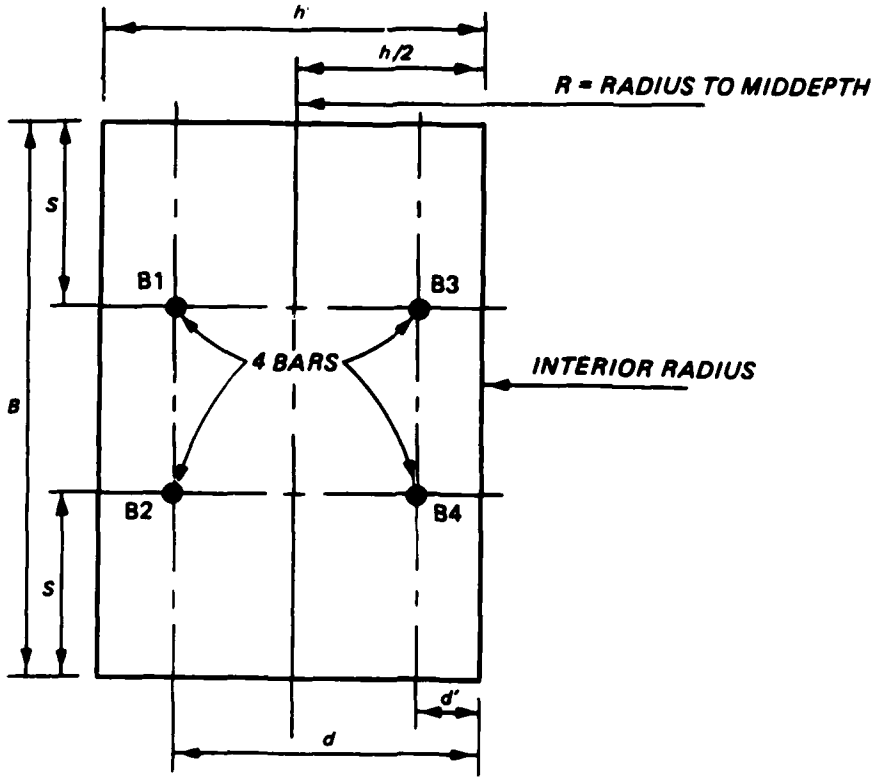

Figure 1. Typical test section

before the concrete crushed) or brittle (the concrete crushed before the steel yielded). The crown and springing line sections were the critical sections governing failure of the model conduits.

4. During each test, observations were noted and photographs were taken and are shown in Appendix A. Video records were made of the last seven tests conducted.

5. Observations noted during a later test series are contained in Appendix B. Appendix B, also contains a discussion of the test plan, loading apparatus, instrumentation, data acquisition, test procedure, material properties, and test observations along with tabulated results and plots.

PART II: EXPERIMENTAL PROCEDURE

Test Plan

6. The test plan involved a matrix with three variables: curvature (three values), loading conditions (four values), and steel percentages (three values). The qualitative behavior of R/C circular conduits was observed in each test. Eighteen reinforcement models were planned and populated the test matrix shown in Table 2. At most, only two variables among given tests were duplicated. The 3:1 loading (ratio of load at crown to load at springing line) was considered to be an average design loading, a middle steel percentage of about 1 percent was considered an average design steel percentage, and an intermediate curvature with $R/h = 2.5$ was considered an average curvature. The matrix was first populated along the averages of these three variables. Then tests were planned to check the upper and lower limits of the three variables. The curvatures were bounded between $R/h = 4.5$ and 1.5, which represent a very thin and a very thick conduit, respectively. From more recent surveys, these values are shown to be limits of Corps structures that are being planned or have been constructed. The other three loading conditions were 4:1 (the most eccentric loading), 2:1, and 1:1 (hydrostatic loading). The other steel percentages used were 0.5 and 1.5 percent.

7. The outside diameter of the models was 20 in.* Each model contained two layers of reinforcement, compression and tensile reinforcement, with a total of four bars in a given section. Before the reinforced models were tested, three plain circular conduit models were tested, one of each curvature ($R/h = 1.5$, 2.5, and 4.5). The testing of the plain circular conduit models established a standard testing procedure and identified any problems with the new testing setup.

Loading Apparatus, Instrumentation, and Data Acquisition

8. The loading apparatus used was the same as that for the first series of tests (Chiarito and Mlakar 1986). Instrumentation included strain gages on

---

* A table of factors for converting non-SI units of measurement to SI (metric) units is given on page 3.

the reinforcement and surface concrete strain gages. Deflection gages were also used to measure deflection of the crown and springing line. The locations of the gages are shown in Figures 2 and 3. The data acquisition system employed used a data logger to record the strains and deflections at a given

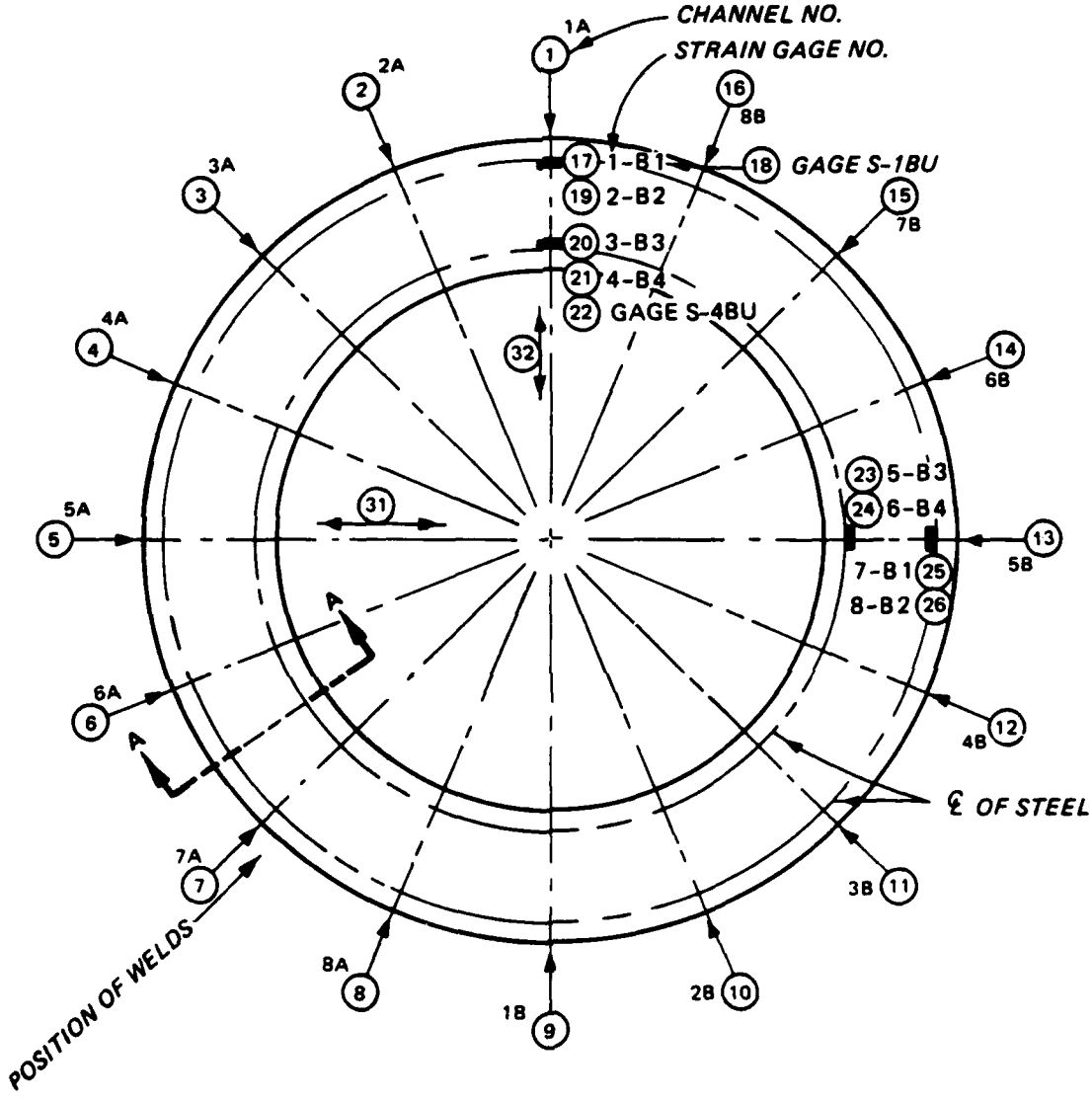

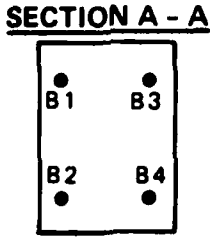

Figure 2. Test scheme and gage locations

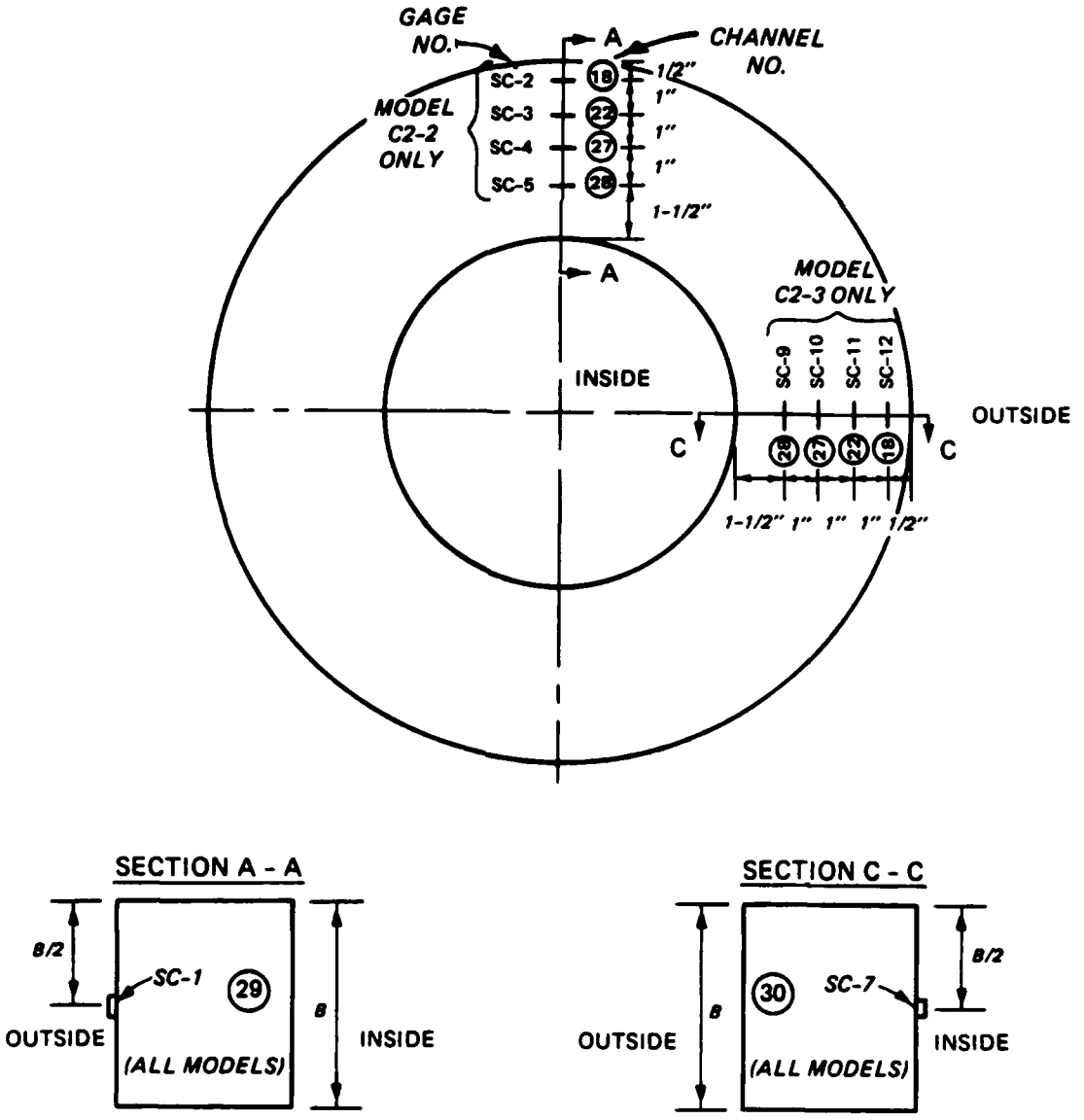

Figure 3. External strain gages

load level onto a cassette tape. This enabled a direct digital output of all strain and deflection results. The experimental equipment is listed in Table 3.

Test Procedure

9. After calibrating a load distribution on the hydraulic controller, a model conduit was placed in the reaction frame so that the center line of the ram aligned with the loading plane of the model. The model was supported at four points by shim plates and two 4- by 4- by 1/2-in. pieces of Teflon.

The Teflon pads were cleaned with a solvent beforehand and provided a very good low-friction surface to allow free translation of the model during loading. With the model in place, the instrumentation channels were connected.

10. Before the model was loaded, each rod of the ram was positioned to just touch the model bearing plates. Then, while the pressures in the jacks were increased, data were recorded on cassette tape with the digital data logger. The loading rate for each of the tests was approximately 100 psi/min (2,000 lb/min in the jack with the largest load).

PART III: TEST RESULTS

Material Properties

11. The material properties listed in Part I (f'_c , E_c , γ_c , f_y , and E_s) were used in analyzing test results. In addition, the Poisson's ratio for the day on which testing was conducted (designated as ν) was also used. Tables 4 and 5, respectively, list the results from the tensile tests of the steel reinforcement and the uniaxial compressive tests. As shown in Table 5, three batches of concrete were mixed, with each batch being used for six models. Thirty-six standard 6- by 12-in. concrete cylinders were tested to obtain material properties on the day of the test. The values of f'_c on the test day were used as parameters for the concrete material property according to Hognestad's constitutive law (Hognestad, Hanson, and McHenry 1955).

12. Table 4 lists the four sizes of steel reinforcement used and the number of bars tested. An average yield strength and modulus of elasticity were computed for each bar type.

Observations

13. Test observations are summarized in Tables 6 through 8. In the five thick models with R/h = 1.5 (C1-1, C2-1, C2-2, C2-3, C3-1), a brittle type of failure was observed as expected. First, tensile cracks occurred at the crown, followed by spalling and crushing at the springing line, and then failure by sudden collapse.

14. As expected, the five thin models with R/h = 3.9 to 4.5 (C7-1, C8-1, C8-2, C8-3, C9-1) had ductile failures with steel yielding before concrete crushing. Four hinges formed in each model as the tension cracked and the compression concrete crushed at crown and invert and both springing line sections.

15. The eight intermediate models with R/h = 2.4 (C4-1, C4-2, C5-1, C5-2, C5-3, C5-4, C6-1, C6-2) had ductile or brittle failures. The brittle failures occurred in the models with 1:1 or 2:1 loading, except for model C5-2 (2:1 loading) where four hinges formed. Model C5-3 (1:1 loading) collapsed suddenly with initial crushing at the intrados, and models C4-2 and C6-2 (2:1 loading) collapsed suddenly after spalling at the springing line. Ductile

failures with the formation of four hinges occurred in the models with 3:1 and 4:1 loading.

Load Distributions

16. Data from the load cells are presented in radial load distribution plots in Appendix C for each test. Load distributions at a given time are plotted on the same axis to show growing load distribution with increasing pressure. Star symbols represent the predicted load distribution for the last load step. In Table 9, the ratios of crown to springing line loads are listed for two load levels per model.

Load Strain and Load Deflection Plots

17. Data from the largest load, cell 1 or 9, were used. The data from the strain gages on the steel reinforcement and concrete are plotted as load versus strain. Also, the data from the deflection gages are plotted as load versus deflection. These plots are shown in Appendix D for all tests. Note that the positive moment and the negative moment sections refer to crown and springing line sections, respectively.

Strain Distributions

18. Data from the strain gages at the crown and springing line sections for the same time load step are plotted in Appendix E. This gives a graphical view of the strain distribution and scatter.

19. The strain distributions of the positive and negative moment sections were fitted with both a hyperbolic and a linear curve, as shown in Appendix E. The formulations for the curve fits are included in Appendix F. A least-squares criterion was used for the curve fit.

20. In Table 10, the results from the curve fits are listed. The two values solved by the curve fits are the depth of section in compression, c, or the maximum compressive strain, ε_u. The results in the column labelled r^2 are the values of the correlation coefficient squared. This value is a measure of the scatter in data from the assumed strain distribution (linear or hyperbolic).

Resultant Moments and Thrusts

21. Moments and thrusts were computed for each strain distribution using the section properties in Table 1, the material properties in Tables 4 and 5, the neutral axis location and the maximum compressive strain obtained from the curve fits. The hyperbolic curve fit was used with a curved beam analysis computer program, and the linear fit was used with a straight beam analysis computer program.

22. Moment and thrust values are plotted on curved beam analysis interaction diagrams (plot of thrust and moment capacity of a section) shown in Appendix G. In the interaction diagrams, the box symbols represent the resolved moment and thrust from curved beam analysis, and the triangle symbols represent the resolved moment and thrust from straight beam analysis.

23. Predicted load paths using a two-dimensional (2-D) (Airy stress function) and a one-dimensional (1-D) or thin-ring linear elastic structural analysis are also plotted on the interaction diagrams. The Airy stress and 1-D linear elastic solutions appear in Anderson, Haelsig, and Reifel (1966). The 2-D and 1-D load paths are shown as a solid line and a dashed line, respectively.

PART IV: DISCUSSION OF EXPERIMENTAL RESULTS

24. All specimens failed in flexure. The progression to failure is described in the test observations in Part III. None of the models had shear-type failures, which were typical of pipes loaded in the Three-Edge-Bearing Tests (American Concrete Institute 1970). Curvature and loading appear to be the two most important variables in the test. Very thick, thick, and thin models corresponded to respective R/h values of 1.5, 2.4, and 4.5.

25. All models, except the model under hydrostatic loading, failed at a load higher than predicted by 2-D or 1-D linear elastic analyses. Failure loads, modes, and other observations are summarized in Tables 6 through 8. Model C5-3 (1:1 load, R/h = 2.4) failed at the predicted linear elastic failure load.

26. The predicted failure loads at crown and springing line sections were obtained by reading the failure thrust at the intersection of the 2-D or 1-D load paths with the interaction diagrams from Appendix G. As discussed below, the failure loads were calculated from the failure thrust using Airy stress and thin-ring linear elastic structural analyses.

27. According to 1-D or thin-ring theory (Anderson, Haelsig, and Reifel 1966), the thrust T is:

$$T = a_1 RW \tag{1}$$

where

T = thrust, kips

a_1 = factor that is a function of location on ring and ratio of load at crown to load at springing line or

$= \left(q + \frac{p}{3}\right)$ at crown, or

$= \left(q - \frac{p}{3}\right)$ at springing line

where

p = varying pressure component magnitude

q = uniform pressure component magnitude

$q = \frac{5}{8}$; $p = -\frac{3}{8}$ (4:1 load)

$$q = \frac{2}{3} \; ; \; p = -\frac{1}{3} \text{ (3:1 load)}$$

$$q = \frac{3}{4} \; ; \; p = -\frac{1}{4} \text{ (2:1 load)}$$

$$q = 1 \; ; \; p = 0 \text{ (1:1 load)}$$

$$\text{pressure} = q + p \cos 2\theta$$

where

θ = angle measured from springing line

R = radius of initial curvature to middepth of section, in.

W = maximum value of distributed normal load, kips/in.

28. The equivalent maximum concentrated normal load occurs at the crown and is

$$P_{cr} = a_2 WR \tag{2}$$

where

P_{cr} = concentrated normal load at crown, kips

a_2 = factor that is a function of ratio of load at crown to load at springing line

29. The factor a_2 was obtained by integrating the distributed load over one-sixteenth of the circumference at the crown.

$$a_2 = 2 \int_{7\pi/16}^{\pi/2} (q + p \cos 2\theta) d\theta = 2\left(q \frac{\pi}{16} + \frac{p}{2} \sin \frac{7\pi}{8}\right)$$

(Refer to discussion of factor a_1 in paragraph 27 for values of q and p.)

30. Substituting the value of distributed load from Equation 1 into Equation 2 produces the following equation for 1-D predicted failure load:

$$P_{cr} = T \frac{a_2}{a_1} \tag{3}$$

Values of P_{cr}, T, a_2, and a_1 for all models are shown in Table 11.

31. According to Airy stress analysis (Anderson, Haelsig, and Reifel 1966), the thrust T is:

$$T = a_3 W \tag{4}$$

where

a_3 = factor that is a function of inner and outer radius of ring, location on ring, and ratio of load at crown to load at springing line

$$= \left[2K_1(R_o - R_i) + 4K_2\left(R_o^3 - R_i^3\right) - 2K_3\left(\frac{1}{R_o^3} - \frac{1}{R_i^3}\right) \right] \cos 2\Theta$$

$$+ 2K_4(R_o - R_i) + K_5\left(\frac{1}{R_o} - \frac{1}{R_i}\right)$$

where

Θ = angle measured from springing line

R_o = outer radius

R_i = inner radius

$$K_1 = 3\lambda \frac{p}{q}\left(R_o^4 + R_i^2 R_o^2 + 2R_i^4\right)$$

$$K_2 = -\lambda \frac{p}{q}\left(R_o^2 + 3R_i^2\right)$$

$$K_3 = \lambda \frac{p}{q}\left(3R_i^4 R_o^4 + R_i^6 R_o^2\right)$$

$$K_4 = -3\lambda\left(R_o^2 - R_i^2\right)^2$$

$$K_5 = 6\lambda R_i^2\left(R_o^2 - R_i^2\right)^2$$

$$\lambda = \frac{qR_o^2}{6\left(R_o^2 - R_i^2\right)^3}$$

p = varying pressure component magnitude

q = uniform pressure component magnitude

(Refer to discussion of factor a_1 in paragraph 27 for values of q and p.)

32. The equivalent maximum concentrated normal load occurs at the crown and is:

$$P_{cr} = a_2 W R_o \tag{5}$$

where

R_o = outer radius of ring, in.

33. As discussed previously, the factor a_2 was obtained by integrating the loading function over one-sixteenth of the circumference. Substituting, the value of distributed load from Equation 4 into Equation 5, the following equation for 2-D predicted failure load is formed:

$$P_{cr} = T R_o \frac{a_2}{a_3} \tag{6}$$

Values of P_{cr}, T, R_o, a_2, and a_3 for all models are shown in Table 11.

34. It is interesting to note that the implosion pressure, P_{im}, observed for model C5-3 agrees with the pressure predicted by a published empirical design equation for long thick-walled cylinders (Chen 1982):

$$P_{im} = f'_c\left(2.17 \frac{t}{D_o} - 0.04\right) \tag{7}$$

where

P_{im} = implosion pressure, psi

f'_c = uniaxial compressive cylinder strength, psi (3,632 psi for model C5-3)

$\frac{t}{D_o}$ = ratio of wall thickness to outside diameter (3.469/19.937 or 0.174 for model C5-3)

Equation 7 predicts implosion in model C5-3 at 1,215 psi, or 1.1 percent less than observed (1,228 psi at a maximum load of 29,190 lb). The theoretical implosion pressure (Chen 1982) is

$$P_{im} = 2f'_c \frac{t}{D_o}\left(1 - \frac{t}{D_o}\right) \tag{8}$$

For model C5-3, Equation 8 predicts implosion at 1,035 psi, or 15.7 percent less than observed. Figure 4 shows the experimental and predicted implosion

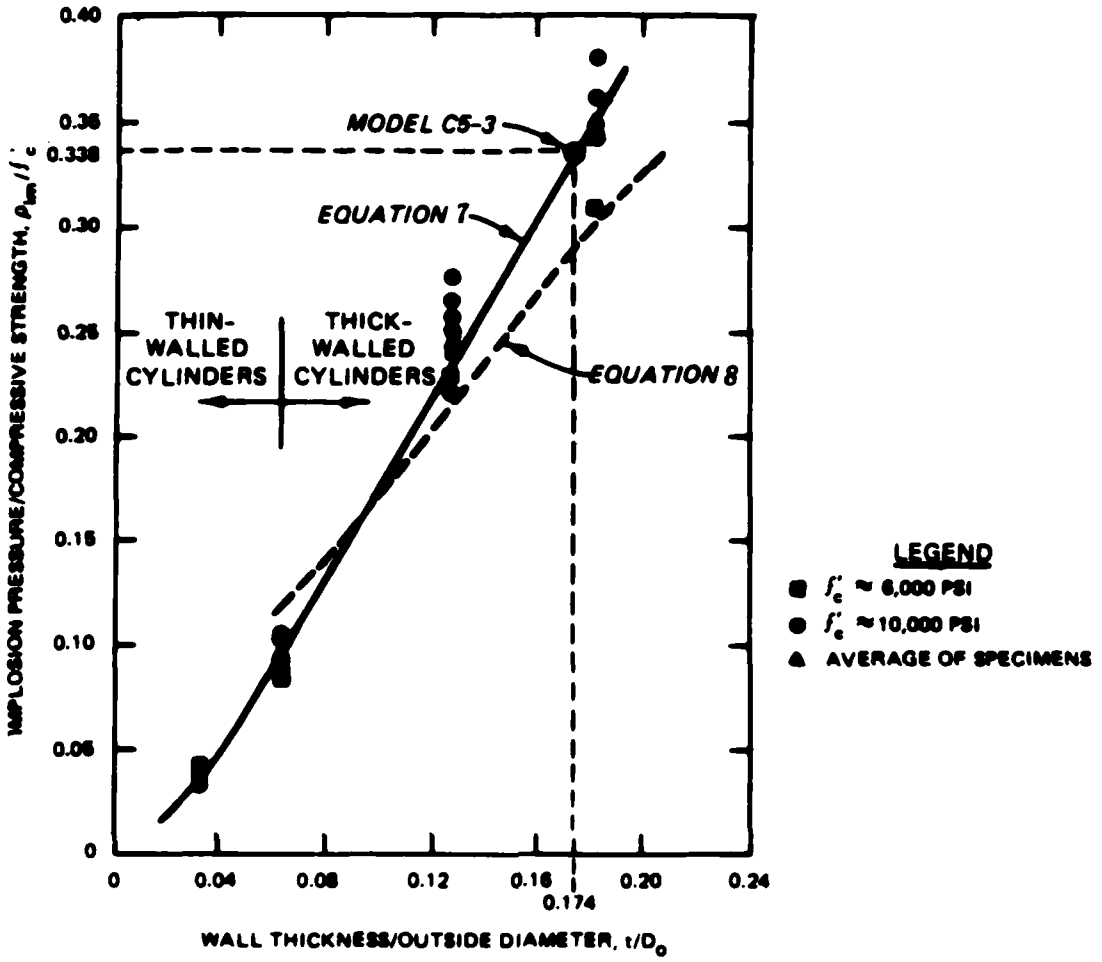

NOTE: ADDITIONAL DATA SHOWN FROM HAYNES (1976): OUTSIDE DIAMETER = 16 INCHES, LENGTH = 64 INCHES. END CLOSURES WERE HEMISPHERES OF SAME WALL THICKNESS AS THE CYLINDER.

Figure 4. Relationship between implosion strength and the t/D_o ratio for concrete cylinders under hydrostatic loading

pressures from Equations 7 and 8. Experimental data from Haynes (1976) is also plotted on the figure.

35. Most of the models redistributed the loads so that the springing line had more load than predicted, as shown in the radial distribution plots in Appendix C. As listed in Table 9, the thicker models had the best comparison of actual to predicted ratio of load at crown to load at springing line (2.1 to 18.0 percent difference). The percent difference between actual and predicted ratio of load at crown to load at springing line ranged from 25.2 to 45.1 percent in the thinner models. Evidently, the thinner models tend to

redistribute the load so that the loading is more uniform around the cylinder.

36. The majority of the predicted failure modes agree with the observed flexural failure modes. Very thick models had brittle failures and thin models had ductile failures. Thick models had ductile failures for the 3:1 and 4:1 loading cases and brittle failures for the 1:1 and 2:1 loading cases. Model C5-2 (R/h = 2.4, 2:1 load) formed four hinges, but a brittle flexural failure was predicted at the crown and springing line. Predicted failure modes at the crown differ from failure modes at the springing line for some models, with ultimate capacity near the balance point on the interaction diagram.

37. Results indicate that the thicker models may be more resistant to cracking than the thinner models. As indicated in Tables 6 through 8, the observed load at which the first crack appears ranges from 0.54 to 1.00 times the observed failure load (P) for models with R/h = 1.5 , from 0.46P to 0.86P for models with R/h = 2.4 , and 0.25P to 0.49P for models with R/h = 3.9 to 4.5 .

38. Appendix G shows that the greatest difference between the experimental load path and the theoretical load paths occurs in the thicker models (R/h = 1.5).

39. It should be noted that the strain data for model C2-1 are not consistent with other models. As shown in Table 10, the effective depth of section in compression (c/h) is more than 50 percent smaller than the effective depth of section in compression for most of the other models. Therefore, the thrust is unusually small, and the difference between theoretical and experimental load paths is large, as shown in Appendix G.

40. In Table 10 the results of the fits to the strain distribution are listed. Statistically, for most models, the hyperbolic fit is better than the linear fit, but no significant difference exists between the fits for a majority of the tests.

41. Straight beam analysis may be sufficient for conduits with R/h as low as 1.5. Results indicate that the linear, straight beam analysis agrees within 20 percent of the curved beam analysis for models with little scatter in the strain data, such as models C1-1 and C2-3. Table 12 shows the experimental moments and thrusts calculated from hyperbolic and linear fits.

42. The difference between the observed and predicted failure loads may be the result of ignoring the biaxial response of concrete in the structural

analysis (Park and Paulay 1975). Uniaxial behavior is assumed, but there is actually a significant compressive confinement pressure present on the extrados of the entire conduit.

PART V: CONCLUSIONS AND FUTURE WORK

Conclusions

43. Initial curvatures of Corps circular conduits affect the flexural-axial resistance, but linear straight beam analysis agrees within 20 percent of the curved beam analysis for conduits with $R/h = 1.5$. Therefore, the normal design practice for computing the moment-thrust resistance of uncurved members may be sufficiently accurate.

44. For most models tested, the observed failure load was larger than predicted by linear elastic analyses. This difference may be due to the neglect of the biaxial response of concrete in the structural analysis.

45. Most models failed in the predicted flexural failure mode. Model conduit failures are summarized as:

R/h	Thickness	Failure
1.5	Very thick	Brittle
2.4	Thick	3:1 loading, ductile 4:1 loading, brittle 1:1 loading, brittle 2:1 loading, brittle
4.5	Thin	Ductile

No shear failures occurred, which may be explained by the loading confinement. Conclusions on test results of models subjected to 2-point, 4-point, and three-edge-bearing loads are included in Appendix B.

Future Work

46. The problems of plastic behavior and shear response of conduits will be addresses in future investigations. Nonlinear finite element analyses will be performed. Ultimate strength flexural and shear design criteria for R/C circular conduits will be formulated.

47. Future work will also include the analysis of oblong-shaped conduits. Ultimate strength design criteria will be developed for oblong conduits.

REFERENCES

American Concrete Institute. 1970. "Models for Concrete Structures," ACI Publication No. 24, Detroit, Mich.

American Society for Testing and Materials. 1983. "Standard Methods of Testing Concrete Pipe, Sections, or Tile," Designation: C497-83, 1983 Book of ASTM Standards, Philadelphia, Pa.

Anderson, R. H., Haelsig, R. T., and Reifel, M. D. 1966 (Mar). "Structural Behavior of Ring Sections Under Nonuniform External Pressure," Technical Report No. AFWL-TR-65-145, Air Force Weapons Laboratory, Kirtland Air Force Base, N. Mex.

Chen, W. F. 1982. Plasticity in Reinforced Concrete, McGraw-Hill, New York.

Chiarito, V. P., and Mlakar, P. 1986. "Strength Design of Reinforced Concrete Hydraulic Structures; Load-Moment Characteristics of Reinforced Concrete Circular Conduits," Technical Report SL-80-4, Report 4, US Army Engineer Waterways Experiment Station, Vicksburg, Miss.

Haynes, H. H. 1976. "Handbook for Design of Undersea, Pressure-Resistant Concrete Structures," Naval Construction Battalion Center, Civil Engineering Laboratory, Port Hueneme, Calif.

Hognestad, E., Hanson, N. W., and McHenry, D. 1955 (Dec). "Concrete Stress Distributions in Ultimate Strength Design," Journal, American Concrete Institute, Title No. 52-28, Vol 27, No. 4, pp 455-479.

Miller, I., and Freund, J. E. 1977. Probability and Statistics for Engineers, 2nd ed., Prentice-Hall, Englewood Cliffs, N. J.

Park, R., and Paulay, T. 1975. Reinforced Concrete Structures, Wiley, New York.

Timoshenko, S. 1941 (Aug). Strength of Materials; Part II, Advanced Theory and Problems, 2nd ed., Chapter II, Van Nostrand, New York.

Table 1

Summary of Models

Model	R/h	Total Steel Ratio, ρg percent	Load Distri-bution	Batch No.	Steel Rein-forcement	R in.	h in.	B in.	d in.	d' in.	S in.
C1-1	1.5	0.408	3:1	1	D3*	7.476	5.031	6.047	4.25	0.75	2.1
C2-1	1.5	0.760	3:1	1	#2	7.468	5.000	5.266	4.25	0.75	1.5
C2-2	1.5	0.758	2:1	1	#2	7.461	5.016	5.250	4.25	0.75	1.5
C2-3	1.5	0.712	4:1	1	#2	7.461	4.984	5.633	4.25	0.75	1.5
C3-1	1.5	1.471	3:1	1	#3	7.453	4.984	6.00	4.25	0.75	2.0
C4-1	2.4	0.432	3:1	2	D3	8.250	3.500	8.203	3.0	0.5	2.9
C4-2	2.4	0.446	2:1	3	D3	8.242	3.437	8.094	3.0	0.5	2.9
C5-1	2.4	0.919	3:1	2	#2	8.265	3.500	6.219	3.0	0.5	2.0
C5-2	2.4	0.957	2:1	3	#2	8.242	3.484	6.000	3.0	0.5	2.0
C5-3	2.4	0.951	1:1	3	#2	8.234	3.469	6.062	3.0	0.5	2.0
C5-4	2.4	0.961	4:1	3	#2	8.281	3.469	6.000	3.0	0.5	2.0
C6-1	2.4	1.433	3:1	1	#2	8.233	3.422	4.078	3.0	0.5	1.25
C6-2	2.4	1.418	2:1	3	#2	8.257	3.484	4.047	3.0	0.5	1.25
C7-1	4.1	0.371	3:1	2	D1*	8.906	2.156	5.000	1.86	0.46	1.5
C8-1	4.0	0.877	3:1	2	D3	9.015	2.250	6.281	1.95	0.62	2.0
C8-2	4.2	0.943	4:1	2	D3	8.875	2.125	6.187	1.59	0.49	2.0
C8-3	4.5	1.017	2:1	3	D3	8.937	2.000	6.094	1.78	0.36	2.0
C9-1	3.9	1.225	3:1	2	D3	8.875	2.250	4.500	1.81	0.61	1.4

Note: ρg = total steel ratio.

* D1 and D3 bars are deformed model rebars. Their properites are listed in Table 3.

Table 2

Test Matrix

ρg*	Loading							
	1:1		2:1		3:1		4:1	
0.0041-0.0045			14**	C4-2	2	C1-1		
					5	C4-1		
					7	C7-1		
0.0071-0.0096	18	C5-3	13	C2-2	1	C2-1	10	C2-3
			15	C5-2	6	C5-1	12	C5-4
			17	C8-3	8	C8-1	11	C8-2
0.010-0.015			16	C6-2	3	C3-1		
					4	C6-1		
					9	C9-1		

* ρg = total steel ratio.
** Numbers preceding test designations indicate testing sequence.

Table 3

Experimental Equipment

Hydraulic System	
Hydraulic cylinder jacks	Double acting Hydroline series Hydroline cylinders Model: N2R, Serial suffix: 01R, *Bore-5 in., stroke-6 in.* Rated for 58.9 kips at 3,000 psi
Hydraulic power supply	3,000-psi water-cooled pump
Hydraulic controller (pressure regulator)	Hydraulic load maintainer Challenger Model 10M Serial No. 5M1142 rated for 5,000 psi
Instrumentation	
Load cells	Interface Model: 1220 AR50K, Precision Universal load cells, 50 kips
Strain gages	Micro Measurements
Deflection gages	LVDT
Data logger	Model 9300 by Monitor Labs
Photography	
Sony portable video camera and recorder 35-mm Camera	

Table 4

Steel Reinforcement Properties

Type	Heat Treatment	Area $in.^2$	Number of Bars Tested	Average f_y ksi	Average Modulus of Elasticity $E_s \times 10^6$ psi	Average Ultimate Stress ksi	Average Rupture Stress ksi
#2	None	0.05	5	54.2	28.1	71.7	66.1
#3	None	0.11	4	63.1	25.5	98.4	87.8
D3	4-1/2 hr to 4-2/3 hr at 1,000° F	0.031	6	68.2	27.0	74.3	64.9
D1	3-1/2 hr at 1,000° F	0.01	19	81.4	32.7	83.3	67.2

Table 5

Concrete Properties

Batch No.	Models	Number of Cylinders Tested	Dates Tested	Age, days	Average f'_c psi	Average Initial Elastic Concrete Modulus $E_c \times 10^6$ psi	Average Poisson's Ratio	Average Tensile Strength psi
1	C1-1, C2-1,	3	8/10/83	28	3,817	--	--	
1	C2-2, C2-3, C3-1, C6-1	12	8/24/83-9/7/83	42-56	4,213	4.19	0.152	388
2	C4-1, C5-1,	3	8/15/83	28	4,193	--	--	
2	C7-1, C8-1, C8-2, C9-1	9	8/30/83-9/7/83	48-51	4,571	4.49	0.150	470
3	C4-2, C5-2,	3	8/18/83	28	3,527	--	--	
3	C5-3, C5-4, C6-2, C8-3	9	9/7/83-9/9/83	48-50	3,632	4.00	0.157	437

Table 6

Failure Loads and Types (R/h = 1.5)

Model	Load Distribution	ρ_g	(P) Observed Failure Load kips	1-D Predicted Failure Load kips	2-D Predicted Failure Load kips	Test Observations
1-1	3:1	0.0041	46.9 (brittle)	35.3 (brittle at C) 29.9 (brittle at SL)	40.0 (brittle at C) 27.0 (brittle at SL)	Load at first crack: 30.9 kips = 0.66P at C intrados. Plastic hinges started to form at the crown and springing line. Spalling at SL intrados.
2-1	3:1	0.0076	38.5 (brittle)	32.7 (brittle at C) 27.3 (brittle at SL)	36.7 (brittle at C) 24.9 (brittle at SL)	Load at first crack: 29.4 kips = 0.76P at C intrados. Spalling at SL intrados before collapse by crushing.
2-2	2:1	0.0076	43.4 (brittle)	35.9 (brittle at C) 30.5 (brittle at SL)	40.0 (brittle at C) 27.8 (brittle at SL)	Load at first crack: 43.4 kips = 1.00P at C intrados. Cracking at C, crushing and cracking at SL, occurred simultaneously at three points. Crushing - beneath some of the bearing plates.
2-3	4:1	0.0071	36.5 (brittle)	31.0 (ductile at C) 27.1 (brittle at SL)	36.1 (ductile at C) 24.4 (brittle at SL)	Load at first crack: 19.6 kips = 0.54P at C intrados. Diagonal crack all the way through section between C and SL.
3-1	3:1	0.0147	49.0 (brittle)	44.3 (brittle at C) 35.3 (brittle at SL)	49.0 (brittle at C) 32.1 (brittle at SL)	Load at first crack: 36.3 kips = 0.74P at C intrados. Spalling at SL.

Note: C = crown; SL = springing line; ρ_g = total steel ratio.

Table 7

Failure Loads and Types (R/h = 2.4)

Model	Load Distribution	ρ_g	(P) Observed Failure Load kips	1-D Predicted Failure Load kips	2-D Predicted Failure Load kips	Test Observations
4-1	3:1	0.0043	27.3 (ductile)	19.1 (ductile at C) 21.0 (brittle at SL)	22.0 (ductile at C) 19.4 (brittle at SL)	Load at first crack: 14.7 kips = 0.54P at C intrados. Spalling occurred first at SL.
4-2	2:1	0.0045	34.1 (brittle)	23.9 (brittle at C) 21.6 (brittle at SL)	26.3 (brittle at C) 19.9 (brittle at SL)	Load at first crack: 29.4 kips = 0.86P at C intrados. Spalling occurred first at SL.
5-1	3:1	0.0092	19.4 (ductile)	17.8 (ductile at C) 18.0 (ductile at SL)	20.4 (ductile at C) 17.2 (ductile at SL)	Load at first crack: 9.0 kips = 0.46P at C intrados. Four hinges formed.
5-2	2:1	0.0096	28.5 (ductile)	20.5 (brittle at C) 18.1 (brittle at SL)	21.8 (brittle at C) 16.8 (brittle at SL)	Load at first crack: 24.5 kips = 0.86P at C intrados. Spalling occurred first at SL. Four hinges formed. Crushing at C extrados.
5-3	1:1	0.0095	29.2 (brittle)	29.3 (brittle)	29.3 (brittle)	Initial crushing at IA intrados.
5-4	4:1	0.0096	17.5 (ductile)	12.7 (ductile at C) 13.1 (brittle at SL)	13.9 (ductile at C) 12.5 (brittle at SL)	Load at first crack: 8.8 kips = 0.50P at C intrados.
6-1	3:1	0.0143	17.9 (ductile)	13.2 (ductile at C) 12.1 (brittle at SL)	14.8 (ductile at C) 11.3 (brittle at SL)	Load at first crack: 9.8 kips = 0.55P at C intrados.
6-2	2:1	0.0142	20.0 (brittle)	15.2 (brittle at C) 13.1 (brittle at SL)	16.1 (brittle at C) 12.4 (brittle at SL)	Load at first crack: 15.7 kips = 0.79P at C intrados. Sudden collapse at SL.

Note: C = crown; SL = springing line; ρ_g = total steel ratio.

Table 8

Failure Loads and Types ($R/b = 4.1$)

Model	Load Distribution	ρ_g	(P) Observed Failure Load kips	I-D Predicted Failure Load kips	F-T Predicted Failure Load kips	Test Observations
7-1	3:1	0.0037	5.3 (ductile)	1.1 (ductile at C) 2.0 (ductile at SL)	1.1 (ductile at C) 2.0 (ductile at SL)	Load at first crack: 1.9 kips = 0.36P at C intrados. Four hinges formed.
8-1	3:1	0.0088	7.3 (ductile)	4.8 (ductile at C) 6.1 (ductile at SL)	4.8 (ductile at C) 6.1 (ductile at SL)	Load at first crack: 2.0 kips = 0.27P at C intrados. Crack almost through crown.
8-2	4:1	0.0094	5.? (ductile)	3.9 (ductile at C) 3.8 (ductile at SL)	3.9 (ductile at C) 3.8 (ductile at SL)	Load at first crack: 2.0 kips = 0.38P at C intrados. Four hinges formed.
8-3	2:1	0.0102	11.5 (ductile)	7.2 (ductile at C) 6.7 (brittle at SL)	7.5 (ductile at C) 6.5 (brittle at SL)	Load at first crack: 5.7 kips = 0.49P at C intrados. Crushing by collapse at C. Four hinges formed.
9-1	3:1	0.01225	5.5 (ductile)	4.1 (ductile at C) 5.0 (brittle at SL)	4.3 (ductile at C) 4.9 (brittle at SL)	Load at first crack: 1.4 kips = 0.25P at C intrados. Spalling at SL. Four hinges formed. Diagonal cracks at C.

Note: C = crown; SL = springing line; ρ_g = total steel ratio.

Table 9

Ratios of Load at Crown to Load at Springing Line

Model	Load at Crown kips	Load at Springing Line kips	Predicted Load at Springing Line kips	Percent Difference**
C1-1	5.35	2.10 (2.55:1)*	1.78 (3:1)*	+18.0
	47.0	17.28 (2.72:1)	15.67 (3:1)	+10.3
C2-1	5.65	1.92 (2.94:1)	1.88 (3:1)	+2.1
	38.48	12.22 (3.15:1)	12.83 (3:1)	-4.8
C2-2	5.19	2.70 (1.92:1)	2.60 (2:1)	+3.8
	43.43	23.46 (1.85:1)	21.72 (2:1)	+8.0
C2-3	2.13	0.51 (4.18:1)	0.53 (4:1)	-3.8
	36.53	10.38 (3.52:1)	9.13 (4:1)	+13.7
C3-1	5.47	2.01 (2.72:1)	1.82 (3:1)	+10.4
	49.01	18.01 (2.72:1)	16.34 (3:1)	+10.2
C4-1	5.39	1.82 (2.96:1)	1.80 (3:1)	+1.1
	27.30	10.51 (2.60:1)	9.10 (3:1)	+15.5
C4-2	2.33	1.33 (1.75:1)	1.17 (2:1)	+13.7
	35.79	20.35 (1.77:1)	17.90 (2:1)	+13.1
C5-1	2.59	0.74 (3.5:1)	0.86 (3:1)	-14.0
	19.58	7.43 (2.64:1)	6.53 (3:1)	+13.8
C5-2	5.18	2.76 (1.88:1)	2.59 (2:1)	+6.6
	28.62	16.53 (1.73:1)	14.31 (2:1)	+15.5
C5-3	5.00	4.89 (1.02:1)	5.00 (1:1)	-2.2
	29.17	28.70 (1.02:1)	29.17 (1:1)	-1.6
C5-4	5.21	1.81 (2.87:1)	1.30 (4:1)	+39.0
	17.63	5.69 (3.10:1)	4.41 (4:1)	+29.0
C6-1	5.47	1.93 (2.83:1)	1.82 (3:1)	+6.0
	18.18	7.22 (2.52:1)	6.06 (3:1)	+19.1

(Continued)

* Values in parentheses denote ratio of load at crown to load at springing line.

** Values in this column are the percent differences of the measured loads at springing line from the predicted loads at springing line.

Table 9 (Concluded)

Model	Load at Crown kips	Load at Springing Line kips	Predicted Load at Springing Line kips	Percent Difference
C6-2	2.41	1.29 (1.87:1)	1.21 (2:1)	+6.6
	20.51	11.42 (1.80:1)	10.26 (2:1)	+11.3
C7-1	2.17	1.00 (2.17:1)	0.72 (3:1)	+38.9
	5.26	2.54 (2.07:1)	1.75 (3:1)	+45.1
C8-1	3.37	1.41 (2.39:1)	1.12 (3:1)	+25.9
	7.30	3.50 (2.09:1)	2.43 (3:1)	+44.0
C8-2	2.38	0.84 (2.83:1)	0.60 (4:1)	+40.0
	5.40	2.13 (2.54:1)	1.35 (4:1)	+57.8
C8-3	2.77	1.74 (1.59:1)	1.39 (2:1)	+25.2
	11.81	7.45 (1.59:1)	5.91 (2:1)	+26.1
C9-1	2.61	1.05 (2.49:1)	0.87 (3:1)	+20.7
	5.57	2.58 (2.16:1)	1.86 (3:1)	+38.7

Table 10

Strain Distributions Fitted to Hyperbolic and Linear Curves

Load Level kips	Hyperbolic Fit			Linear			r^2	
	c , in.	c/h	ε_u millionths	c , in.	c/h	ε_u millionths	Hyper-bolic	Linear
			Model C1-1, Crown					
10.1	2.716	0.540	279.0	2.243	0.446	319.3	0.967	0.965
19.5	2.664	0.530	640.5	2.188	0.435	740.9	0.959	0.956
27.8	2.619	0.521	1,104.6	2.149	0.427	1,268.9	0.970	0.969
30.1	2.597	0.516	1,225.3	2.184	0.434	1,524.8	0.972	0.971
			Model C1-1, Springing Line					
10.1	4.036	0.802	450.0	4.050	0.805	433.6	0.985	0.952
19.5	3.790	0.753	1,087.7	3.878	0.771	1,057.3	0.974	0.929
27.8	3.606	0.717	1,923.3	3.745	0.744	1,886.0	0.962	0.909
30.1	3.537	0.703	2,200.8	3.685	0.732	2,174.5	0.952	0.893
			Model C2-1, Crown					
9.4	1.136	0.272	65.1	1.116	0.223	87.9	0.957	0.972
20.1	1.381	0.276	175.1	1.124	0.225	231.2	0.973	0.974
29.1	1.485	0.297	401.4	1.241	0.248	562.0	0.935	0.920
33.7	1.440	0.288	584.5	1.171	0.234	780.7	0.958	0.946
36.7	1.408	0.282	764.1	1.143	0.229	1,013.5	0.967	0.954
			Model C2-1, Springing Line					
9.4	0.576	0.115	60.3	0.701	0.140	41.7	0.993	0.996
20.1	0.724	0.145	205.2	0.948	0.190	159.7	0.962	0.990
29.4	0.786	0.157	445.8	1.045	0.209	358.1	0.952	0.987
33.7	1.073	0.215	905.1	1.244	0.249	598.7	0.998	0.998
36.7	1.095	0.219	1,294.0	1.310	0.262	910.8	0.971	0.970
			Model C2-2, Crown					
5.2	5.011	1.000	123.2	4.721	0.941	149.2	0.724	0.493
10.0	5.159	1.029	225.9	4.924	0.982	272.3	0.715	0.475
19.3	5.353	1.067	459.9	5.291	1.055	558.4	0.720	0.414
24.1	5.212	1.039	669.0	5.110	1.019	812.7	0.733	0.454
29.1	5.142	1.025	923.8	4.925	0.982	1,141.6	0.711	0.420
			Model C2-2, Springing Line					
5.2	4.221	0.842	231.1	3.800	0.758	236.4	0.853	0.737
10.1	4.178	0.833	467.5	3.762	0.750	481.0	0.844	0.724

(Continued)

Table 10 (Continued)

Load Level kips	Hyperbolic Fit			Linear			r^2	
	c , in.	c/h	ε_u millionths	c , in.	c/h	ε_u millionths	Hyper-bolic	Linear
			Model C2-2, Springing Line (Continued)					
19.3	4.145	0.826	964.7	3.619	0.722	1,034.8	0.793	0.604
24.1	4.024	0.802	1,398.6	3.575	0.713	1,496.4	0.799	0.611
29.1	4.014	0.800	1,984.3	3.680	0.734	2,044.9	0.851	0.708
			Model C2-3, Crown					
5.0	4.177	0.838	125.9	4.071	0.817	134.4	0.968	0.952
10.0	4.256	0.854	252.4	4.136	0.830	272.6	0.942	0.921
19.4	4.045	0.812	553.3	3.714	0.745	619.9	0.889	0.860
24.3	3.914	0.785	817.8	2.484	0.699	940.4	0.858	0.818
28.8	3.777	0.758	1,192.9	3.239	0.650	1,431.6	0.811	0.746
			Model C2-3, Springing Line					
5.0	3.740	0.750	216.6	3.767	0.756	195.4	0.992	0.968
10.0	3.615	0.725	437.2	3.685	0.739	393.9	0.994	0.964
19.4	3.099	0.622	1,033.3	3.232	0.649	945.1	0.979	0.909
24.3	2.865	0.575	1,523.4	3.042	0.610	1,404.0	0.969	0.879
28.8	2.687	0.539	2,221.5	2.879	0.578	2,088.0	0.941	0.835
			Model C3-1, Crown					
10.2	4.794	0.962	192.8	5.076	1.018	205.3	0.931	0.952
19.7	4.872	0.978	400.5	5.122	1.028	430.2	0.900	0.924
29.3	4.917	0.987	709.7	5.050	1.031	774.2	0.855	0.885
38.4	5.072	1.018	1,092.6	5.129	1.029	1,211.4	0.804	0.829
			Model C3-1, Springing Line					
10.2	3.658	0.734	326.2	3.000	0.602	429.7	0.603	0.498
19.7	3.502	0.703	683.8	2.787	0.559	1,025.4	0.514	0.410
29.3	2.748	0.551	1,376.0	2.171	0.436	1,988.8	0.504	0.376
38.4	2.614	0.525	2,530.1	2.144	0.430	3,622.2	0.517	0.389
			Model C4-1, Crown					
5.4	2.446	0.699	188.0	2.241	0.640	199.9	0.960	0.948
10.3	2.032	0.581	487.0	1.815	0.519	521.3	0.979	0.975
15.3	1.590	0.454	1,004.0	1.384	0.395	1,096.3	0.980	0.984
19.4	1.527	0.436	1,594.0	1.320	0.377	1,750.6	0.977	0.984

(Continued)

Table 10 (Continued)

Load Level kips	Hyperbolic Fit			Linear			r^2	
	c , in.	c/h	ε_u millionths	c , in.	c/h	ε_u millionths	Hyperbolic	Linear
			Model C4-1, Springing Line					
5.4	2.237	0.639	219.0	2.317	0.662	218.8	0.936	0.905
10.3	1.884	0.538	527.0	1.996	0.570	548.5	0.886	0.848
15.3	1.640	0.469	1,246.0	1.847	0.528	1,322.5	0.902	0.871
19.4	1.805	0.516	2,889.0	2.064	0.590	2,900.4	0.996	0.996
			Model C4-2, Crown					
2.3	2.780	0.809	67.3	2.698	0.785	70.5	0.978	0.971
10.2	2.840	0.826	369.0	2.802	0.815	383.5	0.992	0.989
21.9	2.760	0.803	1,033.0	2.661	0.774	1,082.7	0.971	0.971
27.4	2.724	0.793	1,740.0	2.529	0.736	1,880.1	0.909	0.913
			Model C4-2, Springing Line					
2.3	2.952	0.859	81.4	2.810	0.817	83.8	0.918	0.892
10.2	2.470	0.719	457.0	2.432	0.707	491.4	0.866	0.834
21.9	2.300	0.669	1,605.0	2.392	0.696	1,625.8	0.946	0.924
27.4	2.220	0.646	2,823.0	2.328	0.677	2,863.7	0.944	0.922
			Model C5-1, Crown					
4.1	2.446	0.699	244.0	2.233	0.638	270.0	0.920	0.916
8.7	2.270	0.649	641.1	2.021	0.577	741.5	0.876	0.867
12.0	2.234	0.638	981.2	1.977	0.565	1,152.6	0.860	0.847
14.6	1.723	0.492	1,494.7	1.501	0.429	1,631.1	0.967	0.973
17.3	1.619	0.463	1,981.5	1.403	0.401	2,173.9	0.969	0.975
			Model C5-1, Springing Line					
5.2	1.995	0.570	358.6	2.073	0.592	375.8	0.868	0.815
9.2	1.696	0.485	807.1	1.849	0.528	835.2	0.889	0.844
12.0	1.757	0.502	1,269.7	1.919	0.548	1,277.4	0.922	0.887
14.6	1.670	0.477	1,964.8	1.850	0.529	1,955.7	0.935	0.903
16.3	1.607	0.459	2,530.0	1.794	0.512	2,517.3	0.936	0.903
			Model C5-2, Crown					
10.0	2.810	0.807	453.2	2.620	0.752	501.9	0.891	0.892
15.8	2.770	0.795	825.2	2.560	0.735	921.6	0.881	0.882
19.3	2.710	0.778	1,008.0	2.331	0.669	1,260.6	0.739	0.737
24.1	2.733	0.784	2,110.0	2.653	0.761	2,258.5	0.989	0.989

(Continued)

Table 10 (Continued)

Load Level kips	Hyperbolic Fit c , in.	Hyperbolic Fit c/h	Hyperbolic Fit ε_u millionths	Linear c , in.	Linear c/h	Linear ε_u millionths	r^2 Hyperbolic	r^2 Linear
			Model C5-2, Springing Line					
10.0	2.440	0.700	469.0	1.967	0.565	697.1	0.517	0.471
15.8	2.280	0.654	936.0	1.884	0.541	1,456.6	0.500	0.451
19.3	2.250	0.646	1,433.0	1.970	0.565	1,960.4	0.595	0.544
24.1	2.200	0.632	2,508.5	2.082	0.597	2,954.8	0.735	0.688
			Model C5-4, Crown					
2.2	2.550	0.735	70.0	2.232	0.644	76.7	0.863	0.875
5.0	1.930	0.556	317.0	1.678	0.484	345.8	0.934	0.950
9.0	1.540	0.444	650.0	1.322	0.381	718.5	0.953	0.968
12.8	1.400	0.404	1,096.0	1.198	0.345	1,226.3	0.953	0.966
			Model C5-4, Springing Line					
2.2	2.500	0.721	86.5	2.313	0.667	105.8	0.723	0.680
5.0	2.046	0.590	386.0	2.068	0.596	470.3	0.753	0.712
9.0	2.088	0.602	1,354.9	2.293	0.661	1,383.0	0.976	0.976
12.8	1.970	0.568	2,767.0	2.195	0.633	2,831.6	0.974	0.974
			Model C6-1, Crown					
2.7	2.710	0.792	129.5	2.555	0.747	139.6	0.922	0.931
5.3	2.183	0.638	442.6	1.965	0.574	488.1	0.927	0.929
10.1	2.072	0.606	992.3	1.831	0.535	1,142.3	0.884	0.888
13.6	2.026	0.592	1,436.9	1.829	0.535	1,675.9	0.912	0.912
			Model C6-1, Springing Line					
2.7	2.360	0.690	145.4	2.283	0.667	155.6	0.841	0.805
5.3	1.706	0.499	459.1	1.759	0.514	547.6	0.749	0.710
10.1	1.752	0.512	1,339.1	1.832	0.535	1,492.2	0.815	0.777
10.8	1.800	0.526	1,909.0	1.841	0.538	2,199.2	0.779	0.738
			Model C6-2, Crown					
2.4	2.800	0.804	156.2	2.740	0.786	162.5	0.995	0.992
5.4	2.750	0.789	374.0	2.665	0.765	389.7	0.994	0.993
10.2	2.540	0.729	873.3	2.402	0.690	914.4	0.985	0.993
14.9	2.400	0.689	1,618.8	2.213	0.635	1,711.4	0.974	0.973
19.3	2.240	0.643	2,717.5	2.002	0.575	2,927.7	0.941	0.945

(Continued)

Table 10 (Continued)

Load Level kips	Hyperbolic Fit c , in.	Hyperbolic Fit c/h	Hyperbolic Fit ε_u millionths	Linear c , in.	Linear c/h	Linear ε_u millionths	r^2 Hyperbolic	r^2 Linear
			Model C6-2, Springing Line					
2.4	2.780	0.798	190.9	2.572	0.738	202.0	0.847	0.806
5.4	2.770	0.795	457.8	2.538	0.729	490.1	0.829	0.788
10.2	2.620	0.752	1,105.8	2.527	0.725	1,142.5	0.883	0.848
14.9	2.475	0.710	2,535.1	2.474	0.710	2,557.9	0.919	0.890
			Model C7-1, Crown					
0.3	1.270	0.589	273.0	1.073	0.498	376.7	0.643	0.665
1.4	0.867	0.402	552.0	0.804	0.373	760.6	0.748	0.756
2.2	1.270	0.589	1,403.0	1.119	0.519	1,729.4	0.754	0.773
2.7	1.260	0.584	1,657.8	1.116	0.518	2,030.8	0.762	0.780
3.4	1.230	0.571	1,797.5	1.095	0.508	2,181.7	0.779	0.795
			Model C7-1, Springing Line					
0.3	0.731	0.339	340.5	0.831	0.385	345.1	0.991	0.991
1.4	0.661	0.306	586.0	0.778	0.360	630.1	0.959	0.959
2.2	0.602	0.279	1,221.0	0.730	0.339	1,387.0	0.929	0.929
2.4	0.433	0.201	1,293.0	0.753	0.349	2,888.5	0.664	0.664
			Model C8-1, Crown					
2.2	0.574	0.255	639.1	0.547	0.243	727.0	0.959	0.955
3.4	0.610	0.271	665.3	0.587	0.261	780.4	0.935	0.933
4.5	0.657	0.292	1,285.9	0.619	0.275	1,416.6	0.966	0.968
5.4	0.526	0.234	2,474.1	0.500	0.222	2,789.3	0.967	0.969
			Model C8-1, Springing Line					
2.2	1.200	0.533	499.5	0.644	0.286	880.4	0.326	0.326
3.4	1.337	0.594	630.6	0.653	0.290	1,143.2	0.292	0.292
4.5	1.214	0.540	1,291.2	0.769	0.342	1,776.9	0.492	0.492
5.4	1.590	0.707	1,931.0	0.813	0.361	2,439.5	0.590	0.590
			Model C8-2, Crown					
2.4	0.947	0.446	692.1	0.905	0.426	833.9	0.879	0.886
3.5	0.841	0.396	1,132.0	0.808	0.380	1,317.1	0.930	0.928
4.4	0.687	0.323	1,566.5	0.700	0.329	1,959.3	0.959	0.958
4.4	0.657	0.309	2,111.2	0.784	0.369	3,696.6	0.805	0.805

(Continued)

Table 10 (Concluded)

Load Level kips	Hyperbolic Fit			Linear			r^2	
	c , in.	c/h	ε_u millionths	c , in.	c/h	ε_u millionths	Hyperbolic	Linear
			Model C8-2, Springing Line					
2.4	0.903	0.425	709.1	0.959	0.451	689.7	0.998	0.997
3.5	0.877	0.413	1,155.0	0.932	0.439	1,139.9	0.986	0.978
4.4	0.802	0.377	1,942.0	0.860	0.405	1,918.8	0.983	0.978
4.4	0.719	0.338	2,442.4	0.779	0.366	2,418.5	0.972	0.969
			Model C8-3, Crown					
2.8	1.359	0.680	249.5	1.273	0.637	288.8	0.841	0.848
5.7	1.139	0.570	946.3	1.071	0.535	1,170.3	0.809	0.817
7.8	1.156	0.578	1,594.1	1.083	0.542	2,041.0	0.777	0.786
8.6	1.184	0.592	1,900.0	1.106	0.553	2,420.5	0.777	0.785
			Model C8-3, Springing Line					
2.8	1.392	0.696	322.1	1.389	0.694	329.6	0.926	0.909
5.7	1.071	0.536	975.1	1.110	0.555	1,013.4	0.915	0.896
7.8	0.991	0.496	1,687.0	1.037	0.518	1,775.4	0.905	0.885
8.6	1.034	0.517	2,137.8	1.076	0.538	2,237.9	0.908	0.889
			Model C9-1, Crown					
1.9	0.933	0.415	931.5	0.882	0.392	1,004.9	0.967	0.978
2.7	1.104	0.491	973.5	1.039	0.462	1,067.6	0.927	0.942
3.4	1.043	0.464	1,441.8	0.985	0.438	1,566.4	0.946	0.959
3.7	1.020	0.453	1,669.6	0.962	0.427	1,827.6	0.940	0.953
			Model C9-1, Springing Line					
1.9	0.967	0.430	1,663.4	1.025	0.455	1,628.6	0.970	0.959
2.7	1.031	0.458	1,869.0	1.085	0.482	1,844.0	0.963	0.953
3.4	1.038	0.461	2,667.1	1.092	0.485	2,615.2	0.969	0.960
3.7	0.972	0.432	3,136.2	1.029	0.457	3,125.0	0.949	0.945

Table 11

Predicted Failure Loads

			1-D Analysis			2-D Analysis			
Model	Location	a_2 (Eqs. 2, 5)	Thrust kips	a_1 (Eq. 1)	P_{cr} (Eq. 3) kips	Thrust kips	R_o inches	a_3 (Eq. 4) inches	P_{cr} (Eq. 6) kips
C1-1	C	0.3894	50.3	0.556	35.3	57.1	10.0	5.556	40.0
	SL		59.8	0.778	29.9	54.0		7.778	27.0
C2-1	C	0.3894	46.7	0.556	32.7	52.4	9.985	5.548	36.7
	SL		54.5	0.778	27.3	49.7		7.766	24.9
C2-2	C	0.3902	61.4	0.667	35.9	68.3	10.0	6.667	40.0
	SL		65.1	0.833	30.5	59.3		8.333	27.8
C2-3	C	0.3889	39.8	0.5	31.0	46.2	10.0	5.0	36.1
	SL		52.2	0.75	27.1	46.8		7.5	24.4
C3-1	C	0.3894	63.2	0.556	44.3	70.0	9.992	5.556	49.0
	SL		70.5	0.778	35.3	64.2		7.774	32.1
C4-1	C	0.3894	27.2	0.556	19.1	31.4	10.024	5.570	22.0
	SL		41.9	0.778	21.0	38.7		7.796	19.4
C4-2	C	0.3902	40.8	0.667	23.9	45.0	10.0	6.667	26.3
	SL		46.1	0.833	21.6	42.4		8.333	19.9
C5-1	C	0.3894	25.4	0.556	17.8	29.1	10.0	5.556	20.4
	SL		36.0	0.778	18.0	34.4		7.778	17.2
C5-2	C	0.3902	35.1	0.667	20.5	37.2	10.0	6.667	21.8
	SL		38.7	0.833	18.1	35.9		8.333	16.8

(Continued)

Note: C = crown; SL = springing line.

Table 11 (Concluded)

Model	Location	a_2 (Eqs. 2, 5)	1-D Analysis: Thrust kips	1-D Analysis: a_1 (Eq. 1)	1-D Analysis: P_{cr} (Eq. 3) kips	2-D Analysis: Thrust kips	2-D Analysis: R_o inches	2-D Analysis: a_3 (Eq. 4) inches	2-D Analysis: P_{cr} (Eq. 6) kips
C5-3	All locations	0.3927	74.7	1.000	29.3	74.7	9.985	9.985	29.3
C5-4	C	0.3889	16.3	0.5	12.7	17.9	10.0	5.0	13.9
	SL		25.3	0.75	13.1	24.2		7.5	12.5
C6-1	C	0.3894	18.9	0.555	13.2	21.1	10.008	5.564	14.8
	SL		24.2	0.778	12.1	22.6		7.786	11.3
C6-2	C	0.3902	25.9	0.667	15.2	27.5	10.016	6.677	16.1
	SL		28.0	0.833	13.1	26.4		8.346	12.4
C7-1	C	0.3894	1.6	0.556	1.1	1.6	10.0	5.560	1.1
	SL		3.9	0.778	2.0	3.9		7.780	2.0
C8-1	C	0.3894	6.9	0.556	4.8	6.9	9.992	5.552	4.8
	SL		12.2	0.778	6.1	12.2		7.772	6.1
C8-2	C	0.3889	5.0	0.5	3.9	5.0	9.985	4.992	3.9
	SL		7.4	0.75	3.8	7.4		7.489	3.8
C8-3	C	0.3902	12.3	0.667	7.2	12.8	10.0	6.667	7.5
	SL		14.4	0.833	6.7	13.9		8.334	6.5
C9-1	C	0.3894	5.9	0.556	4.1	6.1	10.0	5.556	4.3
	SL		10.0	0.778	5.0	9.7		7.778	4.9

Table 12

Moments and Thrusts

Load Level kips	Moment			Thrust		
	Hyperbolic ft-lb	Linear ft-lb	Percent Difference	Hyperbolic lb	Linear lb	Percent Difference
			Model C1-1, Crown			
10.1	1,211	1,172	3.2	8,308	7,013	15.6
19.5	2,580	2,497	3.2	17,351	14,615	15.8
27.8	4,019	3,830	4.7	26,515	21,950	17.2
30.1	4,407	4,382	0.6	28,789	25,411	11.7
			Model C1-1, Springing Line			
10.1	1,613	1,726	7.0	14,907	17,786	19.3
19.5	3,425	3,666	7.0	30,824	36,979	20.0
27.8	4,937	5,231	6.0	44,526	53,333	19.8
30.1	5,175	5,427	4.9	46,942	55,945	19.2
			Model C2-1, Crown			
9.4	254	270	6.3	246	270	9.8
20.1	675	702	4.0	705	691	2.0
29.4	1,504	1,649	9.6	2,274	2,561	12.6
33.7	2,125	2,175	2.4	2,704	2,627	2.8
36.7	2,445	2,473	1.1	4,621	4,346	6.0
			Model C2-1, Springing Line			
9.4	137	136	0.7	-321	-333	3.7
20.1	457	487	6.6	-267	-119	55.4
29.4	973	1,068	9.8	-77	411	633.8
33.7	1,954	1,749	10.5	3,686	2,719	26.2
36.7	2,630	2,524	4.0	5,140	4,900	4.7
			Model C2-2, Crown			
5.2	393	577	46.8	7,199	6,327	12.1
10.0	657	951	44.7	13,430	12,112	9.8
19.3	1,143	1,635	43.0	27,280	25,761	5.6
24.1	1,654	2,287	38.3	36,979	34,833	5.8
29.1	2,160	3,037	40.6	47,725	44,478	6.8
			Model C2-2, Springing Line			
5.2	770	894	16.1	7,316	8,338	14.0
10.0	1,493	1,733	16.1	14,191	16,111	13.5

(Continued)

Table 12 (Continued)

Load Level kips	Moment			Thrust		
	Hyperbolic ft-lb	Linear ft-lb	Percent Difference	Hyperbolic lb	Linear lb	Percent Difference
			Model C2-2, Springing Line (Continued)			
19.3	2,784	3,324	19.4	26,896	30,111	12.0
24.1	3,682	4,310	17.1	35,337	39,204	10.9
29.1	4,506	5,001	11.0	44,884	48,908	9.0
			Model C2-3, Crown			
5.0	525	537	2.2	6,255	5,523	11.7
10.0	1,008	1,055	4.7	12,531	11,166	10.9
19.4	2,114	2,288	8.2	24,396	21,393	12.3
24.3	3,013	3,260	8.2	32,879	28,579	13.1
28.8	4,064	4,453	9.6	42,404	36,446	14.1
			Model C2-3, Springing Line			
5.0	771	786	1.9	6,635	7,351	10.8
10.0	1,494	1,526	2.1	12,578	14,012	11.4
19.4	3,110	3,279	5.2	23,492	26,421	12.5
24.3	4,098	4,394	7.2	29,403	33,460	13.8
28.8	4,992	5,486	9.9	34,523	39,751	15.1
			Model C3-1, Crown			
10.2	770	902	17.1	12,481	10,841	13.1
19.7	1,472	1,666	13.1	25,489	22,944	10.0
29.3	2,353	2,717	15.5	43,233	39,011	9.8
38.4	2,967	3,640	22.7	64,135	57,730	10.0
			Model C3-1, Springing Line			
10.2	1,296	1,922	48.3	10,696	13,170	23.1
19.7	2,557	4,132	61.6	20,469	25,642	25.3
29.3	4,481	6,779	51.3	28,847	26,299	8.8
38.4	6,429	8,466	31.7	39,264	33,892	13.7
			Model C4-1, Crown			
5.4	599	598	0.2	7,723	6,874	11.0
10.3	1,431	1,393	2.7	15,231	13,507	11.3
15.3	2,481	2,385	3.9	20,666	18,193	12.0
19.4	3,451	3,272	5.2	27,106	23,378	13.8

(Continued)

Table 12 (Continued)

Load Level kips	Moment			Thrust		
	Hyperbolic ft-lb	Linear ft-lb	Percent Difference	Hyperbolic lb	Linear lb	Percent Difference
			Model C4-1, Springing Line			
5.4	608	656	7.9	6,815	7,790	14.3
10.3	1,322	1,499	13.4	13,143	15,724	19.6
15.3	2,602	3,009	15.6	23,689	29,844	26.0
19.4	4,027	4,224	4.9	41,094	49,322	20.0
			Model C4-2, Crown			
2.3	167	168	0.6	2,619	2,392	8.7
10.2	849	855	0.7	13,959	12,928	8.0
21.9	2,041	2,076	1.7	33,188	30,560	7.9
27.4	2,818	2,942	4.4	47,164	42,348	10.2
			Model C4-2, Springing Line			
2.3	180	197	9.4	2,672	2,949	10.4
10.2	958	1,092	14.0	12,019	13,999	16.5
21.9	2,616	2,770	5.9	32,089	36,488	13.7
27.4	3,200	3,265	2.0	40,695	45,334	11.4
			Model C5-1, Crown			
5.2	623	646	3.7	7,672	7,062	8.0
9.2	1,522	1,613	6.0	17,090	15,921	6.8
12.0	2,174	2,310	6.3	23,986	22,276	7.1
14.6	2,979	2,879	3.4	22,417	19,256	14.1
16.3	3,443	3,242	5.8	24,805	20,977	15.4
			Model C5-1, Springing Line			
5.2	770	877	13.9	7,547	8,871	17.5
9.2	1,546	1,764	14.1	13,136	15,788	20.2
12.0	2,254	2,489	10.4	19,758	23,189	17.4
14.6	3,004	3,284	9.3	24,837	29,109	17.2
16.3	3,340	3,625	8.5	26,093	30,509	16.9
			Model C5-2, Crown			
10.0	849	912	7.4	12,826	11,905	7.2
15.8	1,432	1,544	7.8	21,530	19,816	8.0
19.3	1,688	1,996	18.2	24,487	22,884	6.5
24.1	2,579	2,609	1.2	40,595	37,972	6.5

(Continued)

Table 12 (Continued)

Load Level kips	Moment			Thrust		
	Hyperbolic ft-lb	Linear ft-lb	Percent Difference	Hyperbolic lb	Linear lb	Percent Difference
			Model C5-2, Springing Line			
10.0	806	1,233	53.0	9,382	11,437	21.9
15.8	1,474	2,234	51.6	16,212	19,450	20.0
19.3	2,044	2,702	32.2	22,411	24,855	10.9
24.1	2,737	3,025	10.5	30,269	30,164	0.3
			Model C5-4, Crown			
2.2	145	152	4.8	1,879	1,634	13.0
5.0	642	633	1.4	5,615	4,886	13.0
9.0	1,239	1,207	2.7	7,335	6,243	14.9
12.8	1,966	1,908	3.0	8,939	7,430	17.0
			Model C5-4, Springing Line			
2.2	158	208	31.6	1,879	2,331	24.1
5.0	661	863	30.6	6,551	8,554	30.6
9.0	1,950	2,122	8.8	19,882	24,001	20.7
12.8	2,858	2,925	2.3	27,670	32,080	15.9
			Model C6-1, Crown			
2.7	205	213	3.9	2,942	2,701	8.2
5.3	703	716	1.8	7,141	6,485	9.2
10.1	1,445	1,507	4.3	13,344	12,153	8.9
13.6	1,936	2,012	3.9	16,968	15,911	6.2
			Model C6-1, Springing Line			
2.7	206	240	16.5	2,332	2,638	13.1
5.3	608	795	30.8	4,882	6,162	26.2
10.1	1,546	1,852	19.8	12,560	14,787	17.7
10.8	1,990	2,356	18.4	16,537	18,447	11.5
			Model C6-2, Crown			
2.4	223	224	0.4	3,217	2,986	7.2
5.4	518	518	0.0	7,275	6,704	7.8
10.2	1,136	1,130	0.5	14,059	12,742	9.4
14.9	1,844	1,839	0.3	20,774	18,495	11.0
19.3	2,339	2,381	1.8	22,757	19,577	14.0

(Continued)

Table 12 (Continued)

Load Level kips	Moment			Thrust		
	Hyperbolic ft-lb	Linear ft-lb	Percent Difference	Hyperbolic lb	Linear lb	Percent Difference
			Model C6-2, Springing Line			
2.4	244	280	14.8	3,155	3,426	8.6
5.4	558	647	15.9	7,254	7,837	8.0
10.2	1,208	1,334	10.4	15,006	16,283	8.5
14.9	2,004	2,083	3.9	24,605	25,724	4.5
			Model C7-1, Crown			
0.3	181	223	23.2	3,314	3,604	8.8
1.4	294	362	23.1	4,159	4,946	18.9
2.2	719	769	7.0	13,609	13,210	2.9
2.7	794	825	3.9	15,079	14,260	5.4
3.4	823	840	2.1	15,403	14,542	5.6
			Model C7-1, Springing Line			
0.3	161	182	13.0	2,059	2,473	20.1
1.4	252	305	21.0	3,009	3,975	32.1
2.2	442	557	26.0	4,853	6,856	41.3
2.4	368	755	105.2	3,629	10,217	181.5
			Model C8-1, Crown			
2.2	443	465	5.0	2,035	2,178	7.0
3.4	468	507	8.3	2,624	2,936	11.9
4.5	841	849	1.0	5,259	5,116	2.7
5.4	990	977	1.3	6,588	6,361	3.4
			Model C8-1, Springing Line			
2.2	424	649	53.1	6,182	2,732	55.8
3.4	533	813	52.5	8,676	3,368	61.2
4.5	938	1,119	19.3	13,904	7,790	44.0
5.4	1,198	1,257	4.9	24,809	10,520	57.6
			Model C8-2, Crown			
2.4	500	556	11.2	6,464	6,987	8.1
3.5	728	775	6.5	7,748	8,143	5.1
4.4	872	959	10.0	5,858	7,328	25.1
4.4	952	1,157	21.5	7,071	12,076	70.8

(Continued)

Table 12 (Concluded)

Load Level kips	Moment			Thrust		
	Hyperbolic ft-lb	Linear ft-lb	Percent Difference	Hyperbolic lb	Linear lb	Percent Difference
			Model C8-2, Springing Line			
2.4	461	480	4.1	6,106	6,620	8.4
3.5	684	720	5.3	8,708	9,534	9.5
4.4	946	1,002	5.9	10,432	11,665	11.8
4.4	1,011	1,074	6.2	8,713	10,217	17.3
			Model C8-3, Crown			
2.8	168	187	11.3	3,399	3,498	2.9
5.7	562	641	14.1	9,152	9,820	7.3
7.8	835	939	12.5	13,796	14,406	4.4
8.6	929	1,005	8.2	15,861	15,846	0.1
			Model C8-3, Springing Line			
2.8	197	209	6.1	3,982	4,264	7.1
5.7	526	571	8.6	7,916	8,747	10.5
7.8	794	866	9.1	10,601	11,699	10.4
8.6	911	973	6.8	12,769	13,817	8.2
			Model C9-1, Crown			
1.9	537	536	0.2	5,798	5,569	3.9
2.7	583	595	2.1	7,944	7,696	3.1
3.4	776	779	0.4	9,724	9,299	4.4
3.7	852	855	0.4	10,270	9,776	4.8
			Model C9-1, Springing Line			
1.9	779	820	5.3	8,470	9,267	9.4
2.7	847	891	5.2	10,096	10,979	8.7
3.4	982	1,026	4.5	11,477	12,431	8.3
3.7	1,040	1,096	5.4	10,293	11,266	9.5

APPENDIX A

PHOTOGRAPHS OF TESTED MODEL FAILURES

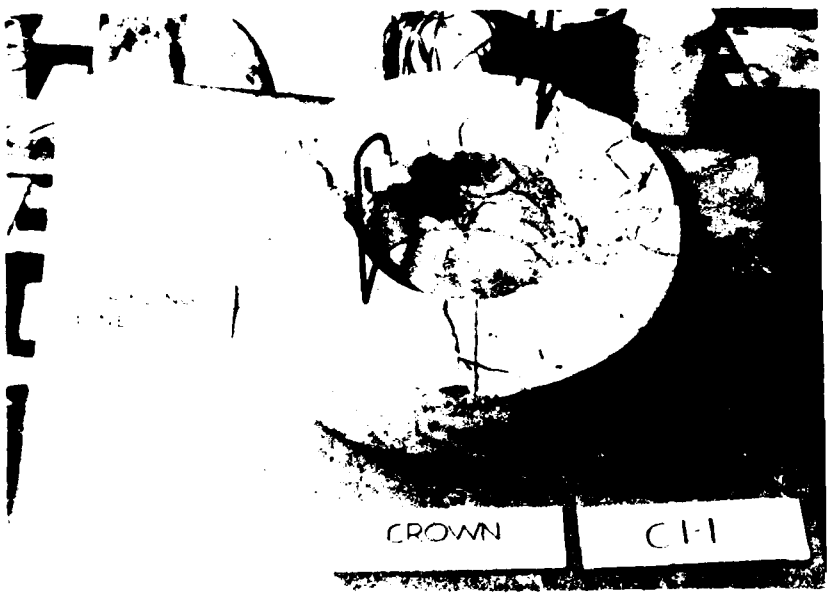

Views of test specimen: C1-1

Date tested: 26 Aug 83

R/h: 1.5

ρg: 0.408%

Loading: 3:1

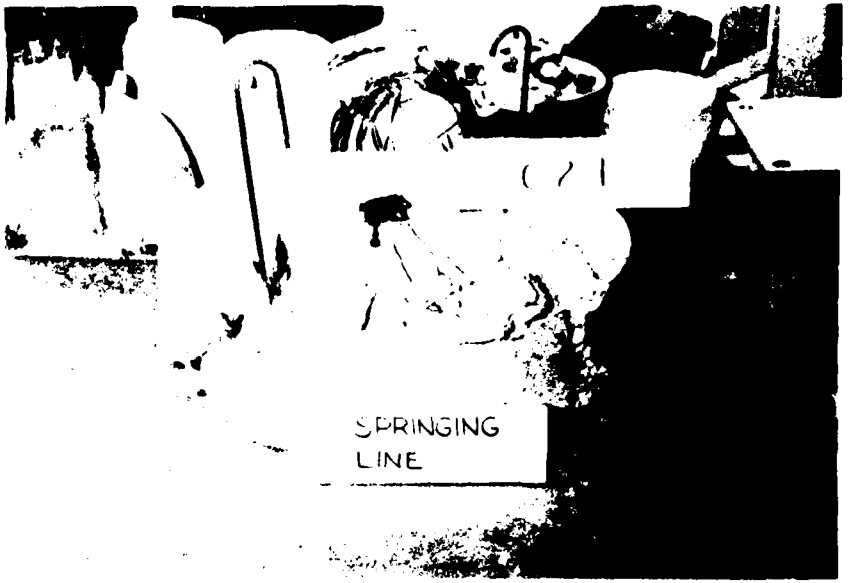

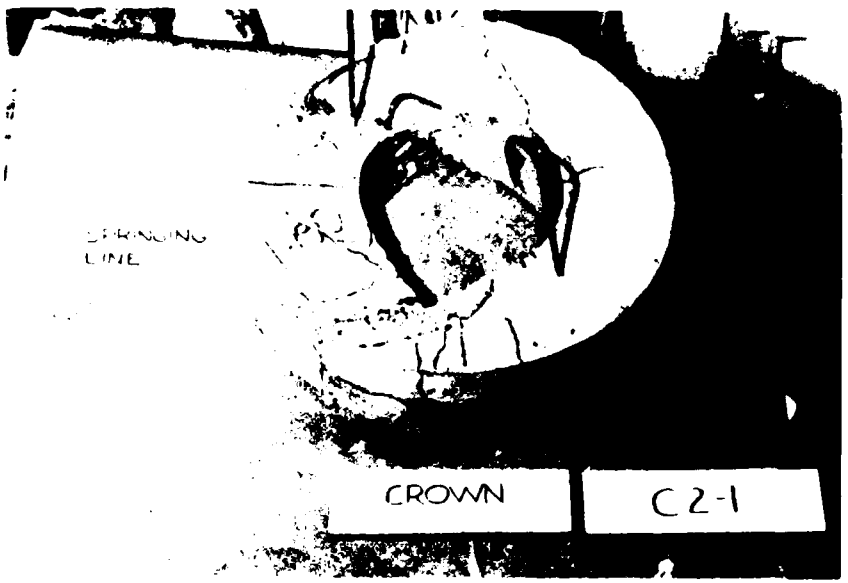

A3

Views of test specimen: C2-1

Date tested: 25 Aug 83

R/h: 1.5

ρg: 0.760%

Loading: 3:1

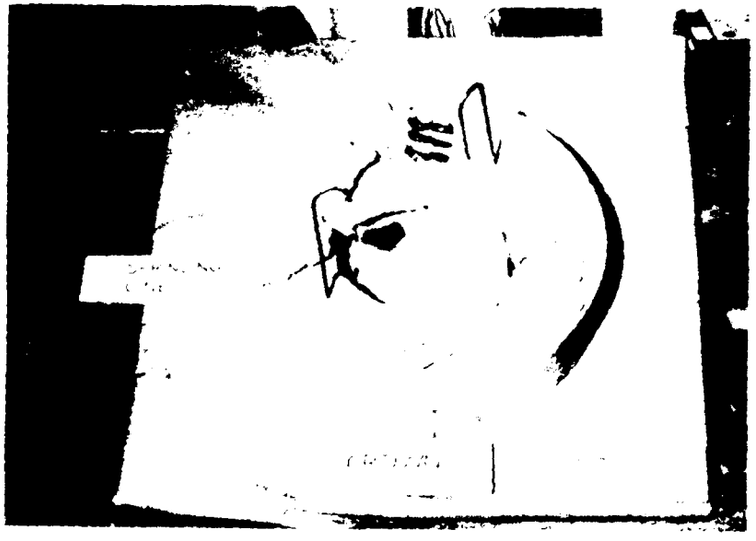

Views of test specimen: C2-2

Date tested: 7 Sep 83

R/h: 1.5

ρg: 0.758%

Loading: 2:1

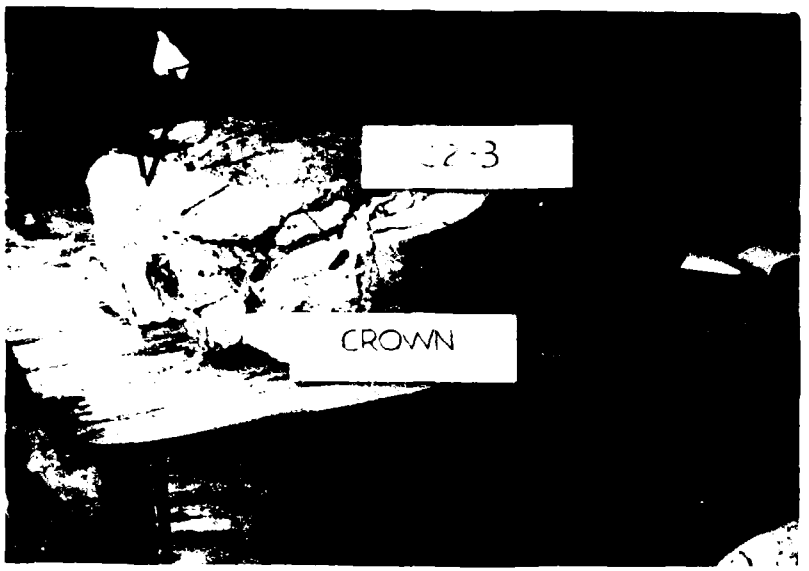

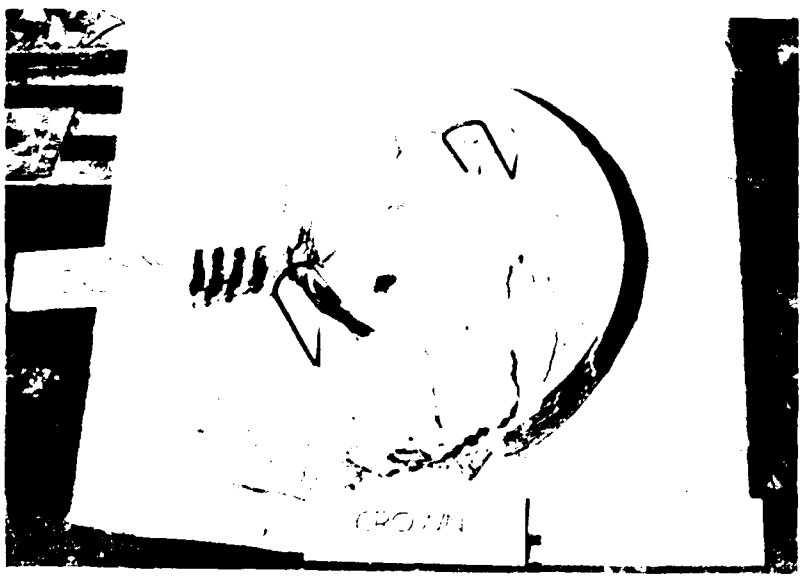

Views of test specimen: C2-3

Date tested: 1 Sep 83

R/h: 1.5

ρg: 0.712%

Loading: 4:1

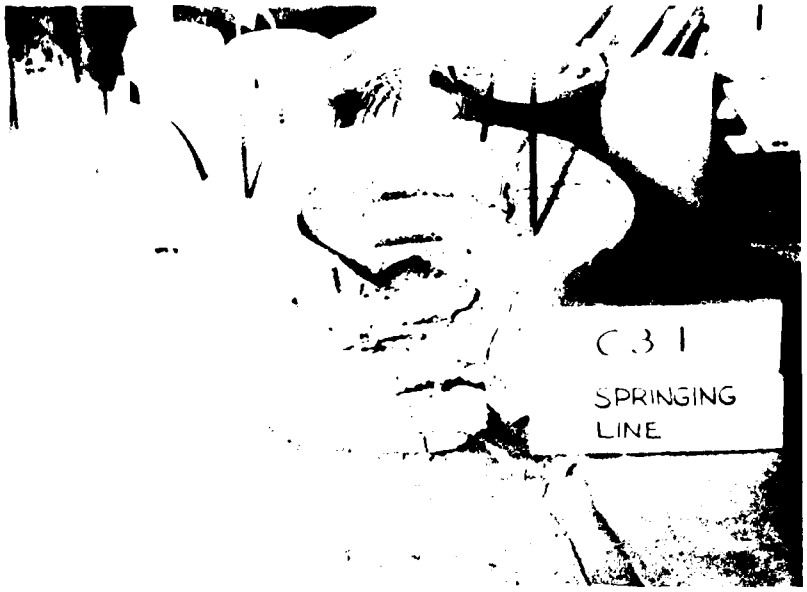

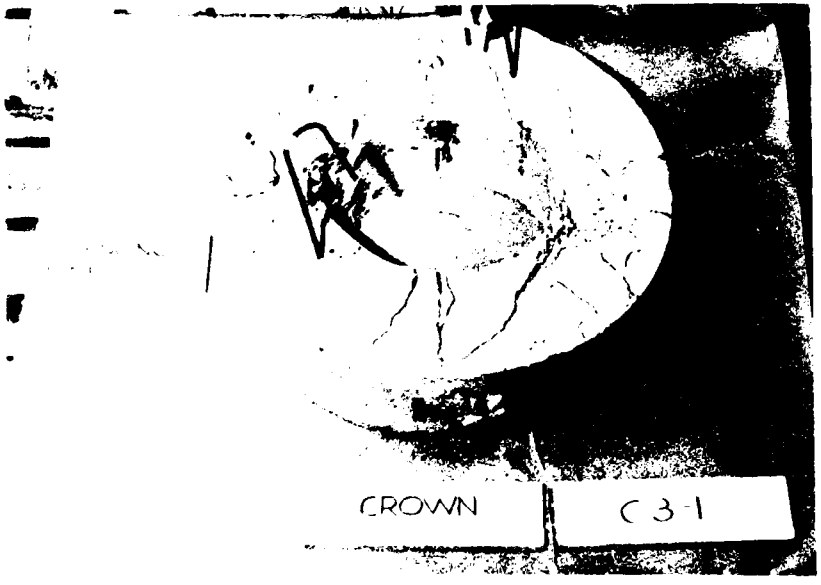

Views of test specimen: C3-1

Date tested: 26 Aug 83

R/h: 1.5

ρg: 1.471%

Loading: 3:1

AE

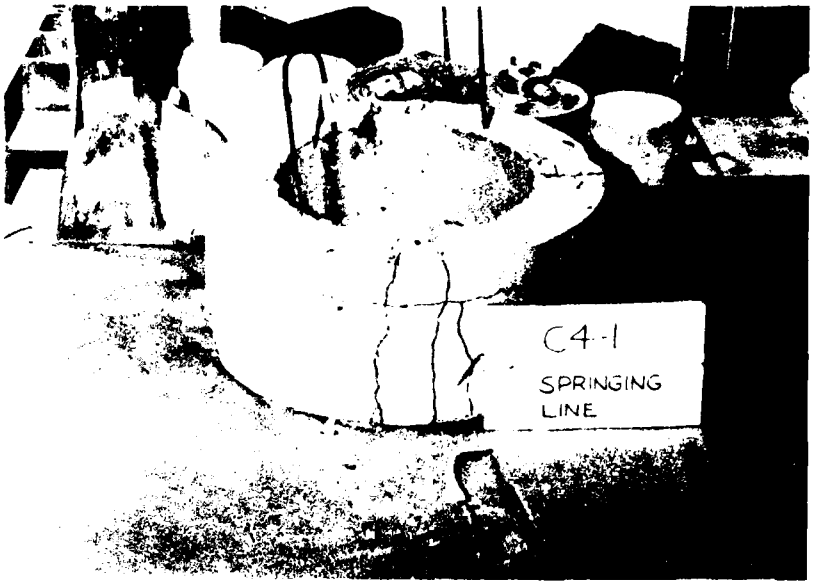

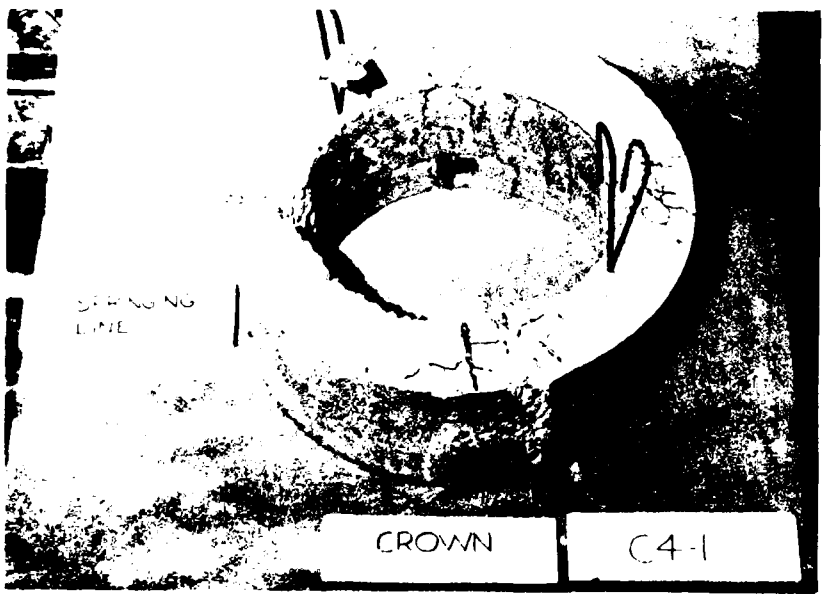

Views of test specimen: C4-1

Date tested: 29 Aug 83

R/h: 2.4

ρg: 0.432%

Loading: 3:1

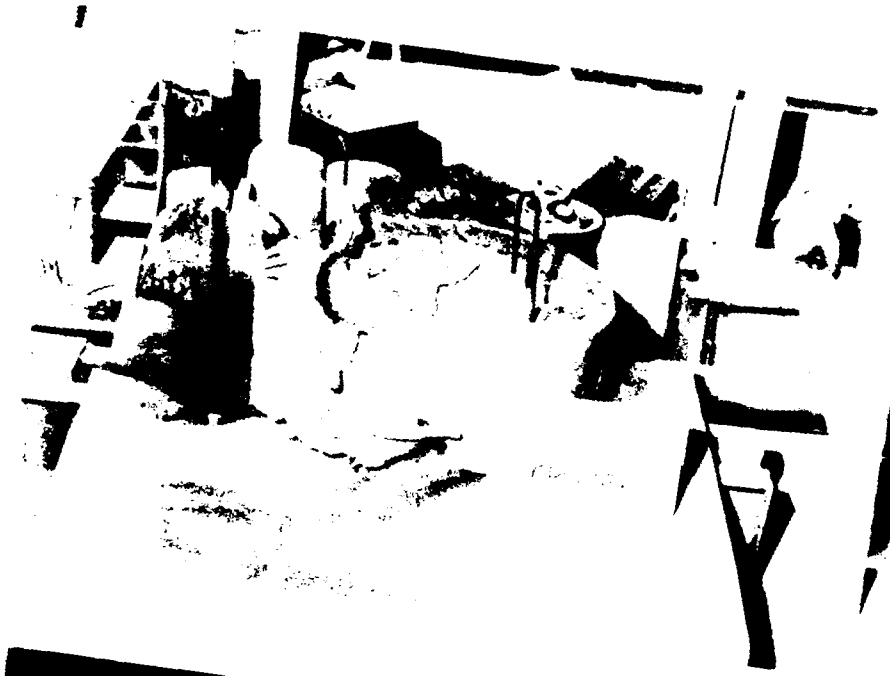

Views of test specimen: C4-2
Date tested: 7 Sep 83
R/h: 2.4
ρg: 0.446%
Loading: 2:1

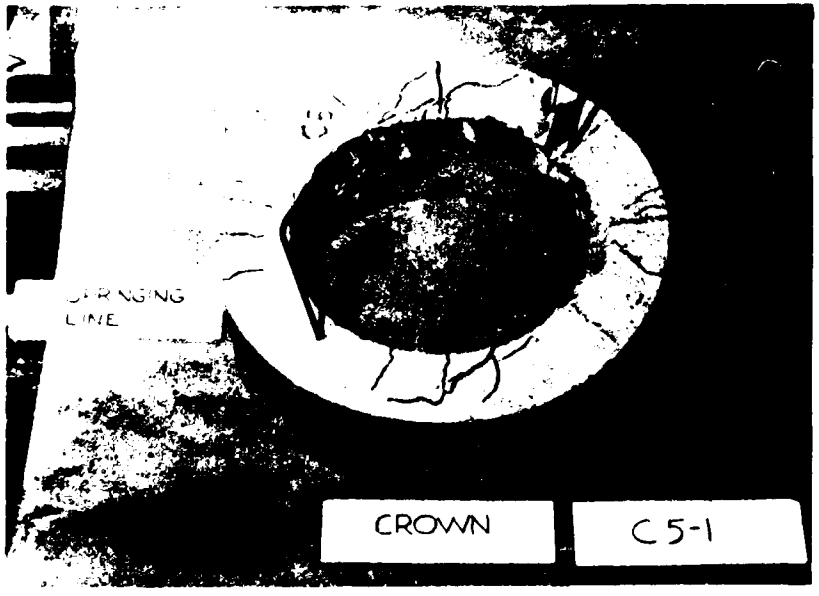

Views of test specimen: C5-1

Date tested: 30 Aug 83

R/h: 2.4

ρg: 0.919%

Loading: 3:1

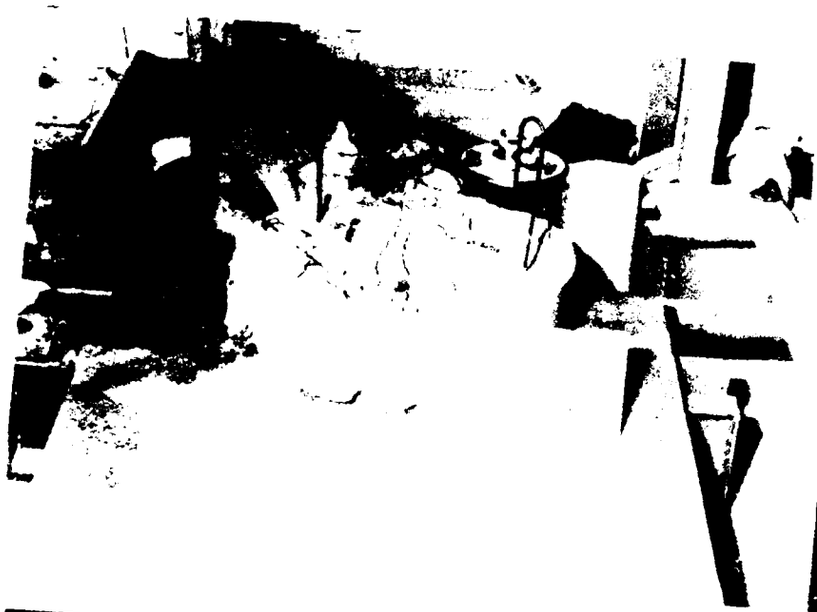

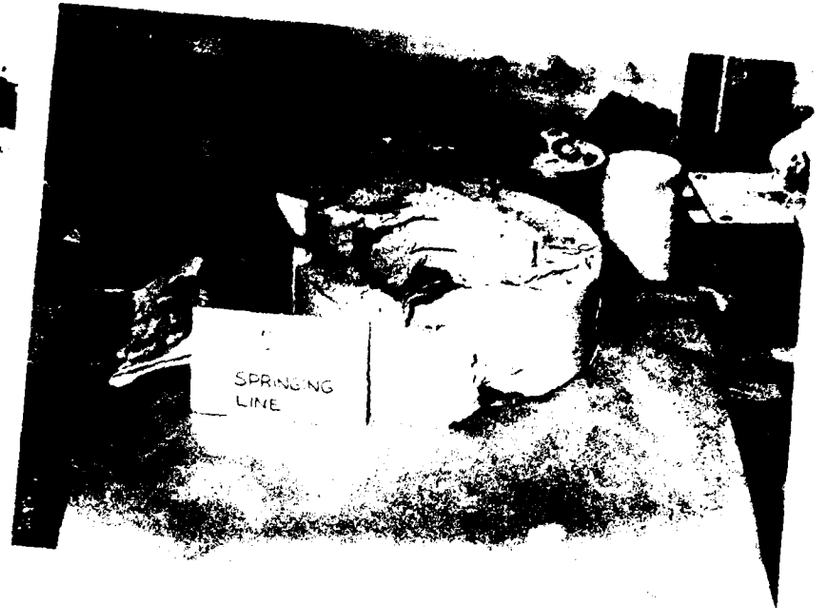

Views of test specimen: C5-2
Date tested: 8 Sep 83
R/h: 2.4
ρg: 0.957%
Loading: 2:1

Views of test specimen: C5-3
Date tested: 9 Sep 83
R/h: 2.4
ρg: 0.951%
Loading: 1:1

Views of test specimen: C5-4
Date tested: 6 Sep 83
R/h: 2.4
ρg: 0.961%
Loading: 4:1

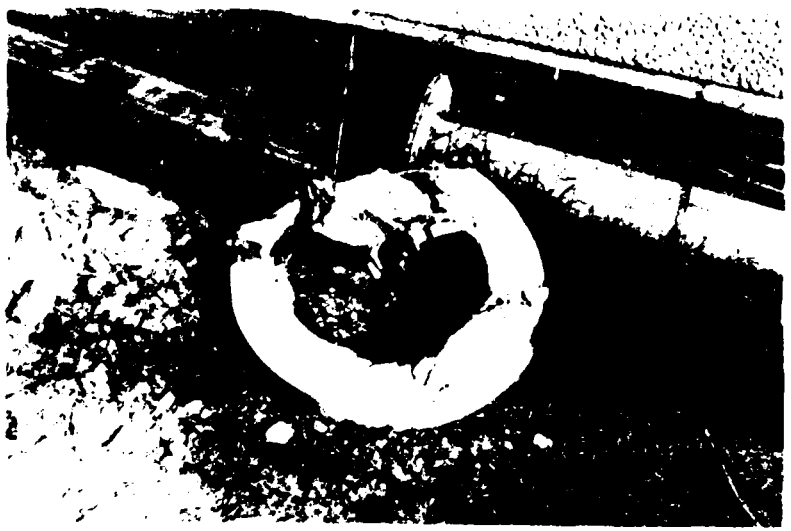

Views of test specimen: C6-1

Date tested: 26 Aug 83

R/h: 2.4

ρg: 1.433%

Loading: 3:1

Views of test specimen: C6-2
Date tested: 8 Sep 83
R/h: 2.4
ρg: 1.418%
Loading: 2:1

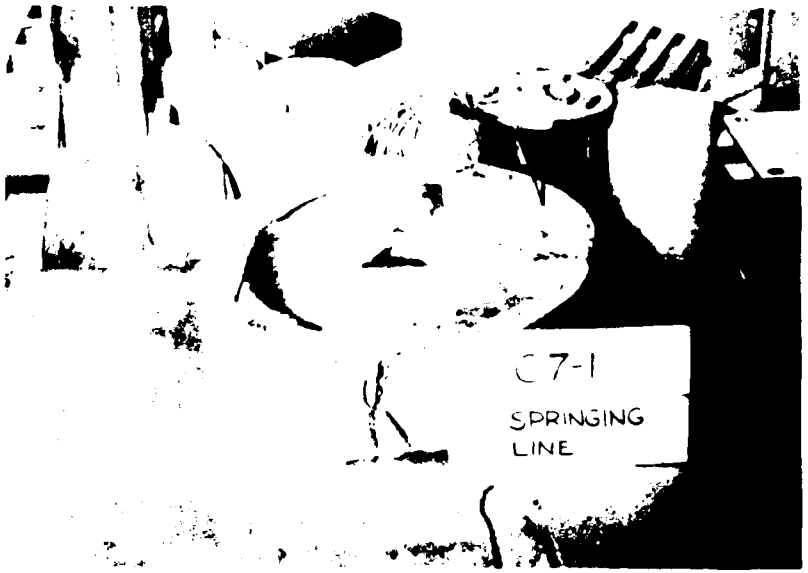

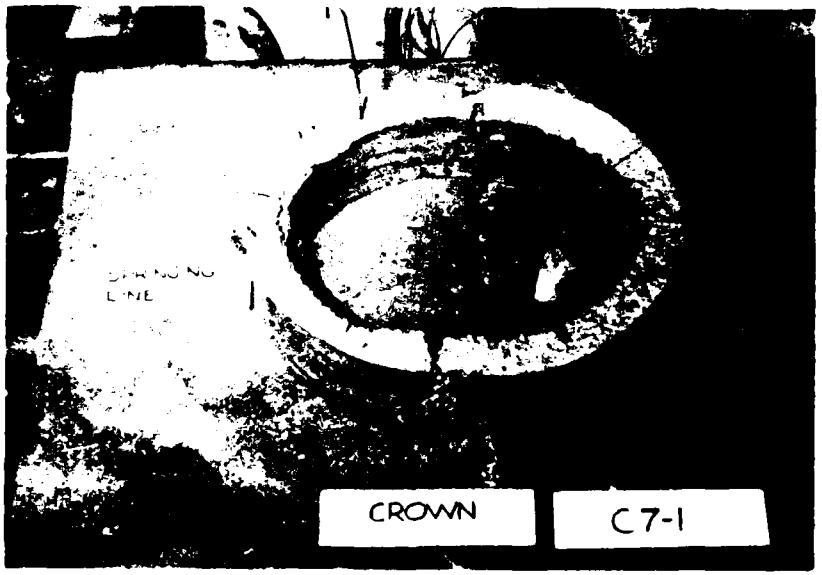

Views of test specimen: C7-1

Date tested: 30 Aug 83

R/h: 4.1

ρg: 0.371%

Loading: 3:1

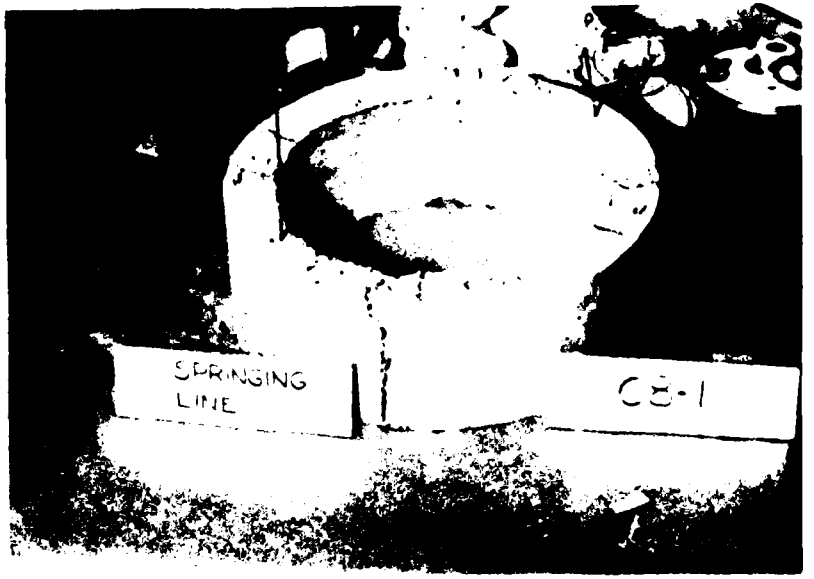

Views of test specimen: C8-1

Date tested: 31 Aug 83

R/h: 4.0

ρg: 0.877%

Loading: 3:1

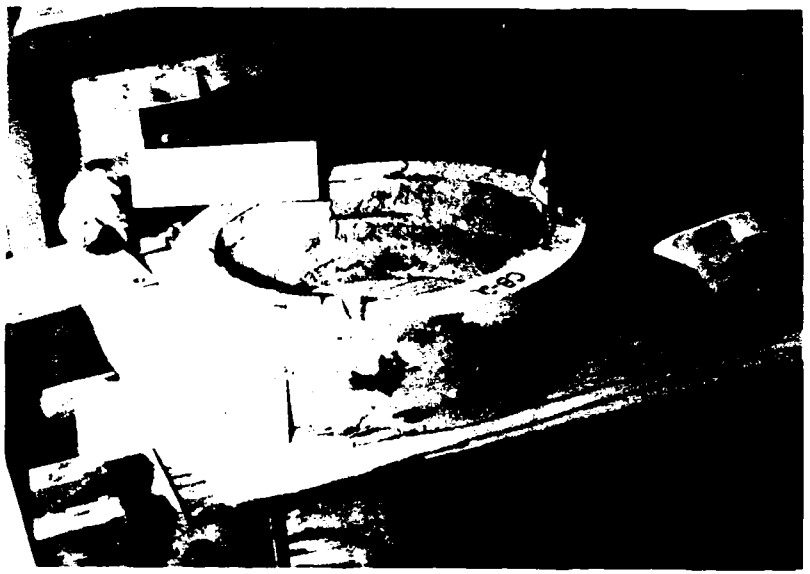

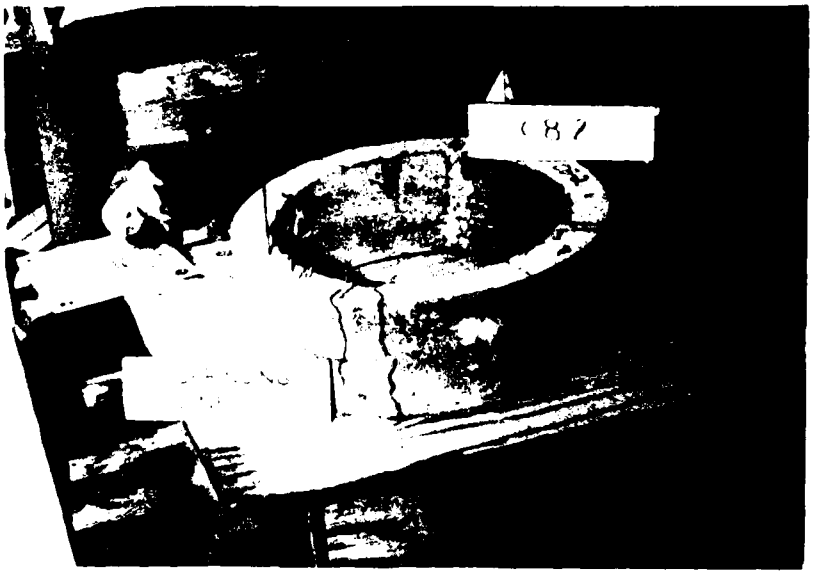

Views of test specimen: C8-2

Date tested: 6 Sep 83

R/h: 4.2

ρg: 0.943%

Loading: 4:1

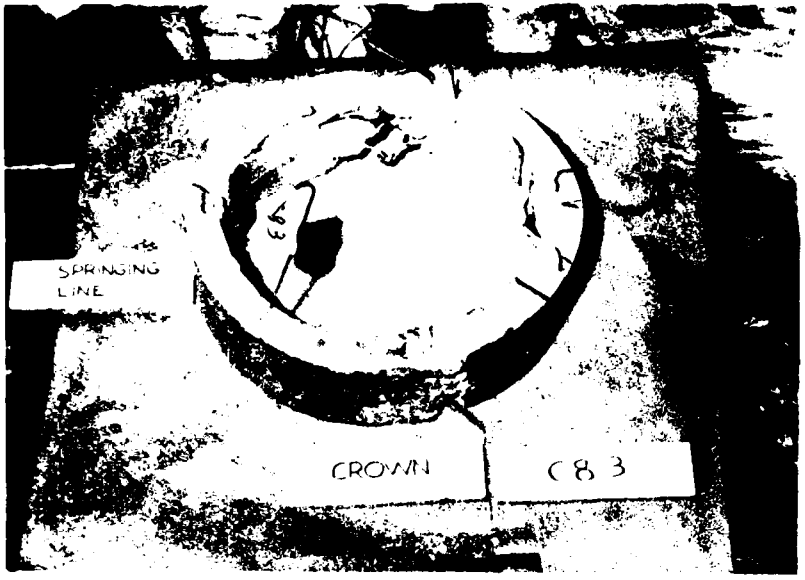

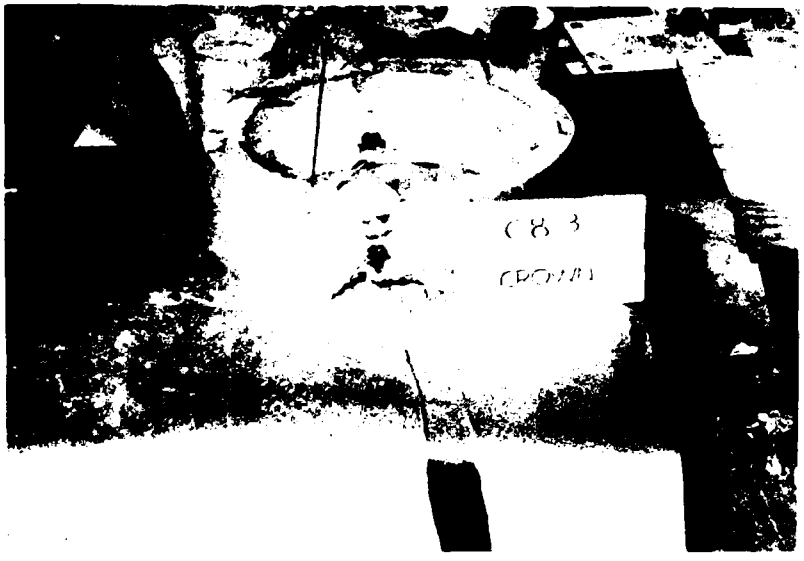

Views of test specimen: C8-3

Date tested: 9 Sep 83

R/h: 4.5

ρg: 1.017%

Loading: 2:1

Views of test specimen: C9-1

Date tested: 31 Aug 83

R/h: 3.9

ρg: 1.225%

Loading: 3:1

APPENDIX B

THE EFFECT OF CONFINING PRESSURES ON THE BEHAVIOR OF REINFORCED CONCRETE CIRCULAR CONDUITS

1. The objective of this work was to observe the convergent effect of confining pressures on the behavior of reinforced concrete (R/C) circular conduits. The only variable was the loading conditions: Radial 2-, 4-, 8-, and 16-point loadings, and a Three-Edge-Bearing Test (American Society for Testing and Materials 1983).* Seven geometrically identical, circular conduits were fabricated, five being reinforced and two unreinforced. The two unreinforced models served as rehearsal test specimens for the 2-point loading and Three-Edge-Bearing Test. Also, a calibration steel specimen was loaded under the radial 2- to 16-point loading as a check on reliability of results.

2. Figure B1 shows a typical test section and Table B1 summarizes the

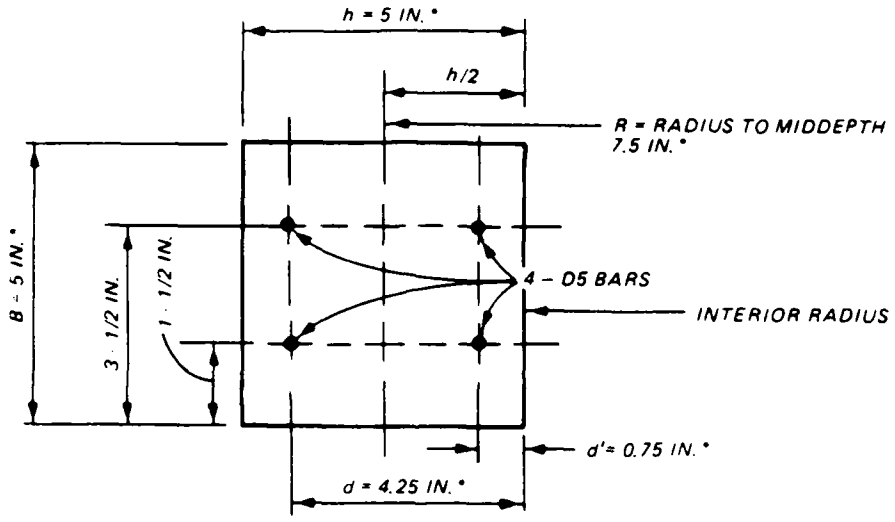

* APPROXIMATE. SEE TABLE B1 FOR MEASURED VALUES

Figure B1. Typical test section

models. Only the models under 2-point, 4-point, and three-edge-bearing loads failed because the concrete developed a compressive strength of 6,678 psi, although 4,000-psi concrete was ordered. These specimen failures were recorded on video cassette.

Test Plan

3. The test plan involved five different loading conditions: radial 2-, 4-, 8-, and 16-point loads (Figure B2), and the Three-Edge-Bearing

* References cited in this appendix are included in the References at the end of the main text.

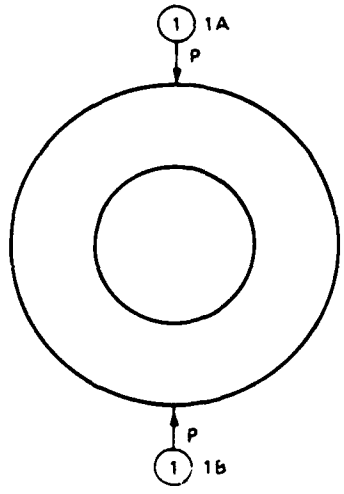

MODEL = 1, 2 PT. LOADING

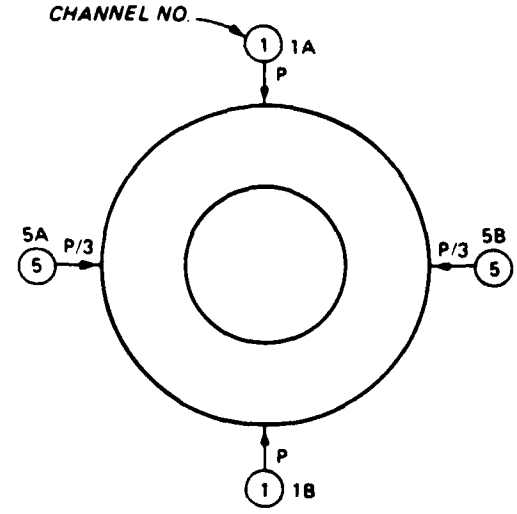

MODEL = 2, 4 PT. LOADING

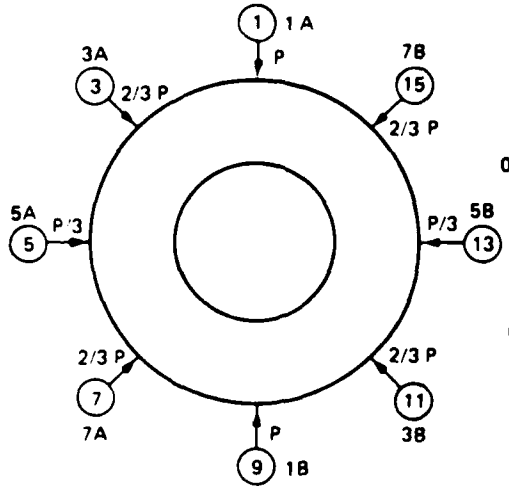

MODEL = 3, 8 PT. LOADING

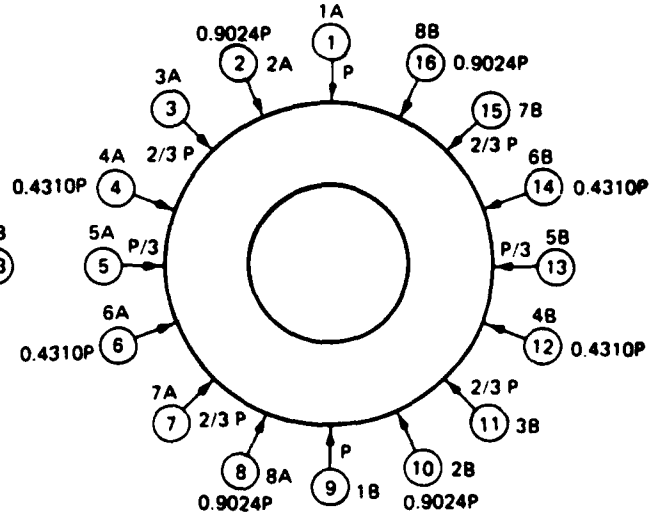

MODEL = 4, 16 PT. LOADING

Figure B2. Load distribution, Models 1, 2, 3, and 4

Test (Figure B3). The 3:1 loading (ratio of load at crown to load at springing line) was used for the 4-, 8-, and 16-point loadings. All models had very similar material and geometric properties and are summarized in Table B1: curvature R/h = 1.5, total steel ratio = 0.8 percent, and outside diameter = 20 in.

4. Before the concrete models were tested, the calibration specimen was loaded under 2-, 4-, 8-, and 16-point radial loads for a comparison to the results of the concrete model tests. Figure B4 shows the dimensions and gage layout of the calibration specimen.

5. Next, one plain concrete model was tested under 2-point loading, followed by tests of the reinforced models under 2- to 16-point radial loads. The locations of the gages are shown in Figure B5. The loading apparatus and data acquisition system used were the same as those for the previous series of tests on concrete conduits.

6. Finally, another plain concrete model and a reinforced model were tested by the three-edge-bearing method, according to ASTM C497-83 (American Society for Testing and Materials 1983). These models were loaded in a hydraulic compression testing machine. The data acquisition system was the same as that used for the other models. The location of the gages is shown in Figure B6.

Test Procedure

7. For the 2-, 4-, 8-, and 16-point loadings, the same test procedure was used as was used for the previously reported second series of tests.

8. For the Three-Edge-Bearing Test, the model was placed on two bottom bearing strips, as shown in Figure B3. A point was marked on top diametrically opposite the point midway between the bearing strips. The top bearing wood block and steel beam, shown in Figure B3, was centered over this top mark and the movable head of the compression machine was lowered to touch the steel beam. The load was then applied at a rate of 1,000 lb/min up to a load of 18,500 lb. At the 18,500-lb point, the top bearing and steel beam became unstable and the loading was restarted with the movable head of the test machine bearing directly on the model. The loading rate was increased to a constant rate of 2,500 lb/min.

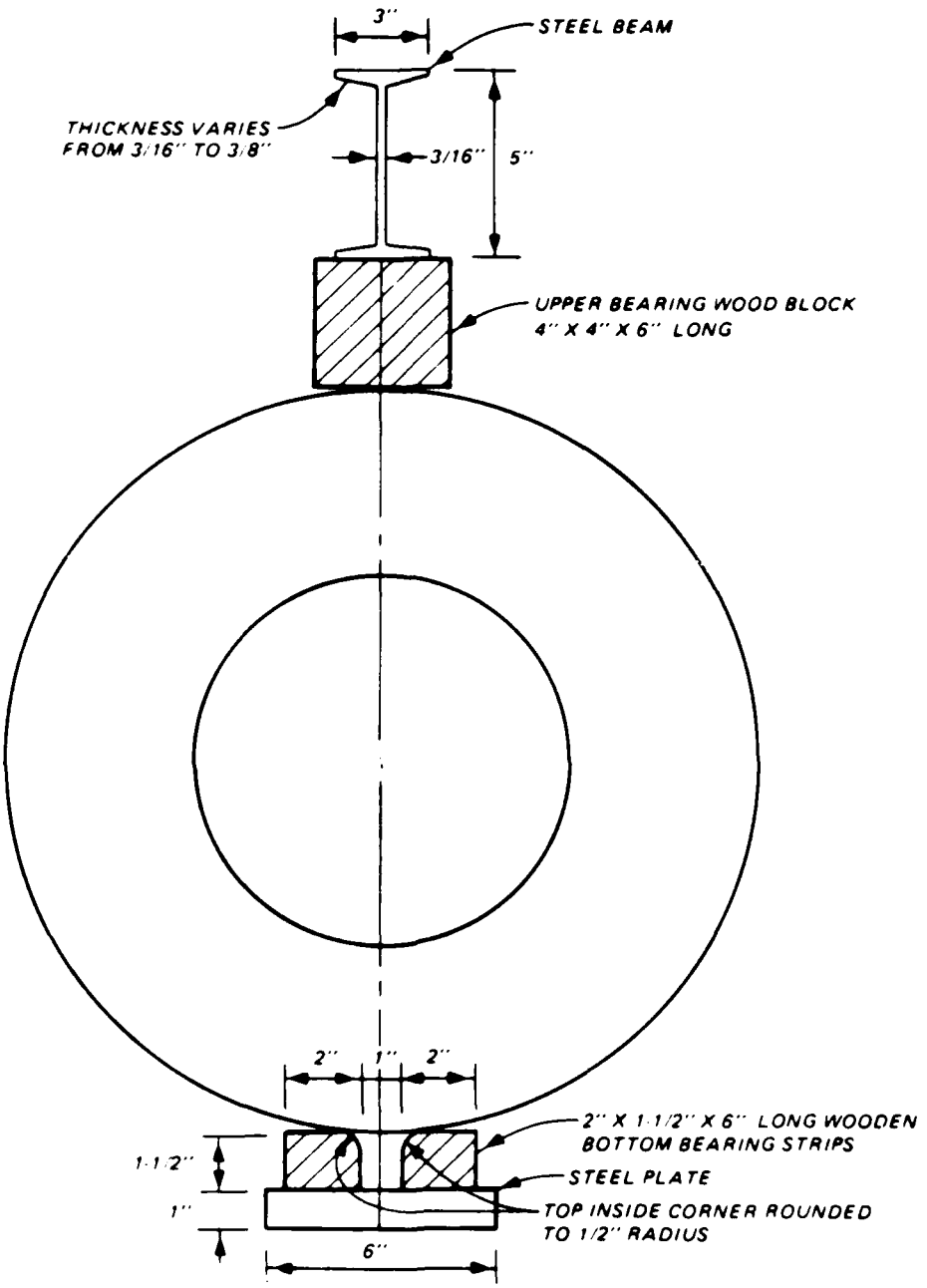

Figure B3. Three-Edge-Bearing Test, Model 5

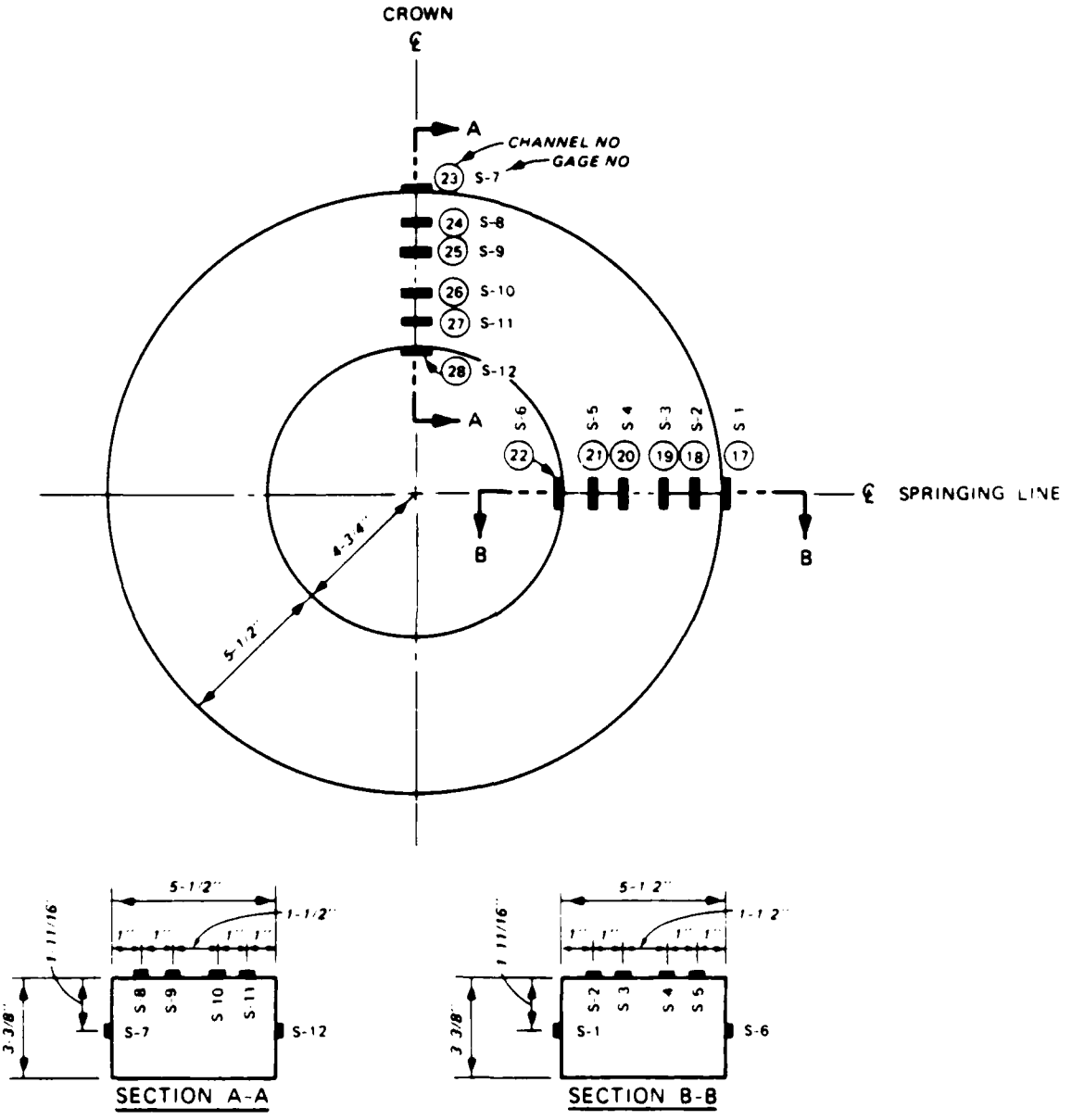

Figure B4. Steel calibration specimen

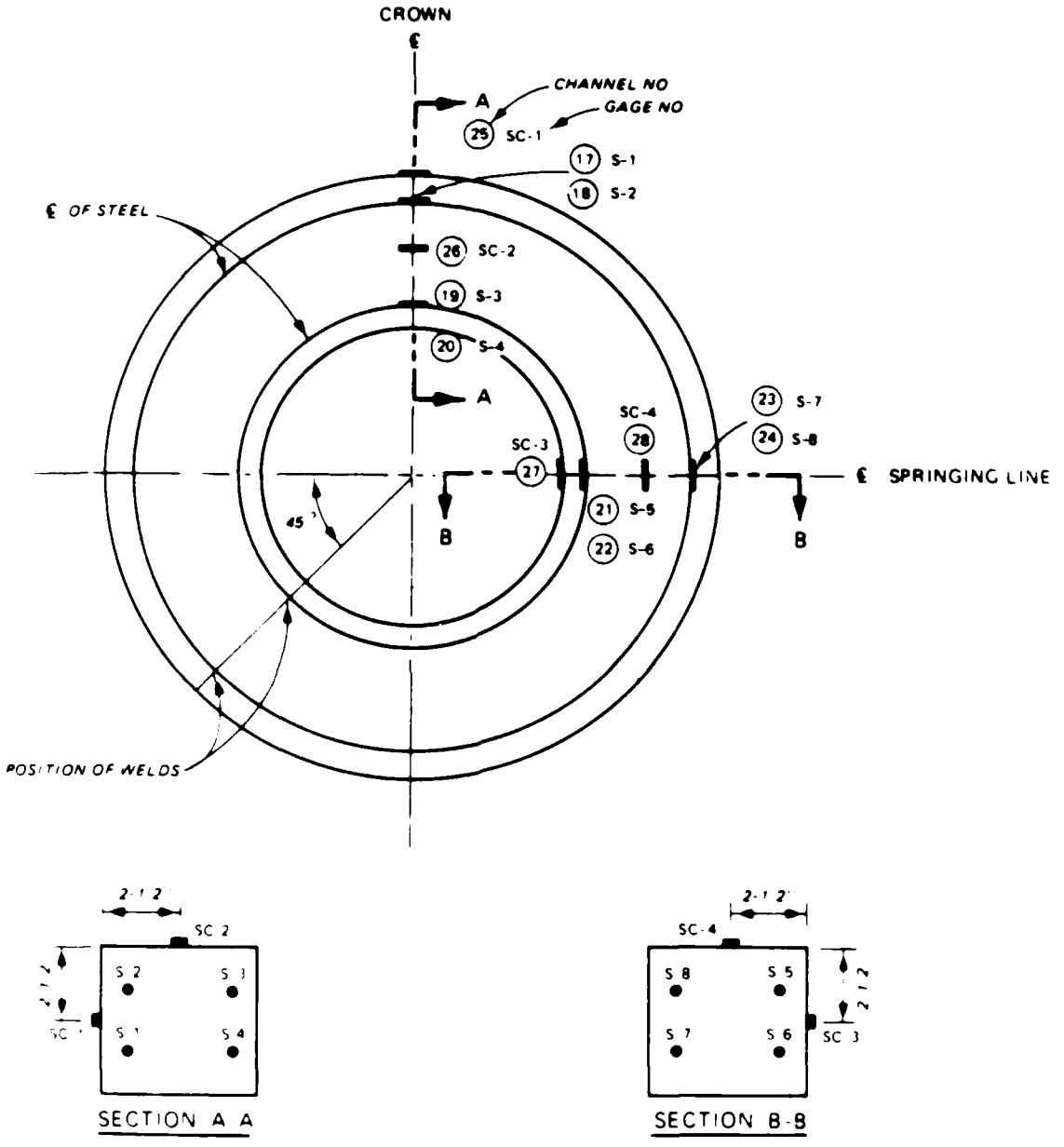

Figure B5. Gage locations for Models 1, 2, 3, and 4

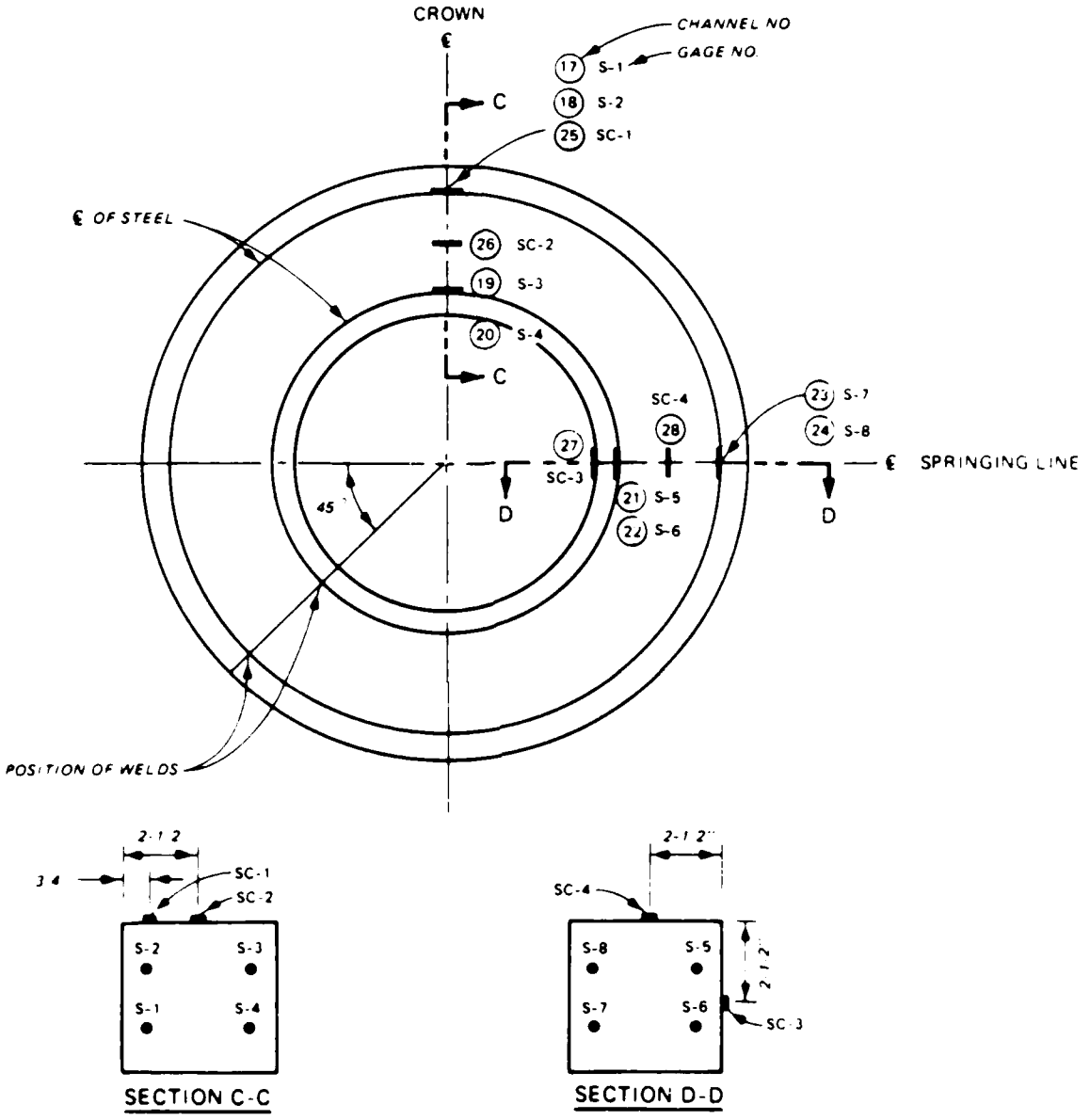

Figure B6. Gage locations for Model 5

Material Properties

9. Tables B2 and B3, respectively, list the results from the tensile tests of the steel reinforcement and the uniaxial compressive concrete tests. These tables list the required material properties for analysis: yield strength and modulus of elasticity of the steel reinforcement, 28-day and day-of-test uniaxial compressive concrete strengths, tensile strength, initial elastic concrete modulus, and Poisson's ratio.

Observations

10. Model 1 was loaded to ultimate failure under a 2-point load. The crack patterns are shown in Figure B7. Tensile cracks occurred first at the crown intrados at an applied load of 11,000 lb, then at the springing line extrados. Radial tension cracks formed at the crown intrados, and the model failed by radial tension at an applied load of 22,150 lb. At failure, the concrete cover spalled off the inner reinforcement, and the reinforcement straightened at the crown.

11. Model 2, under a 4-point load, cracked first at the crown intrados (P = 23,000 lb), then at the springing line extrados (P = 42,000 lb). Next, radial tensions cracks began forming at the crown intrados (P = 47,000 lb). This model failed at P = 56,000 lb , as a diagonal tension crack formed at the crown section. The crack patterns are shown in Figure B8.

12. In the Three-Edge-Bearing Test, Model 5 cracked first at the crown intrados at an applied load of 12,800 lb. Cracks formed at the springing line extrados at an applied load of 13,000 lb. In the same manner as the 2-point load test, the model failed in radial tension at an applied load of 21,300 lb. The crack patterns are shown in Figure B9.

13. Models 3 and 4 under 8-point and 16-point loadings, respectively, were subjected to the maximum possible pressure (P = 57,000 lb) that the hydraulic jacks could produce. No cracking or signs of failure were observed.

14. The two unreinforced models, loaded by 2-point loads and the three-edge-bearing method, each failed by a sudden brittle-type failure. They broke into four approximately equal sections along planes through the crown and springing line sections. The crack patterns are shown in Figure B10. The observed failure load was 10,160 lb for the unreinforced model loaded by the

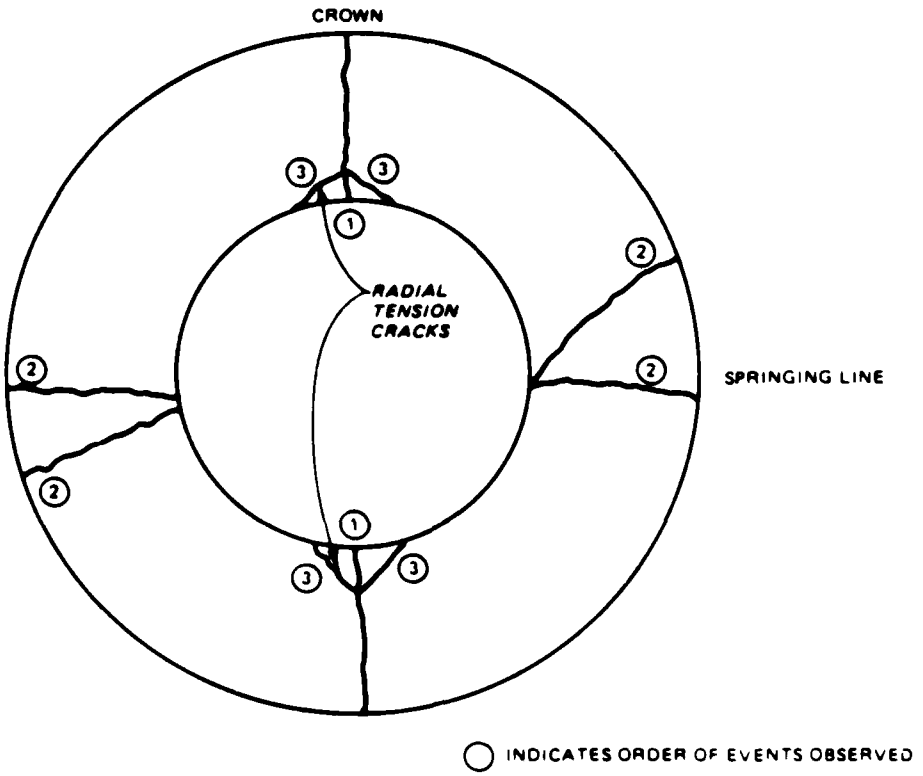

Figure B7. Crack patterns of 2-point loading test

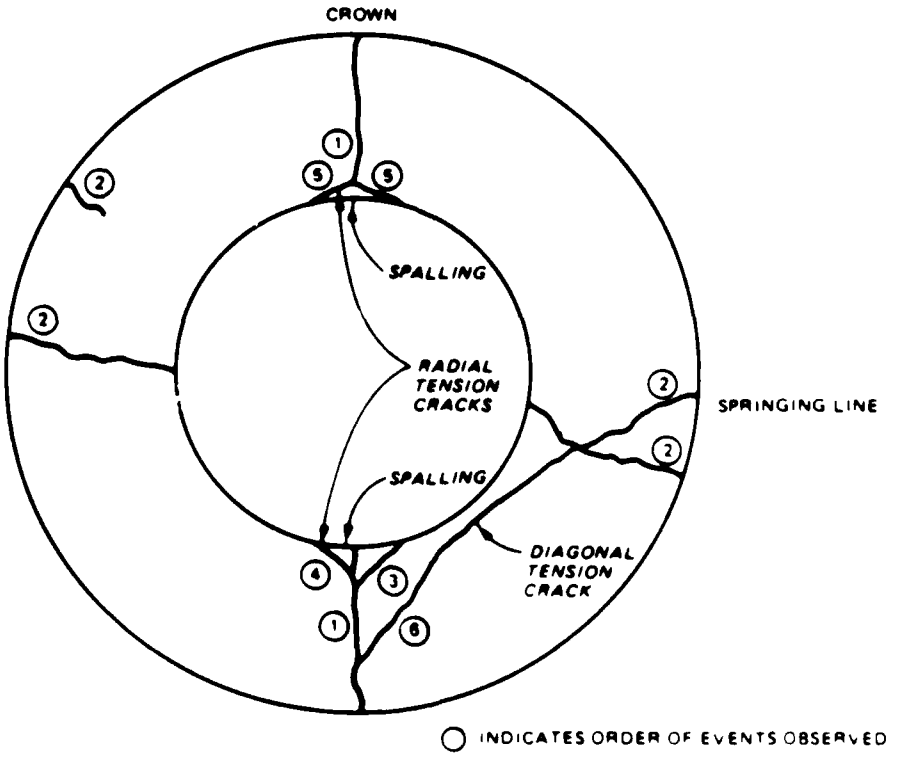

Figure B8. Crack patterns of 4-point loading test

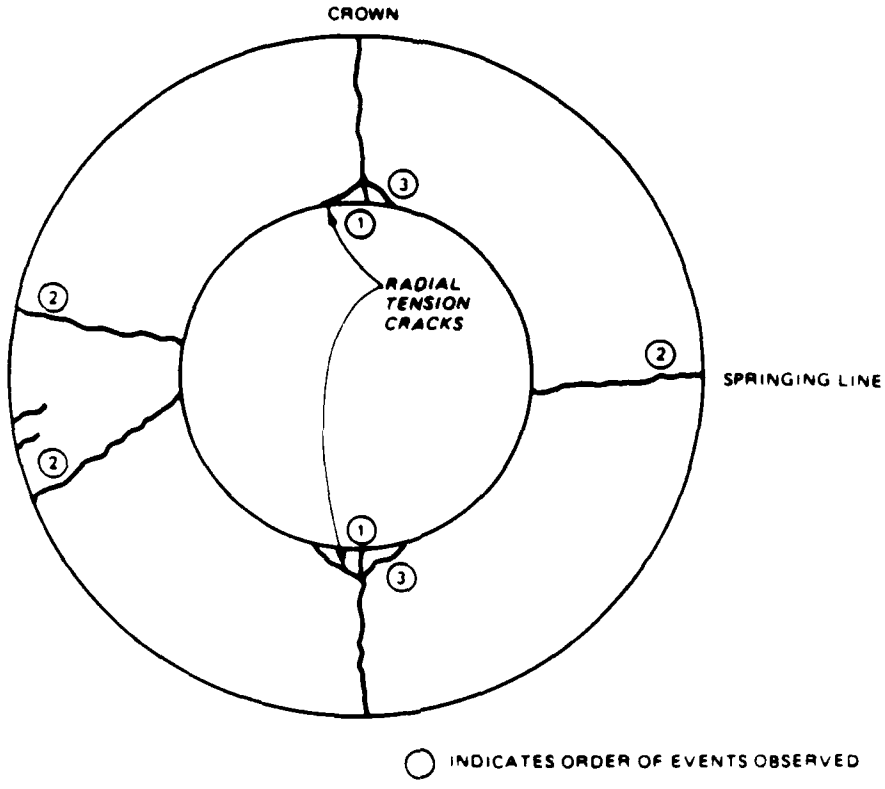

Figure B9. Crack patterns of Three-Edge-Bearing Test

three-edge-bearing method. The failure load for the unreinforced model under the 2-point load was not recorded. Photographs of the failed specimens are shown in Figures B11 to B15.

Conclusions

15. The observed model conduit failures are summarized as follows:

Test	Failure Load, lb	Type of Failure
2-point load	22,150	Radial tension
Three-edge-bearing load	21,300	Radial tension
4-point load	56,000	Radial tension and diagonal tension
Unreinforced, 2-point load	--	Brittle
Unreinforced, three-edge-bearing load	10,160	Brittle

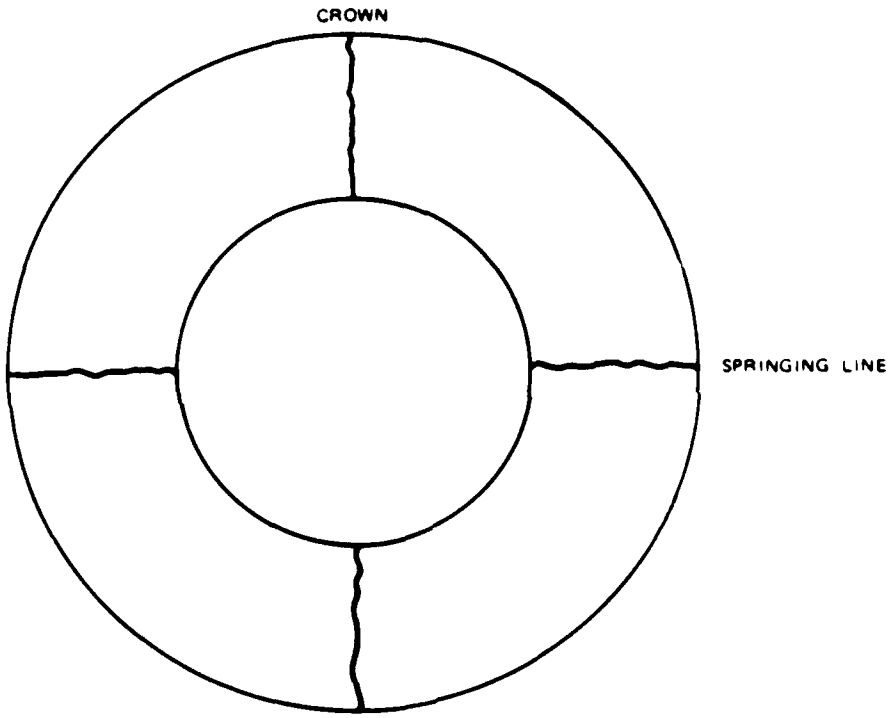

Figure B10. Crack patterns of both unreinforced models

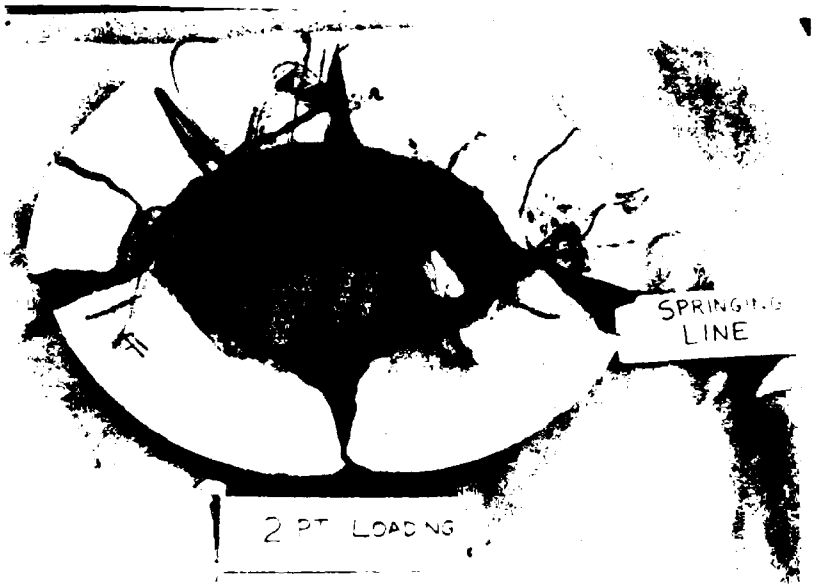

2-point loading
Date tested: 9/17/84
R/h: 1.5
ρ_g: 0.8%

Figure B11. Model 1

4-point loading
Date tested: 9/18/84
R/h: 1.5
ρ_g: 0.8%

Figure B12. Model 2

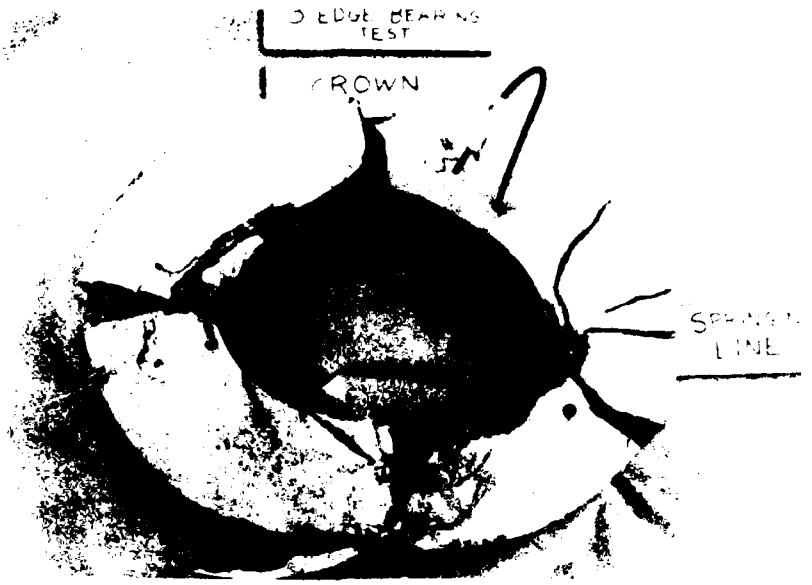

Three-Edge-Bearing Test
Date tested: 9/20/84
R/h: 1.5
ρg: 0.8%

Figure B13. Model 5

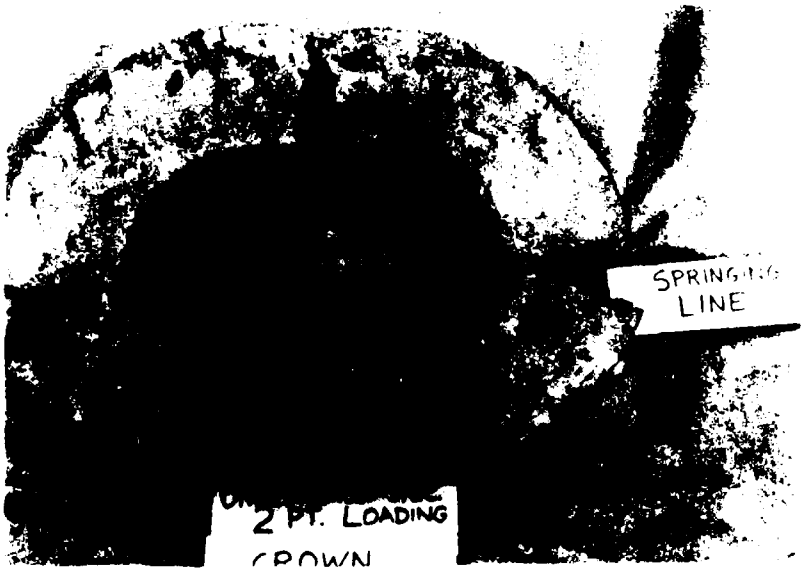

Unreinforced
2-point loading
Date tested: 9/17/84
R/h: 1.5

Figure B14. Rehearsal specimen

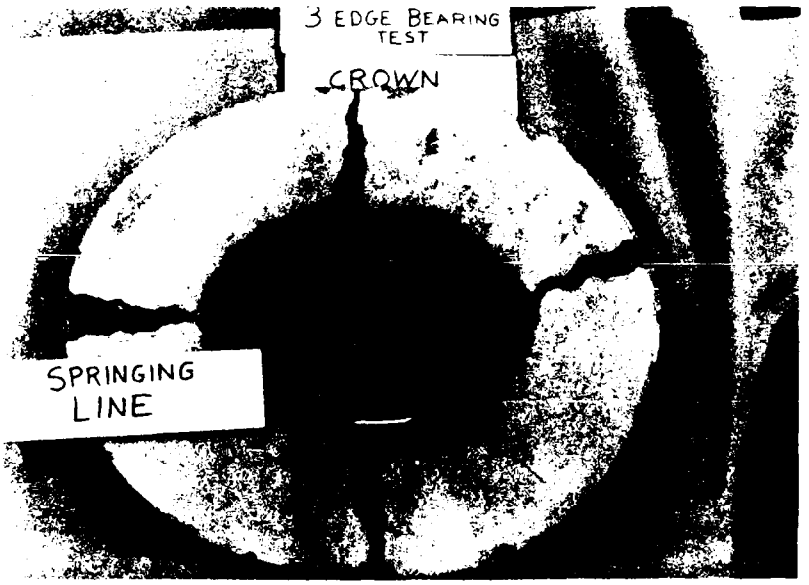

Unreinforced
Three-Edge-Bearing Test
Date tested: 9/20/84
R/h: 1.5

Figure B15. Rehearsal specimen

The increase in failure load for the 4-point over the 2-point and Three-Edge-Bearing tests may be explained by the increase in loading confinement. The type of failure for these tests differed from the previous series of 16-point tests due to the effect of loading confinement.

16. Structural analyses should be performed on the test data to show the effect of confinement on circular conduits. Future analyses should address shear resistance and plastic behavior of concrete.

Table B1

Summary of Models

Model No.	Type of Loading	R/h	Total Steel Ratio, ρg, %	R in.	h in.	B in.	d in.	d' in.
1	2 point	1.502	0.774	7.484	4.984	5.078	4.296	0.766
2	4 point	1.506	0.774	7.485	4.969	5.094	4.266	0.773
3	8 point	1.495	0.777	7.500	5.016	5.031	4.321	0.734
4	16 point	1.503	0.784	7.492	4.984	5.016	4.304	0.758
5	Three-edge-bearing	1.502	0.784	7.508	5.000	5.000	4.289	0.781

Table B2

Steel Reinforcement Properties

Type	Heat Treatment	Area $in.^2$	Number of Bars Tested	Average f_y, psi	Average Modulus of Elasticity $E_s \times 10^6$ psi
D5 deformed wire	3-1/2 hr at 1,050° F	0.049	4	65,695	22.4

Table B3

Concrete Properties

Number of Cylinders Tested	Dates Tested	Age Days	Average f'_c, psi	Average Initial Elastic Concrete Modulus $E_c \times 10^6$ psi	Average Poisson's Ratio	Average Tensile Strength psi
2	8/29/84	28	6,170	--	--	--
5	9/17/84-9/24/84	47-54	6,678	5.78	0.22	--
2	9/18/84-9/19/84	--	--	--	--	543

APPENDIX C

LOAD DISTRIBUTIONS

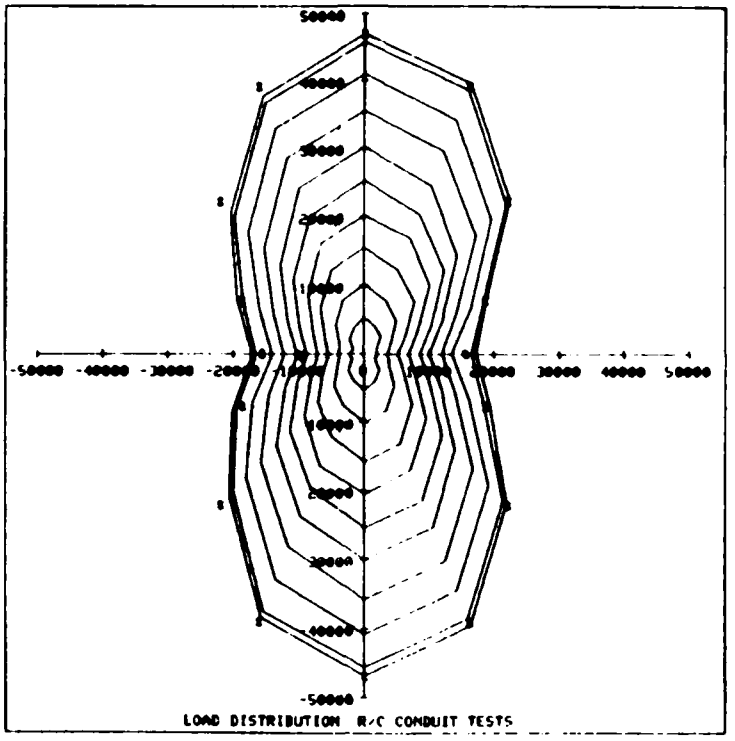

Model C1-1, 3:1 load, 46,900-lb maximum

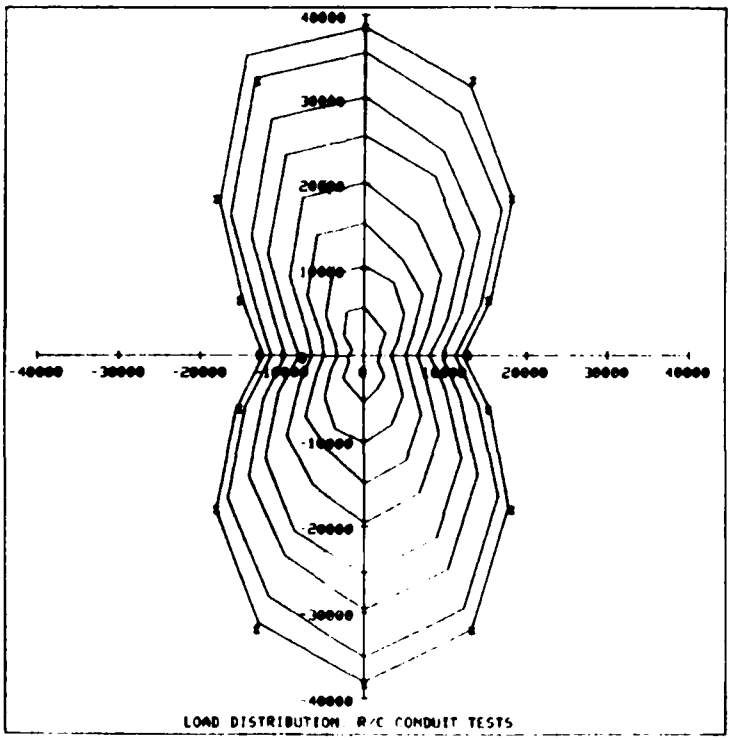

Model C2-1, 3:1 load, 38,500-lb maximum

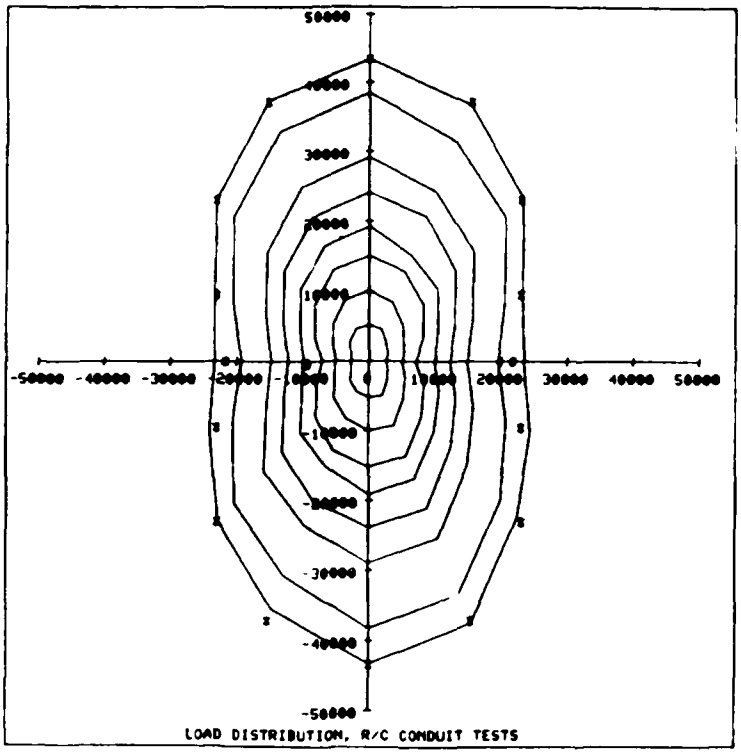

Model C2-2, 2:1 load, 43,400-lb maximum

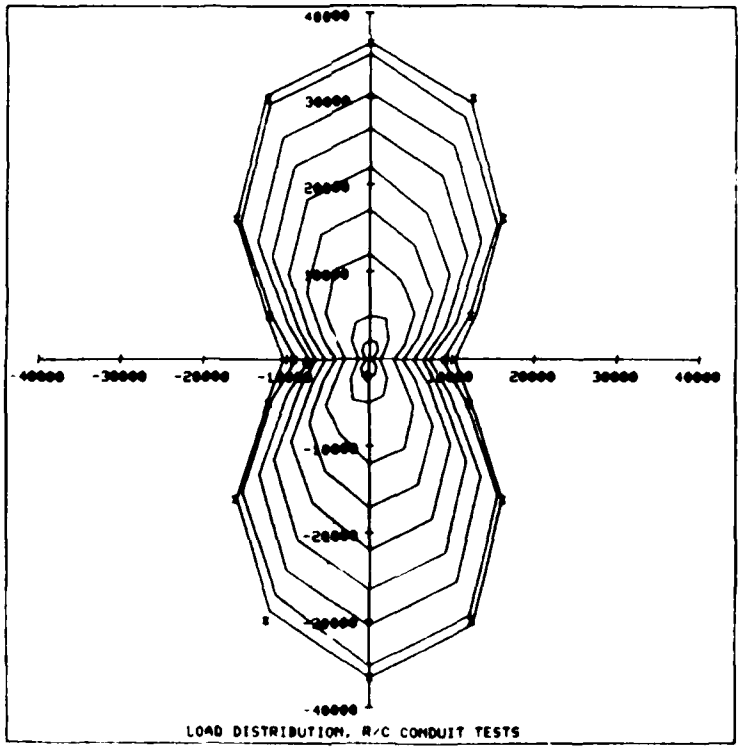

Model C2-3, 4:1 load, 36,500-lb maximum

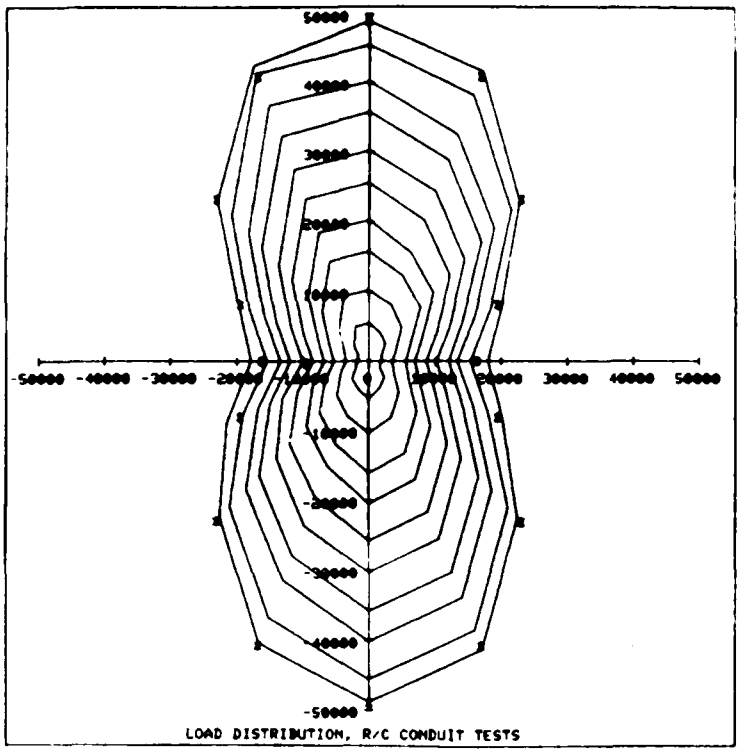

Model C3-1, 3:1 load, 49,000-lb maximum

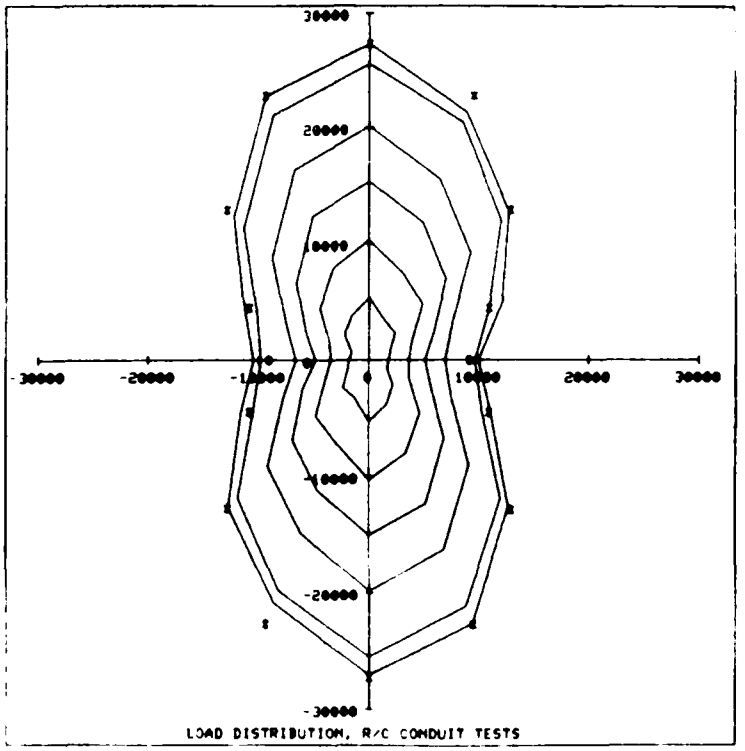

Model C4-1, 3:1 load, 27,300-lb maximum

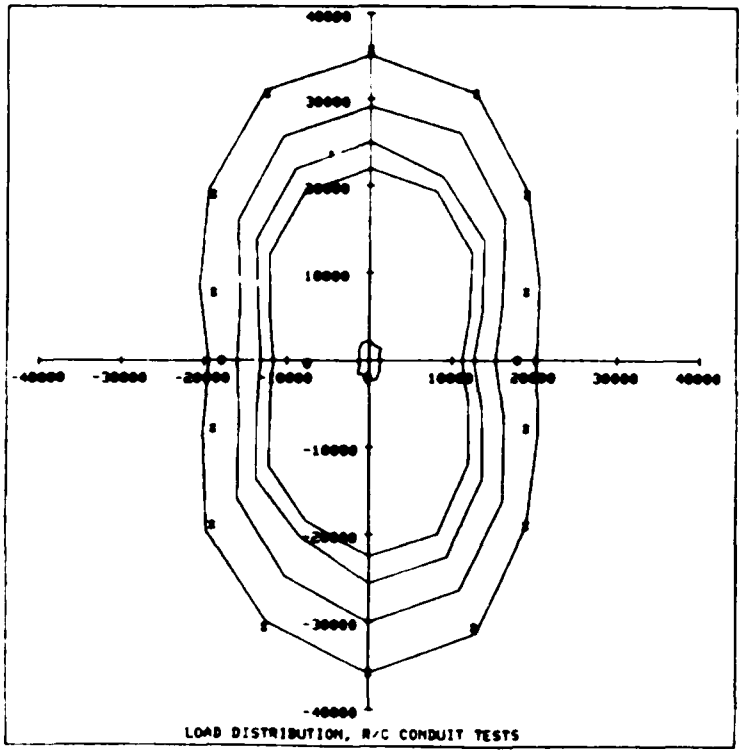

Model C4-2, 2:1 load, 35,800-lb maximum

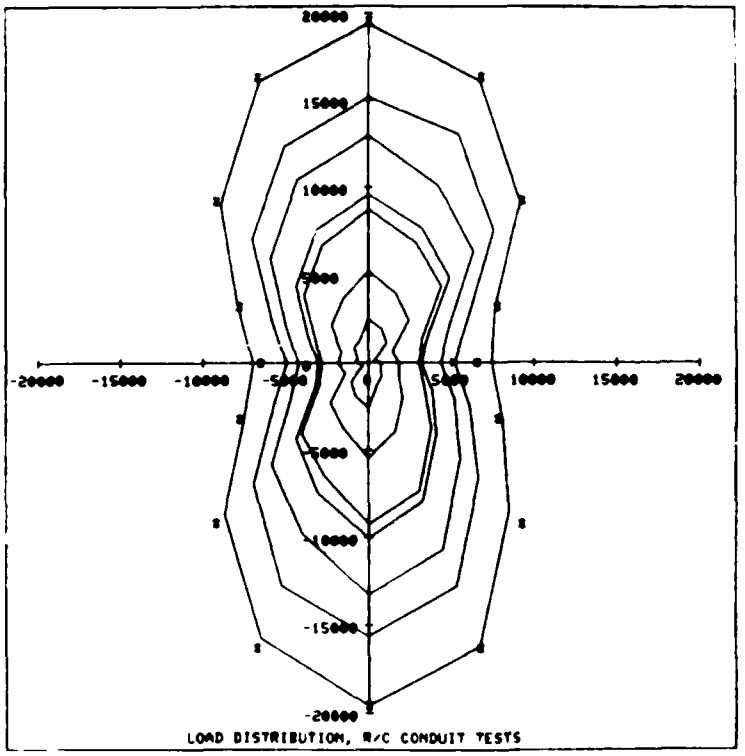

Model C5-1, 3:1 load, 19,500-lb maximum

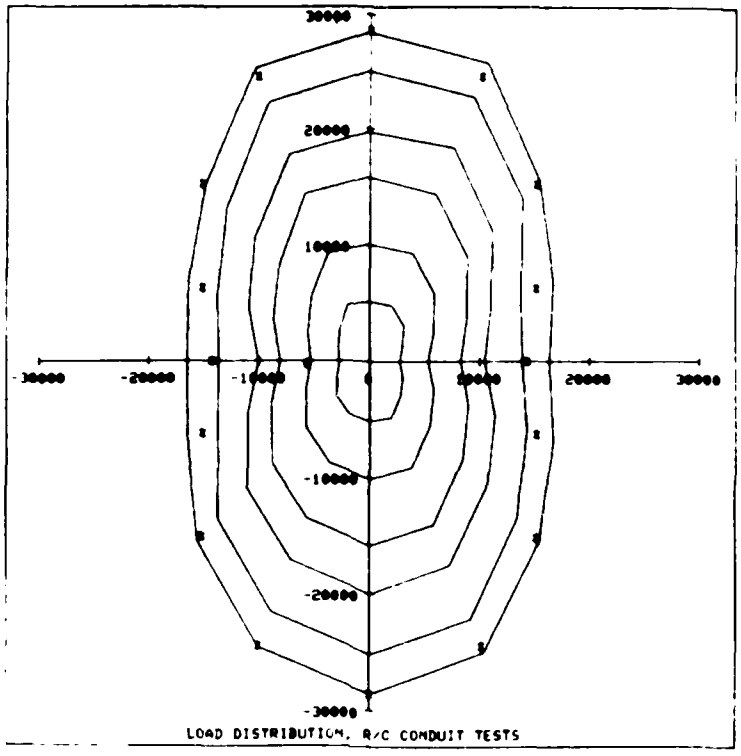

Model C5-2, 2:1 load, 28,500-lb maximum

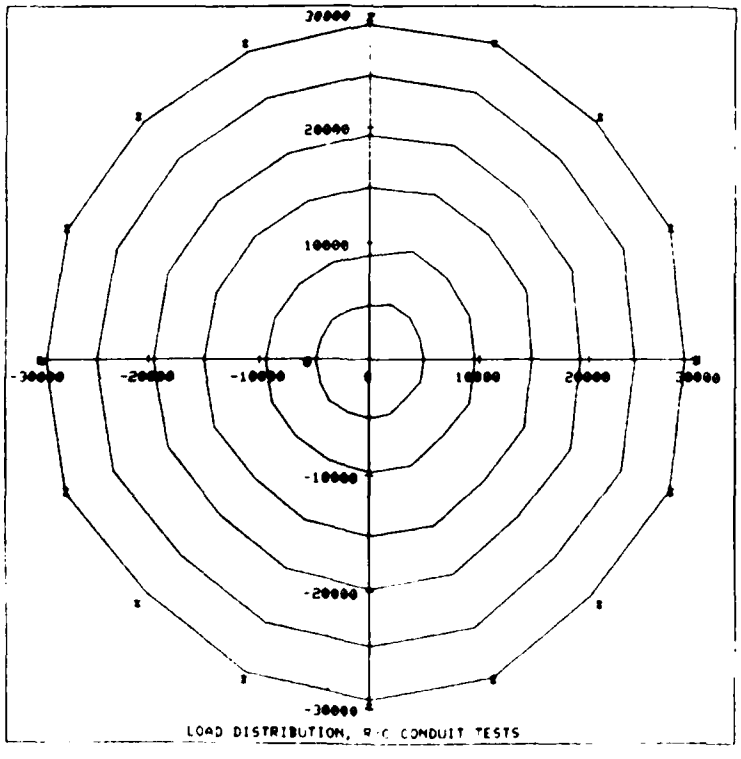

Model C5-3, 1:1 load, 29,700-lb maximum

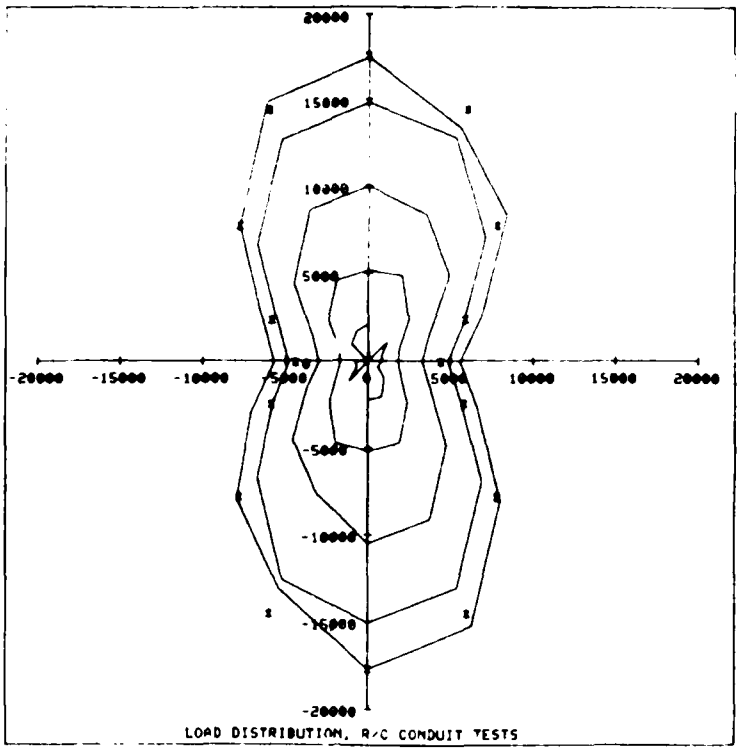

Model C5-4, 4:1 load, 17,600-lb maximum

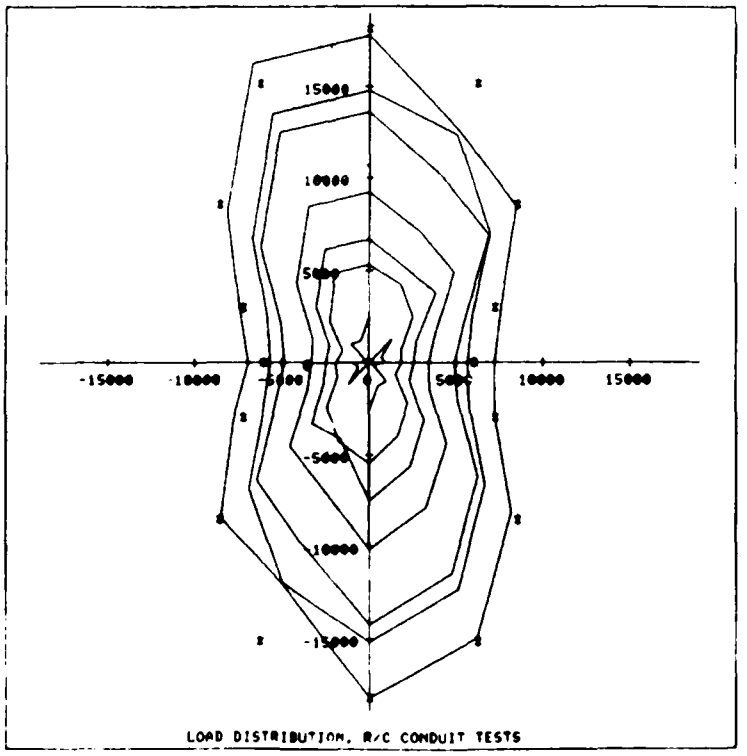

Model C6-1, 3:1 load, 18,100-lb maximum

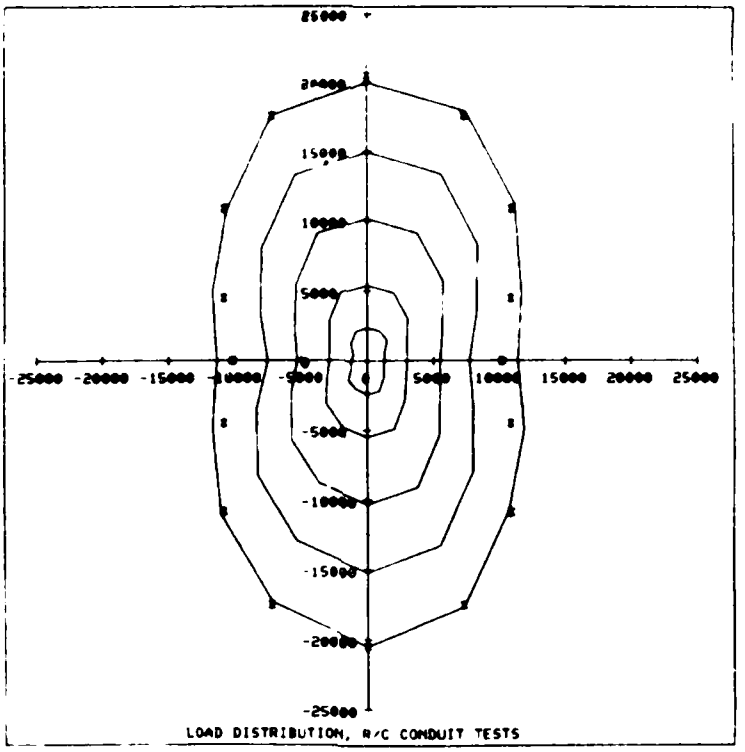

Model C6-2, 2:1 load, 20,500-lb maximum

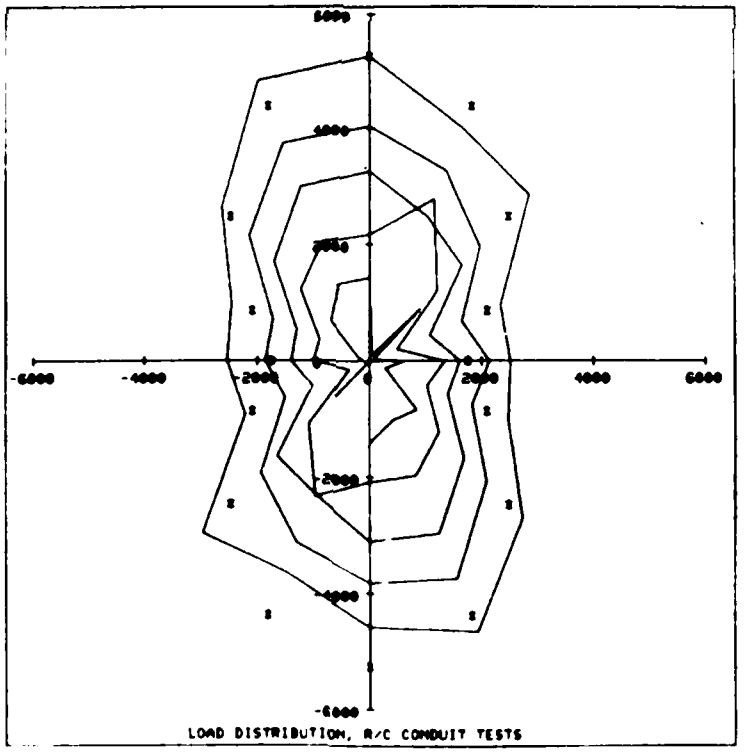

Model C7-1, 3:1 load, 5,260-lb maximum

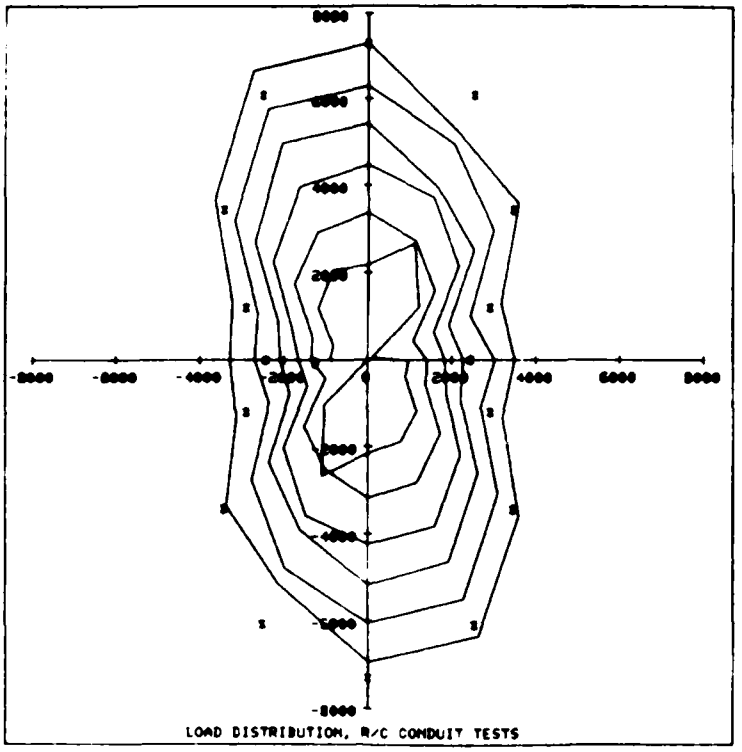

Model C8-1, 3:1 load, 7,300-lb maximum

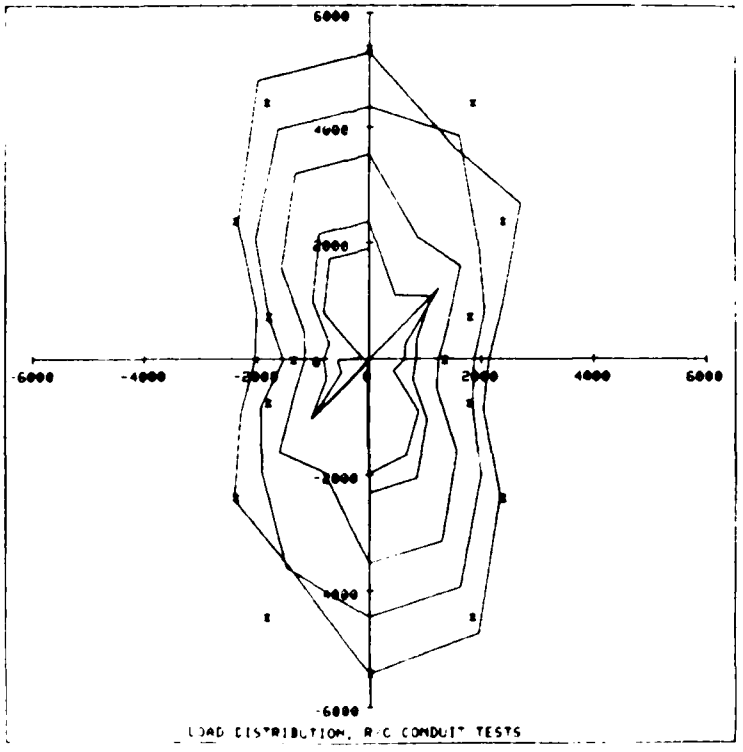

Model C8-2, 4:1 load, 5,400-lb maximum

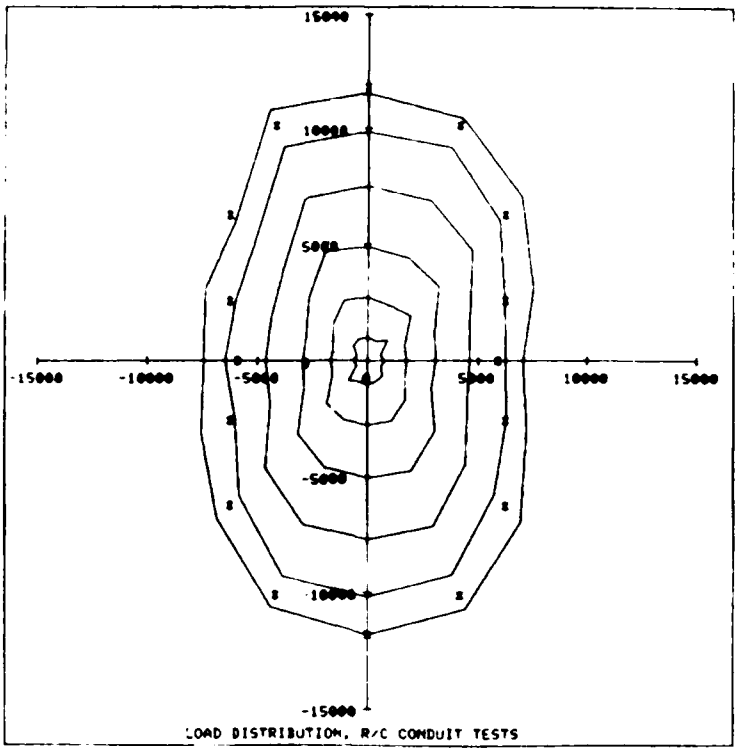

Model C8-3, 2:1 load, 11,800-lb maximum

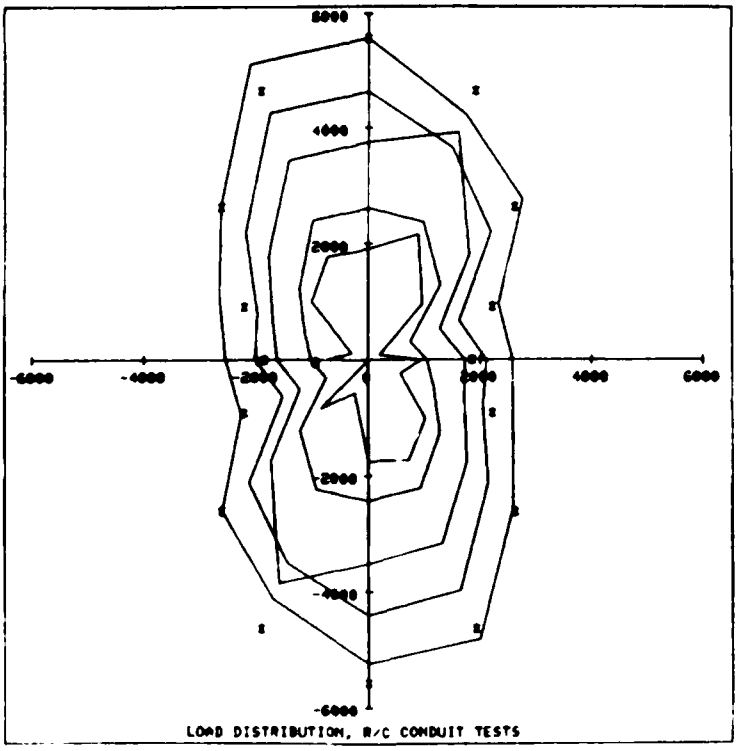

Model C9-1, 3:1 load, 5,700-lb maximum

APPENDIX D

LOAD-STRAIN AND DEFLECTION PLOTS

R/C MODEL C11
LOAD 1 VS. STRAINS

05/10/84

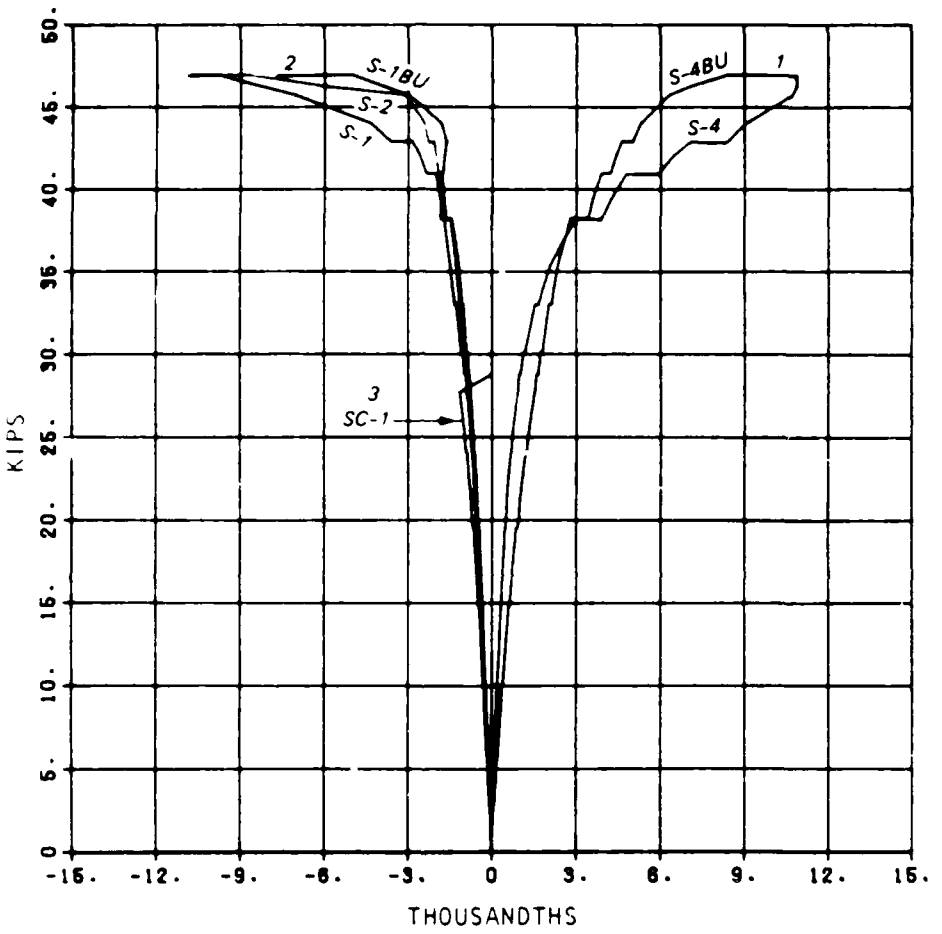

POSITIVE MOMENT
1. INTRADOS STEEL STRAIN 2. EXTRADOS STEEL STRAIN
3. EXTRADOS CONCRETE STRAIN

AD-A182 451 STRENGTH DESIGN OF REINFORCED CONCRETE HYDRAULIC 2/3
STRUCTURES REPORT 5 EXPE (U) ARMY ENGINEER WATERWAYS
EXPERIMENT STATION VICKSBURG MS STRUC
UNCLASSIFIED R S WRIGHT ET AL APR 87 WES/TR/SL-80-4/5 F/G 13/3 NL

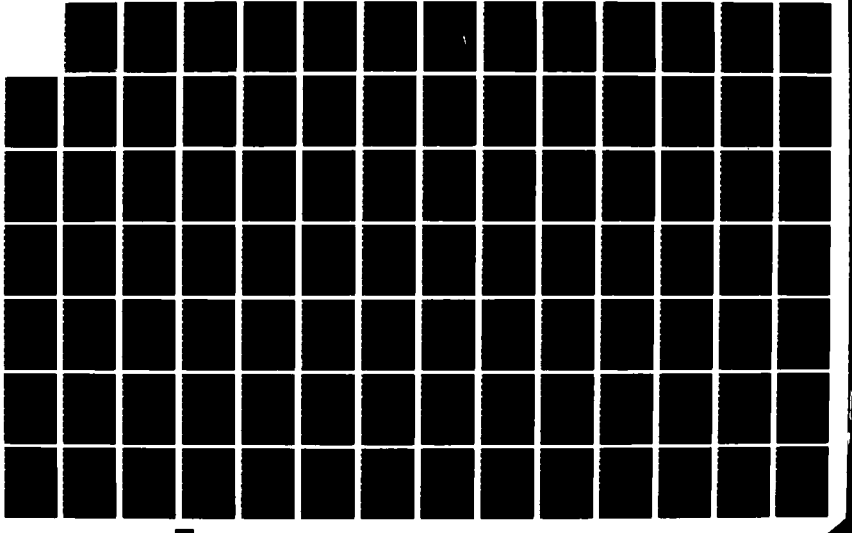

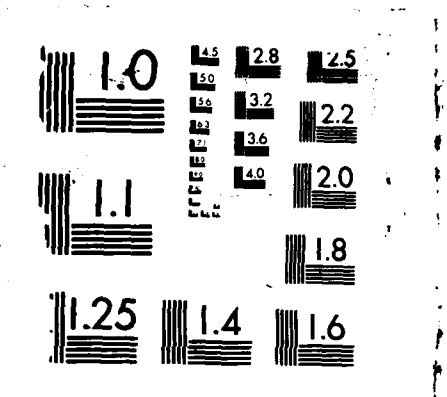

R/C MODEL C11
LOAD 1 VS. DEFL.

05/10/84

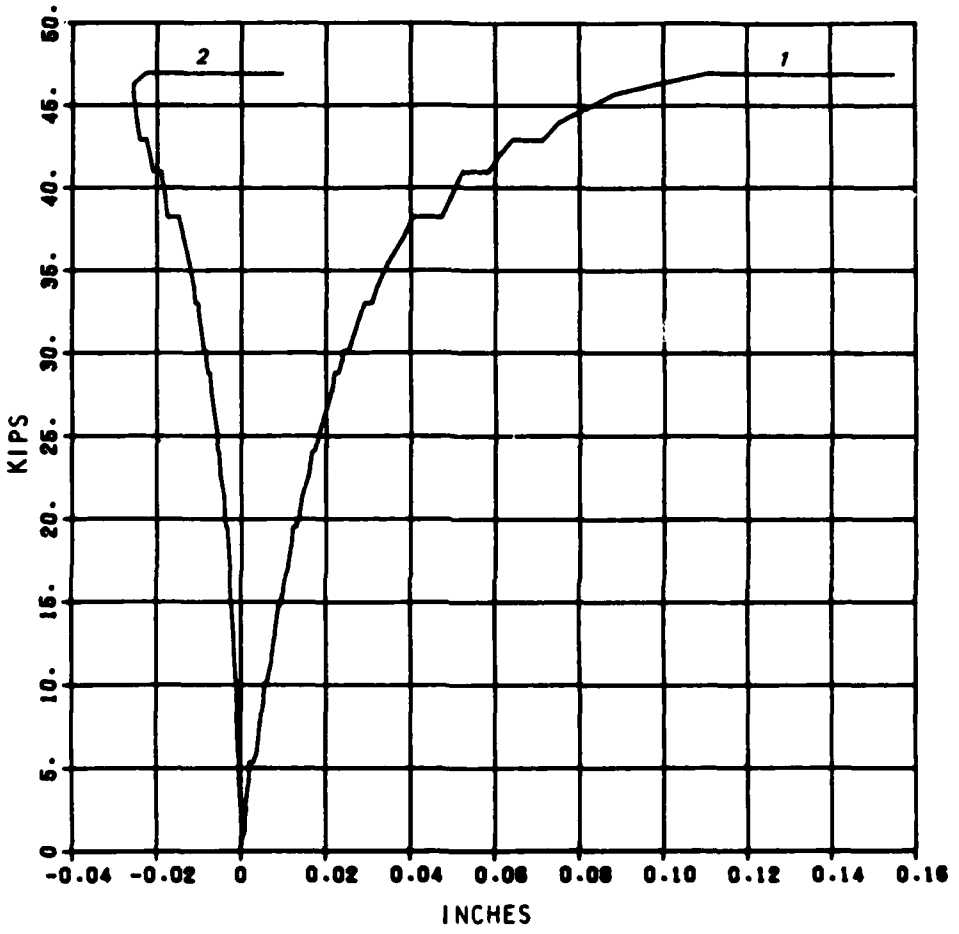

1. CROWN
2. SPRINGING LINE

R/C MODEL C11
LOAD 1 VS. STRAINS

05/10/84

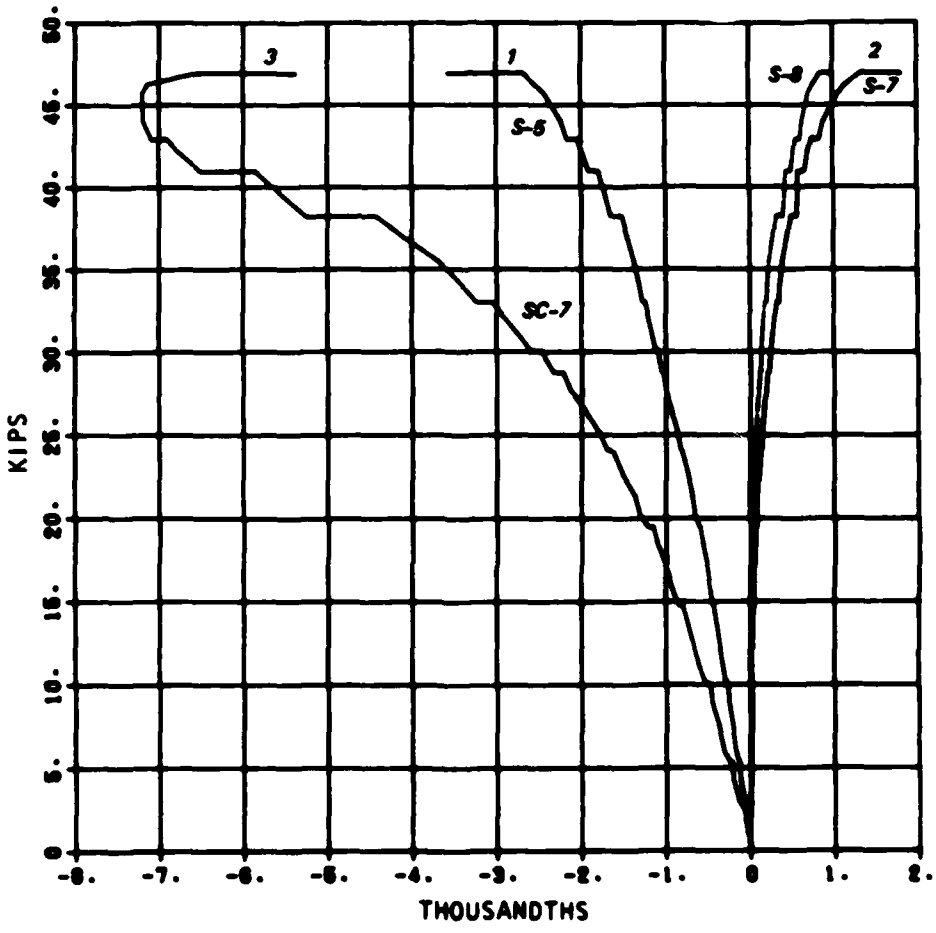

NEGATIVE MOMENT
1. INTRADOS STEEL STRAIN 2. EXTRADOS STEEL STRAIN
3. INTRADOS CONCRETE STRAIN

R/C MODEL C21
LOAD 1 VS. STRAINS

06/10/84

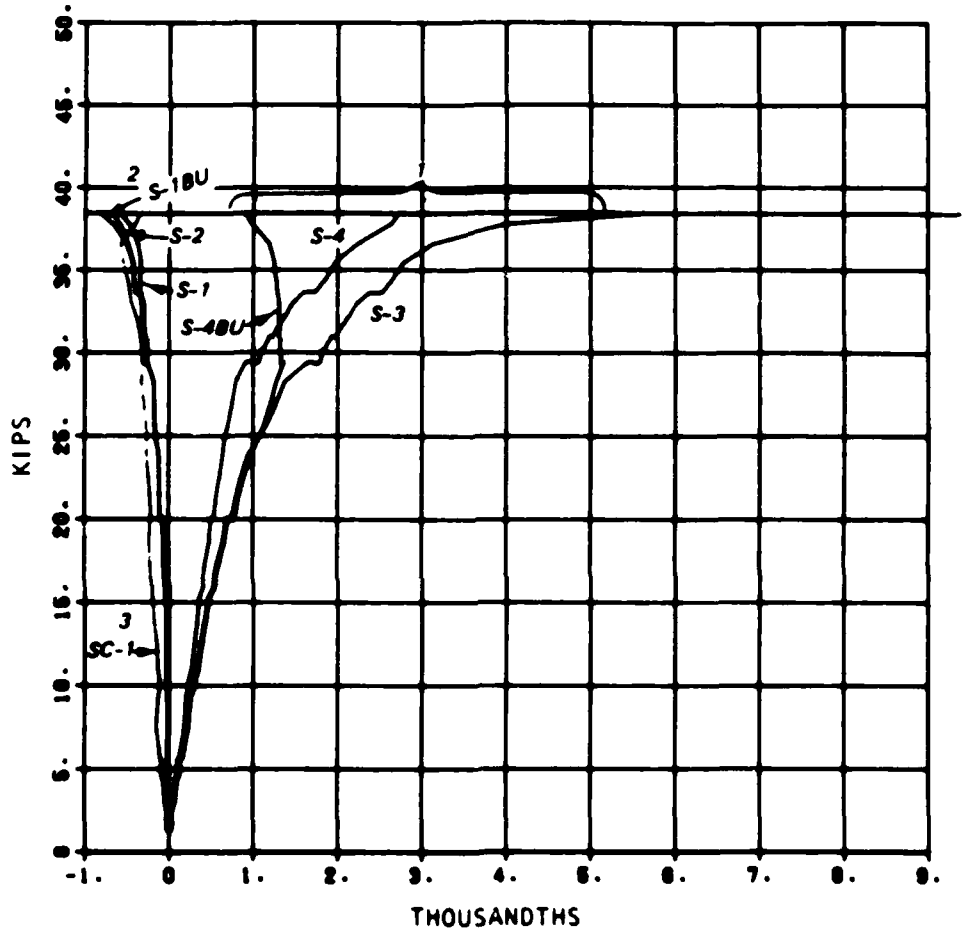

POSITIVE MOMENT
1. INTRADOS STEEL STRAIN 2. EXTRADOS STEEL STRAIN
3. EXTRADOS CONCRETE STRAIN

R/C MODEL C21
LOAD 1 VS. STRAINS

06/10/84

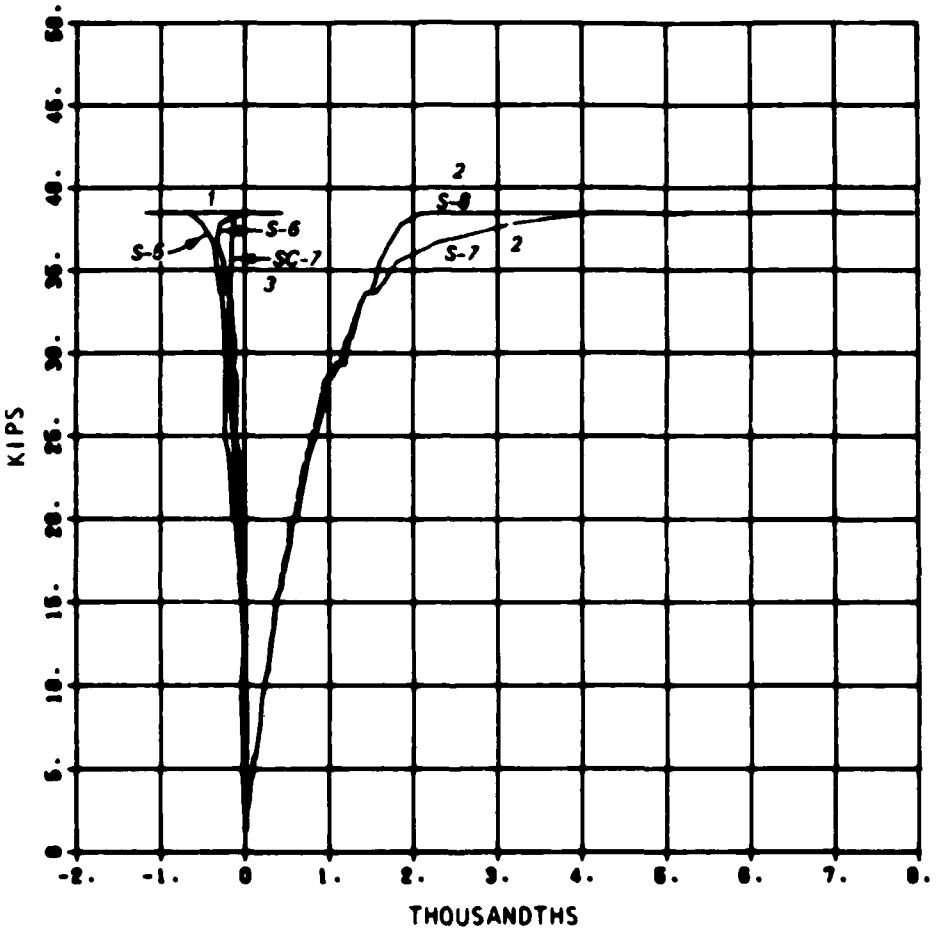

NEGATIVE MOMENT
1. INTRADOS STEEL STRAIN 2. EXTRADOS STEEL STRAIN
3. INTRADOS CONCRETE STRAIN

R/C MODEL C21
LOAD 1 VS. DEFL.

06/10/84

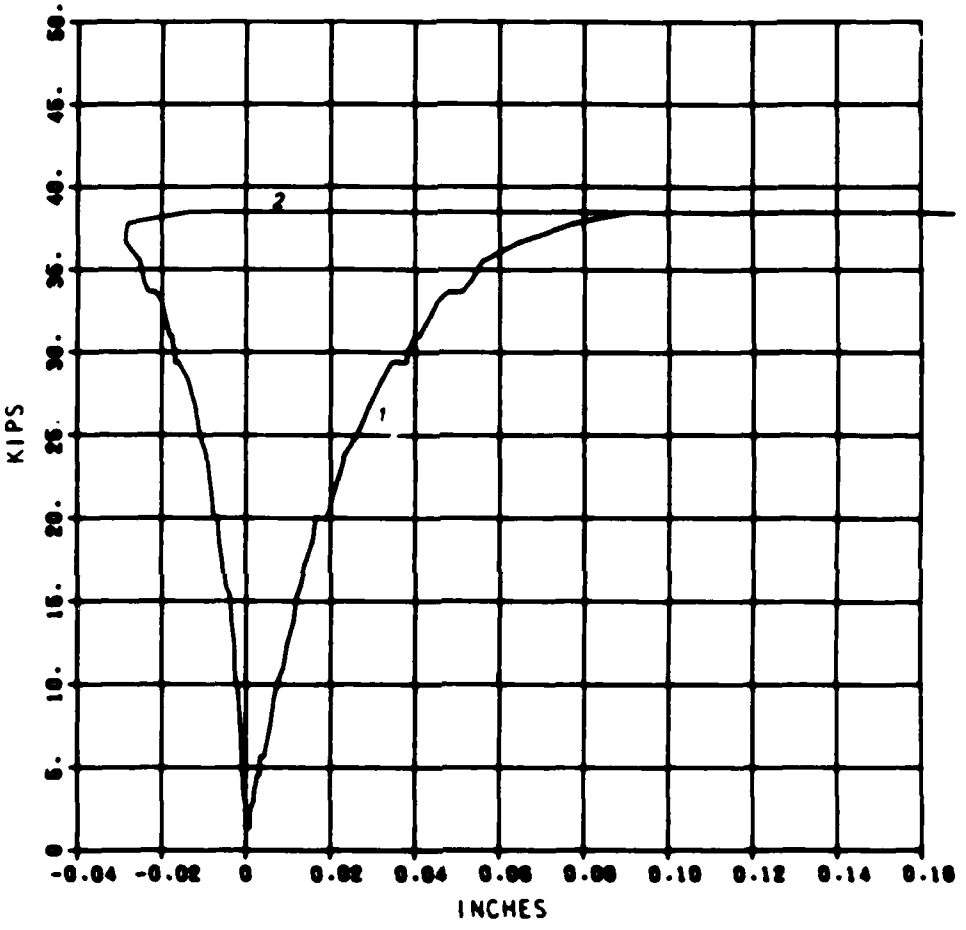

1. CROWN
2. SPRINGING LINE

R/C MODEL C22
LOAD 1 VS. STRAINS

05/10/84

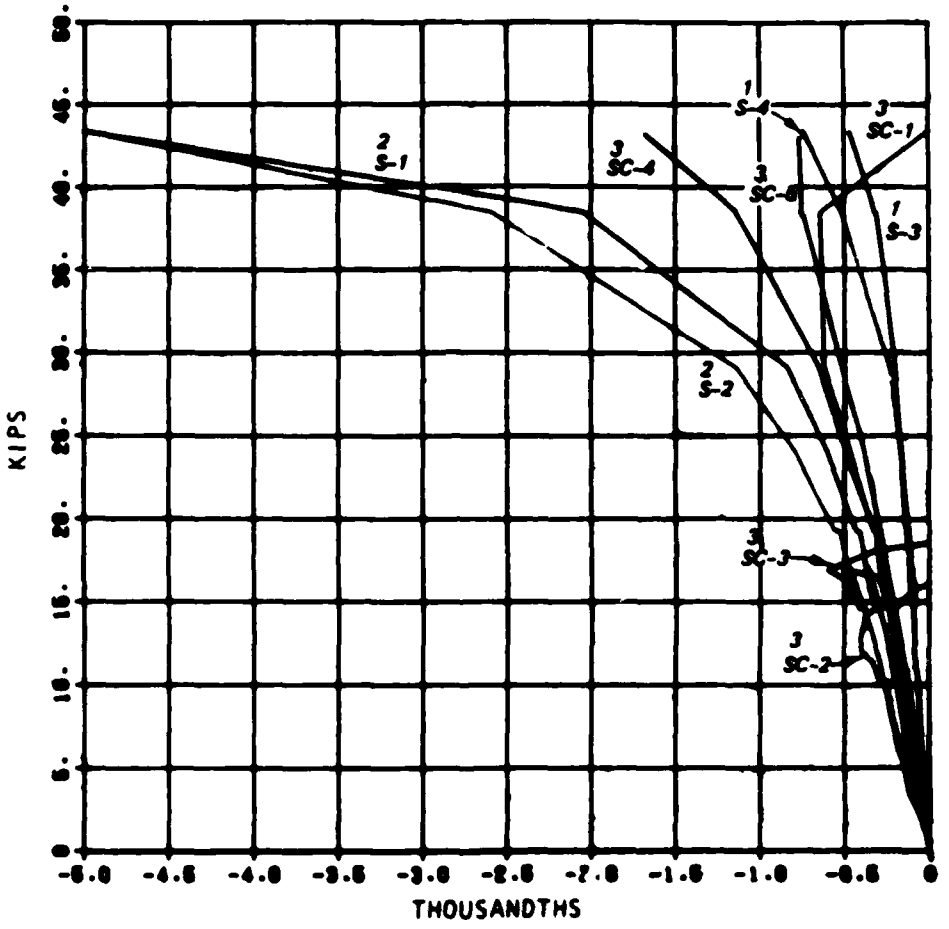

POSITIVE MOMENT
1. INTRADOS STEEL STRAIN 2. EXTRADOS STEEL STRAIN
3. EXTRADOS CONCRETE STRAIN

R/C MODEL C22
LOAD 1 VS. STRAINS

06/10/84

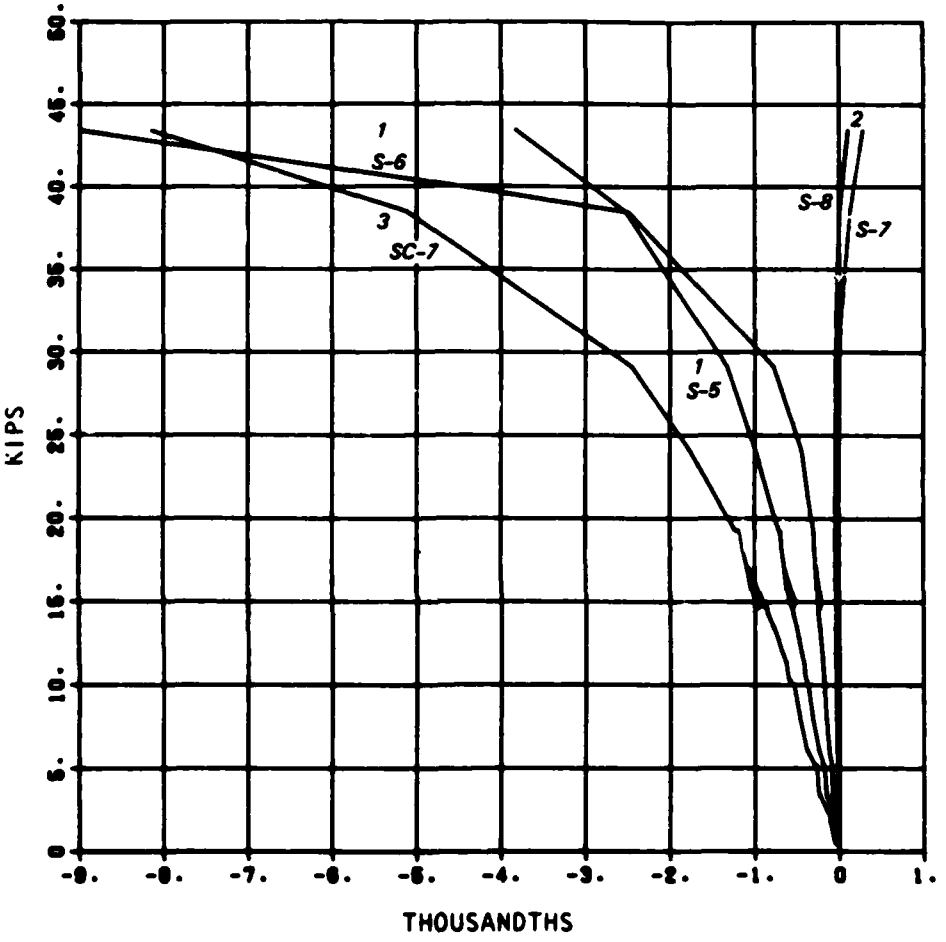

NEGATIVE MOMENT
1. INTRADOS STEEL STRAIN 2. EXTRADOS STEEL STRAIN
3. INTRADOS CONCRETE STRAIN

R/C MODEL C22
LOAD 1 VS. DEFL.

05/11/84

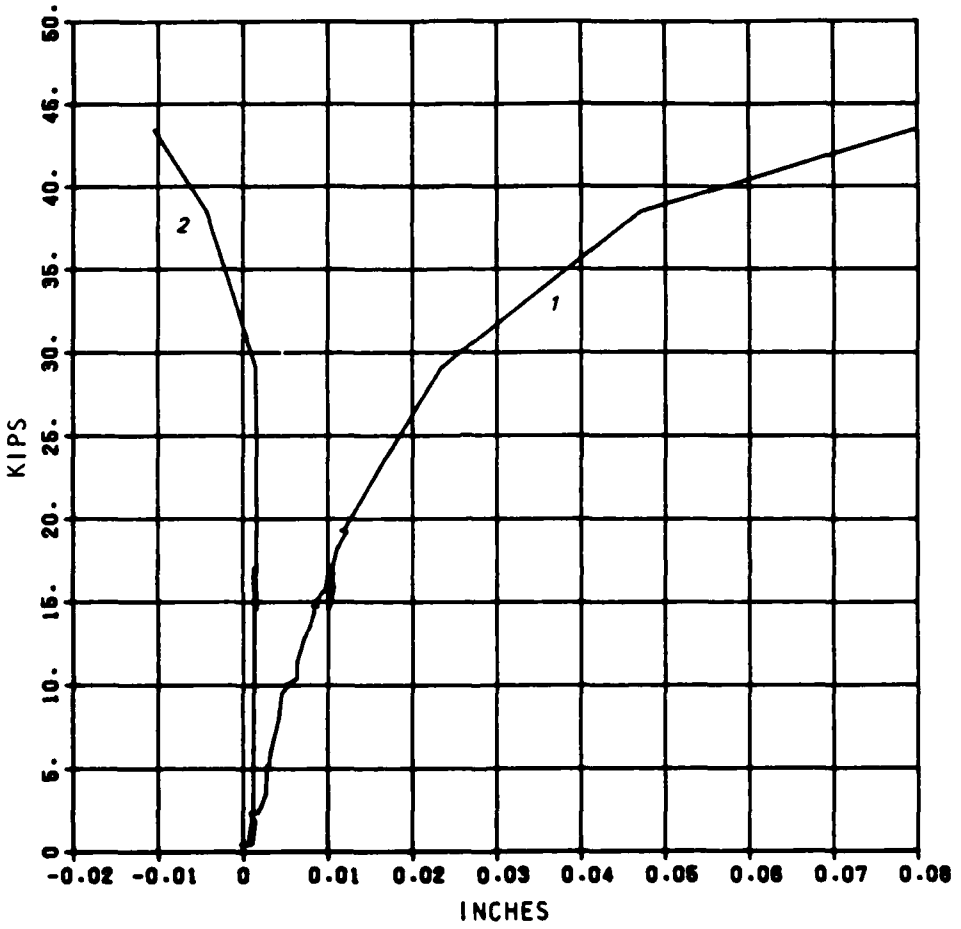

1. CROWN
2. SPRINGING LINE

R/C MODEL C23
LOAD 9 VS. STRAINS

05/10/84

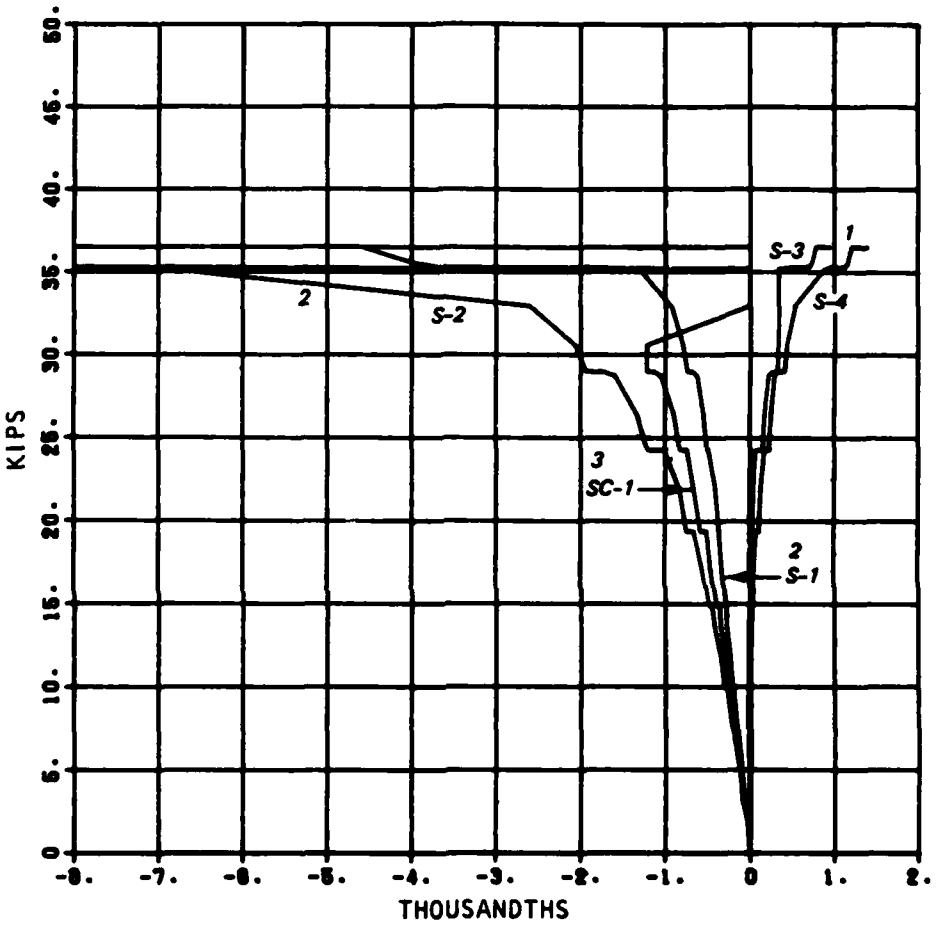

POSITIVE MOMENT
1. INTRADOS STEEL STRAIN 2. EXTRADOS STEEL STRAIN
3. EXTRADOS CONCRETE STRAIN

R/C MODEL C23
LOAD 9 VS. STRAINS

06/10/84

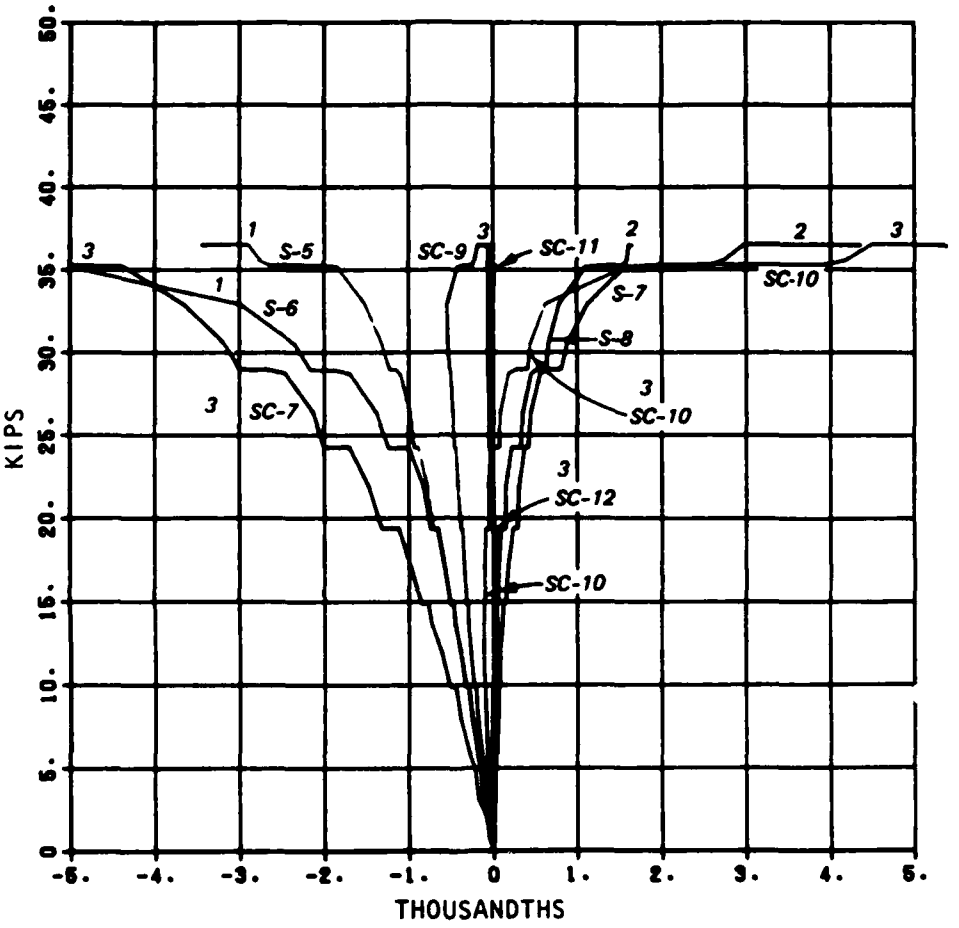

NEGATIVE MOMENT
1. INTRADOS STEEL STRAIN
2. EXTRADOS STEEL STRAIN 3. CONCRETE STRAINS

R/C MODEL C23
LOAD 9 VS. DEFL.

05/10/84

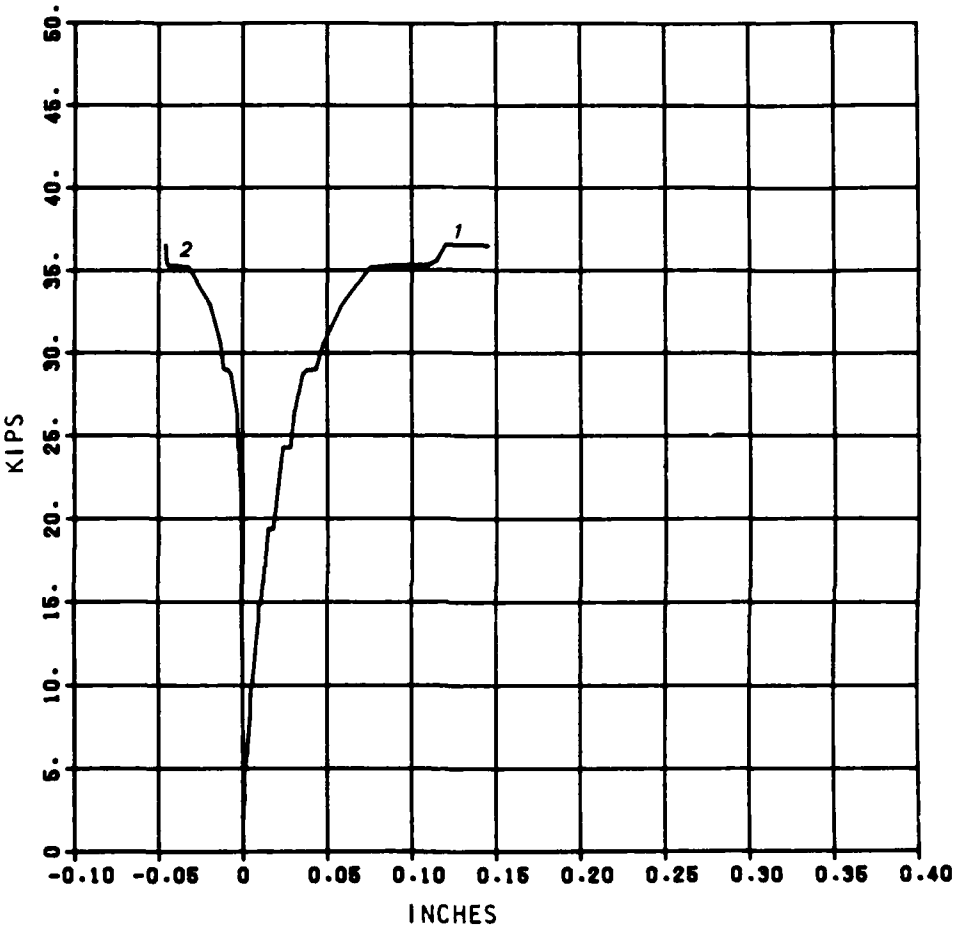

1. CROWN
2. SPRINGING LINE

R/C MODEL C31
LOAD 1 VS. STRAINS

05/10/84

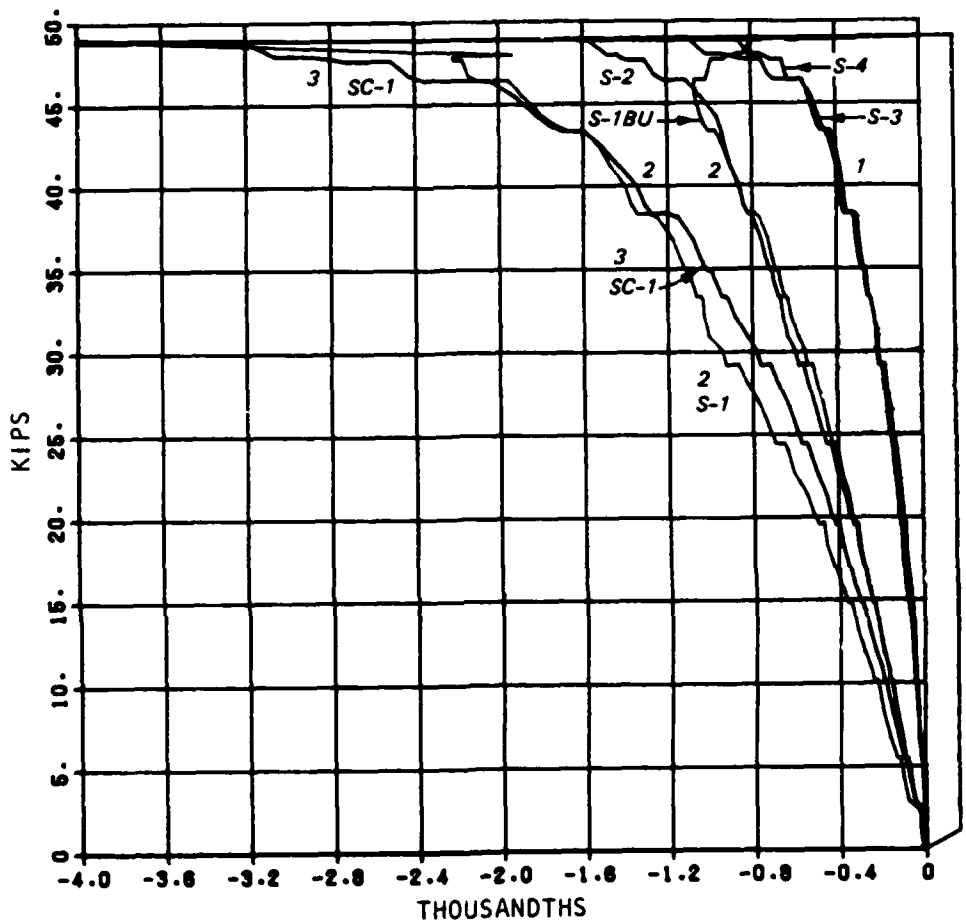

POSITIVE MOMENT
1. INTRADOS STEEL STRAIN 2. EXTRADOS STEEL STRAIN
3. EXTRADOS CONCRETE STRAIN

R/C MODEL C31
LOAD 1 VS. STRAINS

05/10/84

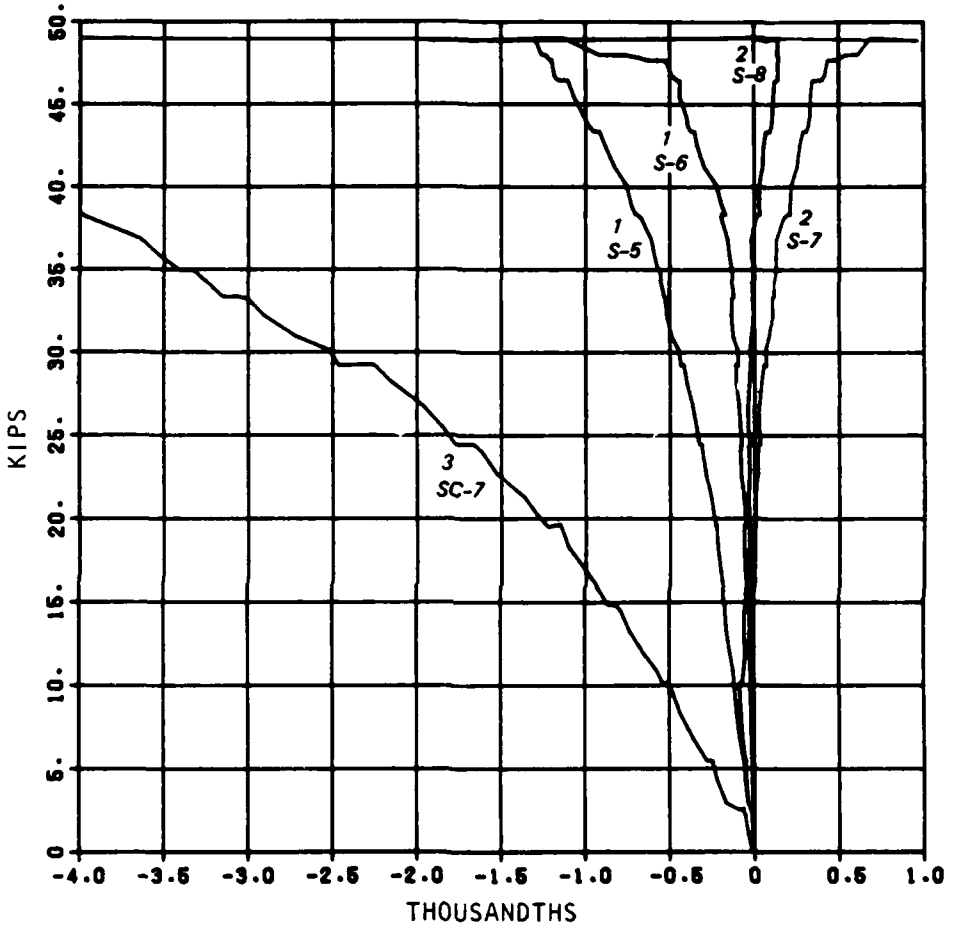

NEGATIVE MOMENT
1. INTRADOS STEEL STRAIN 2. EXTRADOS STEEL STRAIN
3. INTRADOS CONCRETE STRAIN

R/C MODEL C31
LOAD 1 VS. DEFL.

05/10/84

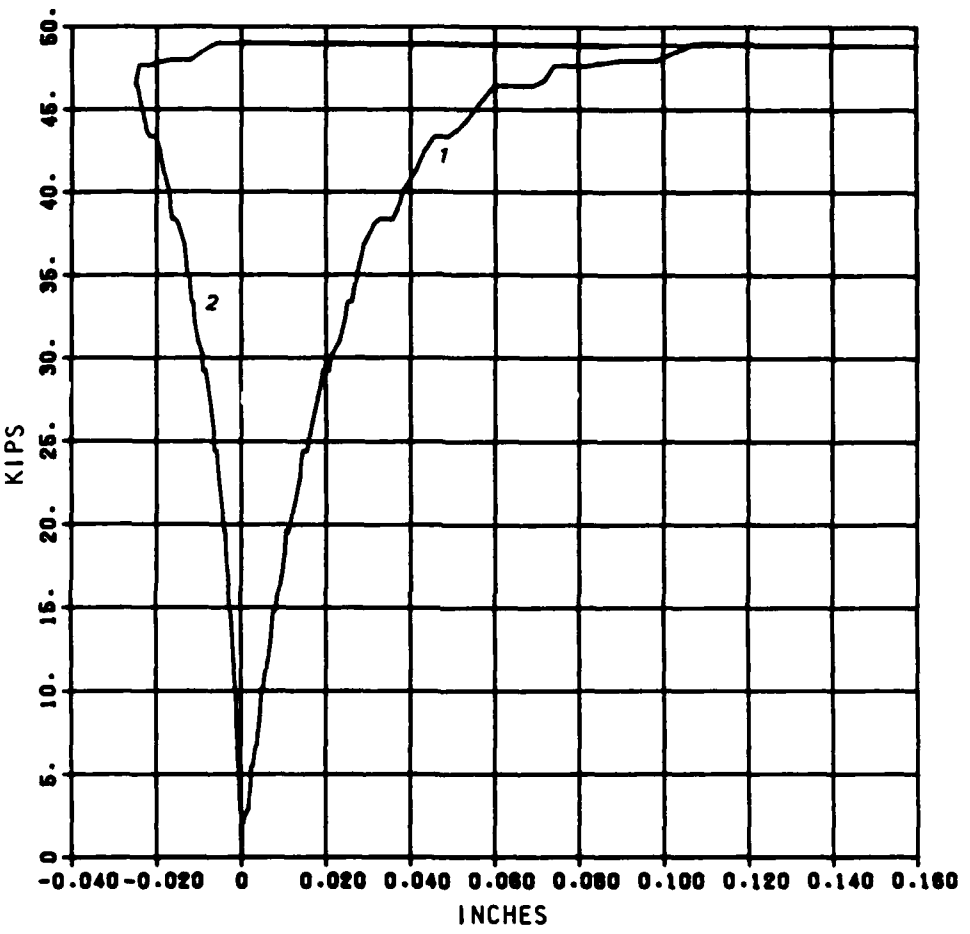

1. CROWN
2. SPRINGING LINE

R/C MODEL C41
LOAD 1 VS. STRAINS

05/11/84

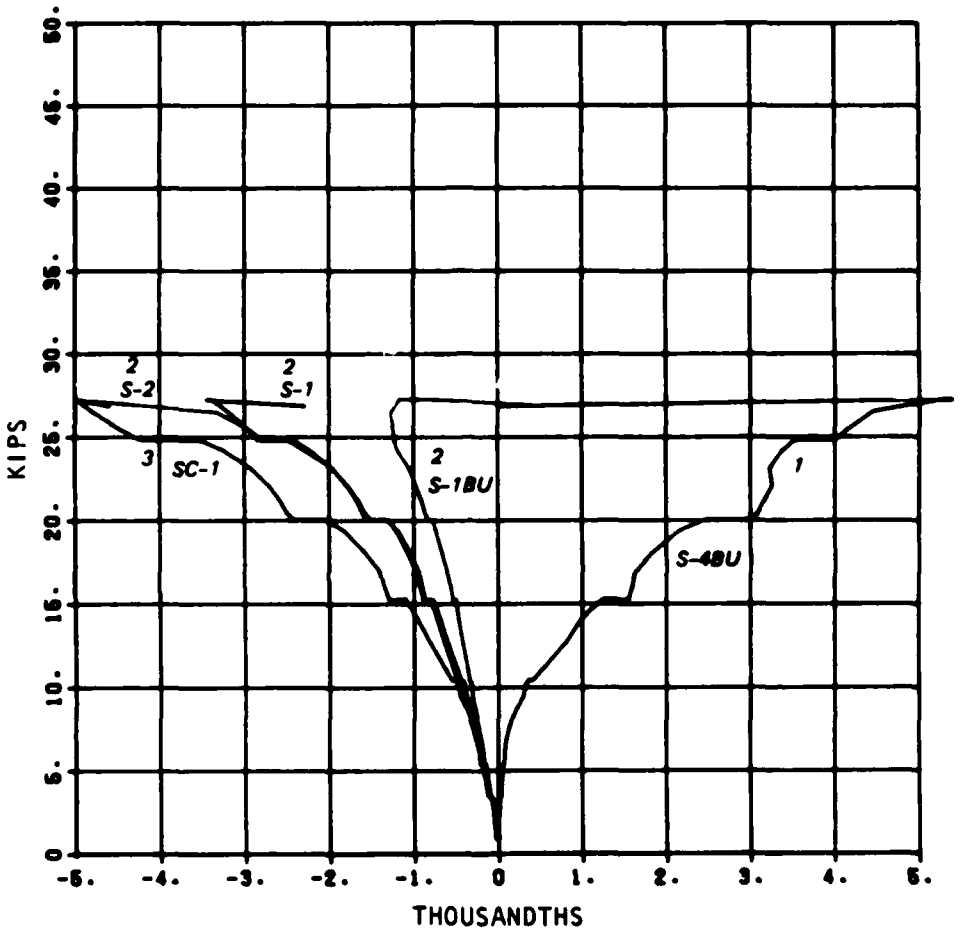

POSITIVE MOMENT
1. INTRADOS STEEL STRAIN 2. EXTRADOS STEEL STRAIN
3. EXTRADOS CONCRETE STRAIN

R/C MODEL C41
LOAD 1 VS. STRAINS

06/11/84

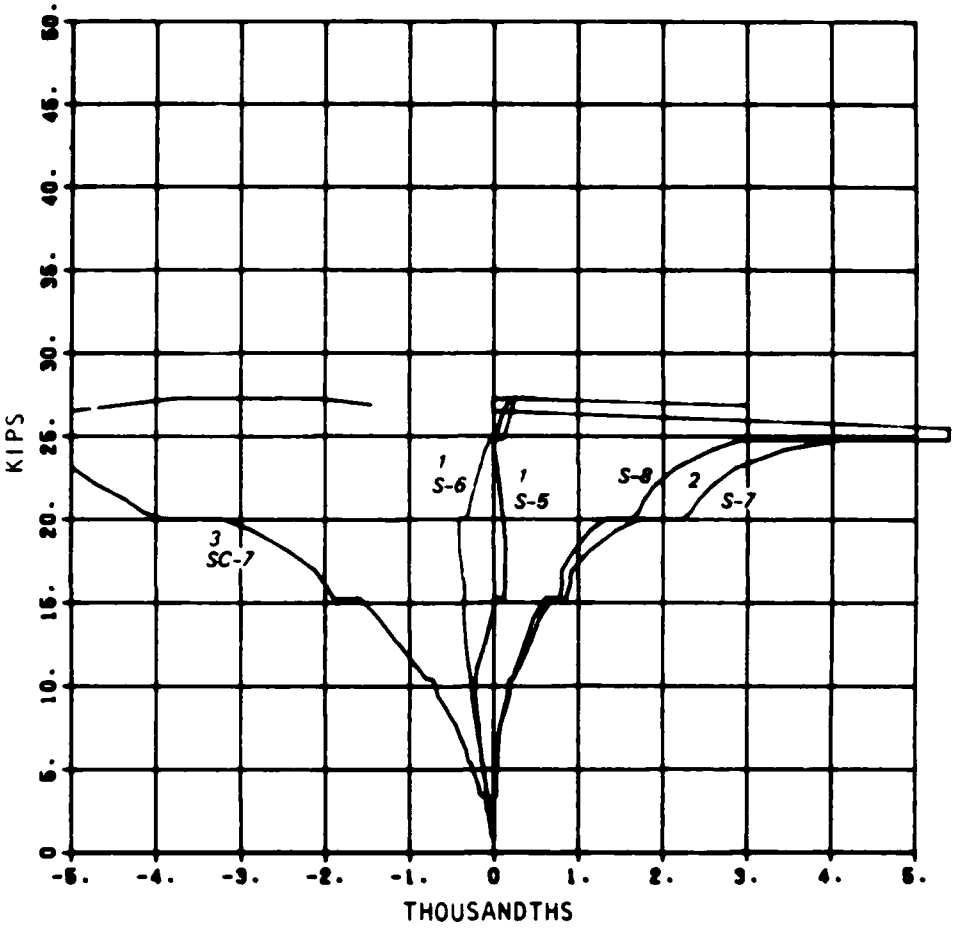

NEGATIVE MOMENT
1. INTRADOS STEEL STRAIN 2. EXTRADOS STEEL STRAIN
3. INTRADOS CONCRETE STRAIN

R/C MODEL C41
LOAD 1 VS. DEFL.

06/15/84

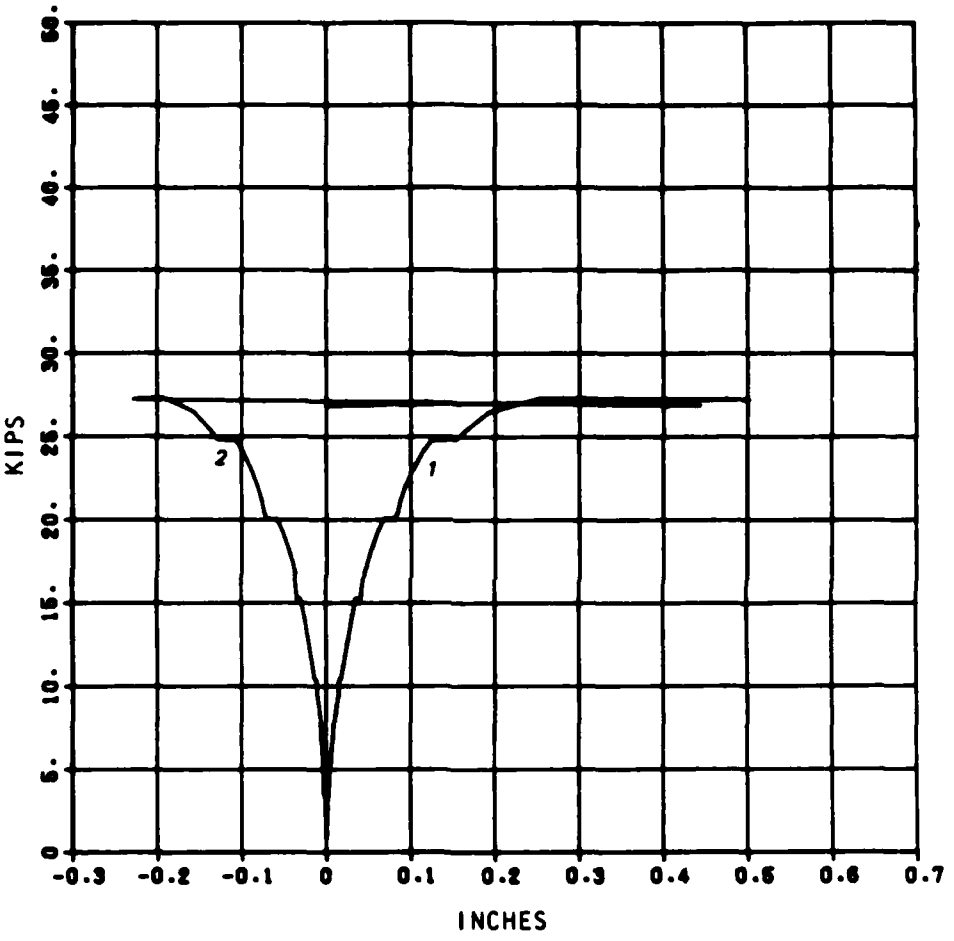

1. CROWN
2. SPRINGING LINE

R/C MODEL C42
LOAD 1 VS. STRAINS

05/15/84

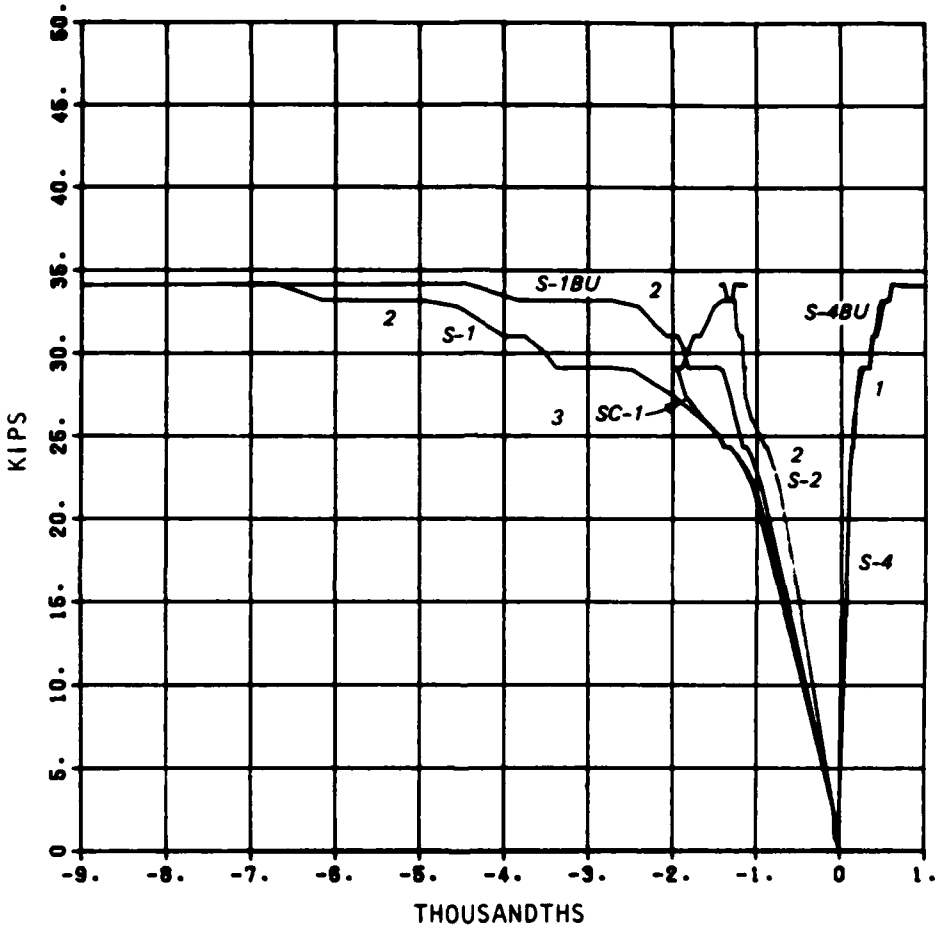

POSITIVE MOMENT
1. INTRADOS STEEL STRAIN 2. EXTRADOS STEEL STRAIN
3. EXTRADOS CONCRETE STRAIN

R/C MODEL C42
LOAD 1 VS. STRAINS

06/15/84

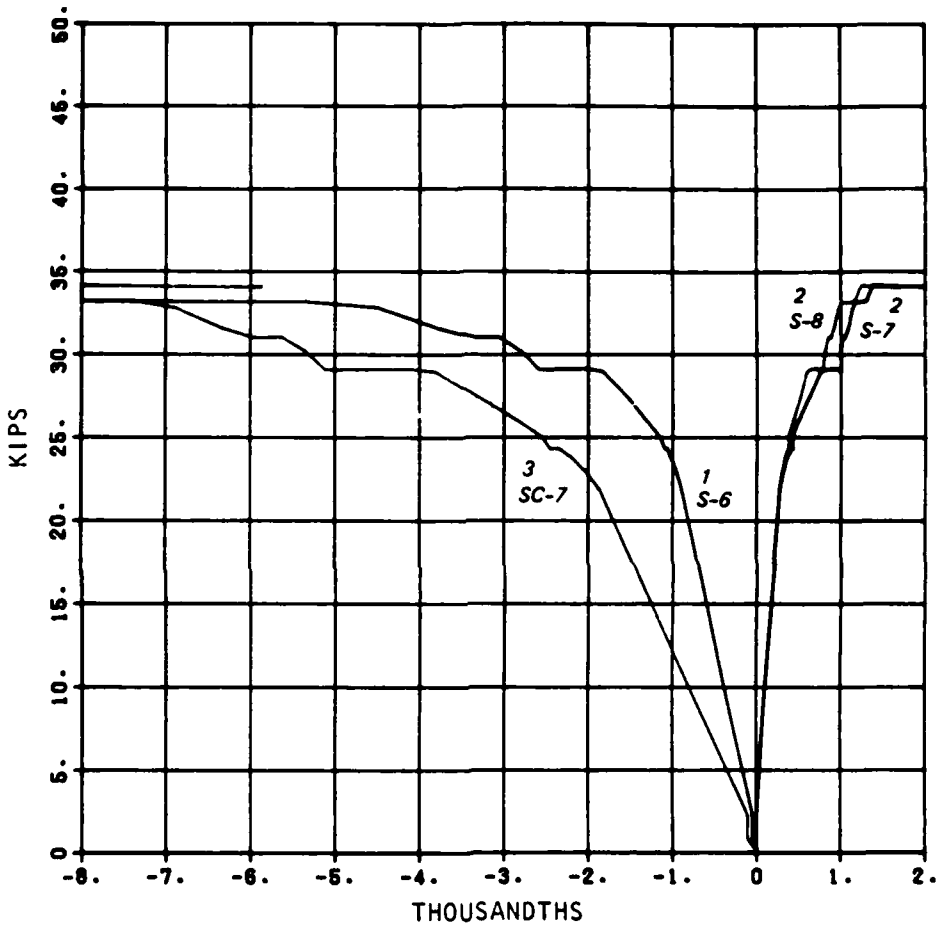

NEGATIVE MOMENT
1. INTRADOS STEEL STRAIN 2. EXTRADOS STEEL STRAIN
3. INTRADOS CONCRETE STRAIN

R/C MODEL C42
LOAJ 1 VS. DEFL.

06/15/84

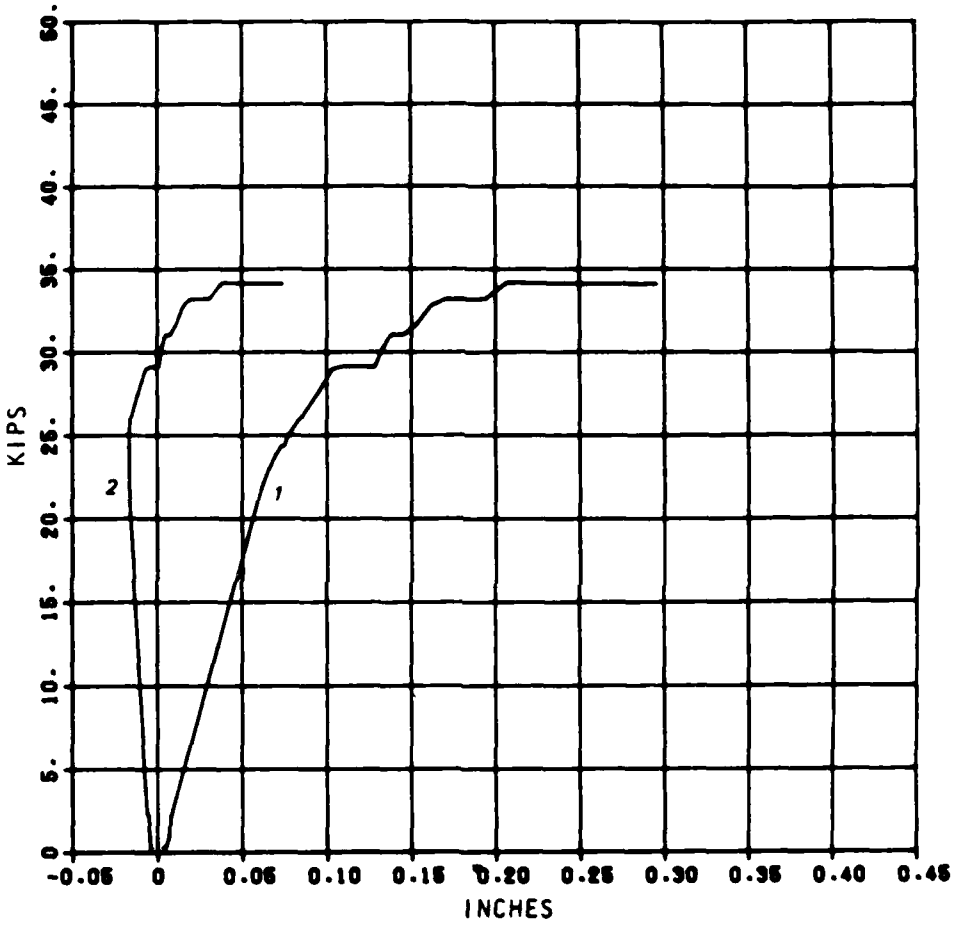

1. CROWN
2. SPRINGING LINE

R/C MODEL C51
LOAD 1 VS. STRAINS

06/10/84

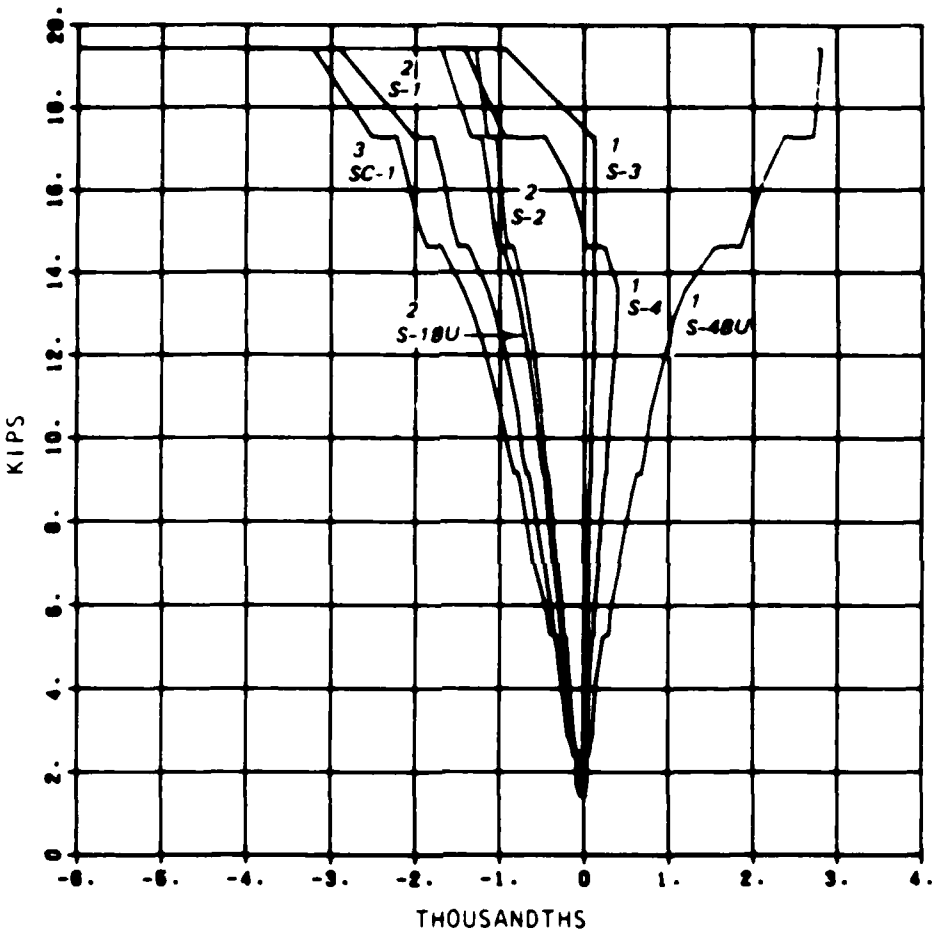

POSITIVE MOMENT
1. INTRADOS STEEL STRAIN 2. EXTRADOS STEEL STRAIN
3. EXTRADOS CONCRETE STRAIN

R/C MODEL C51
LOAD 1 VS. STRAINS

05/10/84

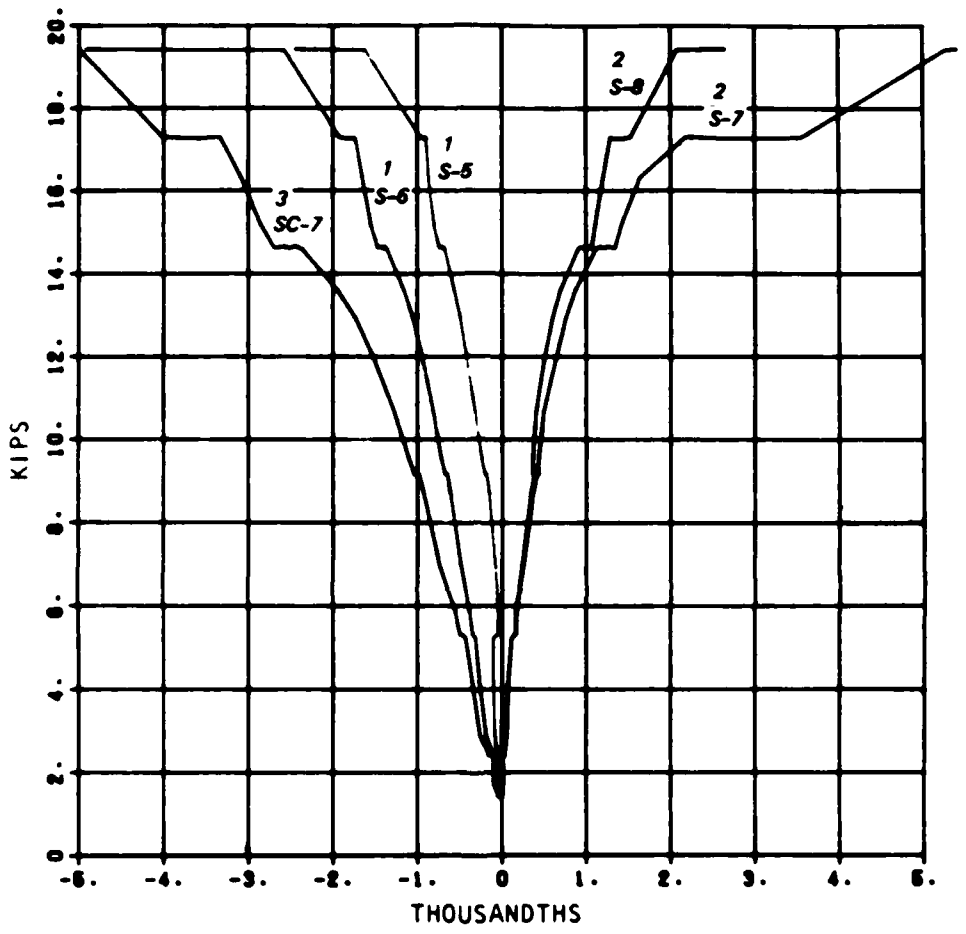

NEGATIVE MOMENT
1. INTRADOS STEEL STRAIN 2. EXTRADOS STEEL STRAIN
3. INTRADOS CONCRETE STRAIN

R/C MODEL C51
LOAD 1 VS. DEFL.

06/10/84

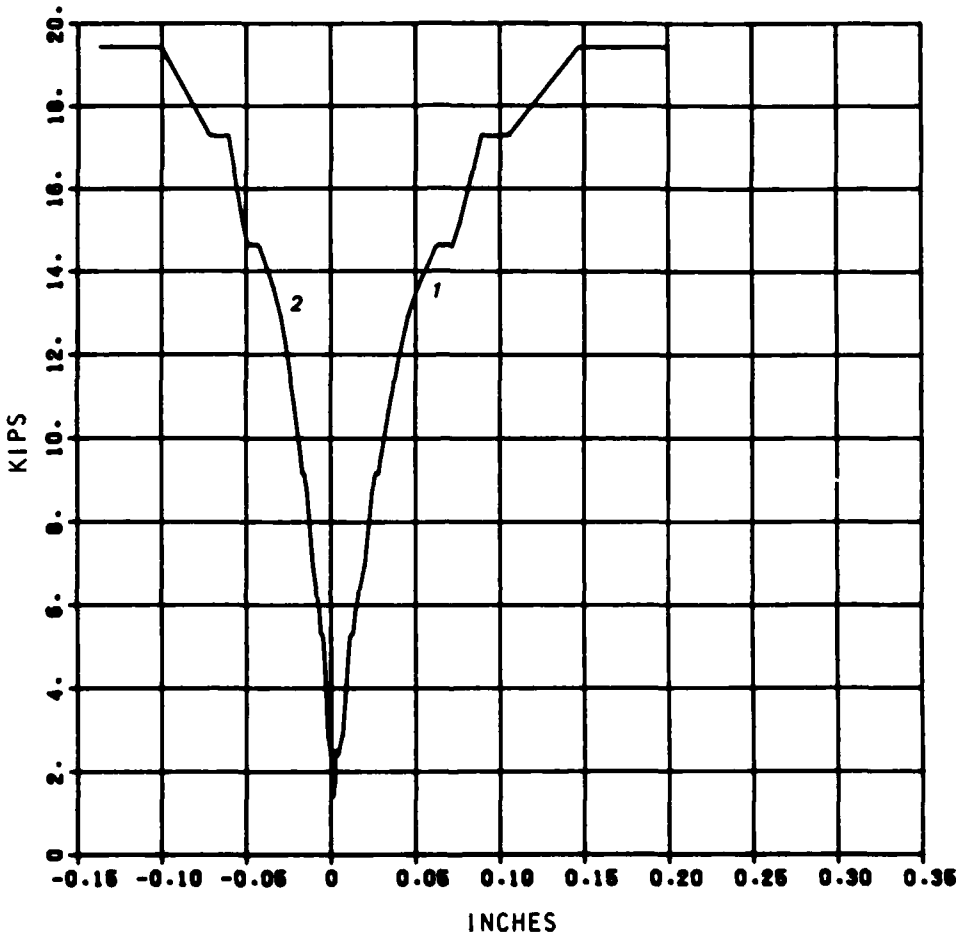

1. CROWN
2. SPRINGING LINE

R/C MODEL C52
LOAD 1 VS. STRAINS

05/10/84

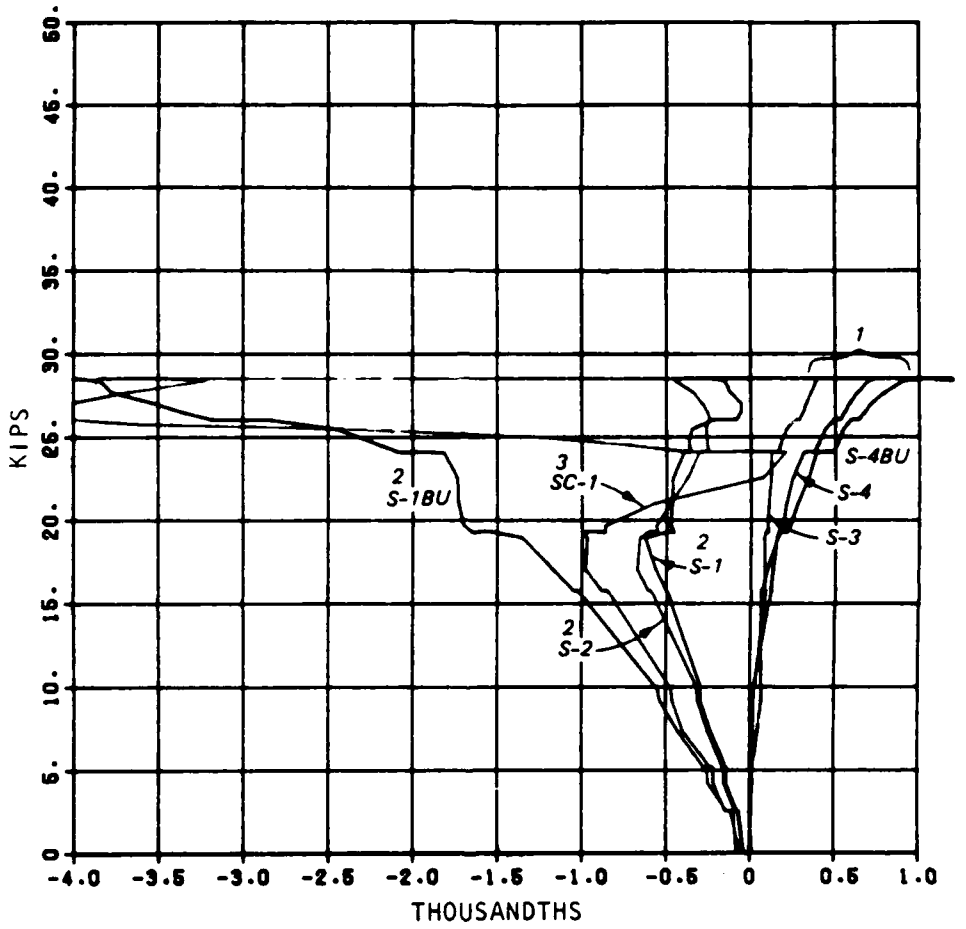

POSITIVE MOMENT
1. INTRADOS STEEL STRAIN 2. EXTRADOS STEEL STRAIN
3. EXTRADOS CONCRETE STRAIN

R/C MODEL C52
LOAD 1 VS. STRAINS

05/10/84

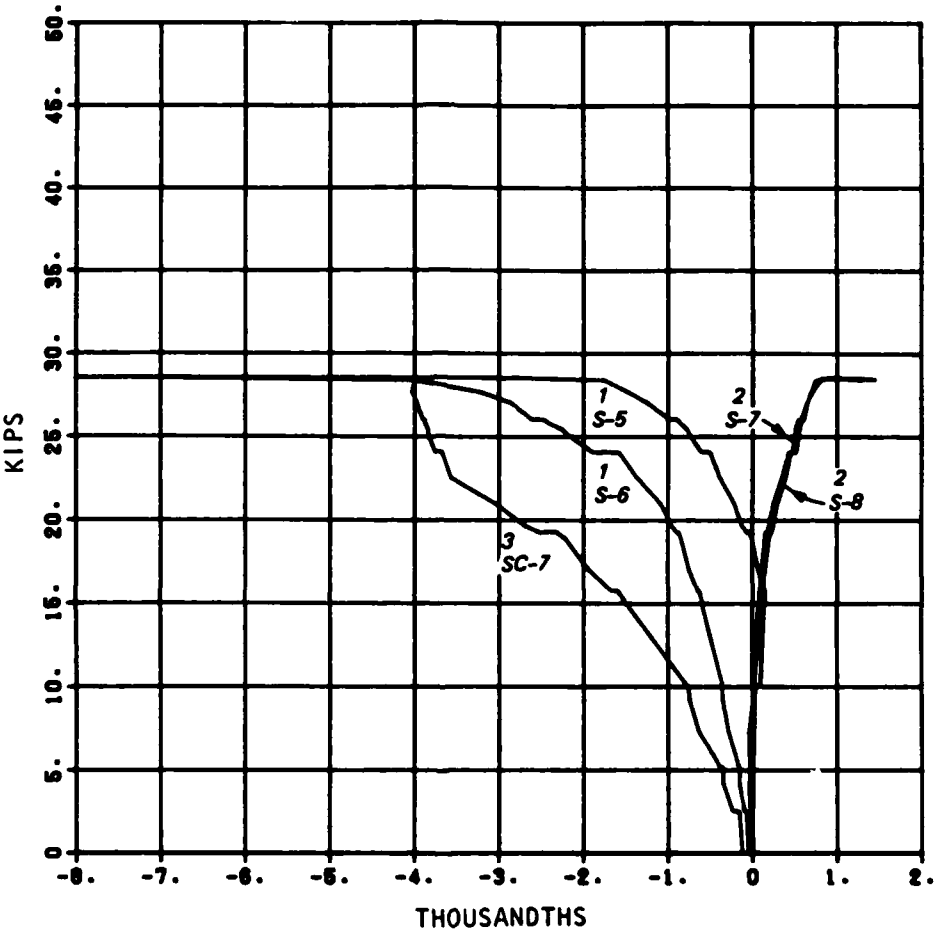

NEGATIVE MOMENT
1. INTRADOS STEEL STRAIN 2. EXTRADOS STEEL STRAIN
3. INTRADOS CONCRETE STRAIN

R/C MODEL C52
LOAD 1 VS. DEFL.

05/10/84

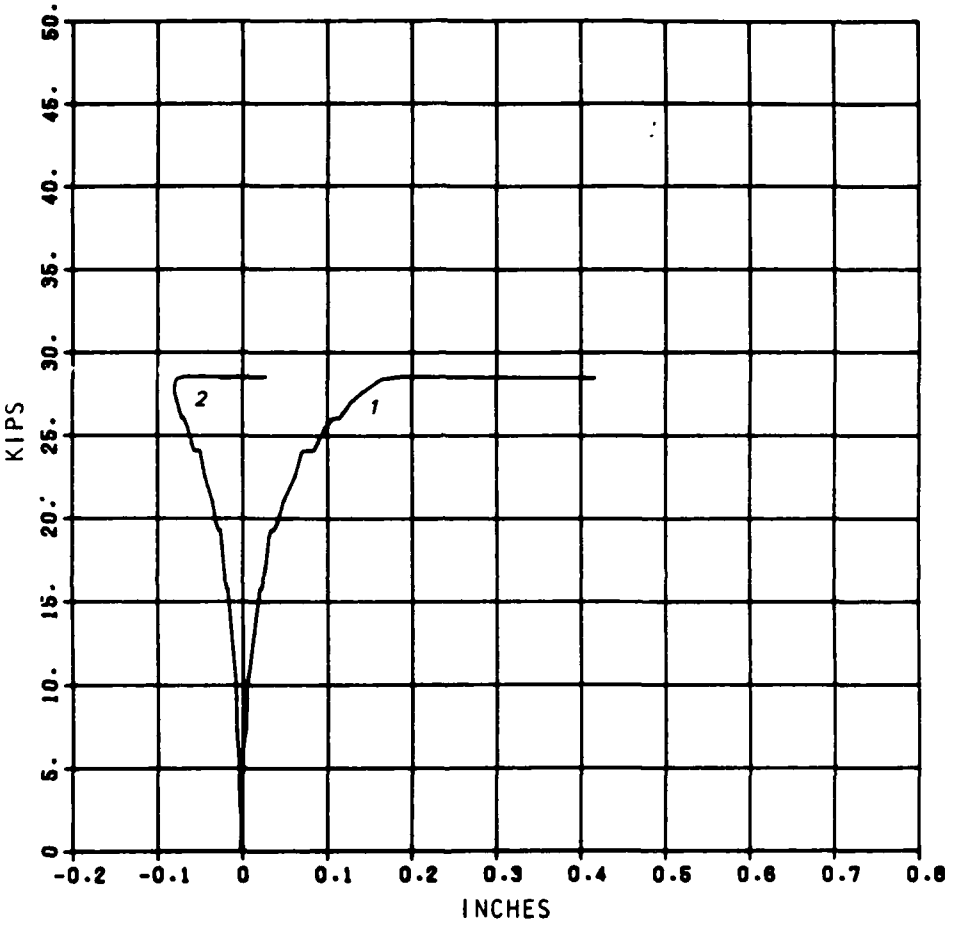

1. CROWN
2. SPRINGING LINE

R/C MODEL C53
LOAD 1 VS. STRAINS

05/10/84

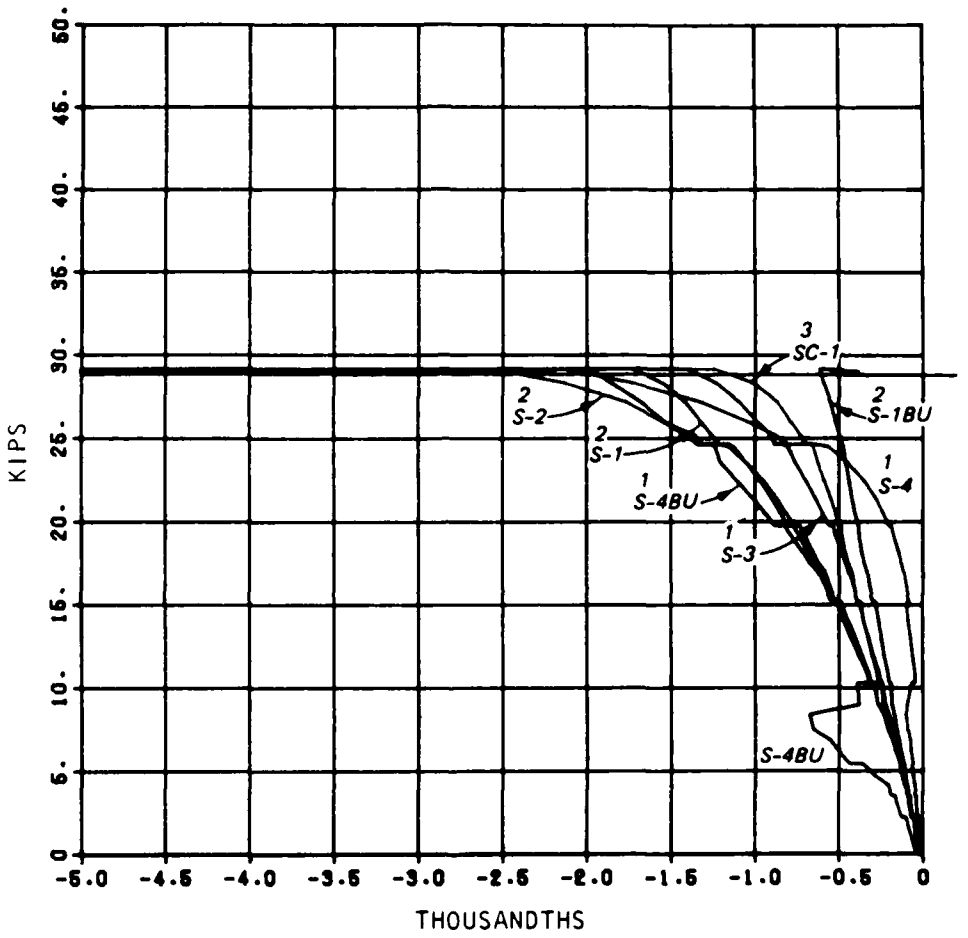

POSITIVE MOMENT
1. INTRADOS STEEL STRAIN 2. EXTRADOS STEEL STRAIN
3. EXTRADOS CONCRETE STRAIN

R/C MODEL C53
LOAD 1 VS. STRAINS

05/10/84

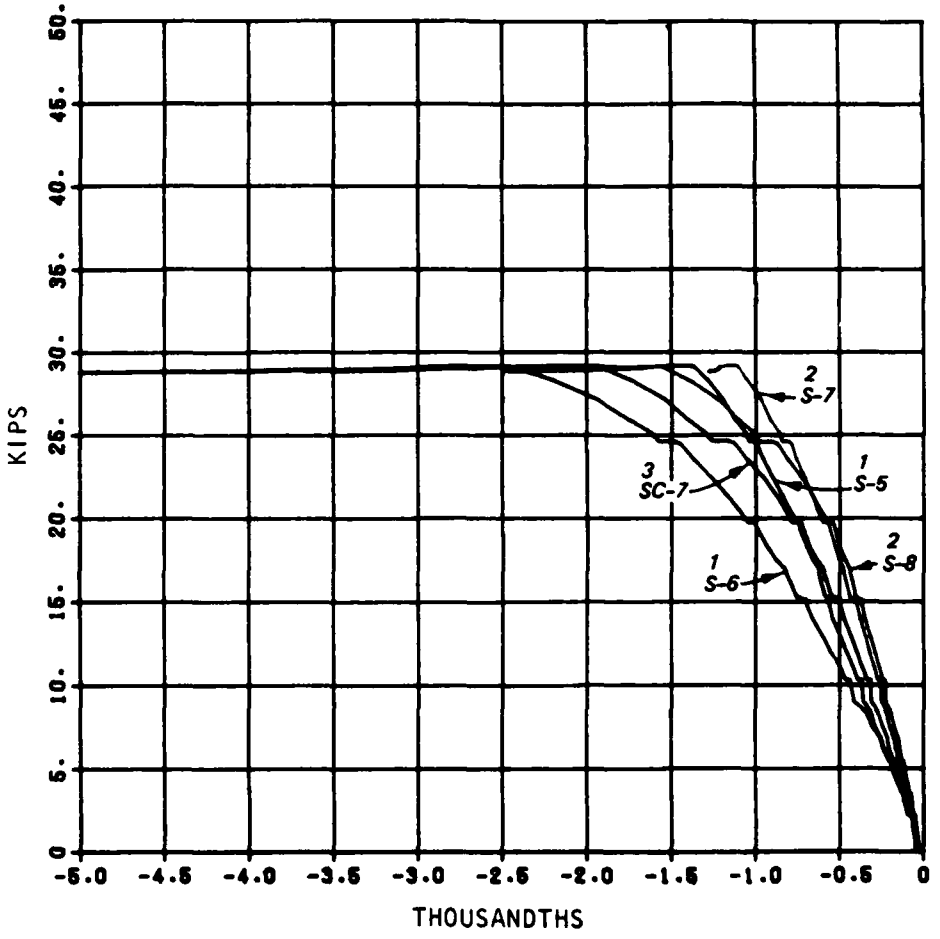

NEGATIVE MOMENT
1. INTRADOS STEEL STRAIN 2. EXTRADOS STEEL STRAIN
3. INTRADOS CONCRETE STRAIN

R/C MODEL C53
LOAD 1 VS. DEFL.

05/10/84

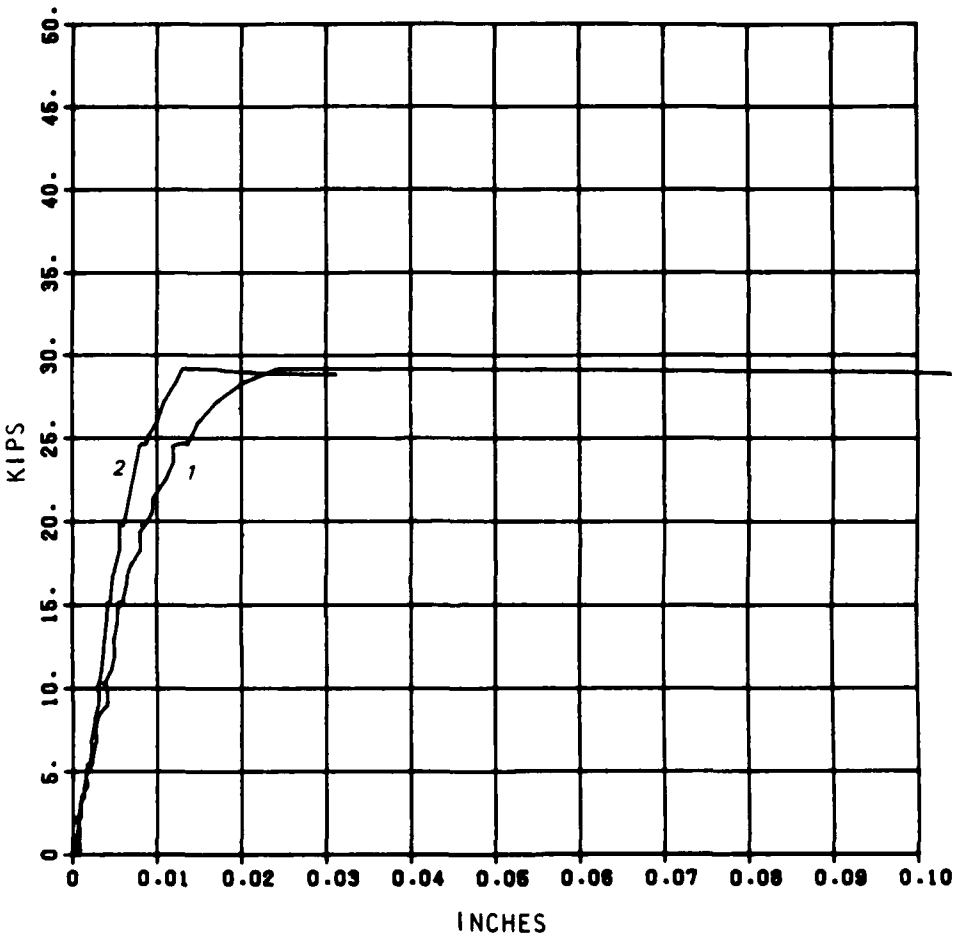

1. CROWN
2. SPRINGING LINE

R/C MODEL C54
LOAD 1 VS. STRAINS

06/10/84

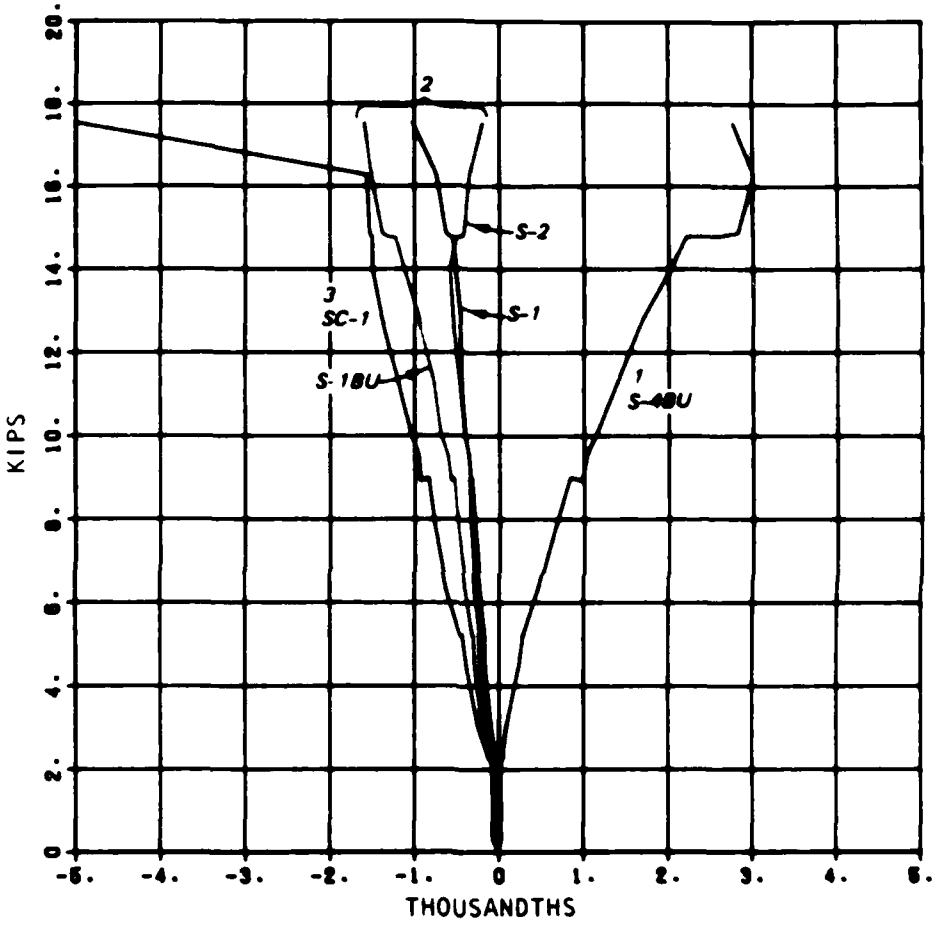

POSITIVE MOMENT
1. INTRADOS STEEL STRAIN 2. EXTRADOS STEEL STRAIN
3. EXTRADOS CONCRETE STRAIN

R/C MODEL C54
LOAD 1 VS. STRAINS

06/18/84

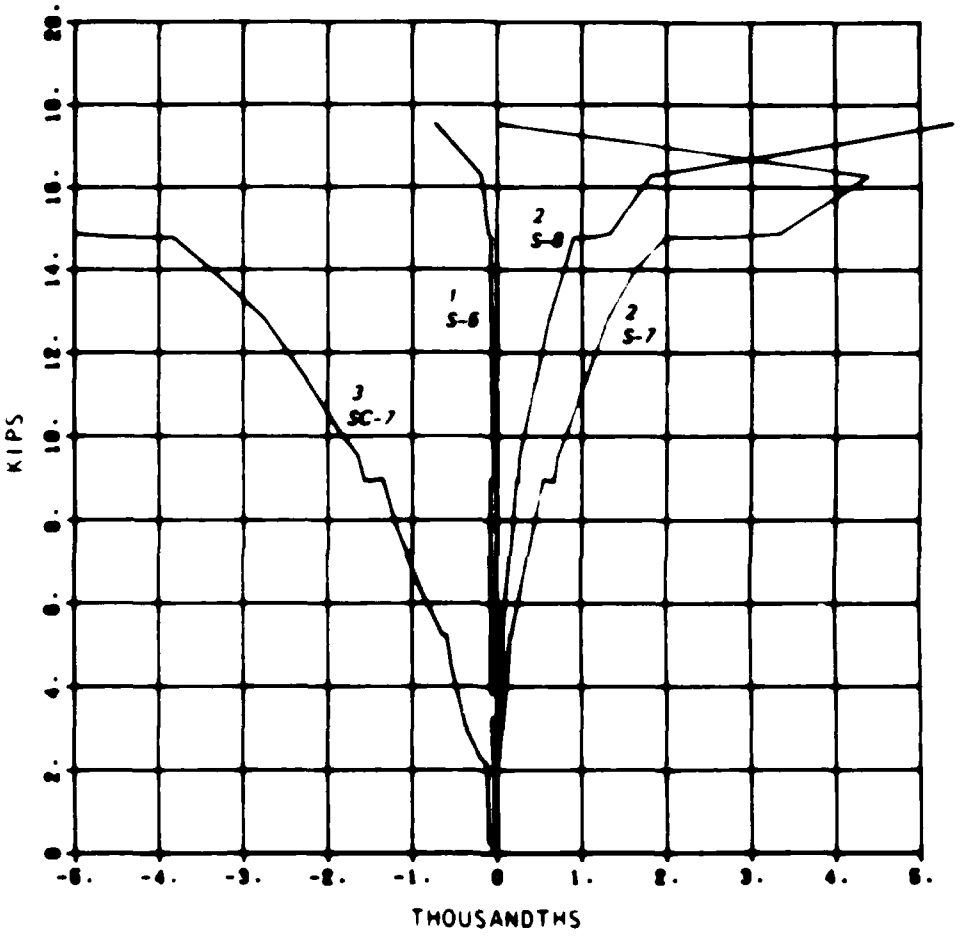

NEGATIVE MOMENT
1. INTRADOS STEEL STRAIN
2. EXTRADOS STEEL STRAIN 3. INTRADOS CONCRETE STR

R/C MODEL C54
LOAD 1 VS. DEFL.

06/10/84

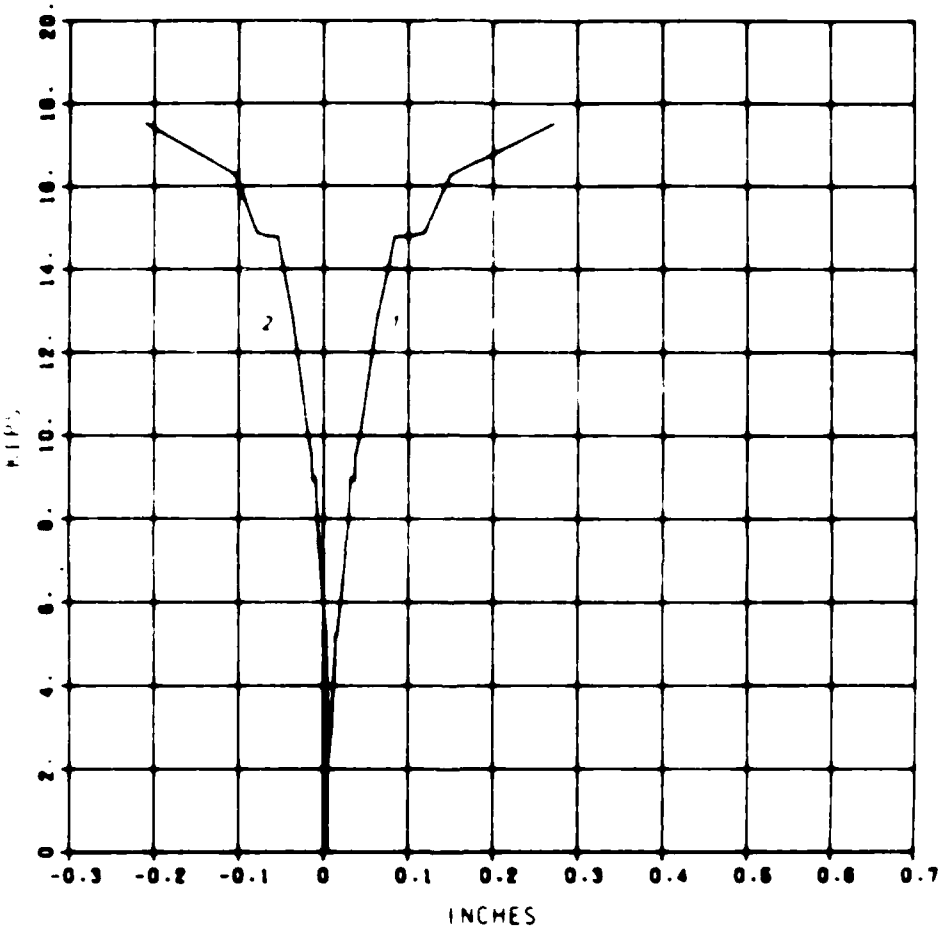

1. CROWN
2. SPRINGING LINE

R/C MODEL C61
LOAD 1 VS. STRAINS

08/10/84

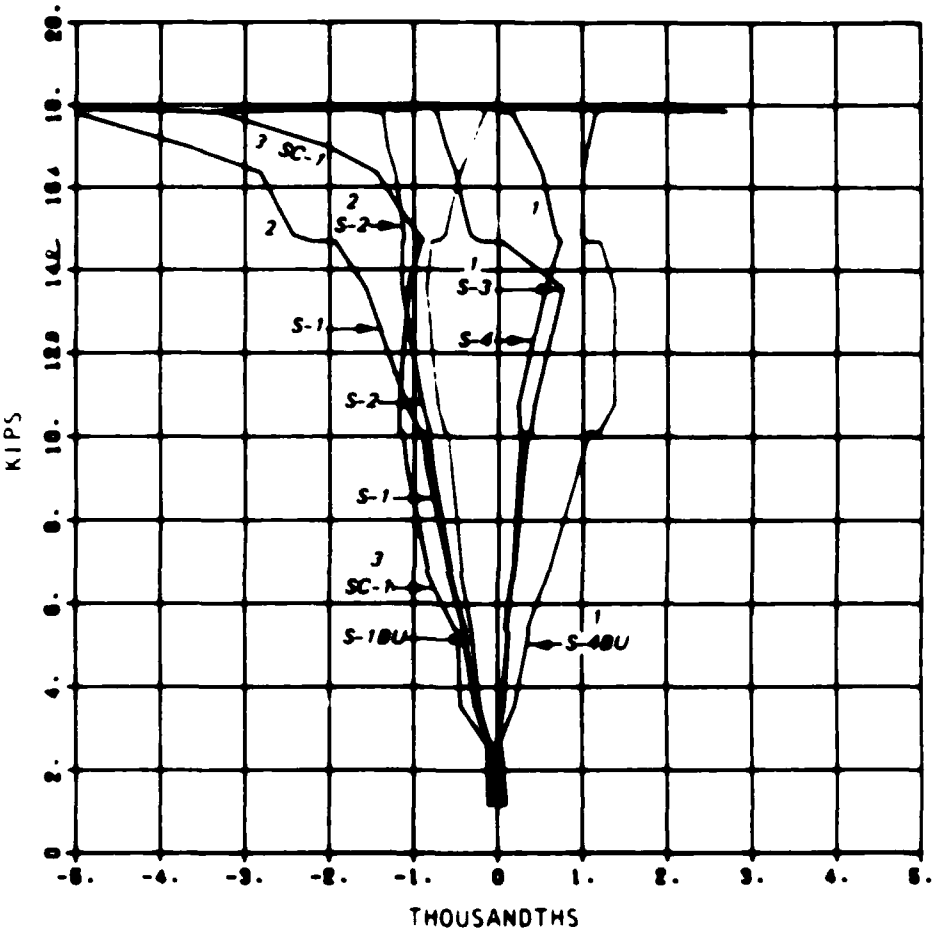

POSITIVE MOMENT
1. INTRADOS STEEL STRAIN 2. EXTRADOS STEEL STRAIN
3. EXTRADOS CONCRETE STRAIN

R/C MODEL C61
LOAD 1 VS. STRAINS

05/10/84

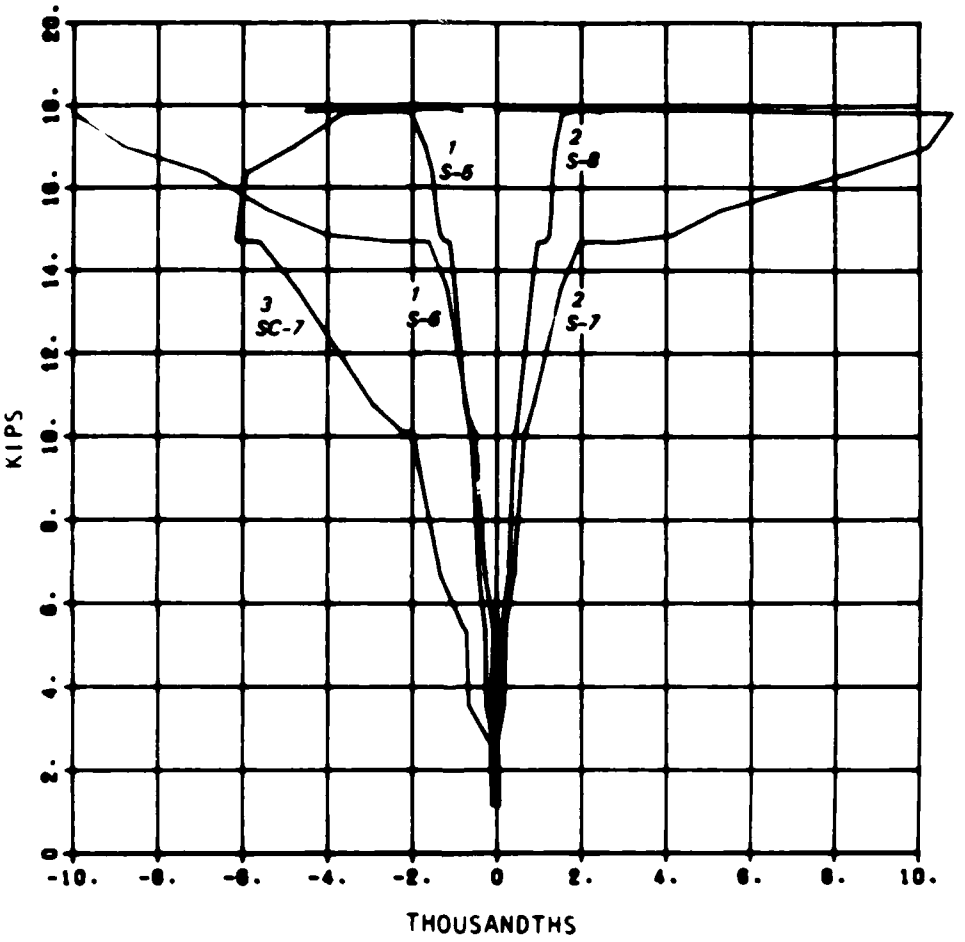

NEGATIVE MOMENT
1. INTRADOS STEEL STRAIN 2. EXTRADOS STEEL STRAIN
3. INTRADOS CONCRETE STRAIN

R/C MODEL C61
LOAD 1 VS. DEFL.

06/10/84

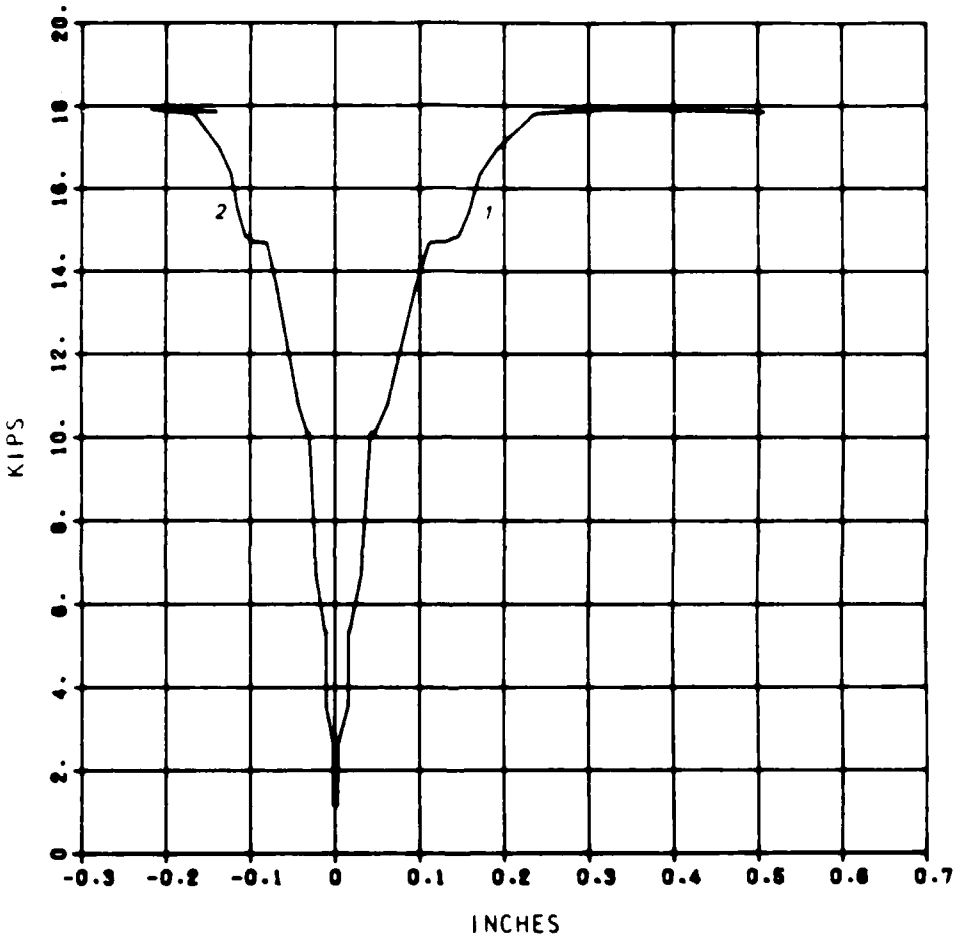

1. CROWN
2. SPRINGING LINE

R/C MODEL C62
LOAD 1 VS. STRAINS

06/10/84

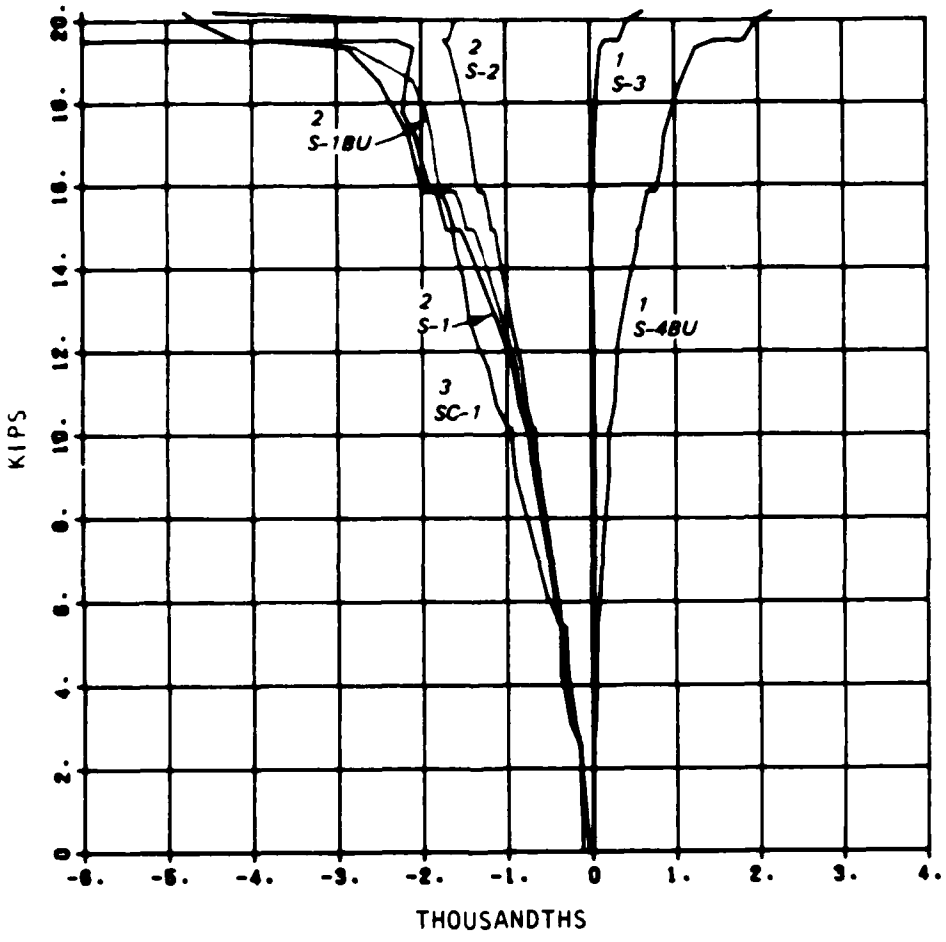

POSITIVE MOMENT
1. INTRADOS STEEL STRAIN 2. EXTRADOS STEEL STRAIN
3. EXTRADOS CONCRETE STRAIN

R/C MODEL C62
LOAD 1 VS. STRAINS

05/10/84

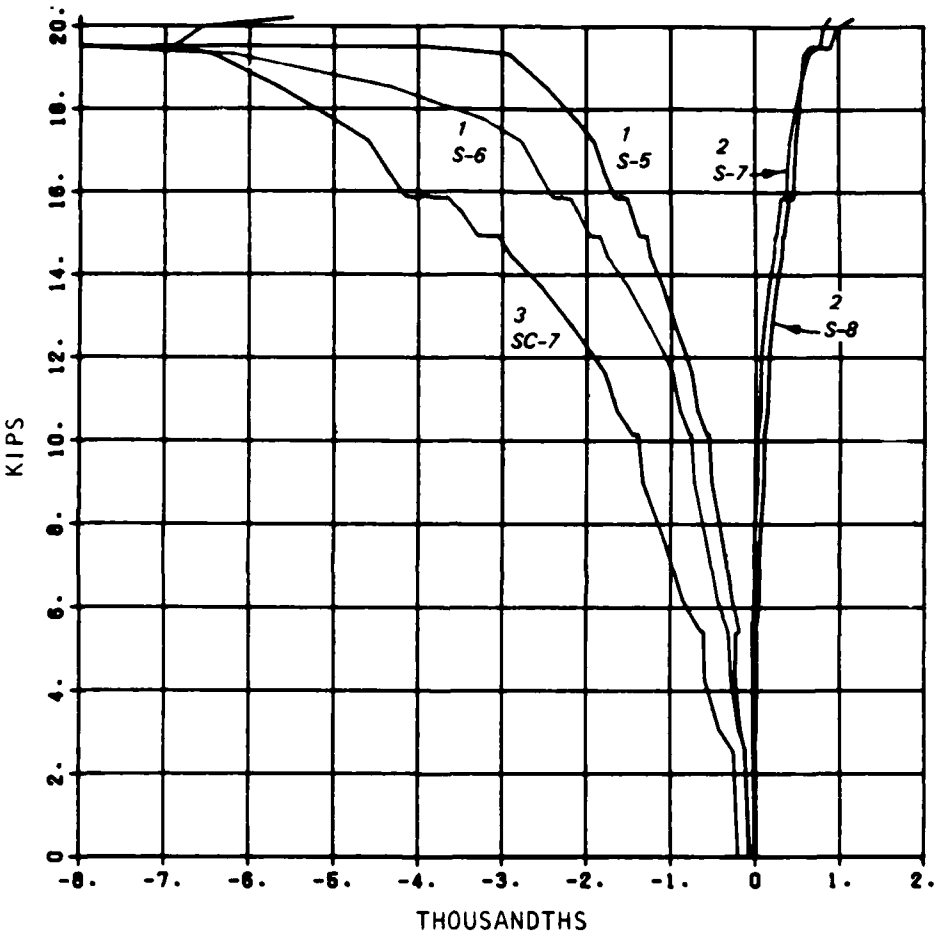

NEGATIVE MOMENT
1. INTRADOS STEEL STRAIN 2. EXTRADOS STEEL STRAIN
3. INTRADOS CONCRETE STRAIN

R/C MODEL C62
LOAD 1 VS. DEFL.

05/10/84

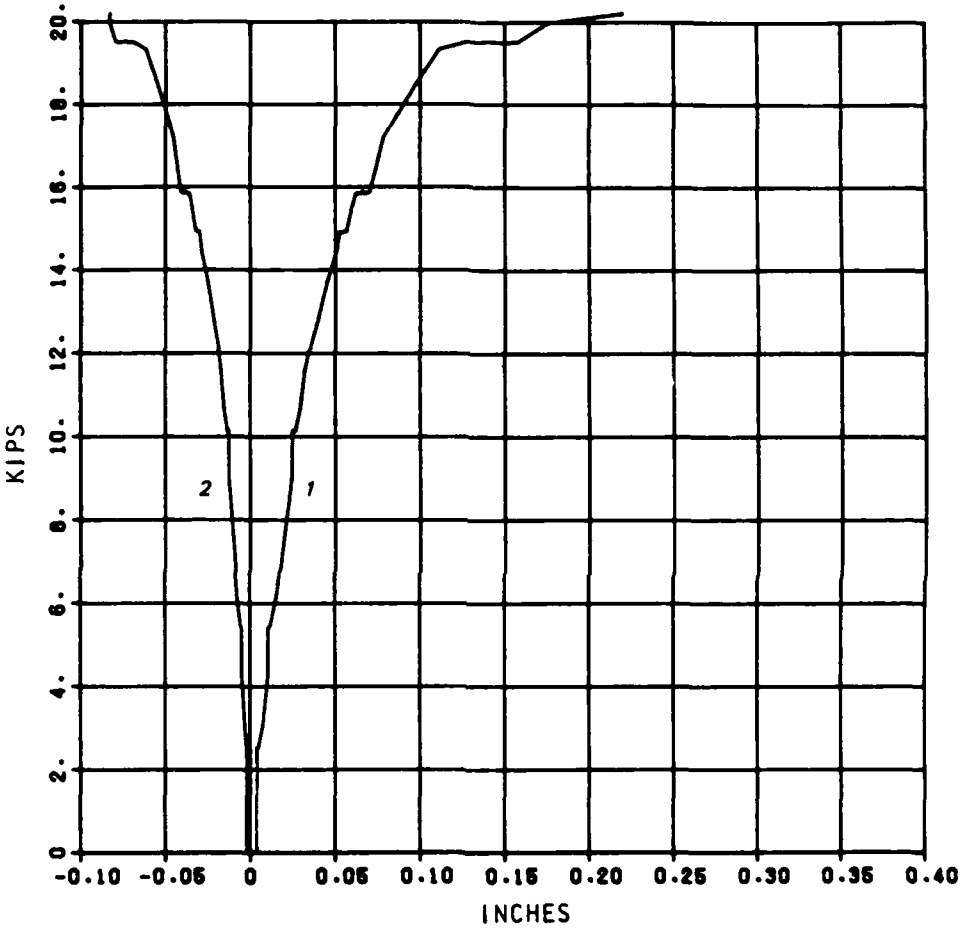

1. CROWN
2. SPRINGING LINE

R/C MODEL C71
LOAD 1 VS. STRAINS

05/10/84

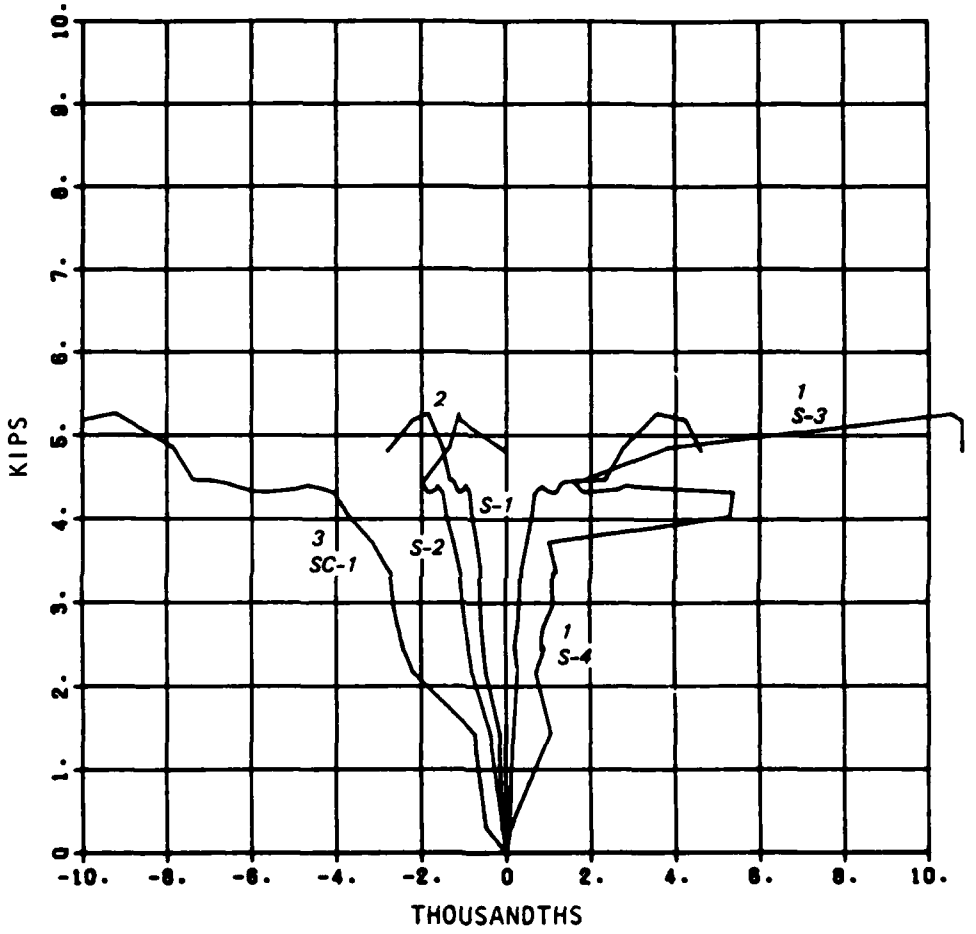

POSITIVE MOMENT
1. INTRADOS STEEL STRAIN 2. EXTRADOS STEEL STRAIN
3. EXTRADOS CONCRETE STRAIN

R/C MODEL C71
LOAD 1 VS. STRAINS

05/10/84

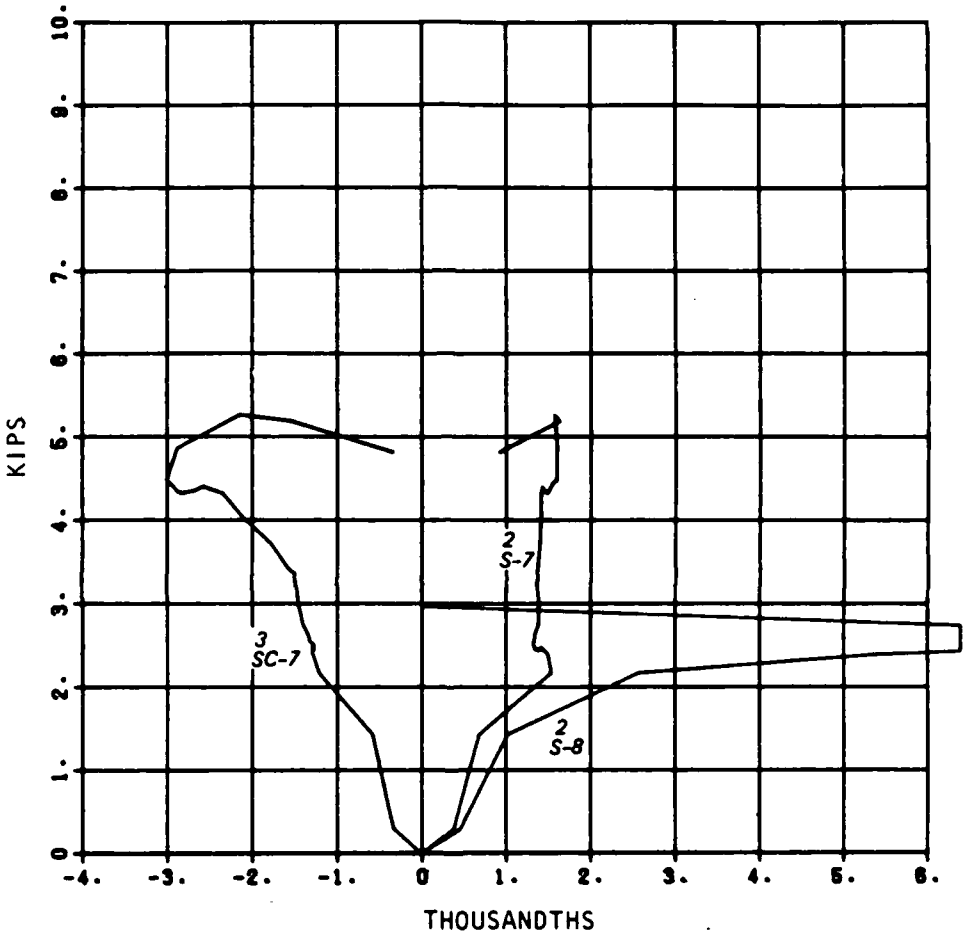

NEGATIVE MOMENT
INTRADOS STEEL STRAIN GAGES NO GOOD
2. EXTRADOS STEEL STRAIN 3. INTRADOS CONCRETE STR

R/C MODEL C71
LOAD 1 VS. DEFL.

05/10/84

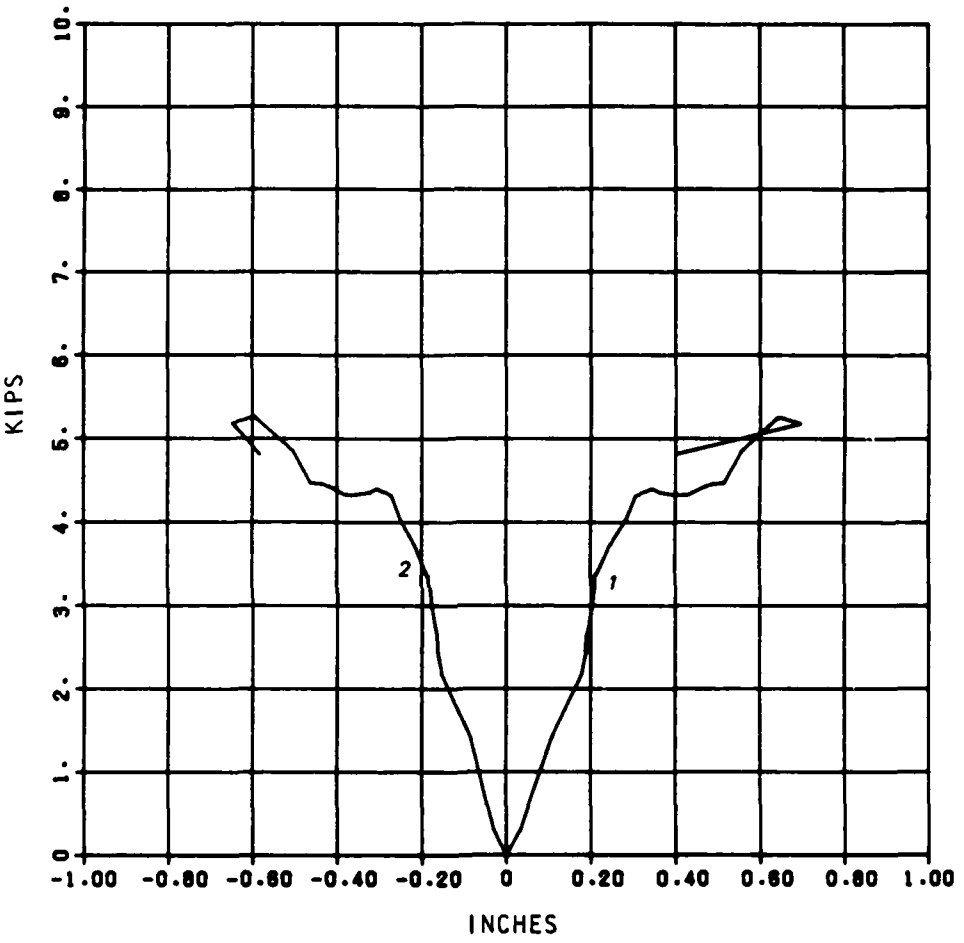

1. CROWN
2. SPRINGING LINE

R/C MODEL C81
LOAD 1 VS. STRAINS

05/10/84

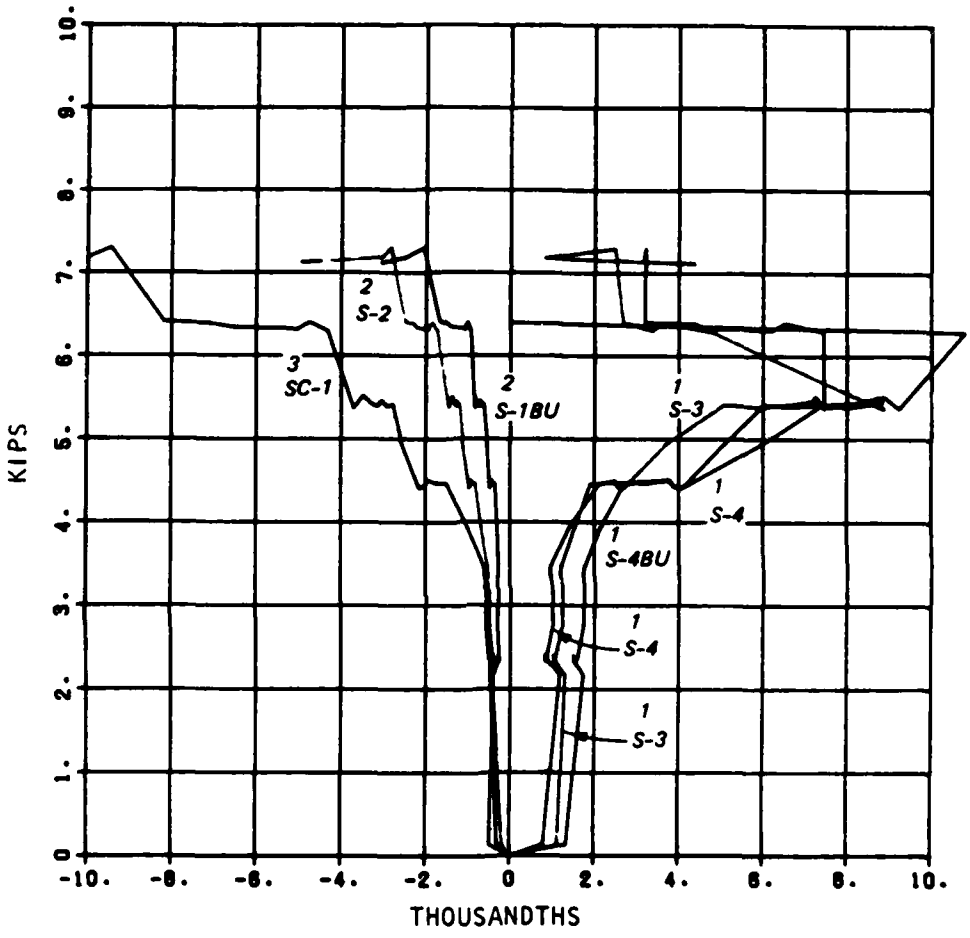

POSITIVE MOMENT
1. INTRADOS STEEL STRAIN 2. EXTRADOS STEEL STRAIN
3. EXTRADOS CONCRETE STRAIN

R/C MODEL C81
LOAD 1 VS. STRAINS

05/10/84

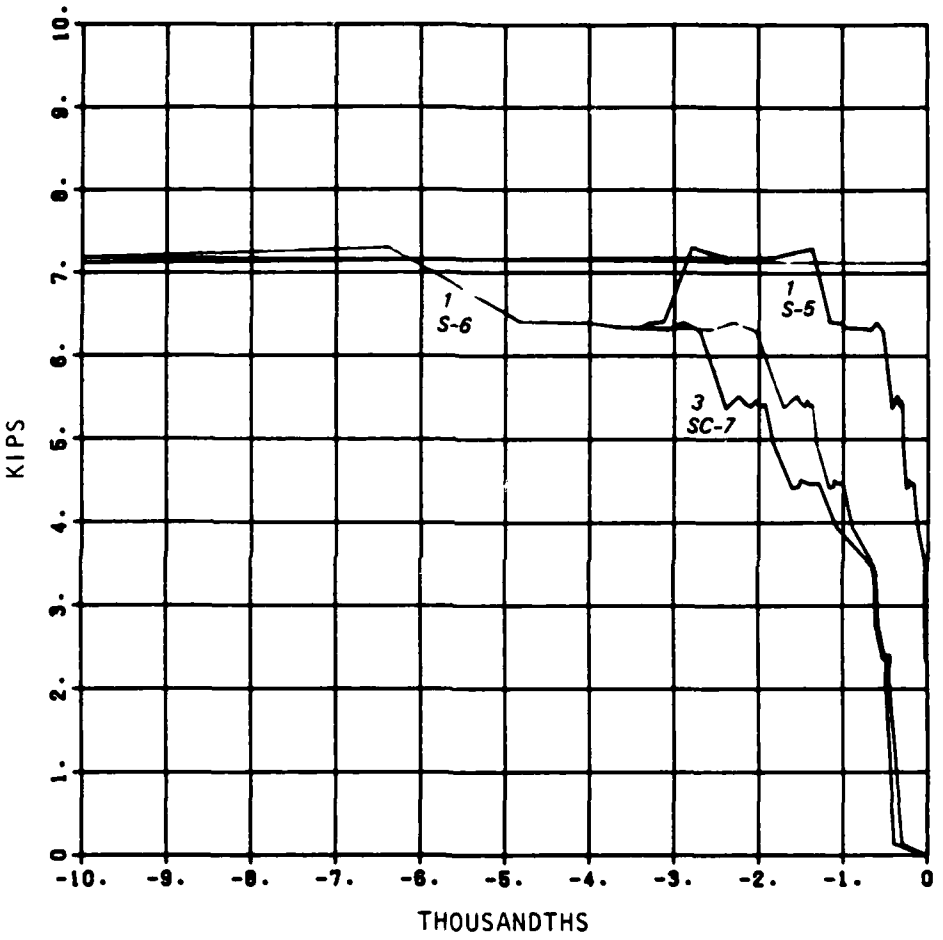

NEGATIVE MOMENT
EXTRADOS STEEL STRAIN GAGES NO GOOD
1. INTRADOS STEEL STRAIN 3. INTRADOS CONCRETE STRA

R/C MODEL C81
LOAD 1 VS. DEFL.

06/10/84

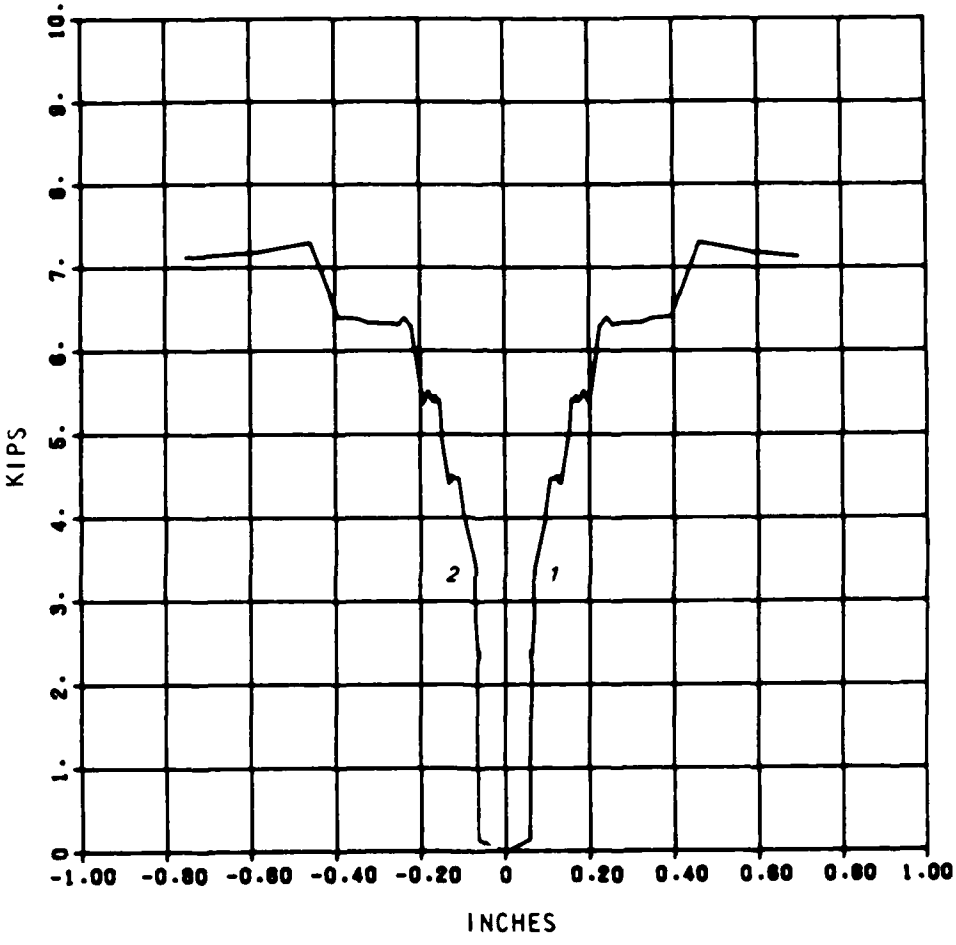

1. CROWN
2. SPRINGING LINE

R/C MODEL C82
LOAD 1 VS. STRAINS

05/05/84

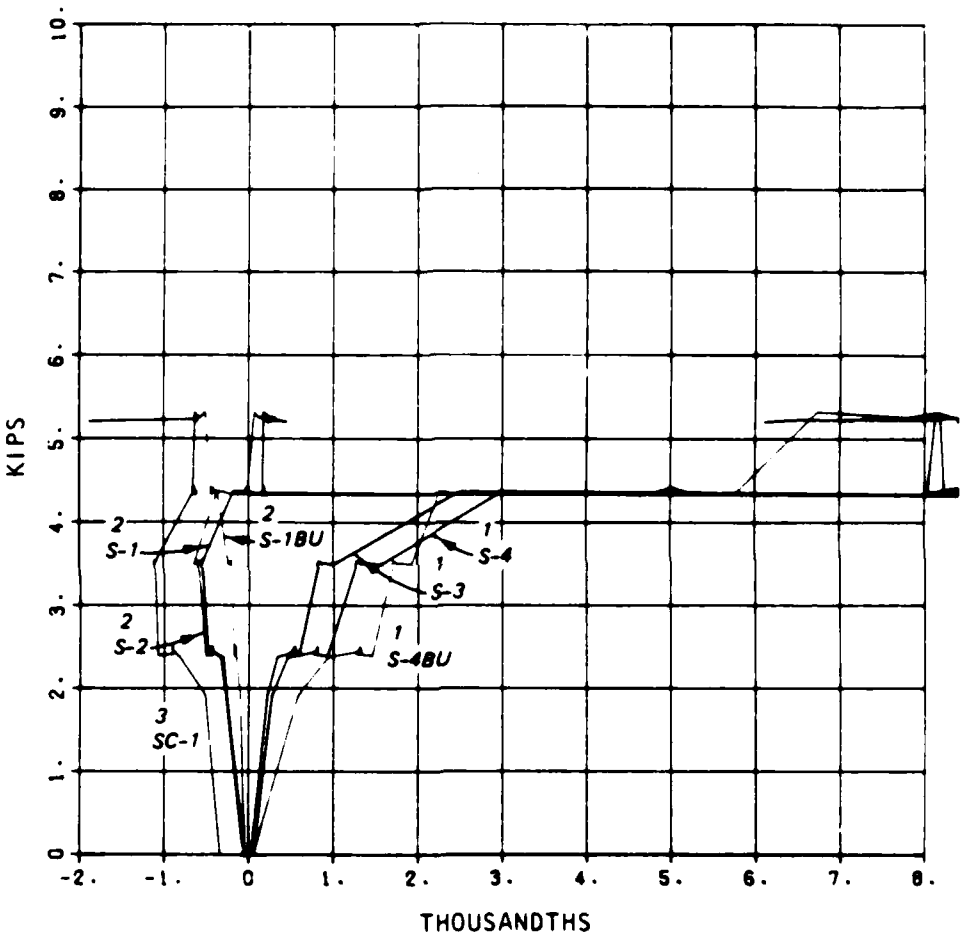

POSITIVE MOMENT
1. INTRADOS STEEL STRAIN 2. EXTRADOS STEEL STRAIN
3. EXTRADOS CONCRETE STRAIN

R/C MODEL C82
LOAD 1 VS. STRAINS

05/05/84

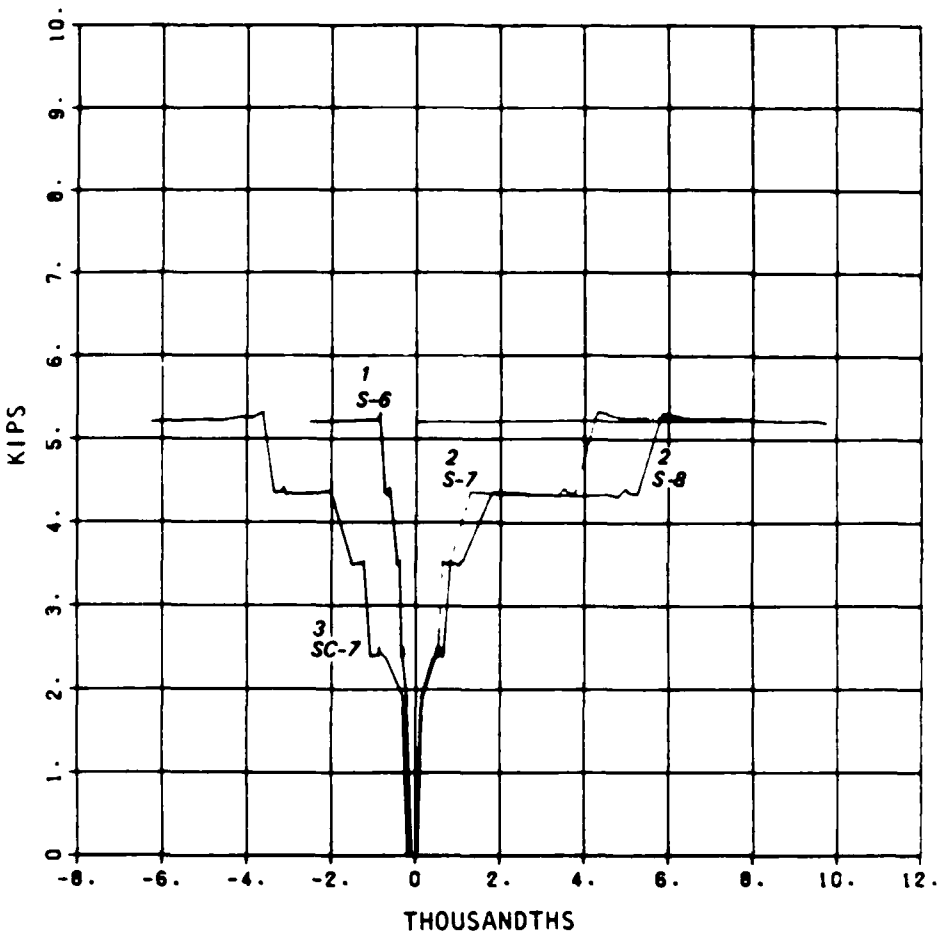

NEGATIVE MOMENT
1.INTRADOS STEEL STRAIN 2.EXTRADOS STEEL STRAIN
3. INTRADOS CONCRETE STRAIN

R/C MODEL C82
LOAD 1 VS. DEFL.

05/05/84

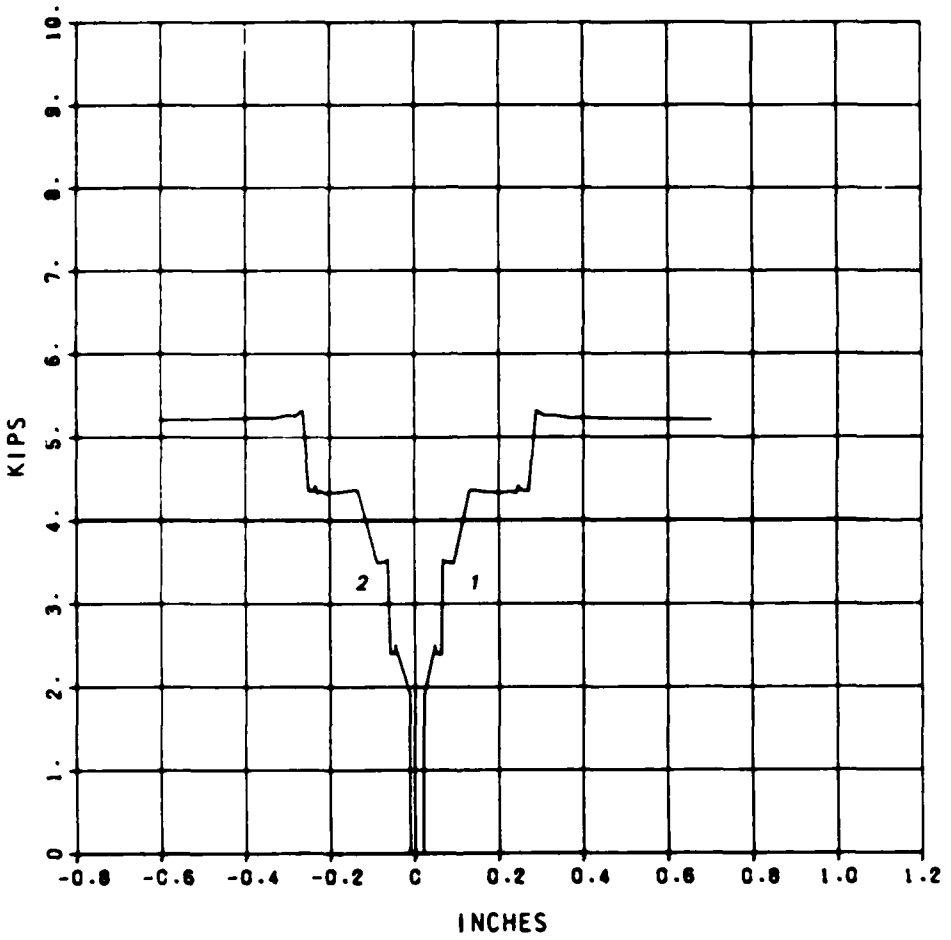

1. CROWN
2. SPRINGING LINE

R/C MODEL C83
LOAD 1 VS. STRAINS

05/05/84

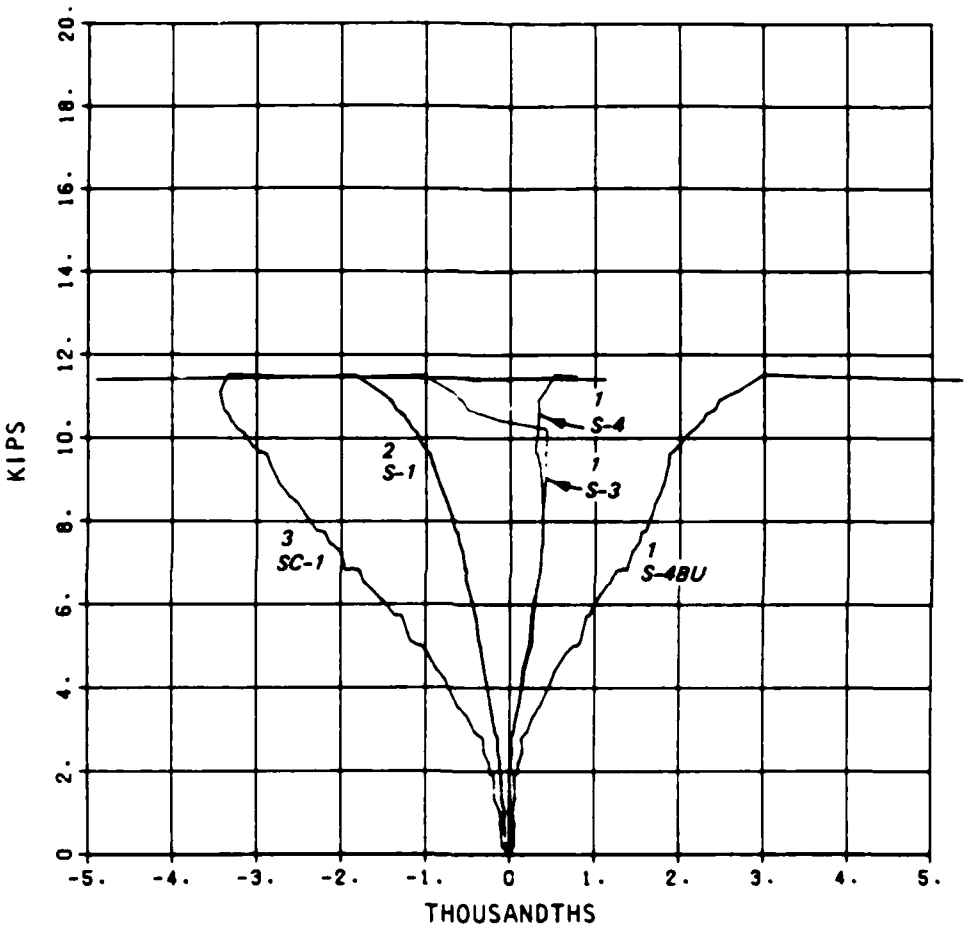

POSITIVE MOMENT
1. INTRADOS STEEL STRAIN 2. EXTRADOS STEEL STRAIN
3. EXTRADOS CONCRETE STRAIN

R/C MODEL C83
LOAD 1 VS. STRAINS

05/05/84

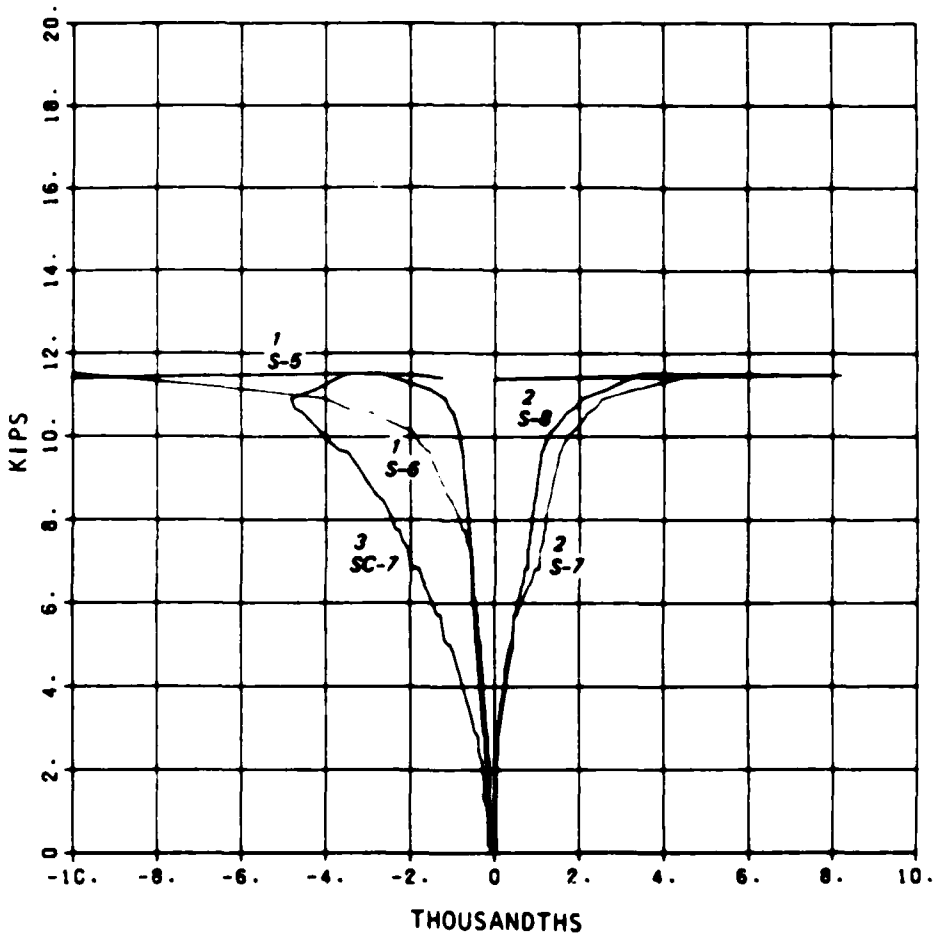

NEGATIVE MOMENT
1. INTRADOS STEEL STRAIN 2. EXTRADOS STEEL STRAIN
3. INTRADOS CONCRETE STRAIN

R/C MODEL C83
LOAD 1 VS. DEFL.

05/05/84

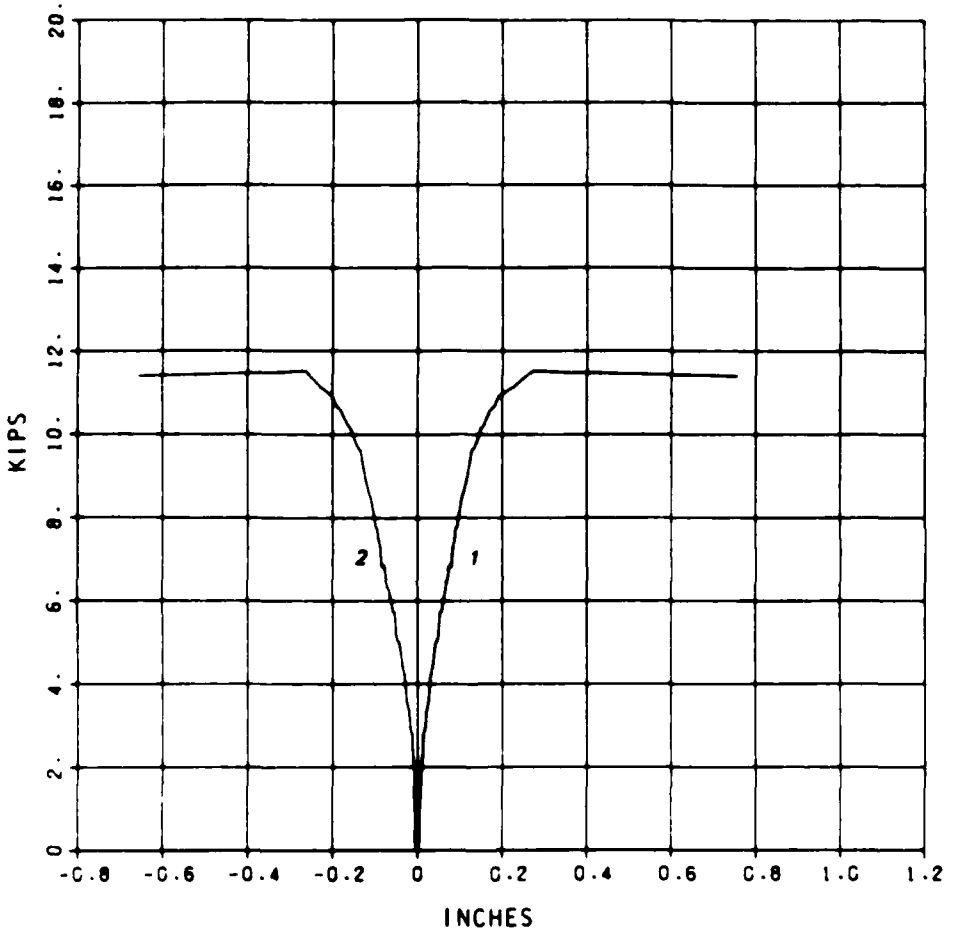

1. CROWN
2. SPRINGING LINE

R/C MODEL C91
LOAD 1 VS. STRAINS

05/05/84

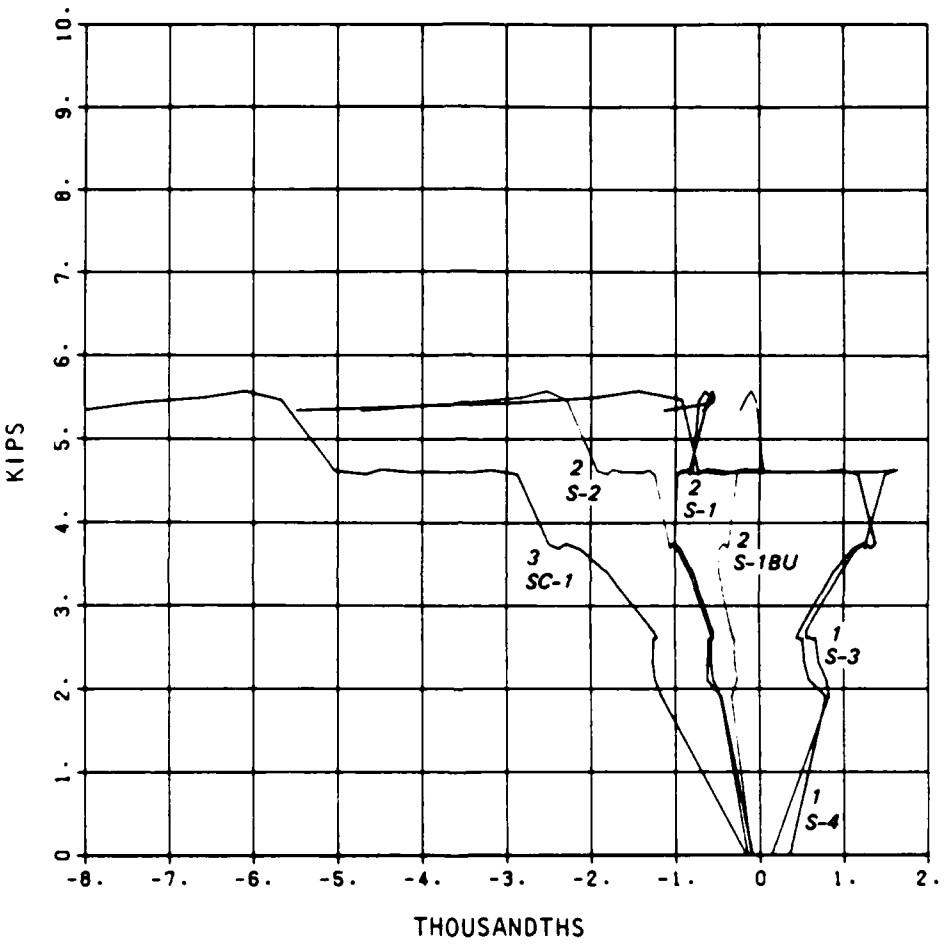

POSITIVE MOMENT
1. INTRADOS STEEL STRAIN 2. EXTRADOS STEEL STRAIN
3. EXTRADOS CONCRETE STRAIN

R/C MODEL C91
LOAD 1 VS. STRAINS

05/05/84

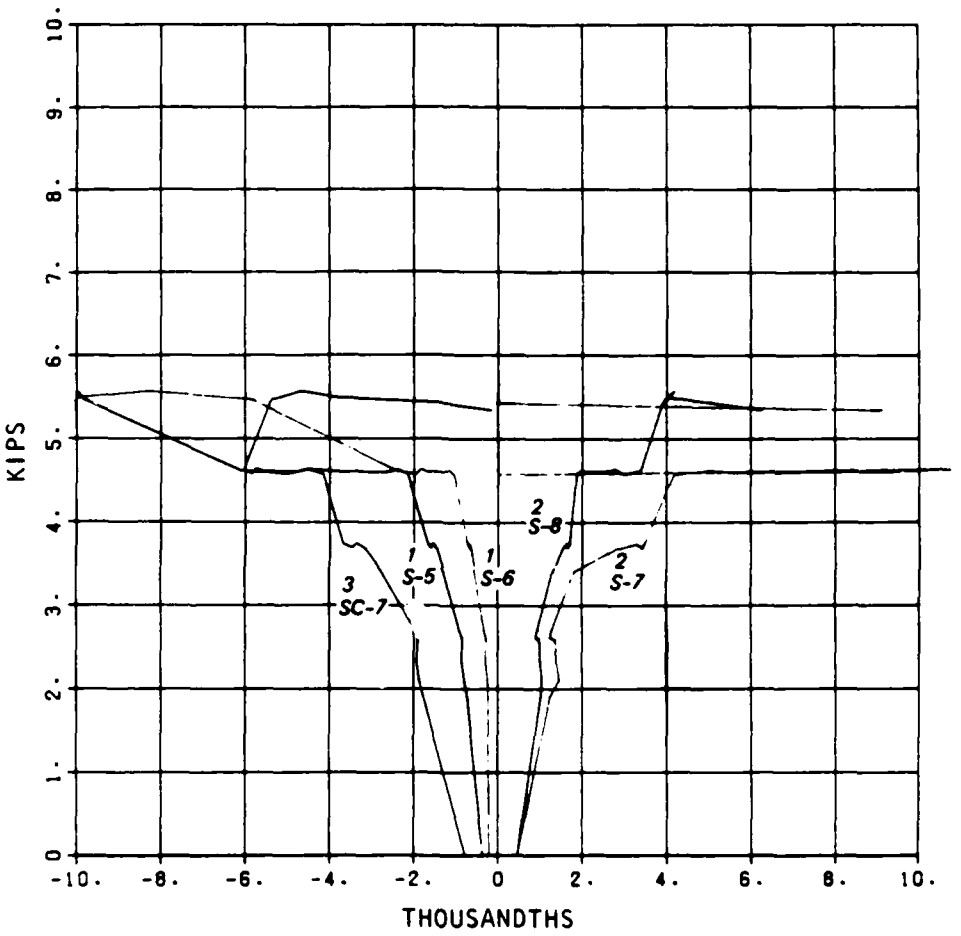

NEGATIVE MOMENT
1. INTRADOS STEEL STRAIN 2. EXTRADOS STEEL STRAIN
3. INTRADOS CONCRETE STRAIN

R/C MODEL C91
LOAD 1 VS. DEFL.

05/05/84

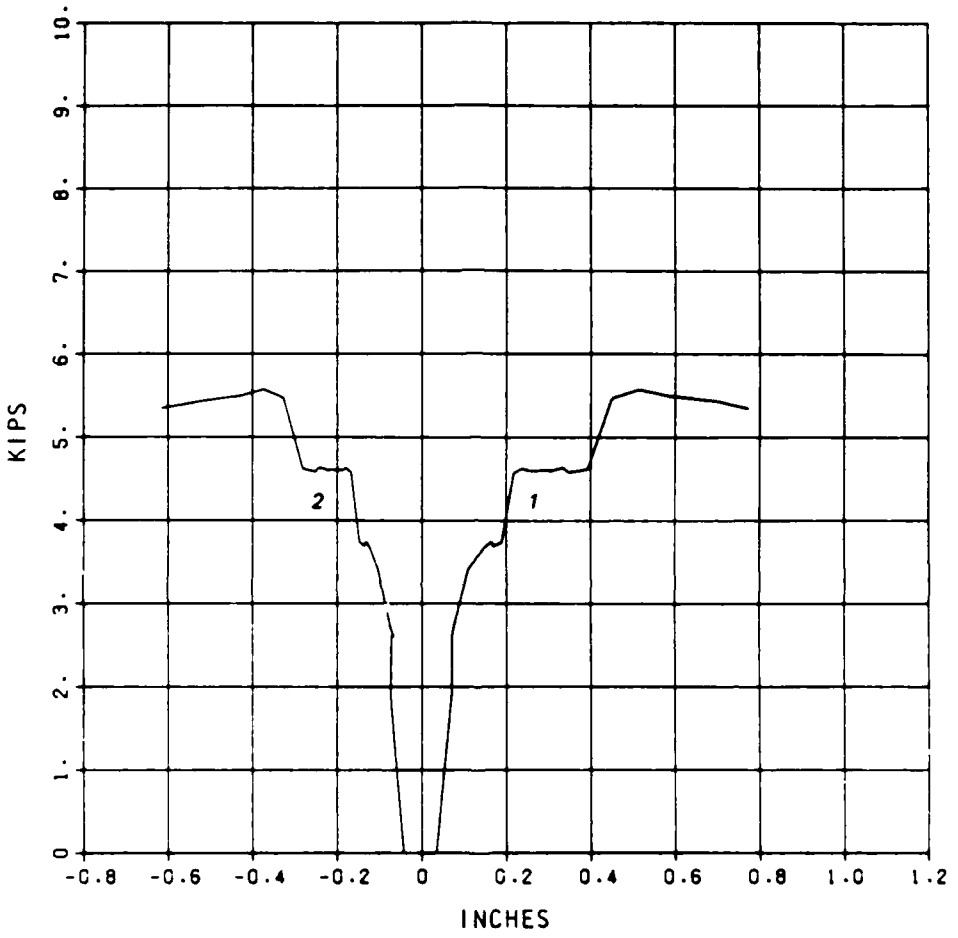

1. CROWN
2. SPRINGING LINE

APPENDIX E

STRAIN DISTRIBUTIONS

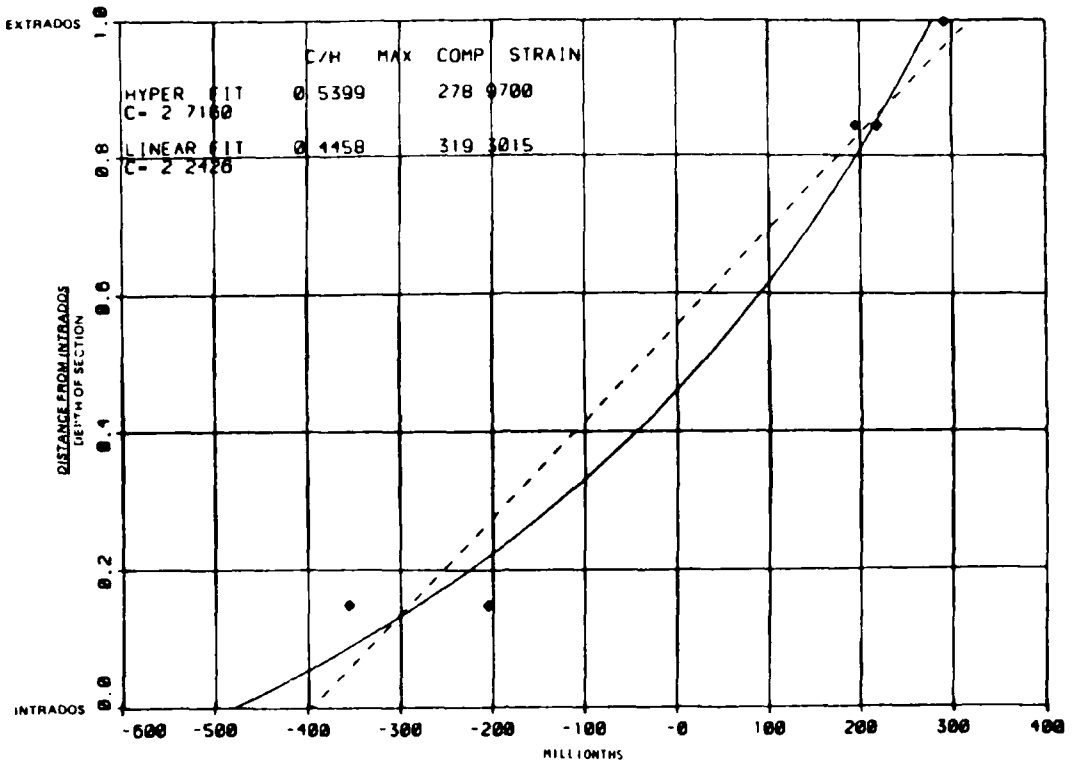

Model C1-1 crown, 10.1 kips

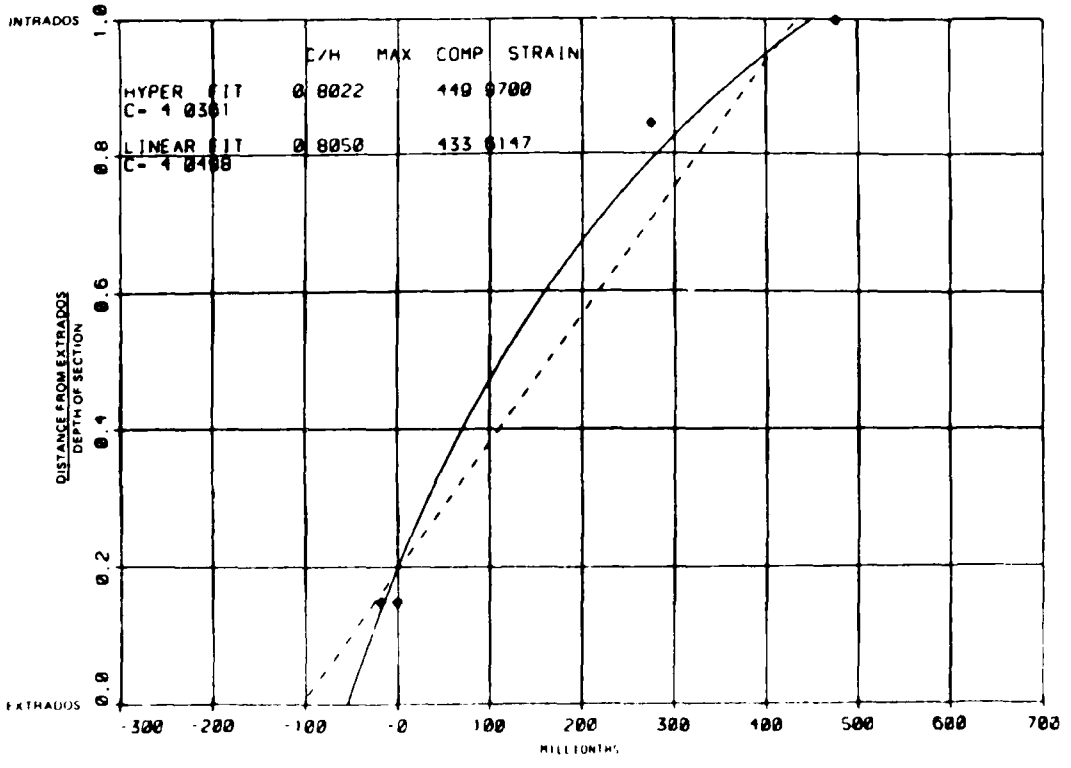

Model C1-1 springing line, 10.1 kips

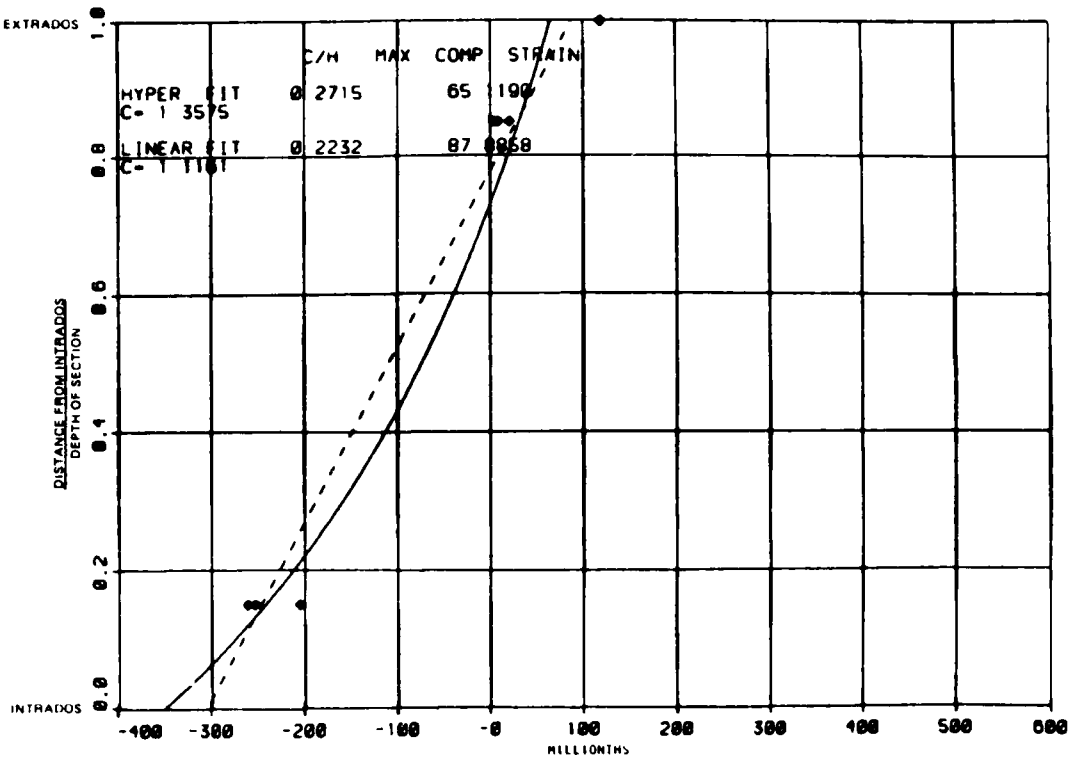

Model C2-1 crown, 9.4 kips

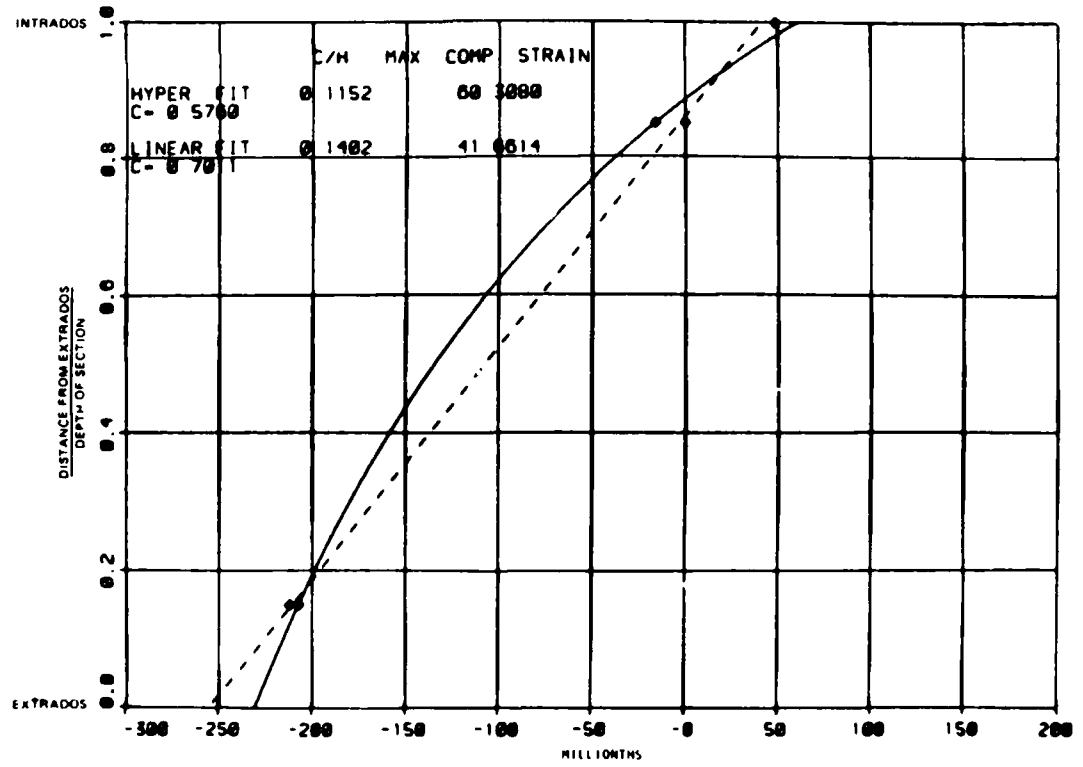

Model C2-1 springing line, 9.4 kips

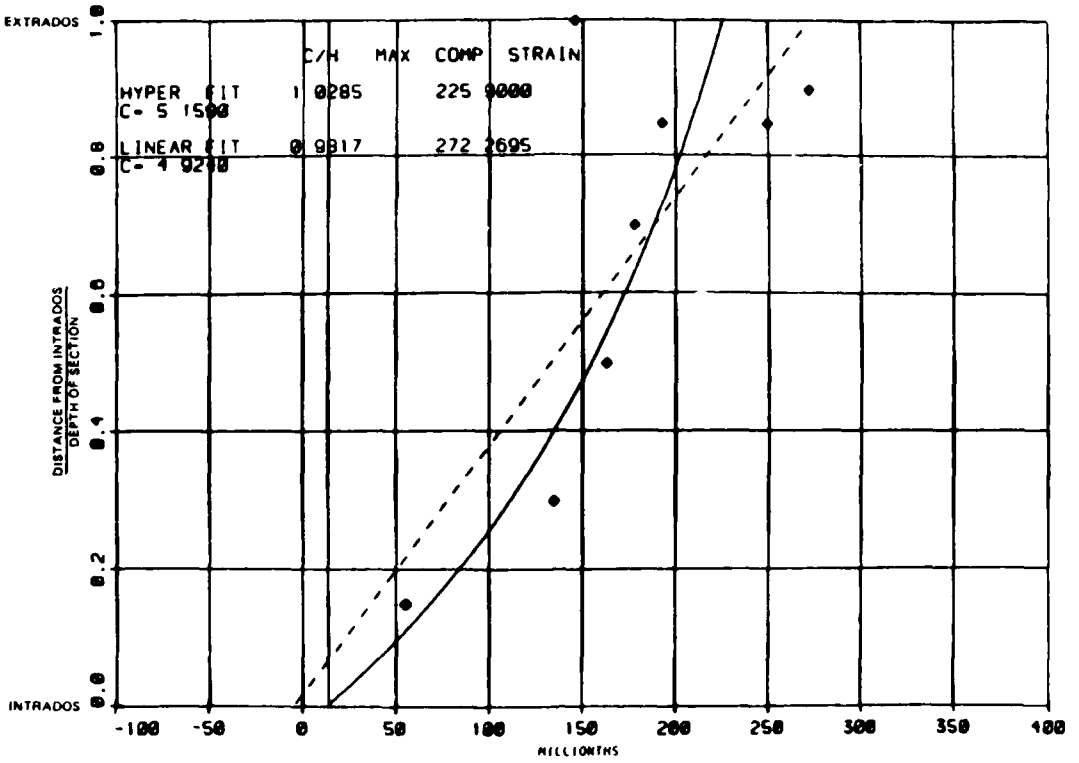

Model C2-2 crown, 10.0 kips

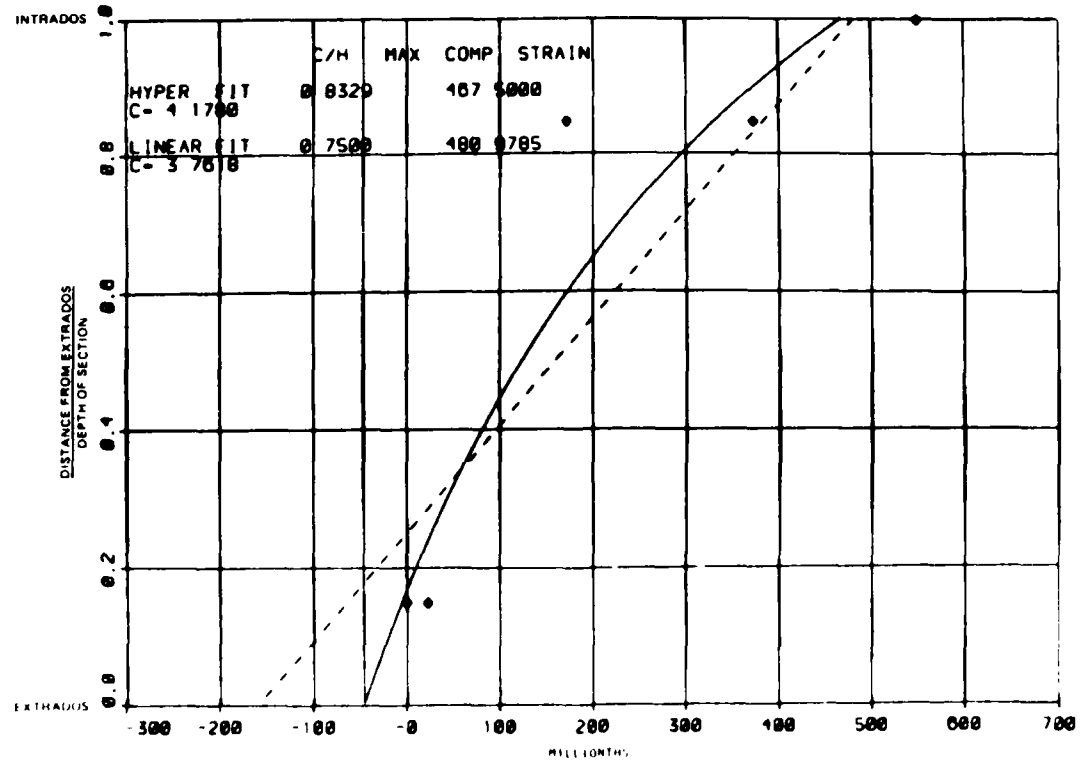

Model C2-2 springing line, 10.0 kips

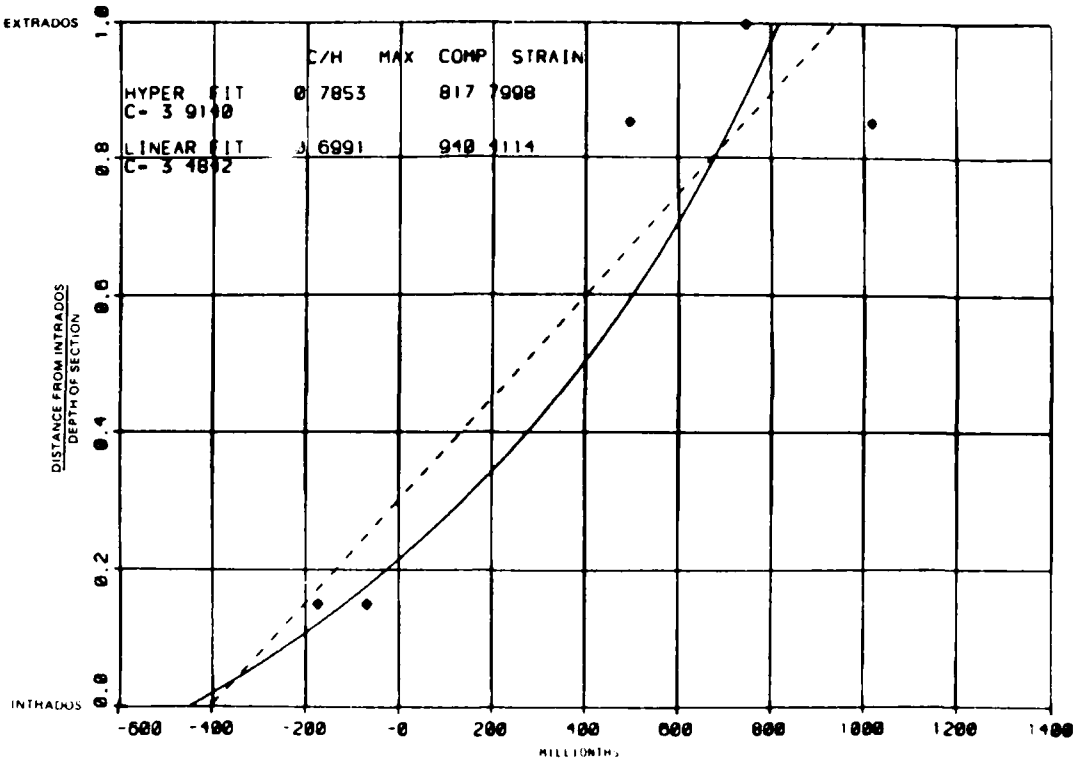

Model C2-3 crown, 24.3 kips

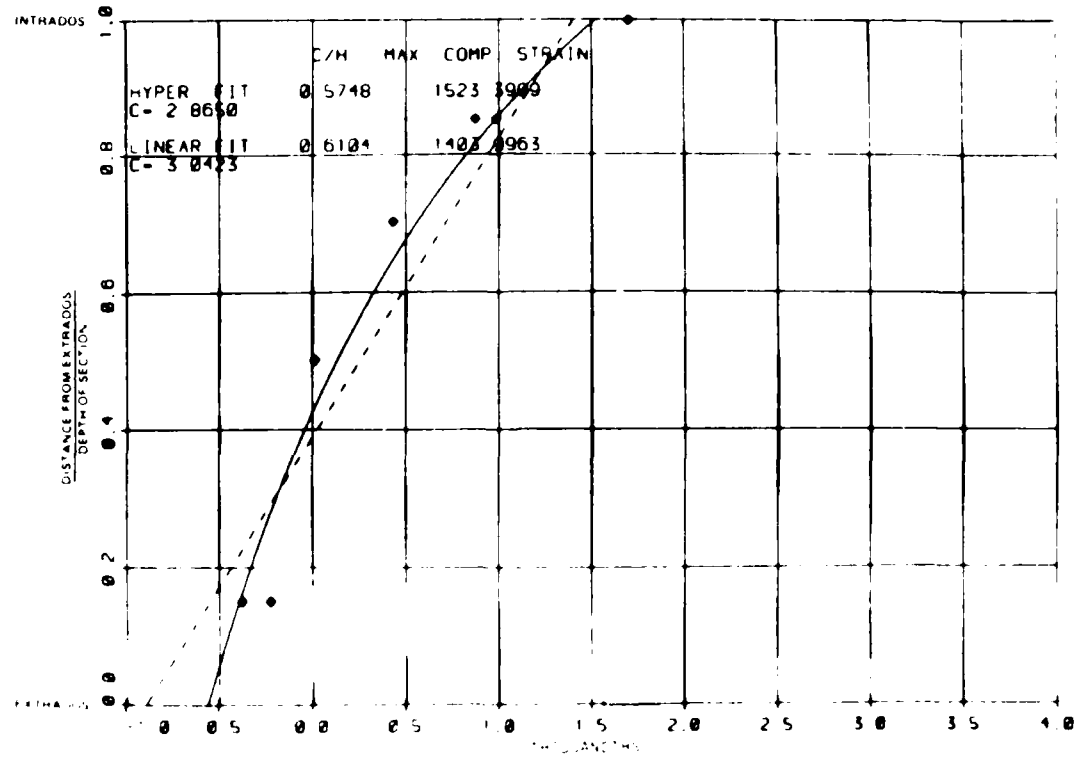

Model C2-3 springing line, 24.3 kips

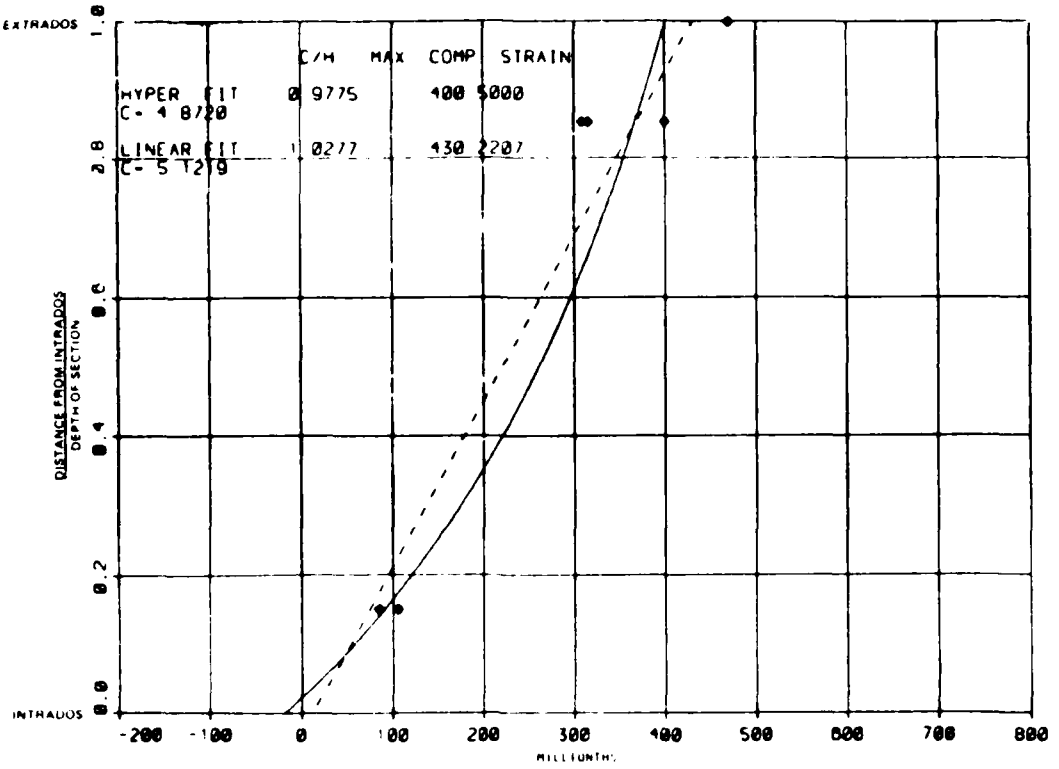

Model C3-1 crown, 20.0 kips

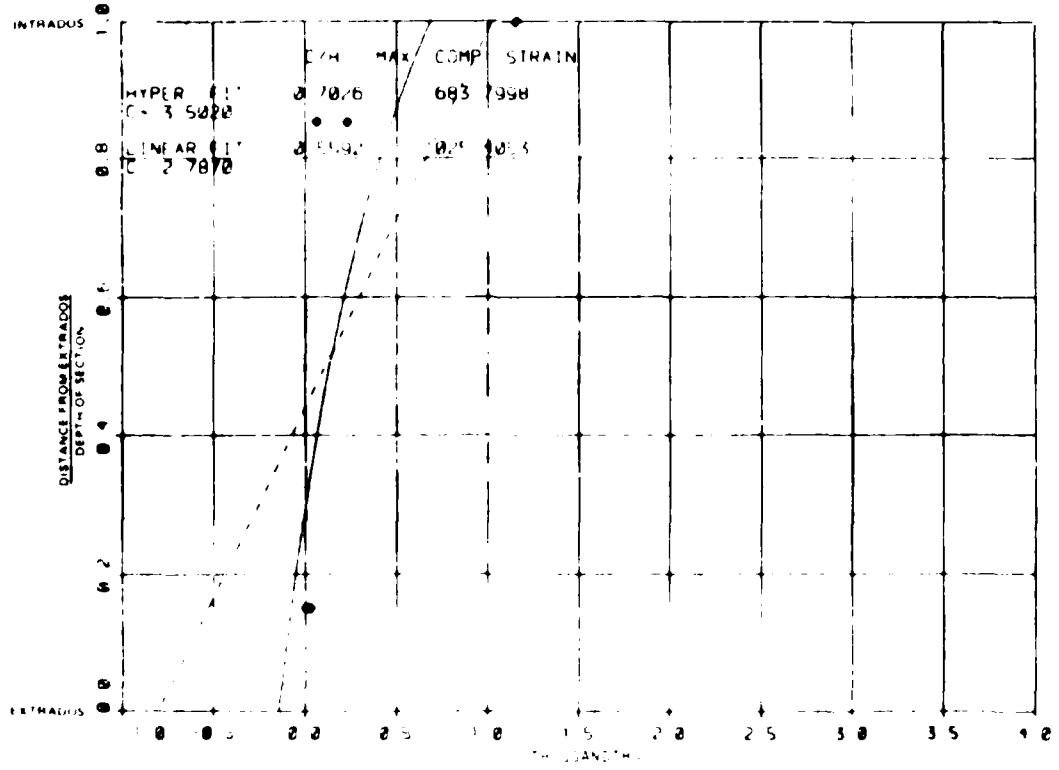

Model C3-1 springing line, 20.0 kips

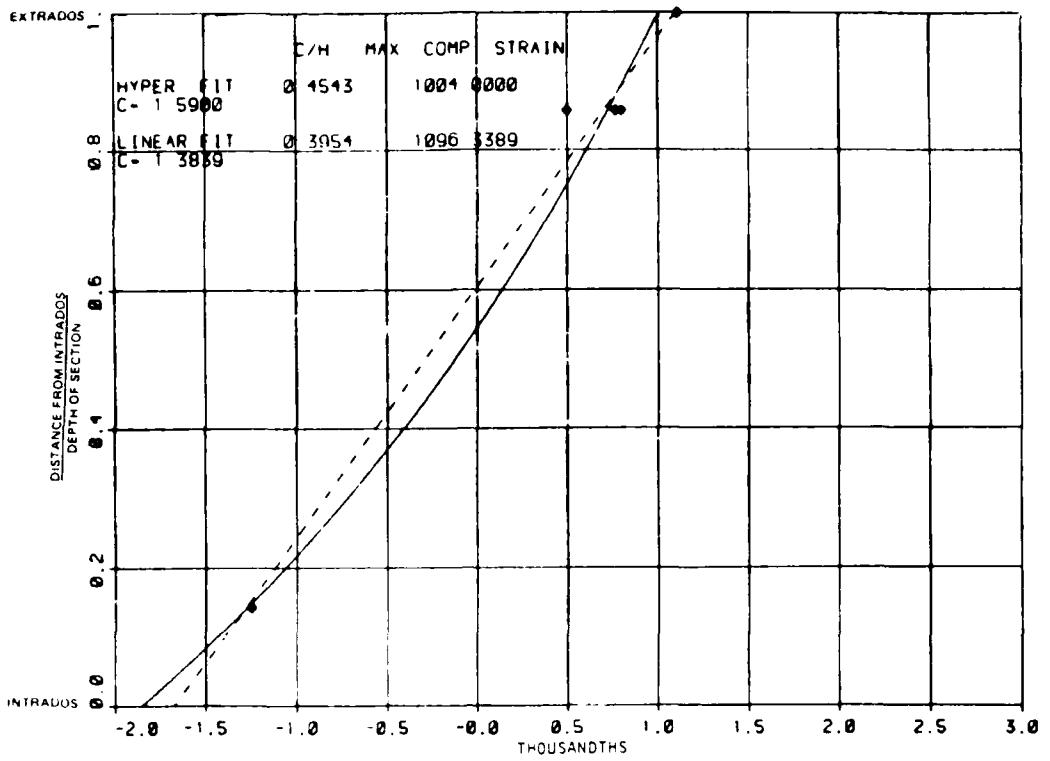

Model C4-1 crown, 15.3 kips

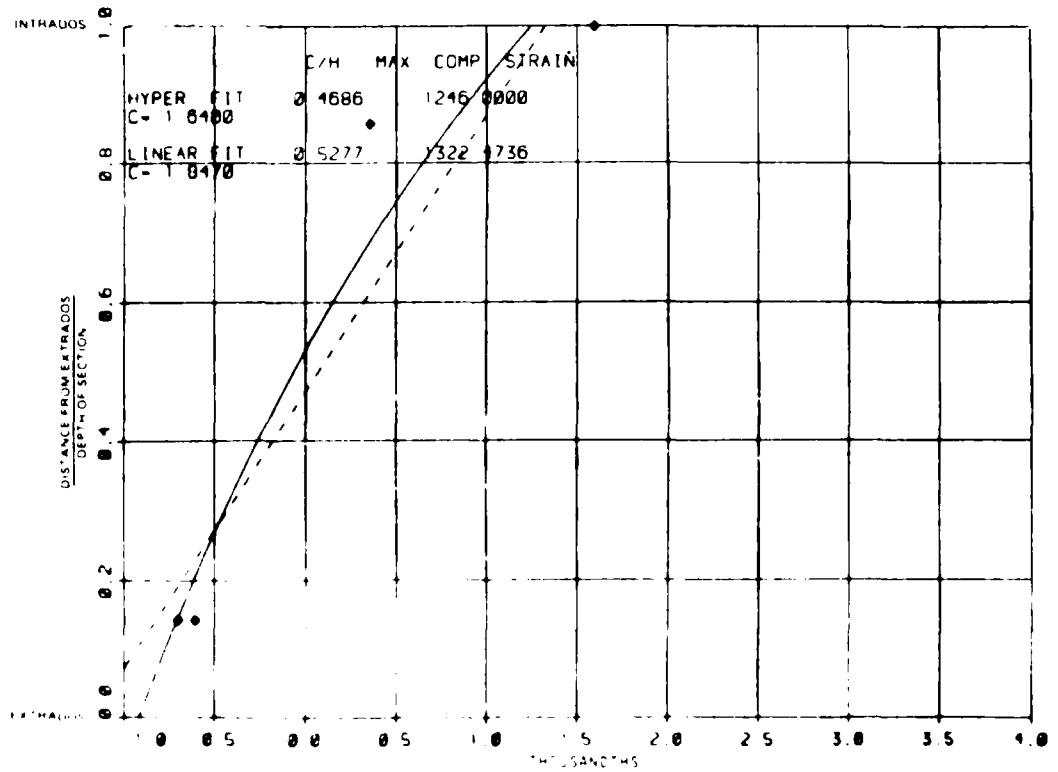

Model C4-1 springing line, 15.3 kips

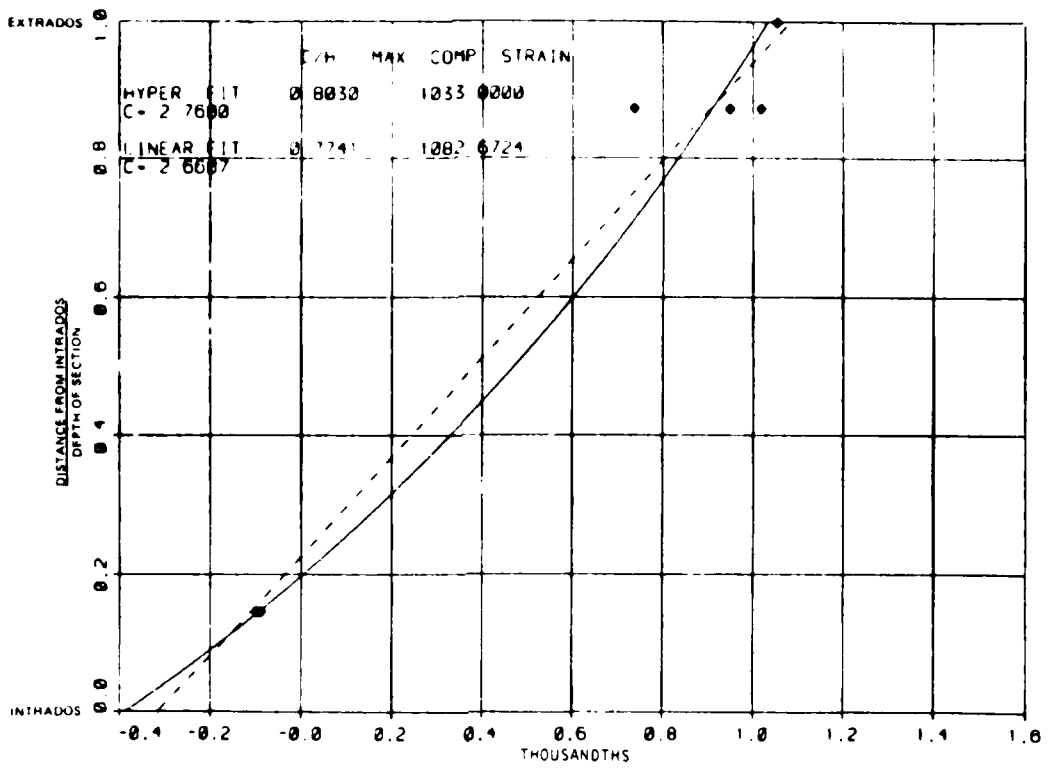

Model C4-2 crown, 21.9 kips

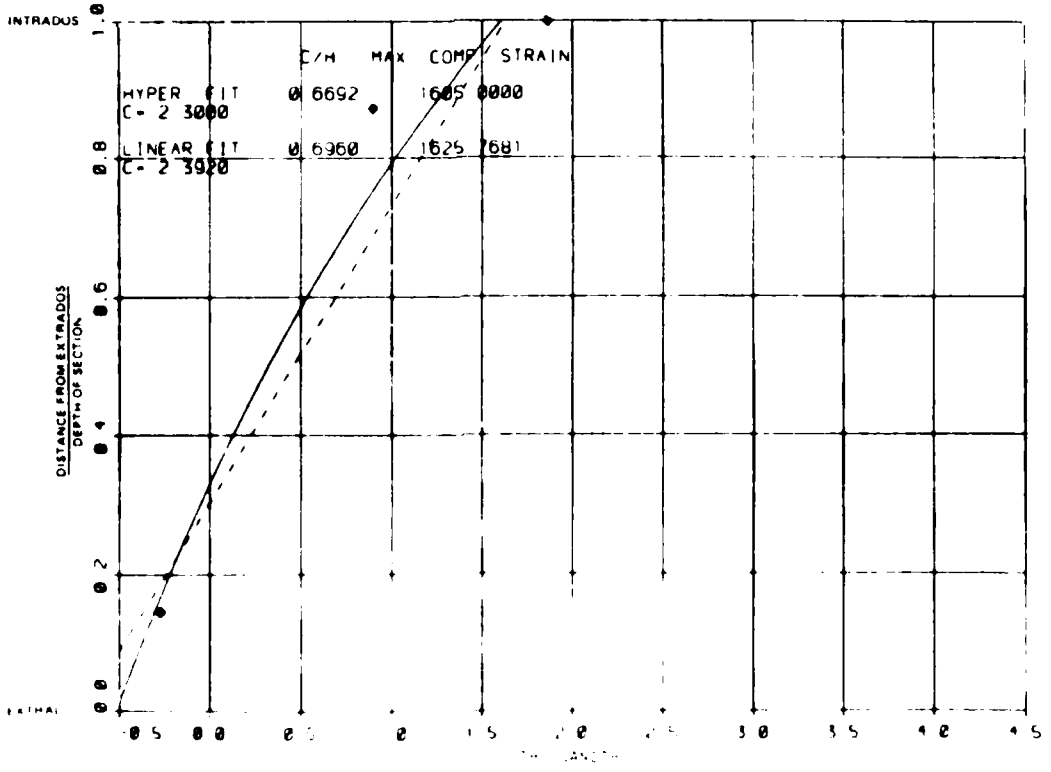

Model C4-2 springing line, 21.9 kips

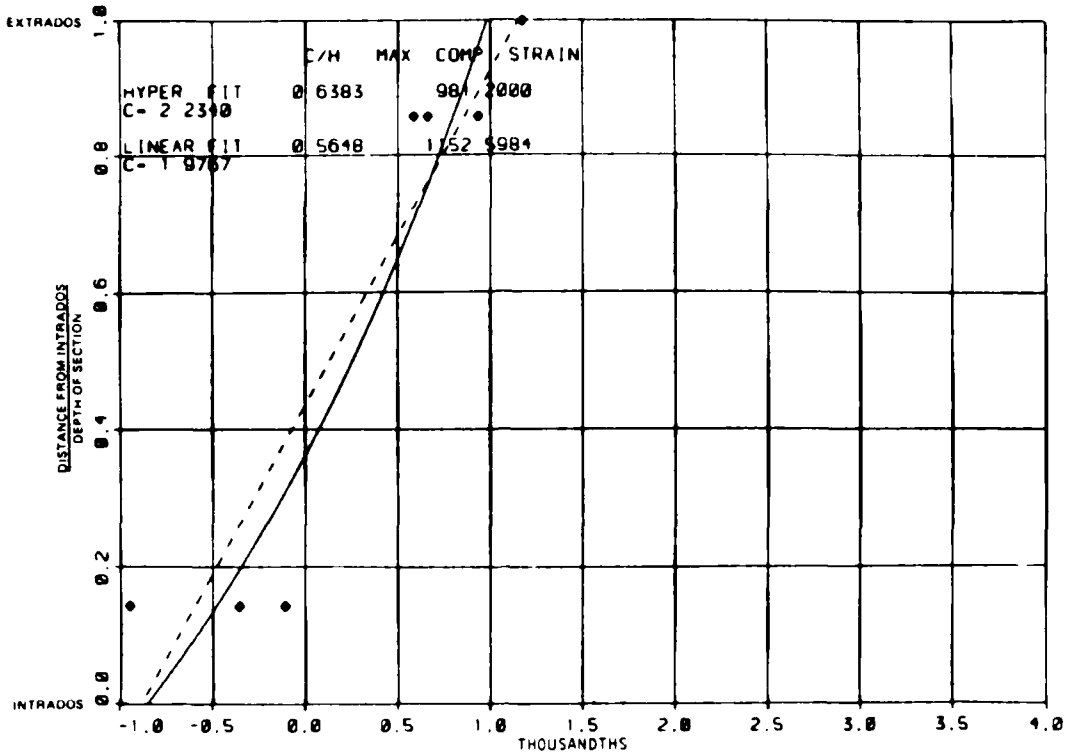

Model C5-1 crown, 12.0 kips

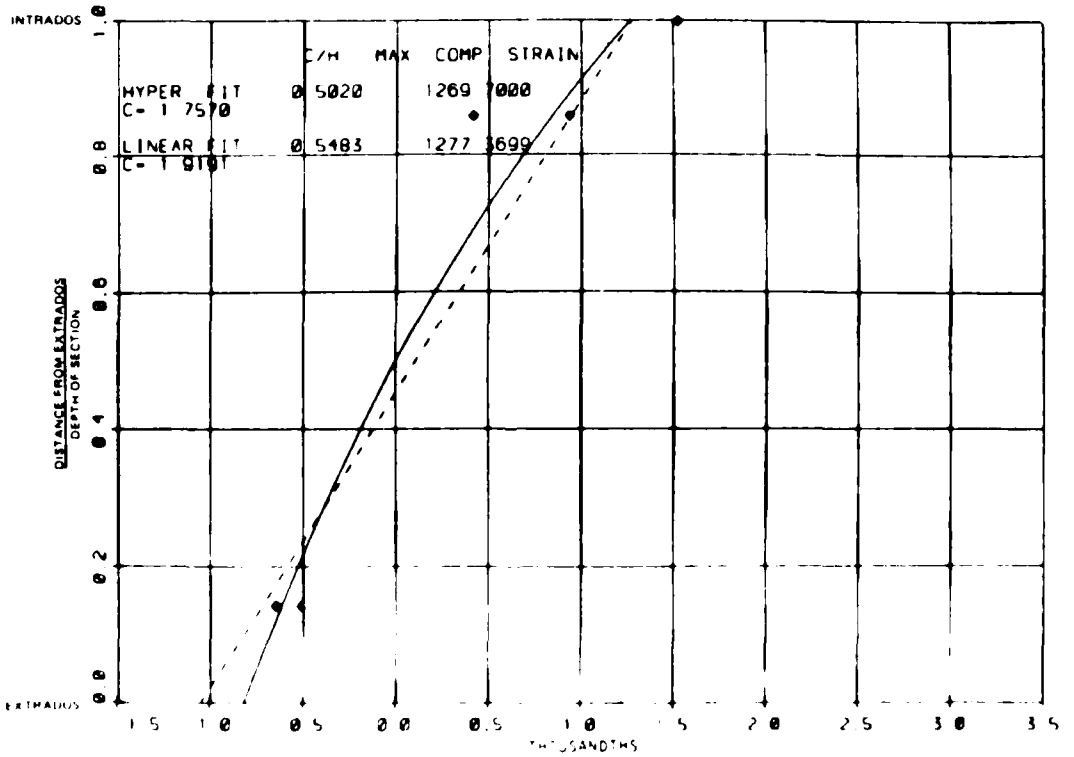

Model C5-1 springing line, 12.0 kips

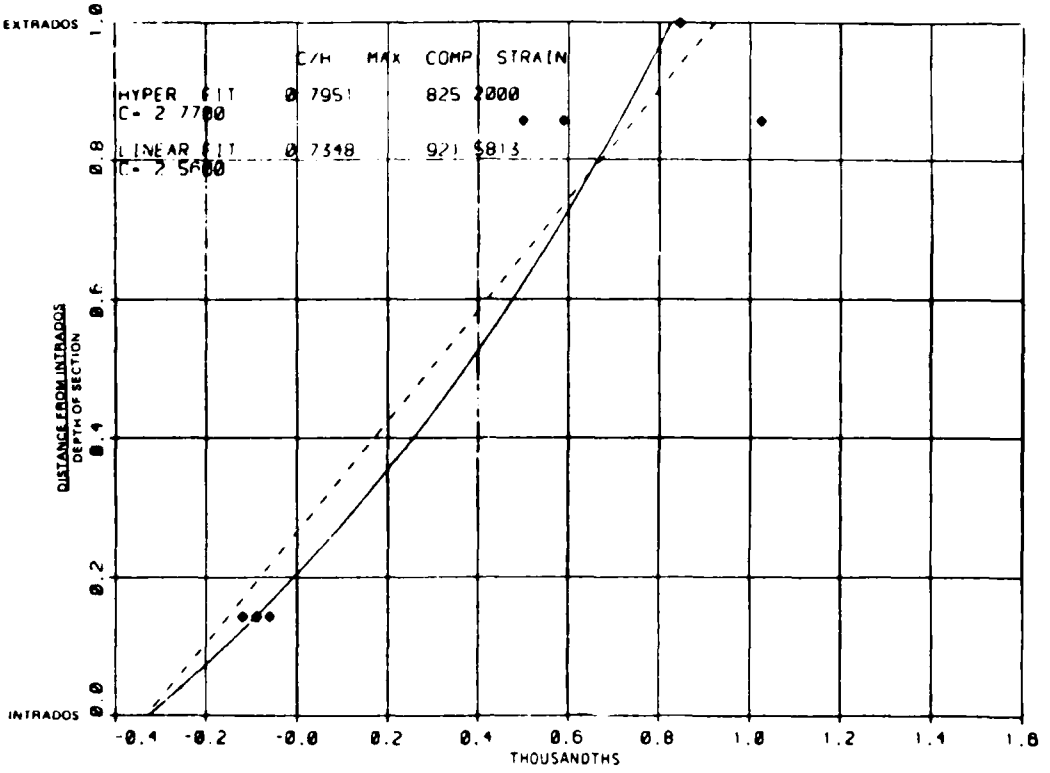

Model C5-2 crown, 15.8 kips

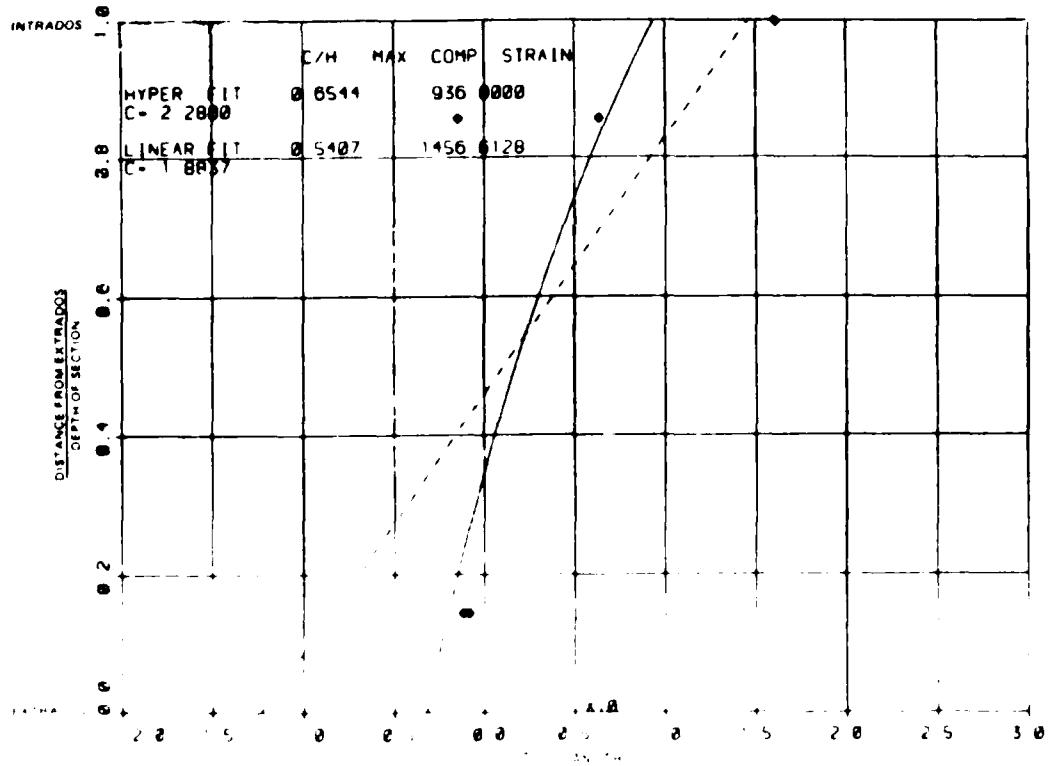

Model C5-2 springing line, 15.8 kips

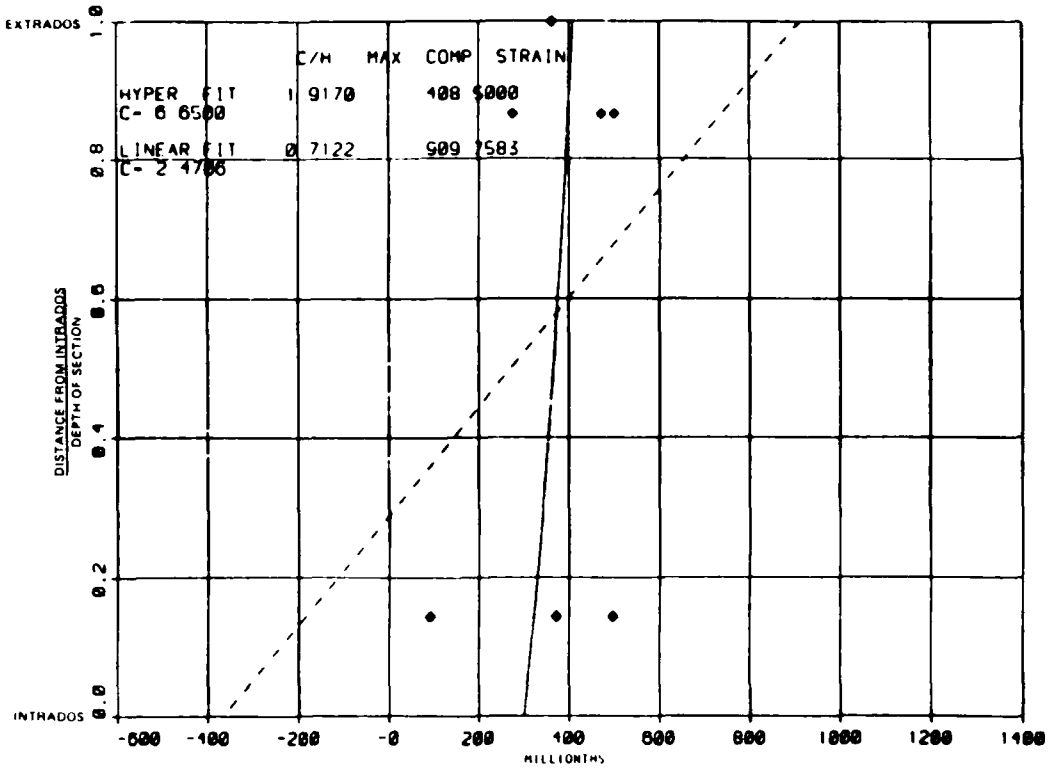

Model C5-3 springing line, 14.8 kips

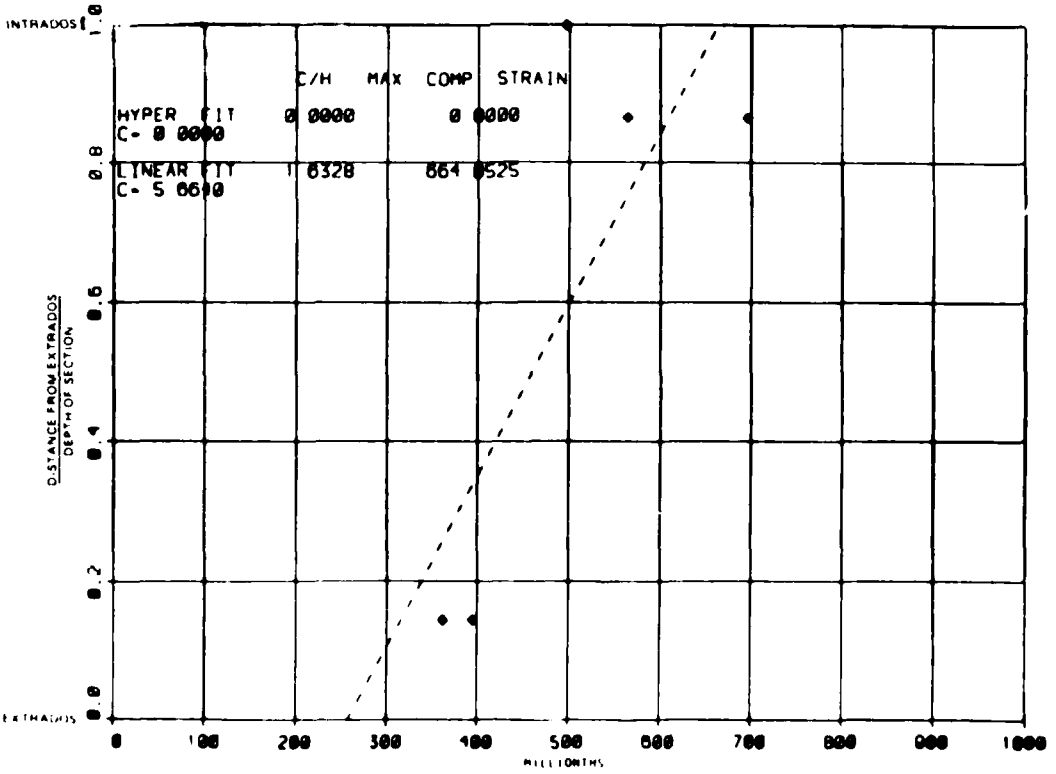

Model C5-3 crown, 14.8 kips

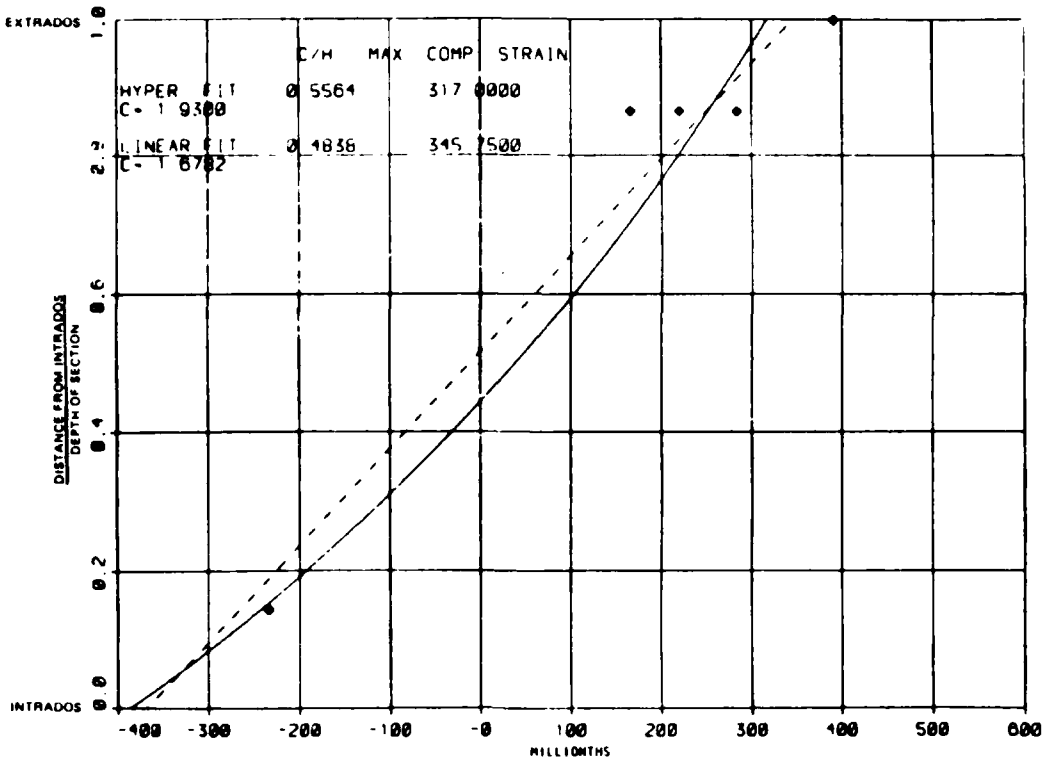

Model C5-4 crown, 4.5 kips

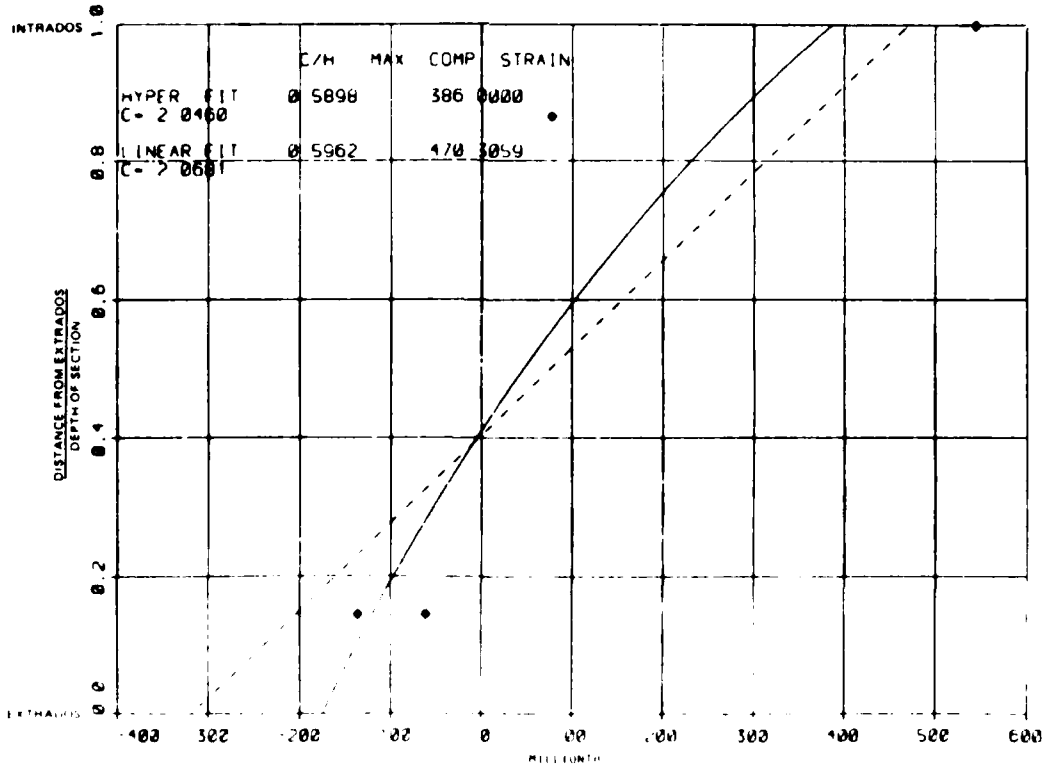

Model C5-4 springing line, 4.5 kips

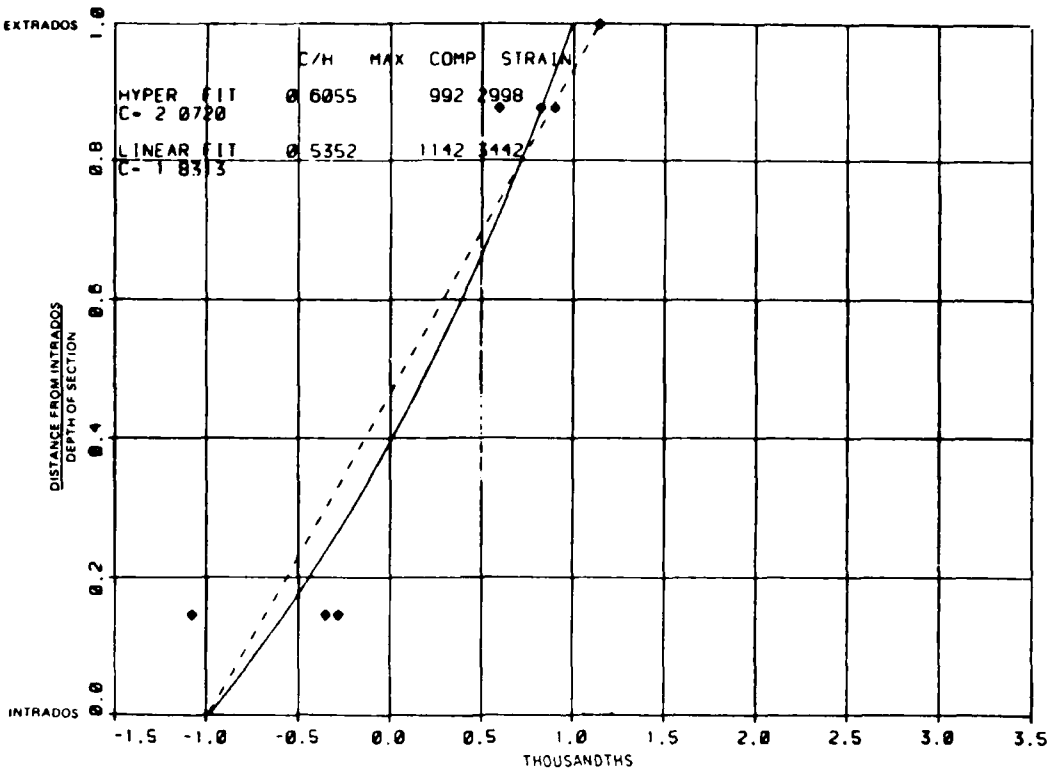

Model C6-1 crown, 10.1 kips

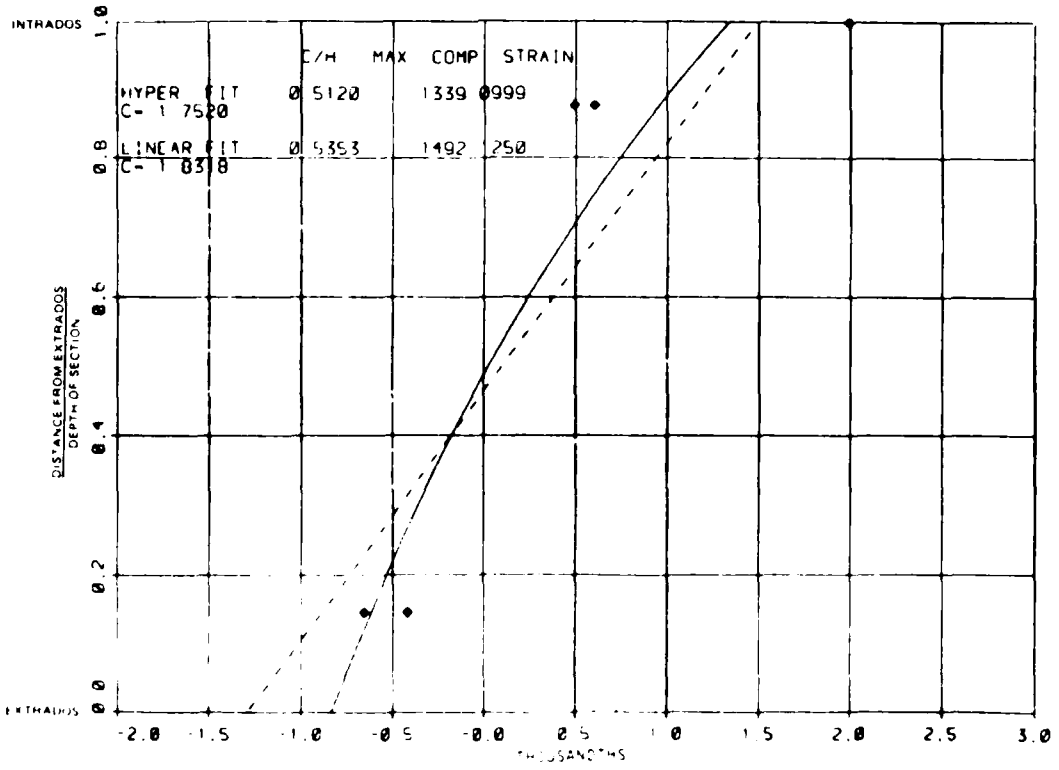

Model C6-1 springing line, 10.1 kips

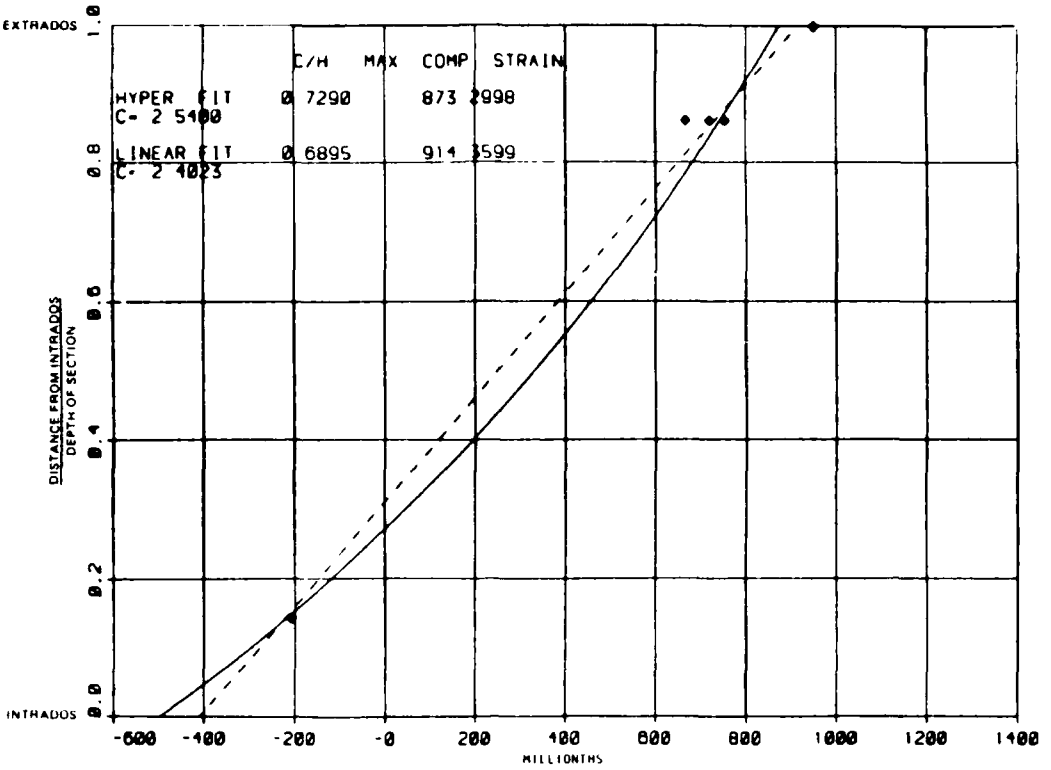

Model C6-2 crown, 10.2 kips

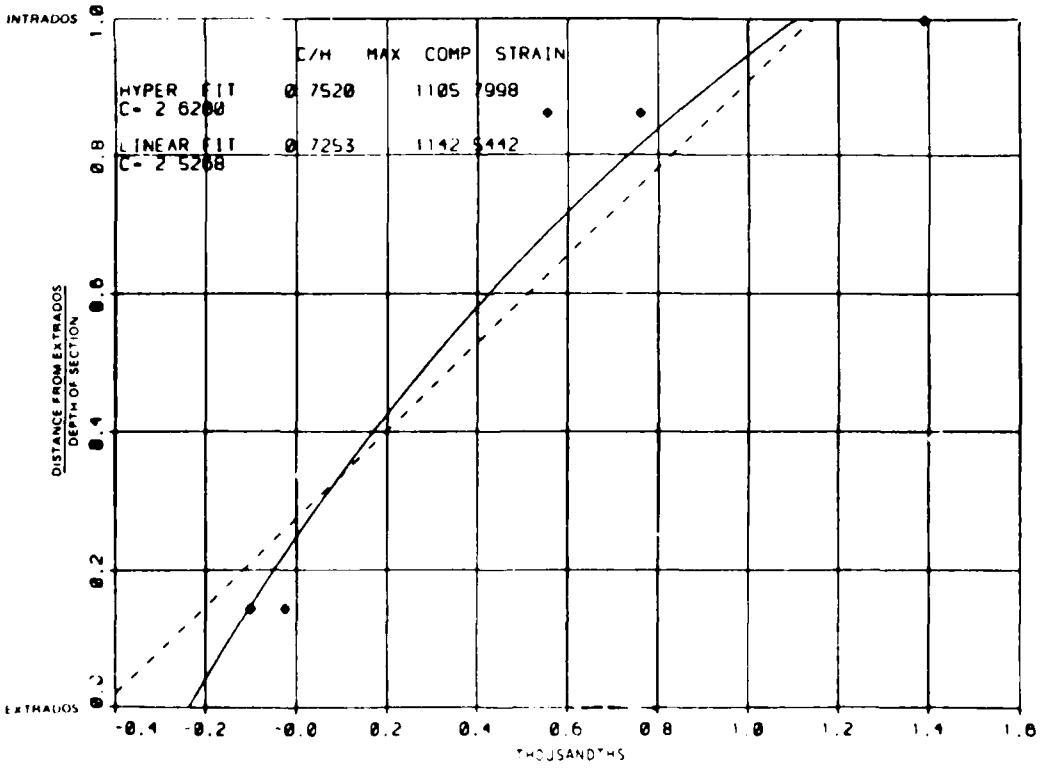

Model C6-2 springing line, 10.2 kips

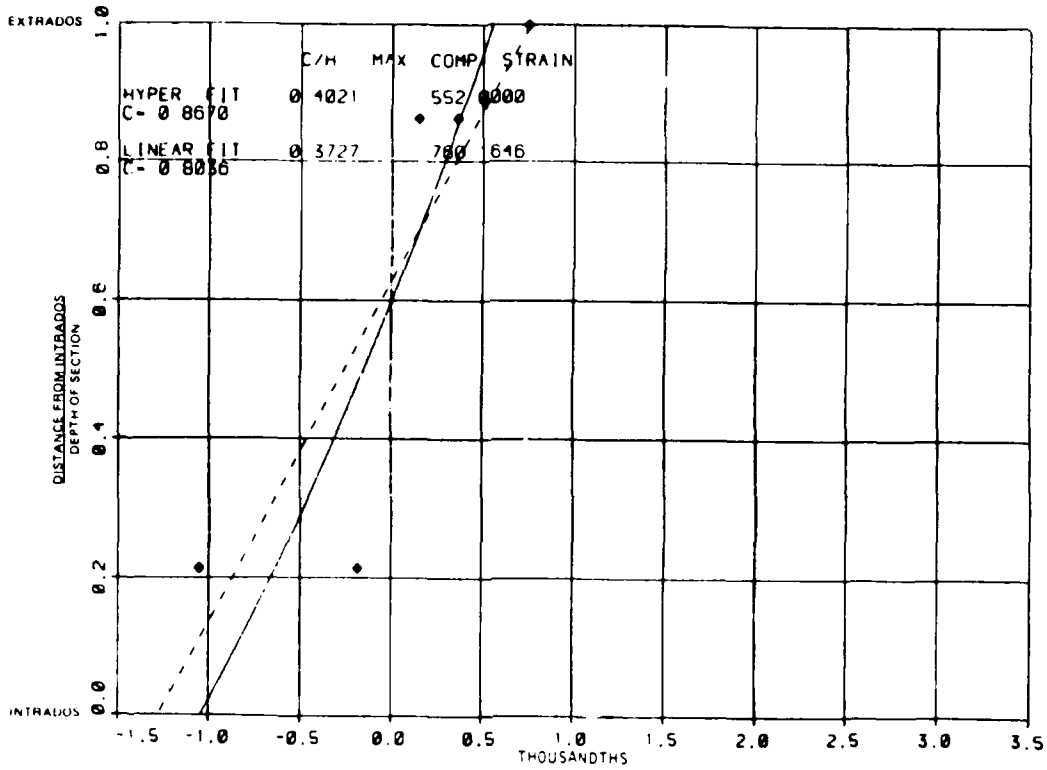

Model C7-1 crown, 1.4 kips

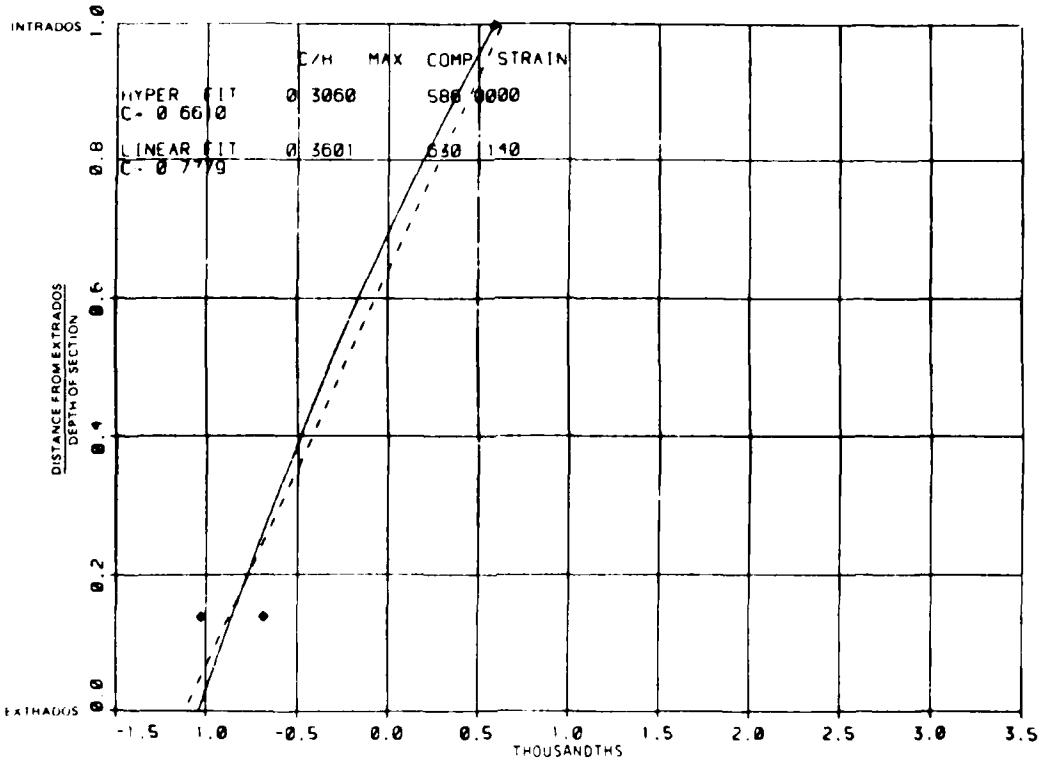

Model C7-1 springing line, 1.4 kips

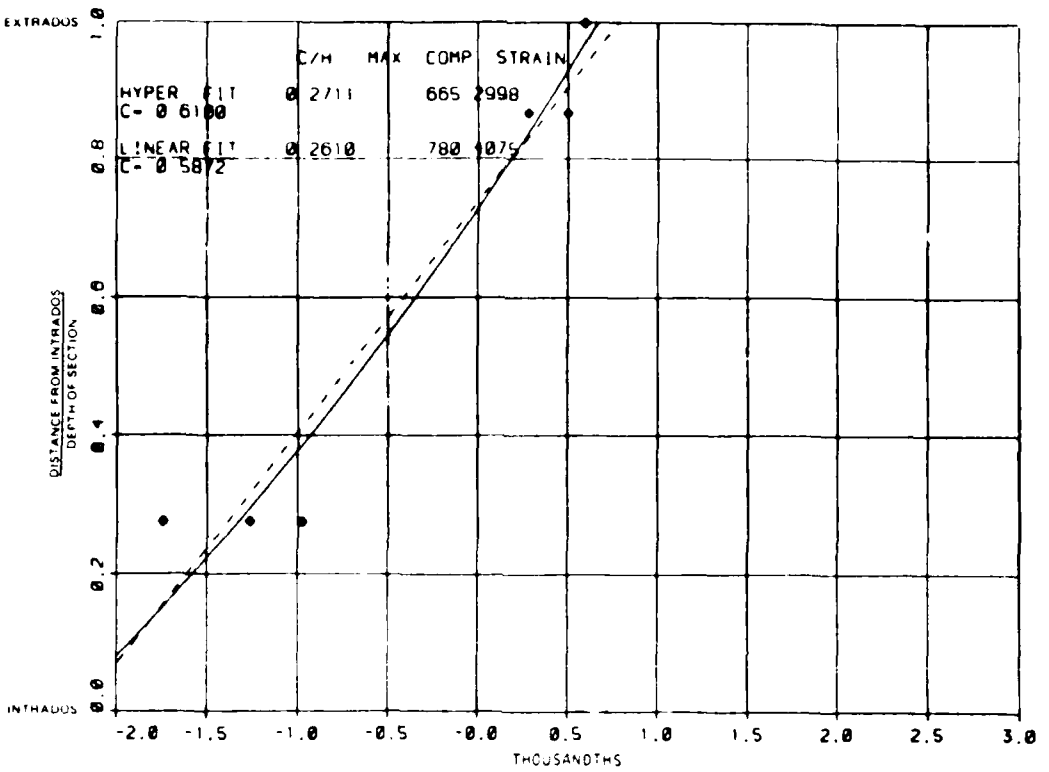

Model C8-1 crown, 3.4 kips

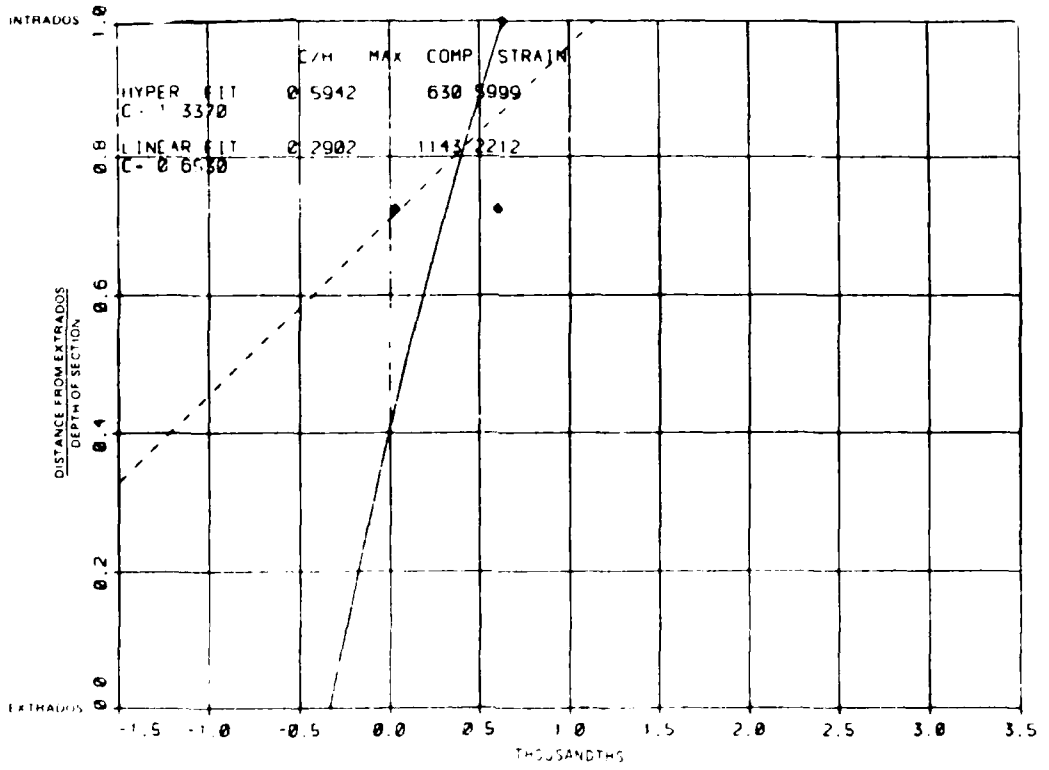

Model C8-1 springing line, 3.4 kips

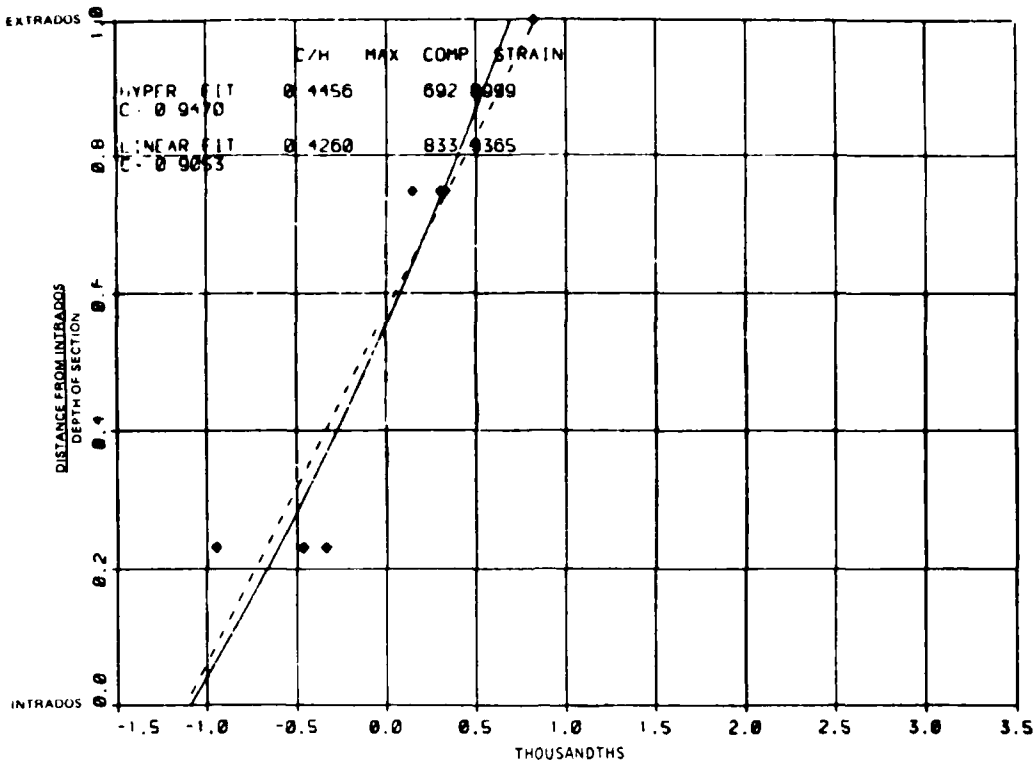

Model C8-2 crown, 2.4 kips

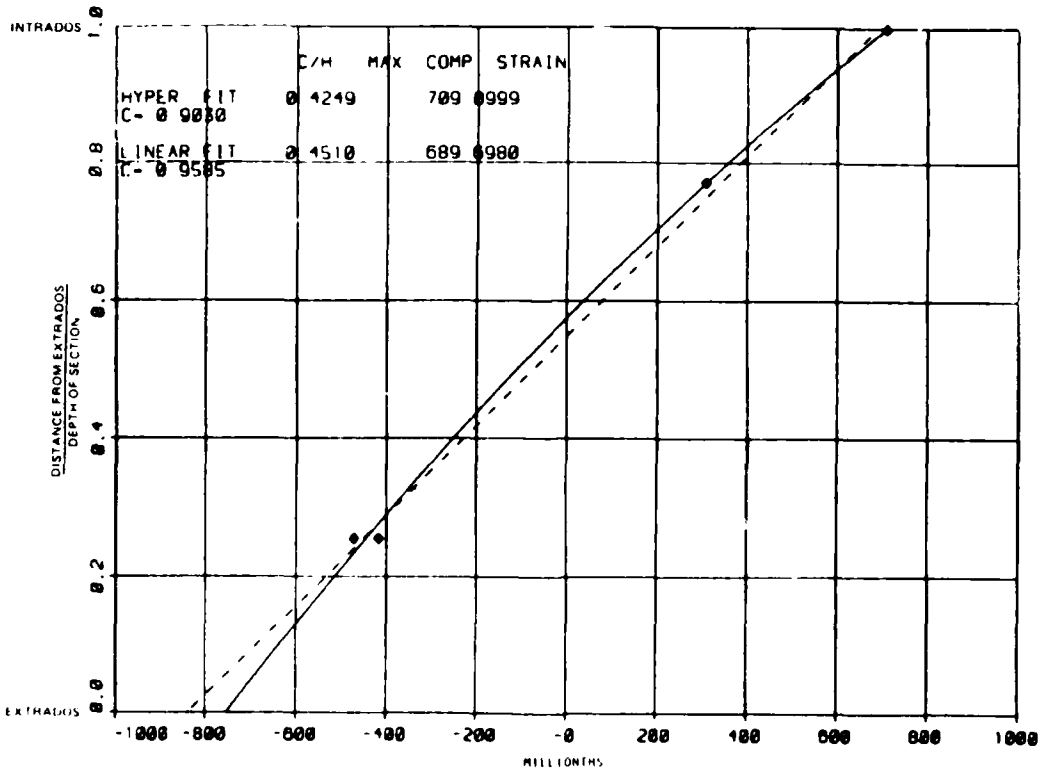

Model C8-2 springing line, 2.4 kips

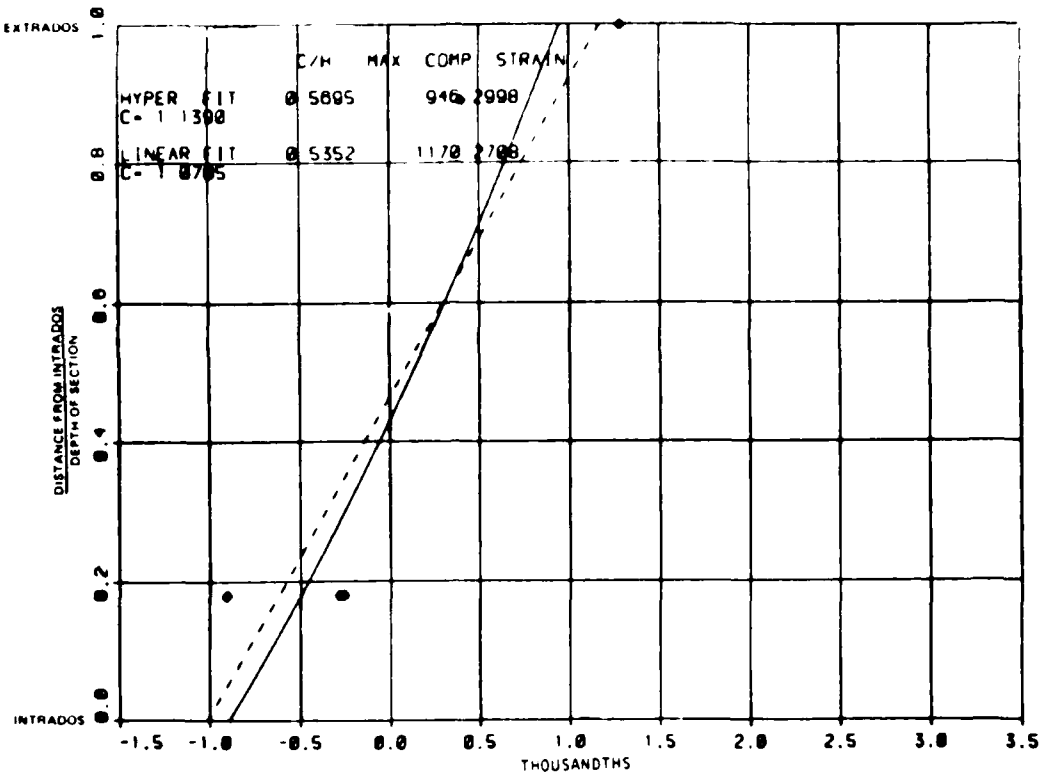

Model C8-3 crown, 5.7 kips

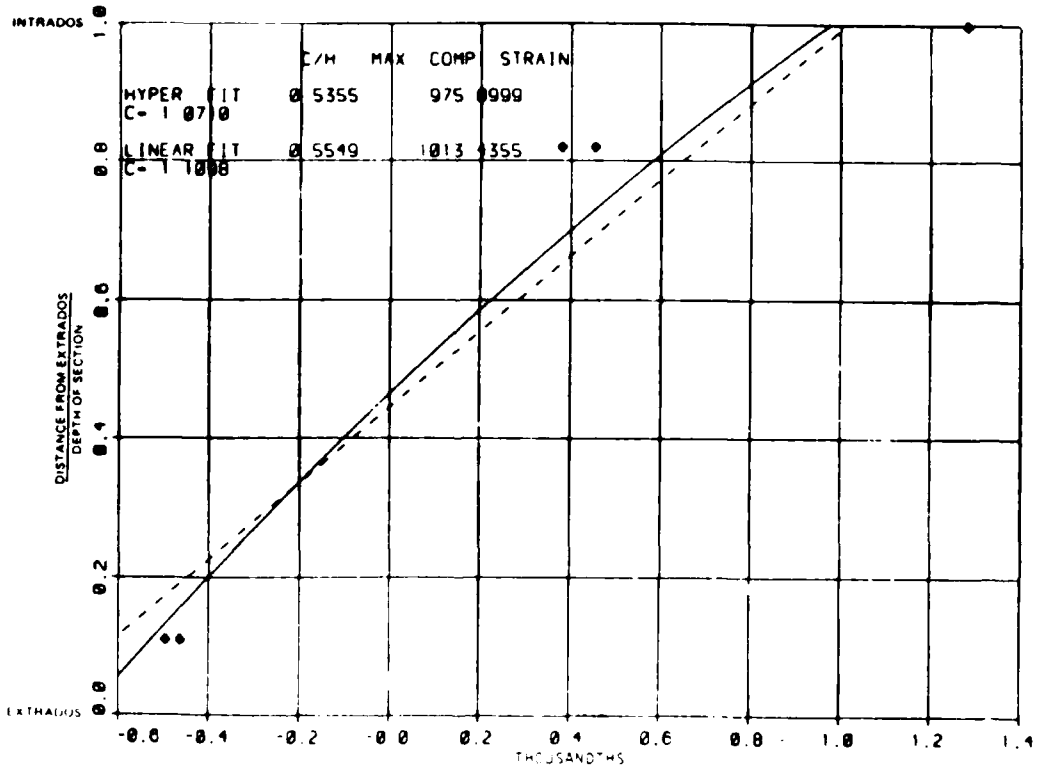

Model C8-3 springing line, 5.7 kips

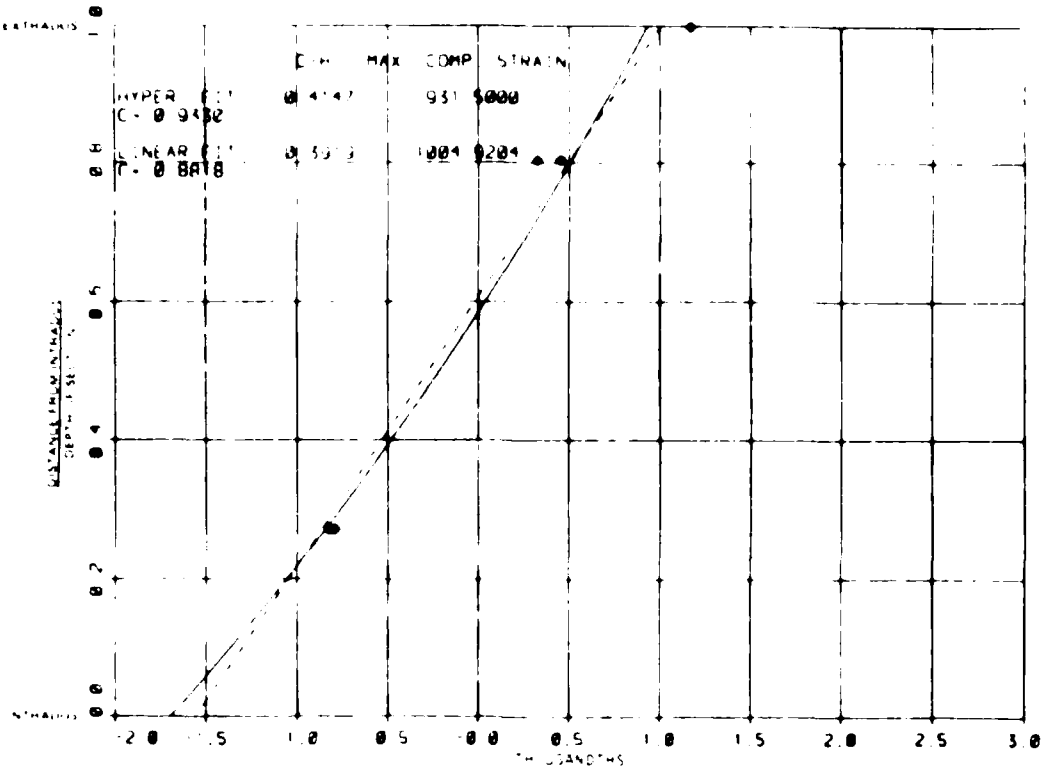

Model C9-1 crown, 1.9 kips

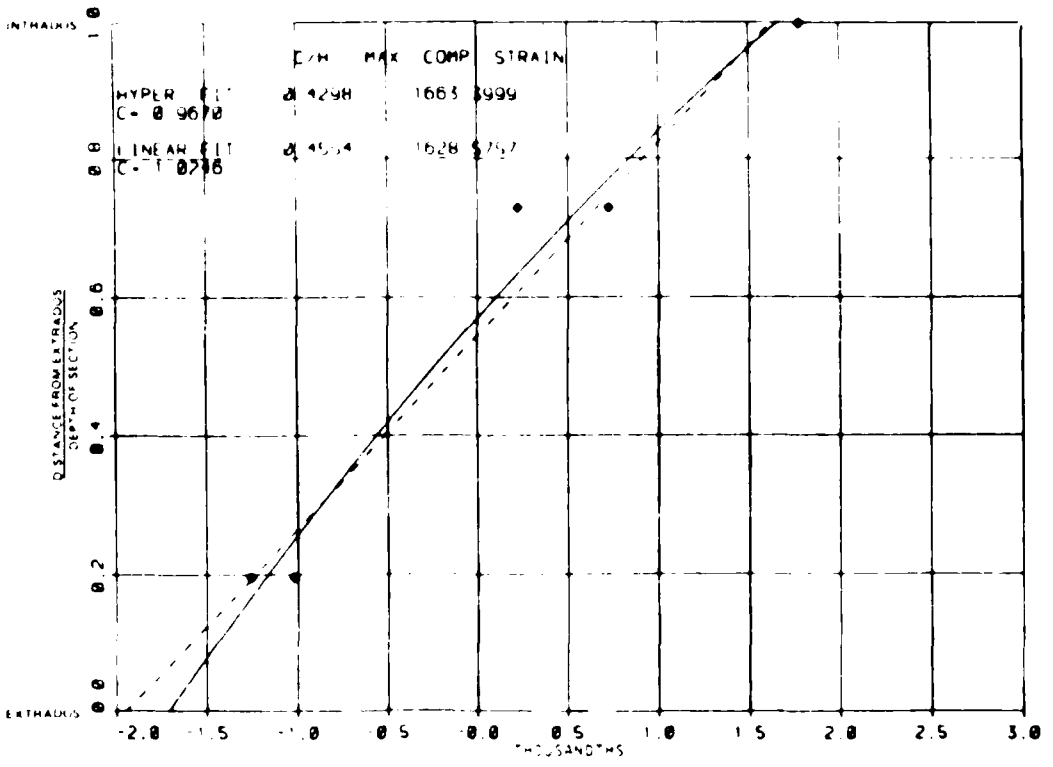

Model C9-1 springing line, 1.9 kips

APPENDIX F

STRAIN DISTRIBUTION FITS

Nonlinear Least Squares Regression Analysis
(Hyperbolic Strain Distribution)

1. The hyperbolic strain distribution according to Timoshenko's curved beam theory (Timoshenko 1941)* is (for the positive-moment case)

$$\varepsilon(y) = \frac{y\left(R + \frac{h}{2}\right)\varepsilon_u}{\left(R + \frac{h}{2} - c + y\right)c}$$

where

ε = strain

y = distance from the neutral axis

R = radius of initial curvature to middepth of section

h = overall depth of section

ε_u = maximum compressive strain

c = depth of section in compression

Replace y with $(y' - h + c)$, where y' is the distance from the intrados. Also, discretely replace $\varepsilon(y)$ with $\varepsilon_i(y_i)$ or ε_i and y' with y'_i. Therefore, the data will be fitted to the curve by the equation:

$$\varepsilon_i = \frac{(y'_i - h + c)K\varepsilon_u}{(y'_i - h + K)c} \qquad \text{(F1)}$$

where

$$K = R + h/2$$

and ε_u and c are the undetermined coefficients to be solved for by the least-squares method.

---

* References cited in this appendix are included in the References at the end of the main text.

2. The error term e_i is:

$$e_i = \varepsilon_i - \frac{(v_i' - h)K\varepsilon_u}{(v_i' - h + K)c} - \frac{K\varepsilon_u}{(v_i' - h + K)} \tag{F2}$$

The sum of the squares of the error term is:

$$\sum_{i=1}^{N} e_i^2 = \sum_{i=1}^{N} \left[\varepsilon_i - \frac{(v_i' - h)K\varepsilon_u}{(v' - h + K)c} - \frac{K\varepsilon_u}{(v' - h + K)} \right]^2 \tag{F3}$$

where N is the number of data pairs $(\varepsilon_1, v_1)...(\varepsilon_N, v_N)$. Let $\varepsilon_u = \alpha$, maximum compressive strain, and $c = \beta$, location of the neutral axis (N.A.), then the term in Equation F3, $\sum_{i=1}^{N} (e_i)^2$, is to be minimized with respect to α and β.

3. To solve for α and β the following equations are formed:

$$\frac{\partial f(\alpha,\beta)}{\partial \alpha} = \sum_{i=1}^{N} \left[\varepsilon_i - \frac{(v_i' - h)K\alpha}{(v_i' - h + K)\beta} - \frac{K\alpha}{(v_i' - h + K)} \right] \left[\frac{(v_i' - h)}{(v_i' - h + K)\beta} + \frac{1}{(v_i' - h + K)} \right] \tag{F4}$$

and

$$\frac{\partial f(\alpha,\beta)}{\partial \beta} = \sum_{i=1}^{N} \left[\varepsilon_i - \frac{(v_i' - h)K\alpha}{(v_i' - h + K)\beta} - \frac{K\alpha}{(v_i' - h + K)} \right] \left[\frac{(v_i' - h)}{(v_i' - h + K)} \right] \tag{F5}$$

where

$$f(\alpha,\beta) = \sum_{i=1}^{N} \left[\varepsilon_i - \frac{(y_i' - h)K\alpha}{(y_i' - h + K)\beta} - \frac{K\alpha}{(y_i' - h + K)} \right]^2$$

Solving Equation F4 for α yields:

$$\alpha = \left\{ \frac{\sum_{i=1}^{N} \left[\varepsilon_i \frac{(y_i' - h + \beta)}{(y_i' - h + K)} \right]}{\sum_{i=1}^{N} \left[\frac{(y_i' - h + \beta)^2}{(y_i' - h + K)^2} \right]} \right\}^{\frac{\beta}{K}} \qquad \text{(F6)}$$

Substituting Equation F6 for α into Equation F5 for β yields:

$$\beta = \frac{\sum_{i=1}^{N} \left[\varepsilon_i \frac{(y_i' - h)}{(y_i' - h + K)} \right] \sum_{i=1}^{N} \left[\frac{(y_i' - h)}{(y_i' - h + K)^2} \right] - \sum_{i=1}^{N} \left[\frac{\varepsilon_i}{(y_i' - h + K)} \right] \sum_{i=1}^{N} \left[\frac{(y_i' - h)^2}{(y_i' - h + K)^2} \right]}{\sum_{i=1}^{N} \left[\frac{1}{(y_i' - h + K)} \right] \sum_{i=1}^{N} \left[\frac{(y_i' - h)}{(y_i' - h + K)^2} \right] - \sum_{i=1}^{N} \left[\frac{\varepsilon_i (y_i' - h)}{(y_i' - h + K)} \right] \sum_{i=1}^{N} \left[\frac{1}{(y_i' - h + K)^2} \right]} \qquad \text{(F7)}$$

Hyperbolic Strain Distribution Fit for the Negative Moment Section

4. The hyperbolic strain distribution for the negative moment case is:

$$\varepsilon(y) = \frac{y\left(R - \frac{h}{2}\right)\varepsilon_u}{\left(R - \frac{h}{2} + c - y\right)c} \qquad \text{(F8)}$$

Replace y with $(y' - h + c)$, where y' is the distance from the extrados. Therefore, the data will be curve-fitted by the equation:

$$\varepsilon_i = \frac{(y_i' - h - c)K\varepsilon_u}{(-y_i' + h + K)c} \qquad \text{(F9)}$$

where

$$K = R - h/2$$

The same solution procedure previously described for the positive moment case is used.

α = Equation F6; however, replace $(v_i' - h + K)$ with $(-v_i' + h + K)$ and $(v_i' - h + K)^2$ with $(-v_i' + h + K)^2$

β = Equation F7; however, replace all terms $(v_i' - h + K)$ with $(-v_i' + h + K)$ and all terms $(v_i' - h + K)^2$ with $(-v_i' + h + K)^2$.

Correlation Coefficient (Miller and Freund 1977)

5. The correlation coefficient squared gives statistical inference to quantify the correlation between the data and the fitted curve. The equation below measures the correlation by:

$$r^2 = 1 - \frac{\sum_{i=1}^{N} (\varepsilon_i - \varepsilon_i')^2}{\sum_{i=1}^{N} (\varepsilon_i - \bar{\varepsilon}_i)^2} \qquad \text{(F10)}$$

where

r^2 = the correlation coefficient squared

ε_i = measured value

ε_i' = predicted value

$\bar{\varepsilon}_i$ = average of measured values

Linear Regression

6. The data that were fitted with the hyperbolic curve were also analyzed by the linear regression method. This gave a comparison of the statistical differences between a hyperbolic and a linear strain distribution

for the same data. The linear regression formulas can be found in most statistics references. And some hand calculators also have linear regression equations preprogrammed by keystroke operations.

APPENDIX G

RESULTANT MOMENTS, THRUSTS, AND LOAD PATHS

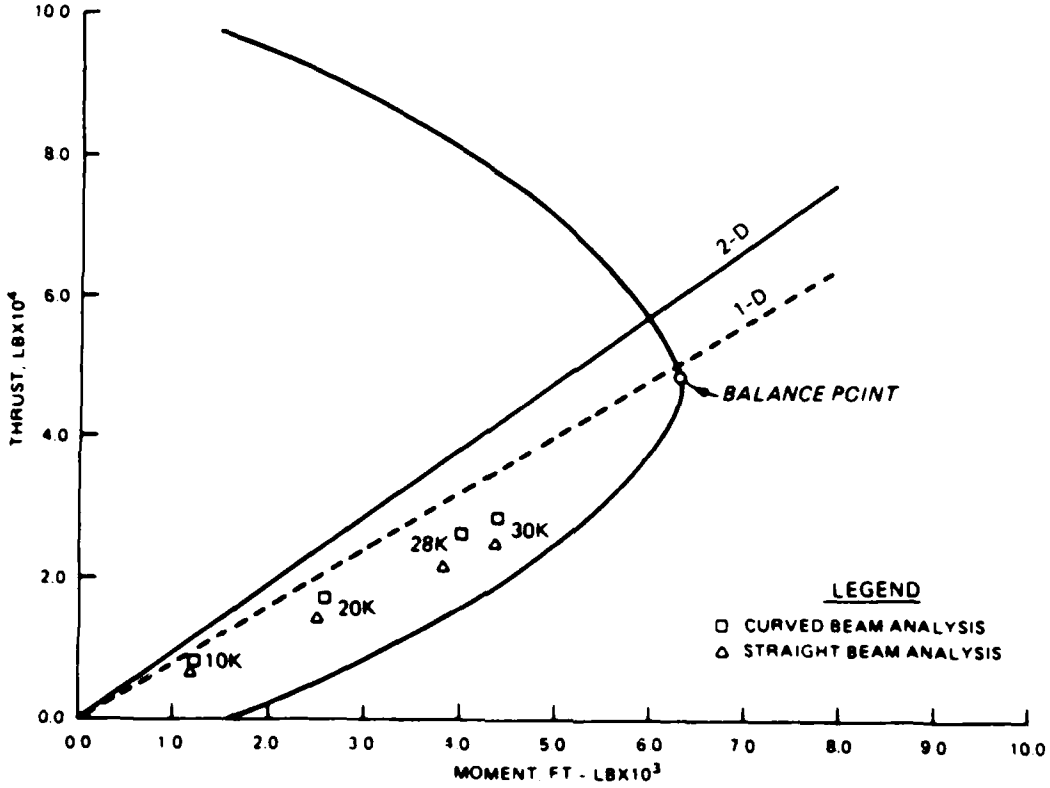

MODEL 1-1, CROWN

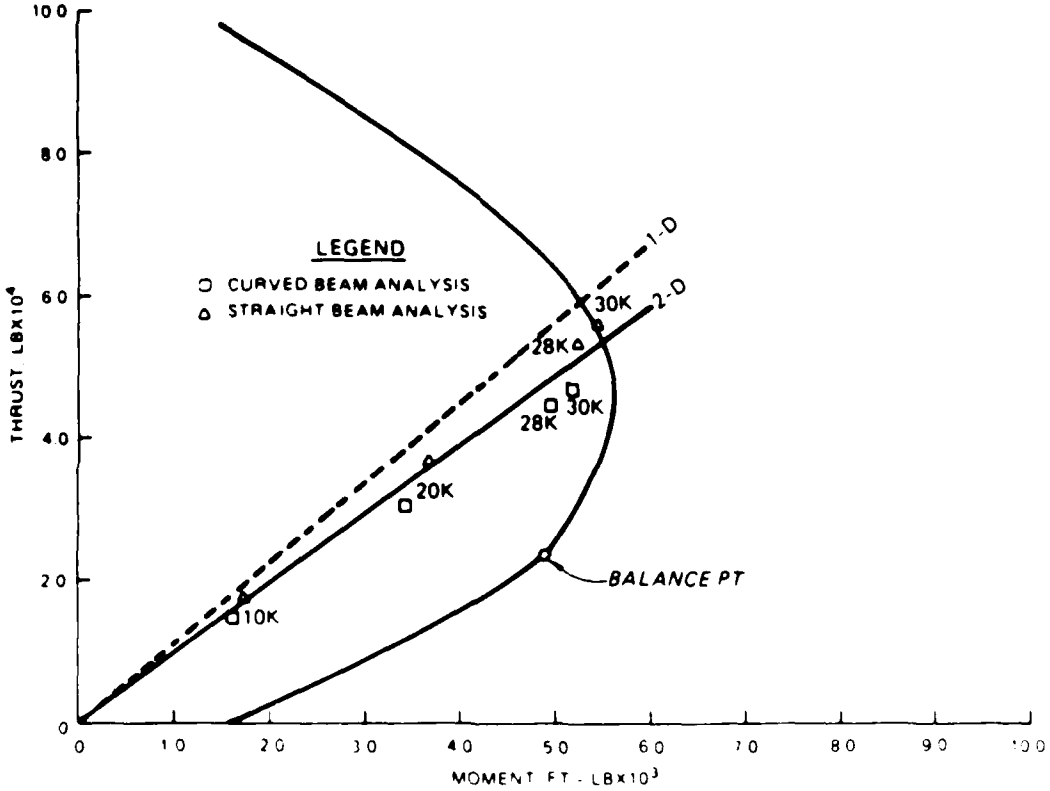

MODEL 1-1, SPRINGING LINE

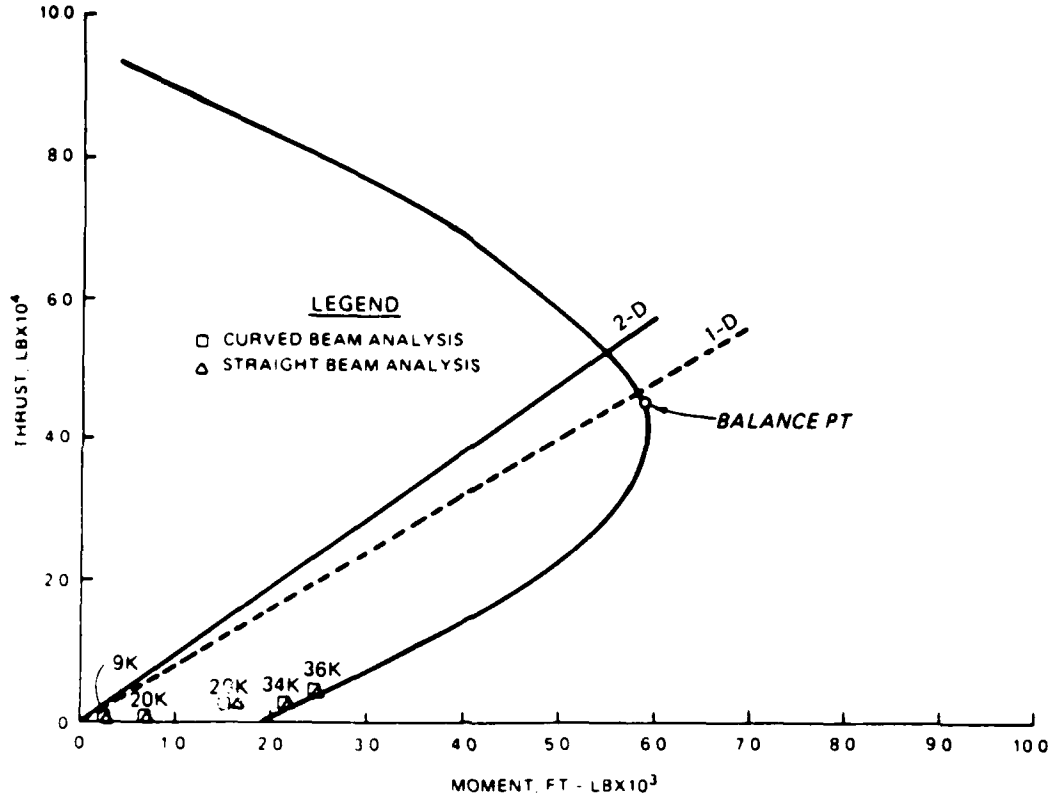

MODEL 2-1, CROWN

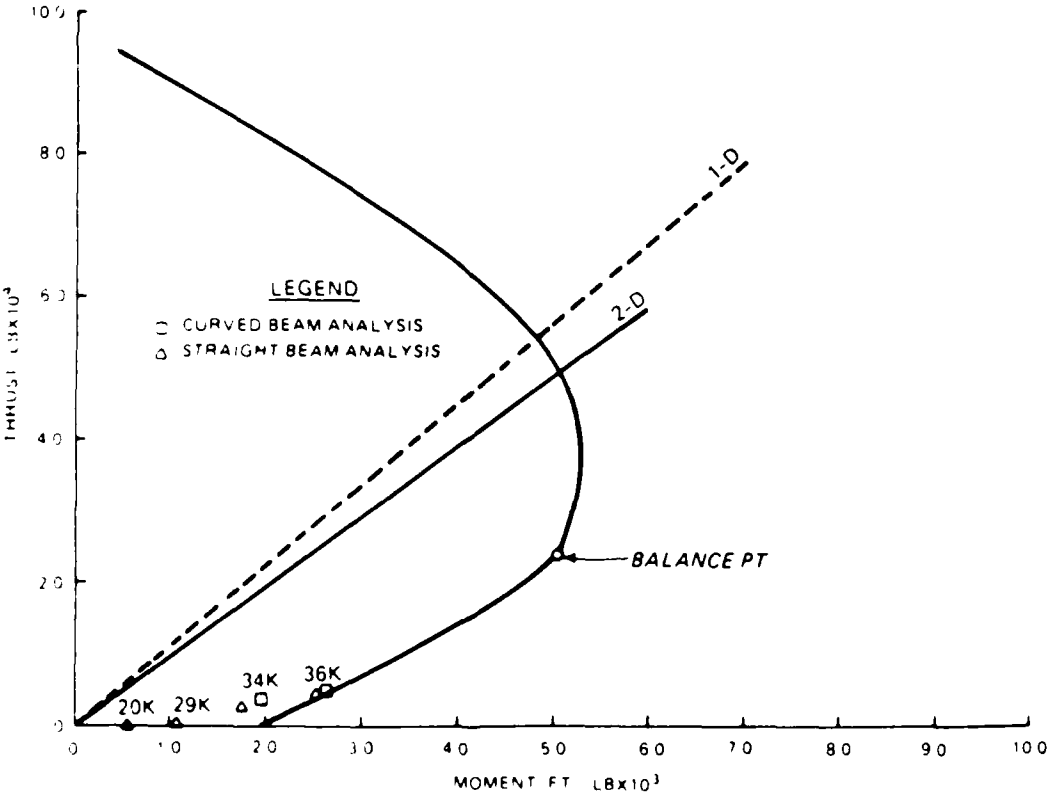

MODEL 2-1, SPRINGING LINE

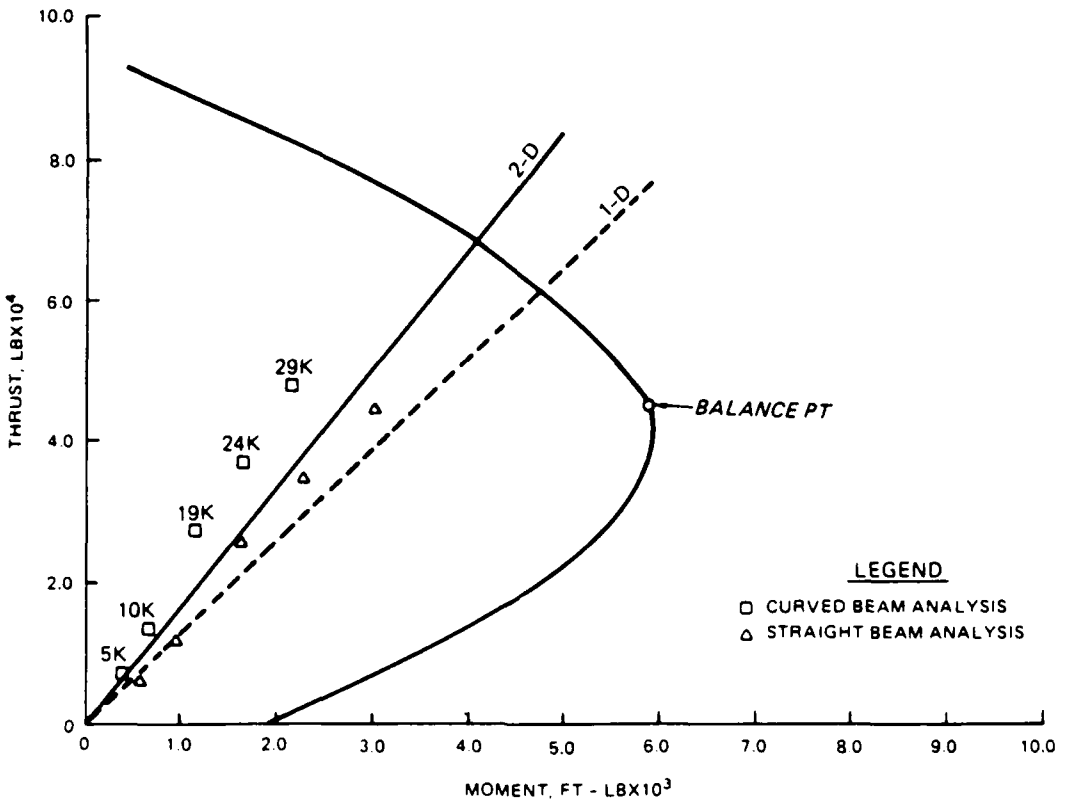

MODEL 2-2, CROWN

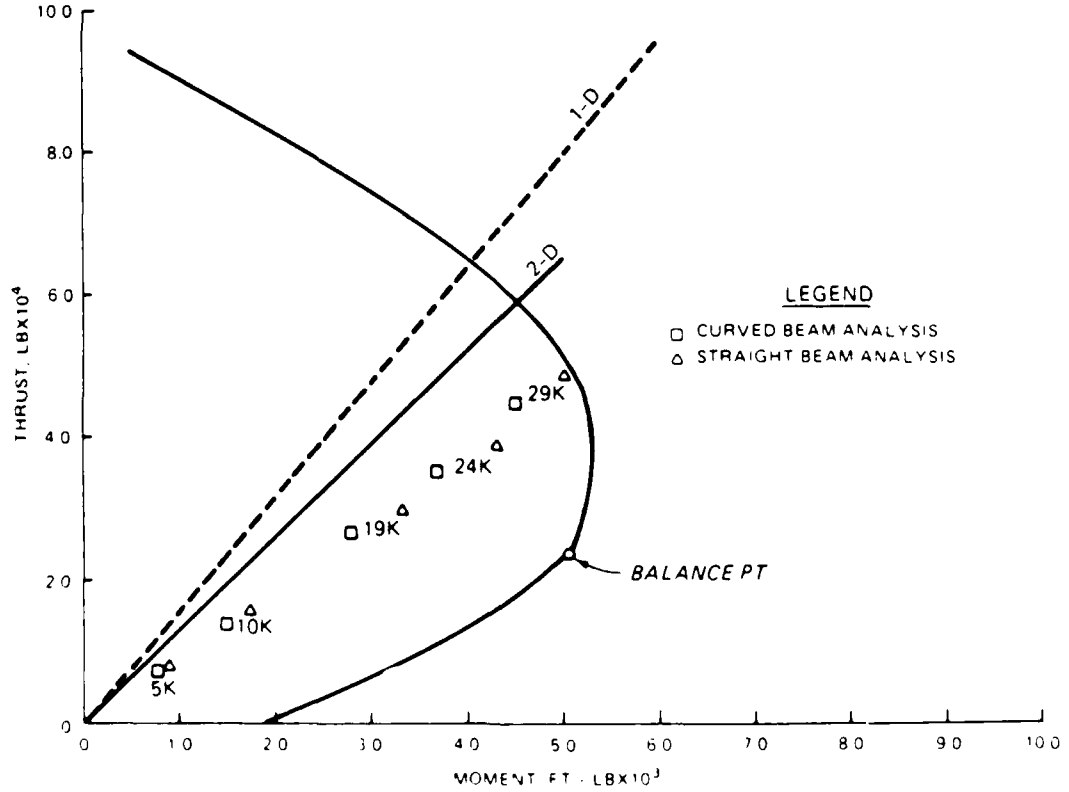

MODEL 2-2, SPRINGING LINE

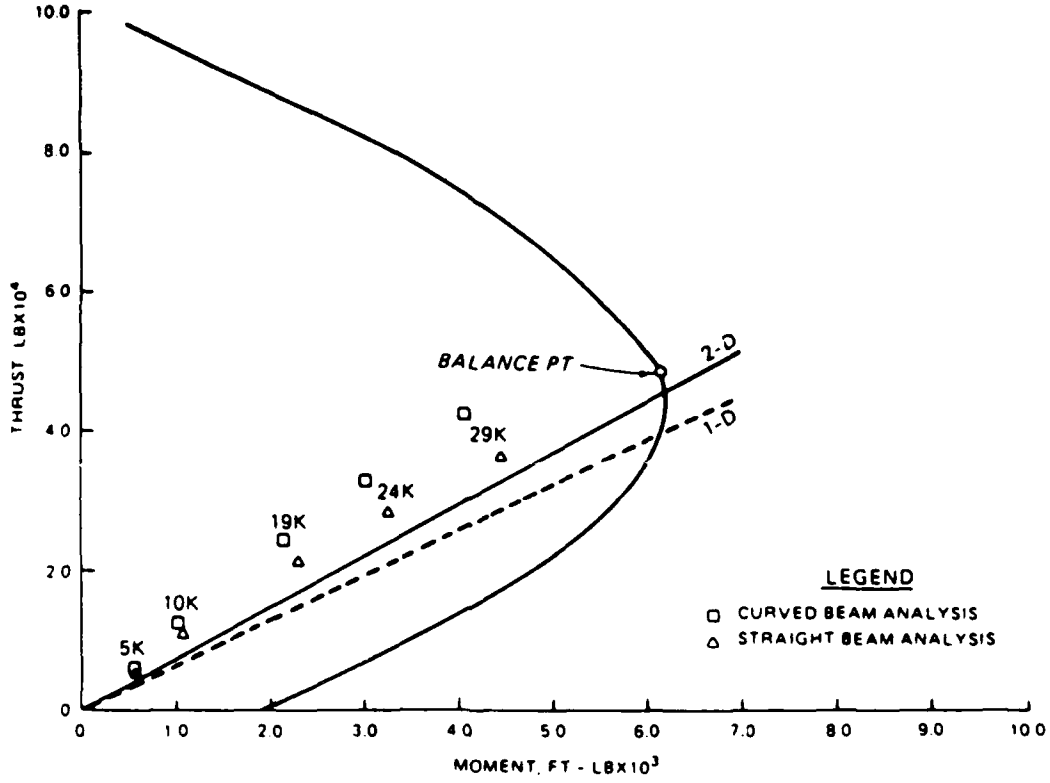

MODEL 2-3, CROWN

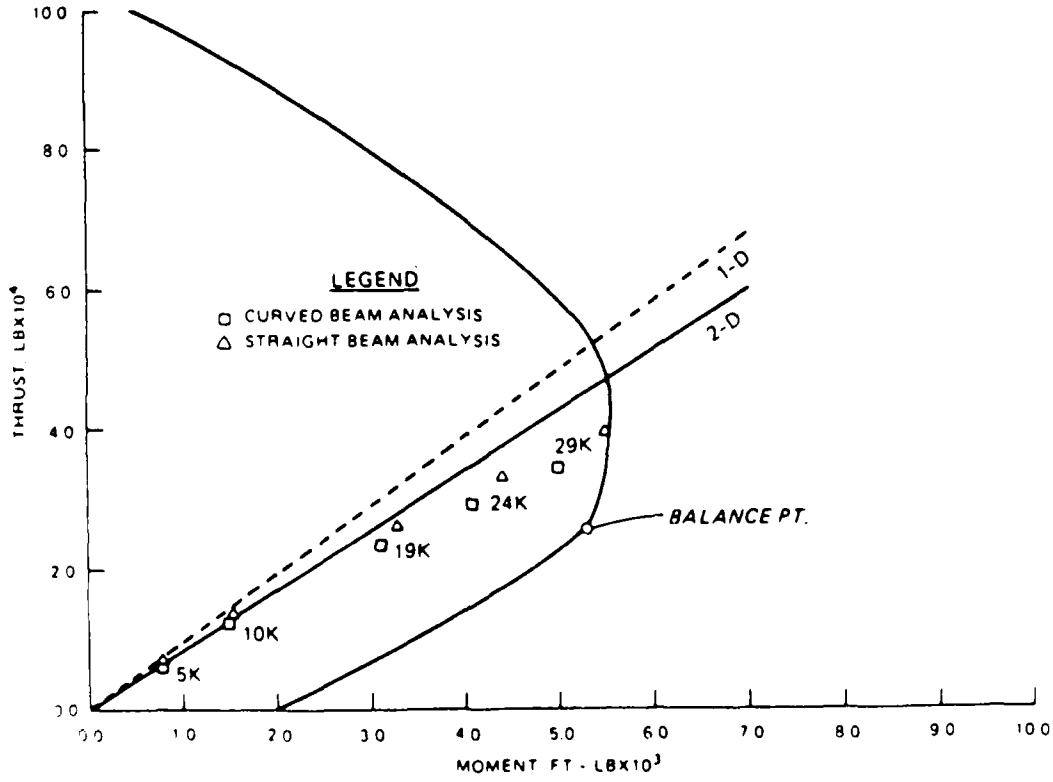

MODEL 2-3, SPRINGING LINE

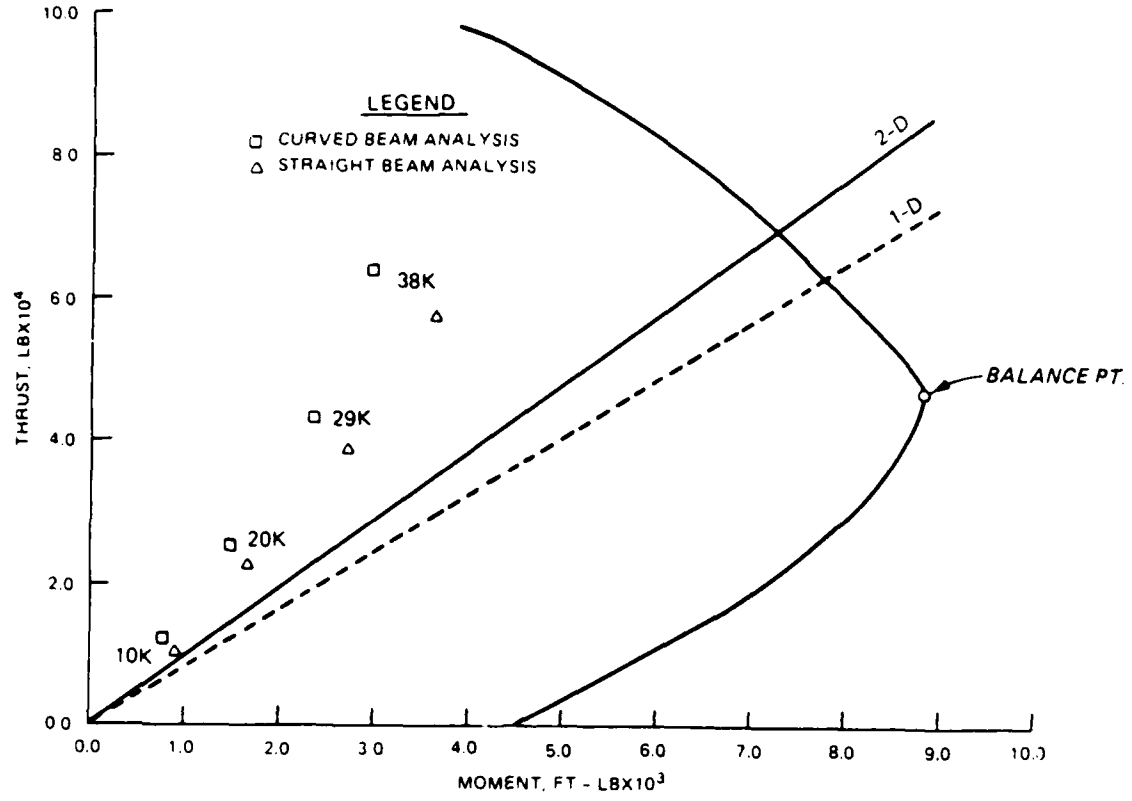

MODEL 3-1, CROWN

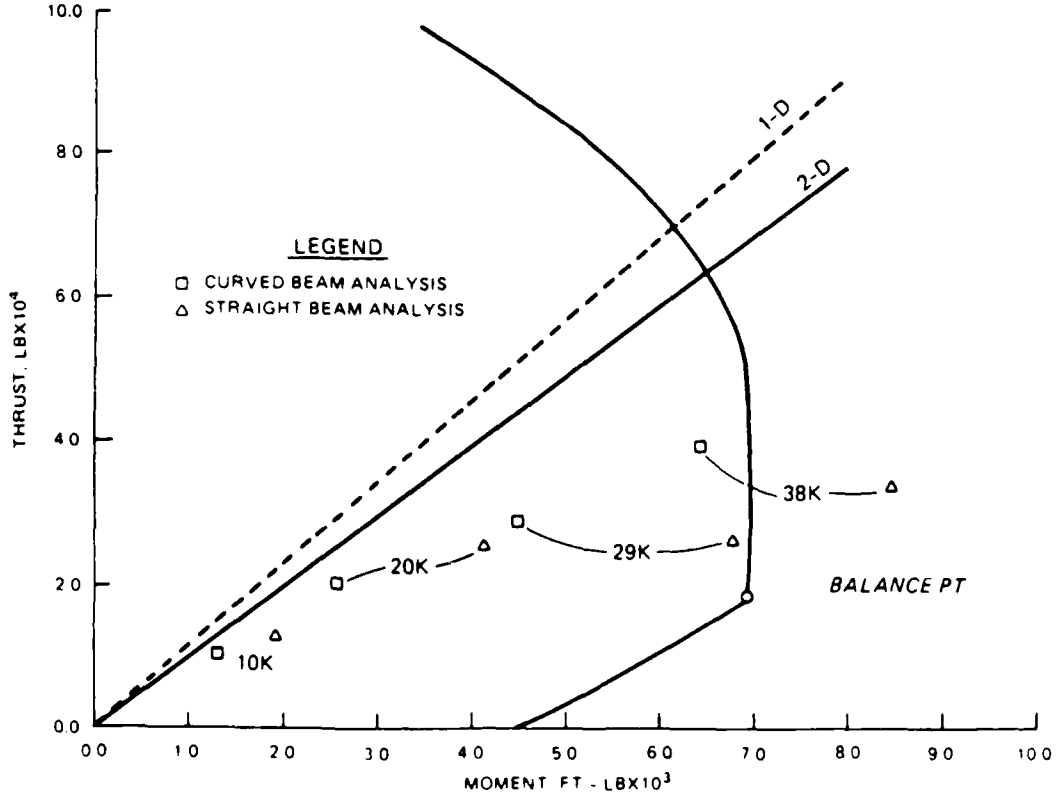

MODEL 3-1, SPRINGING LINE

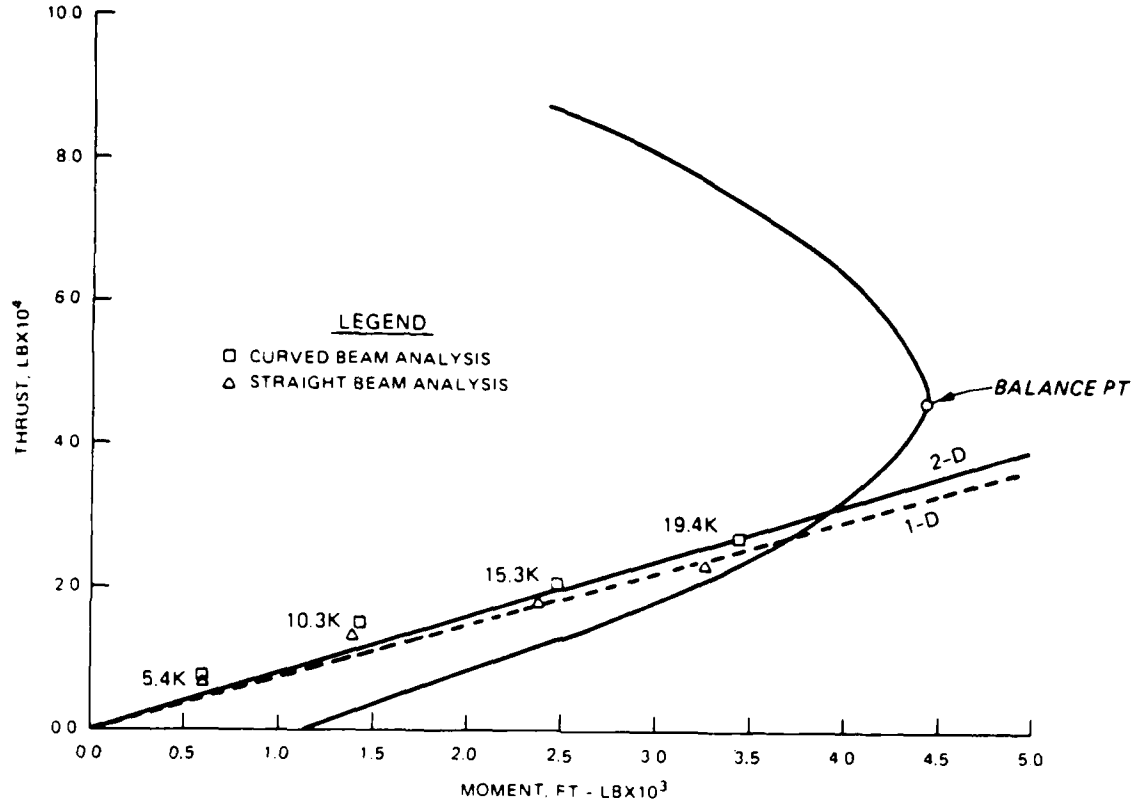

MODEL 4-1, CROWN

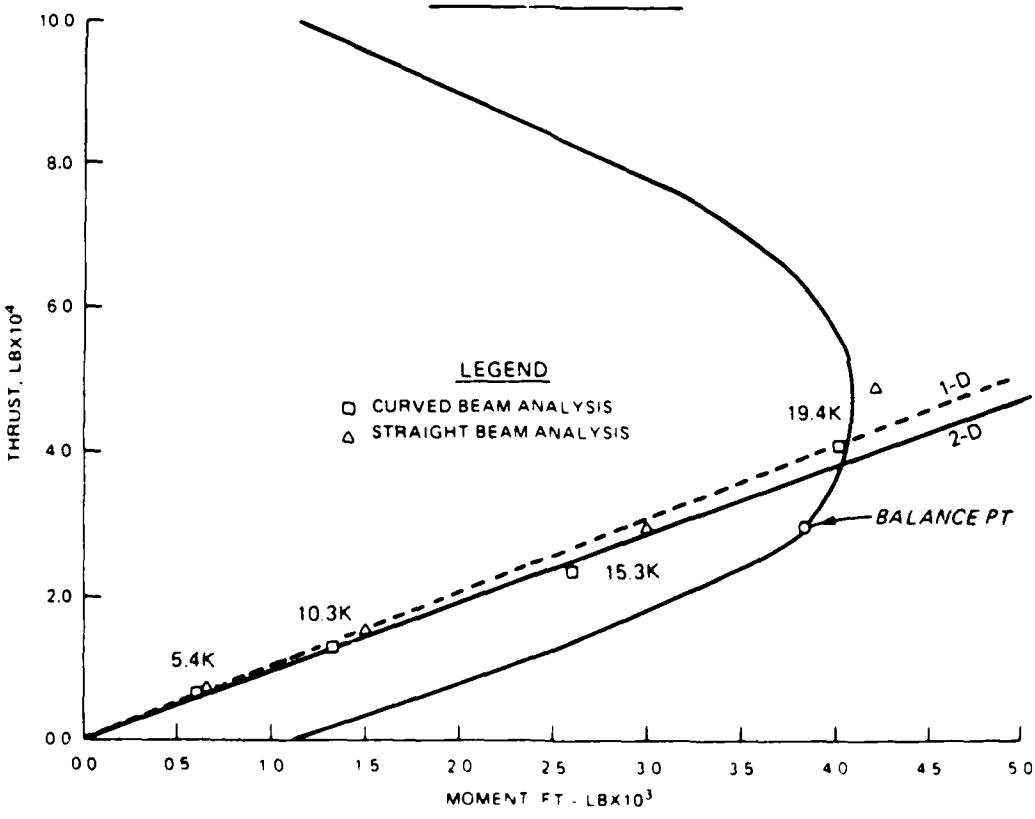

MODEL 4-1, SPRINGING LINE

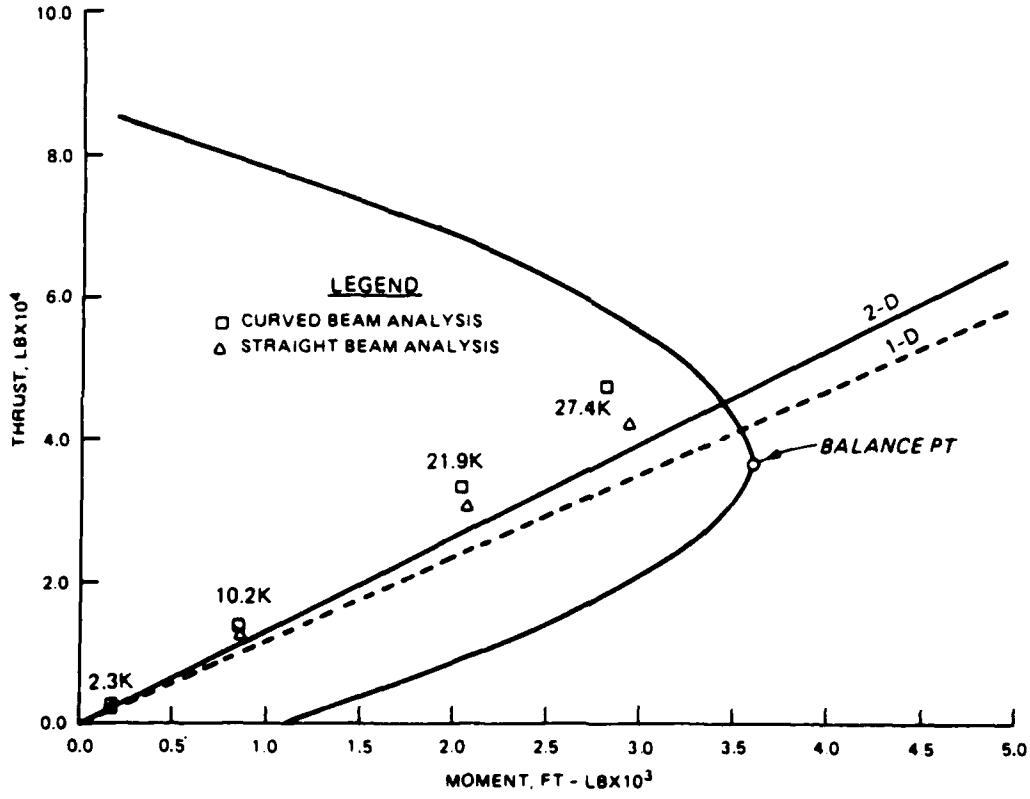

MODEL 4-2, CROWN

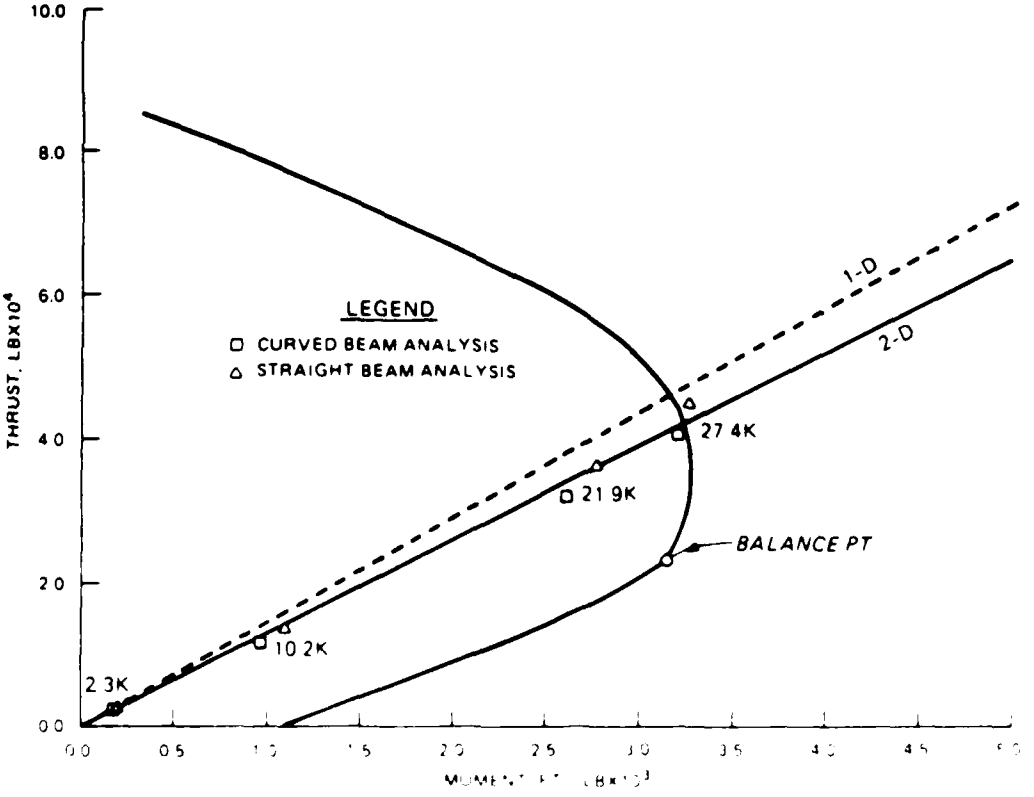

MODEL 4-2 SPRINGING LINE

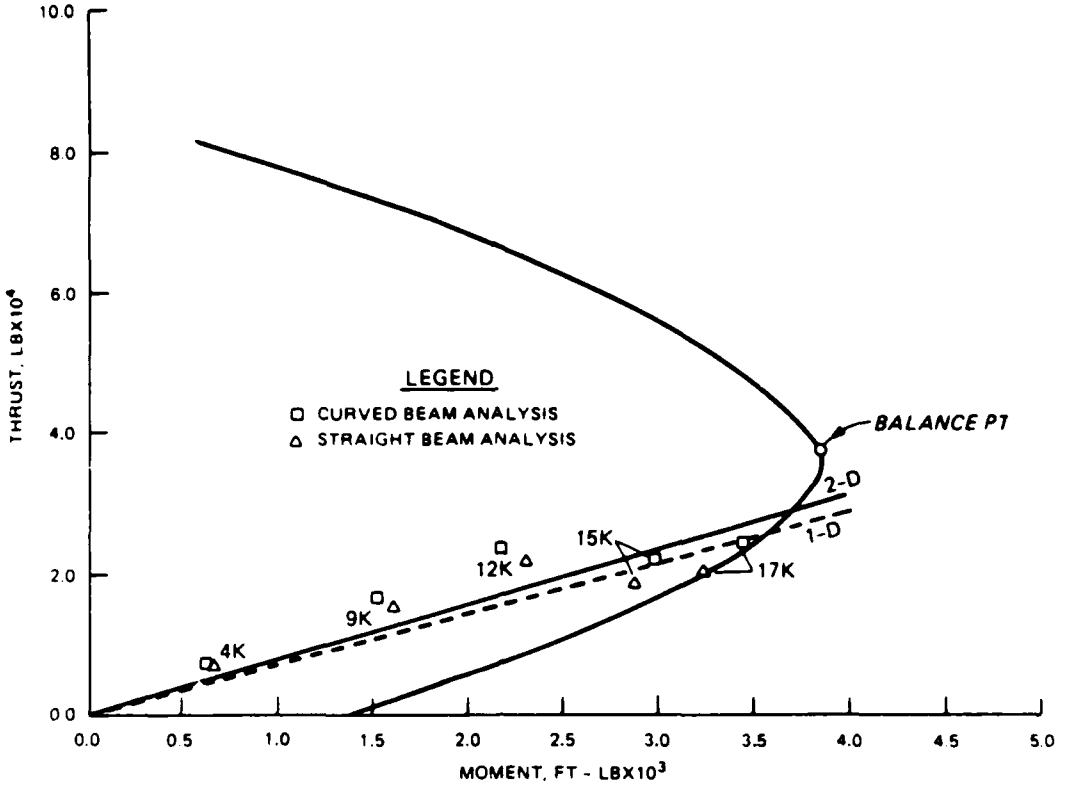

MODEL 5-1, CROWN

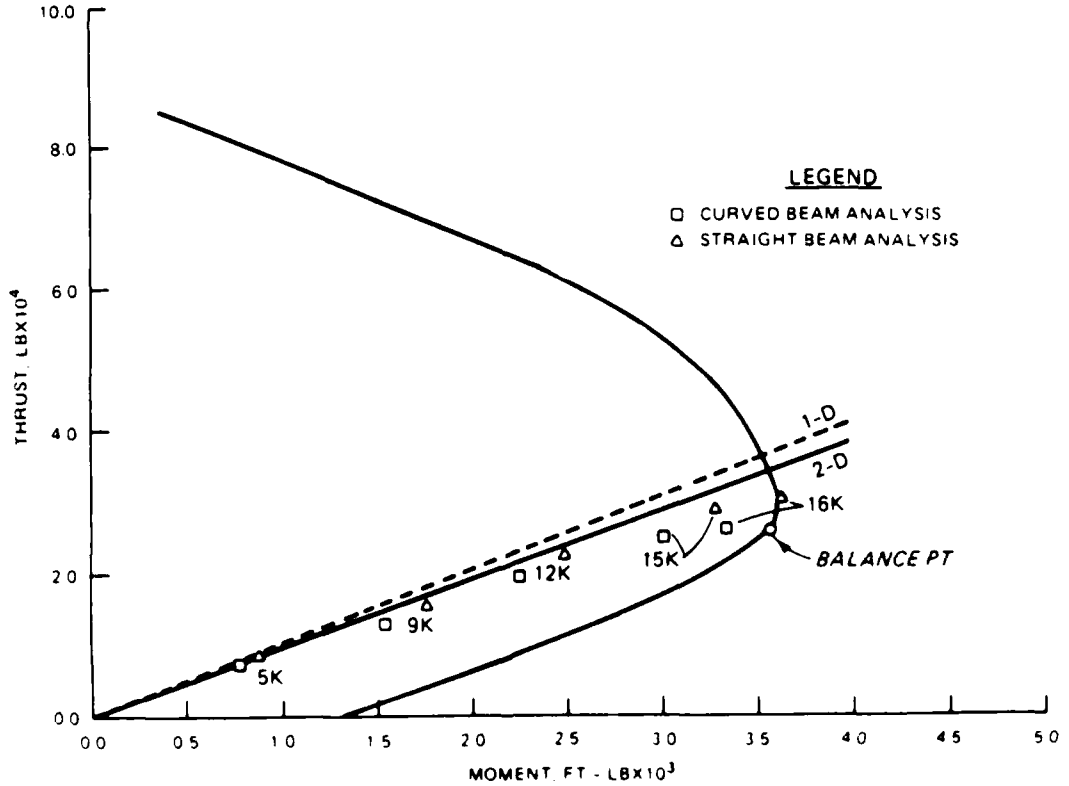

MODEL 5-1, SPRINGING LINE

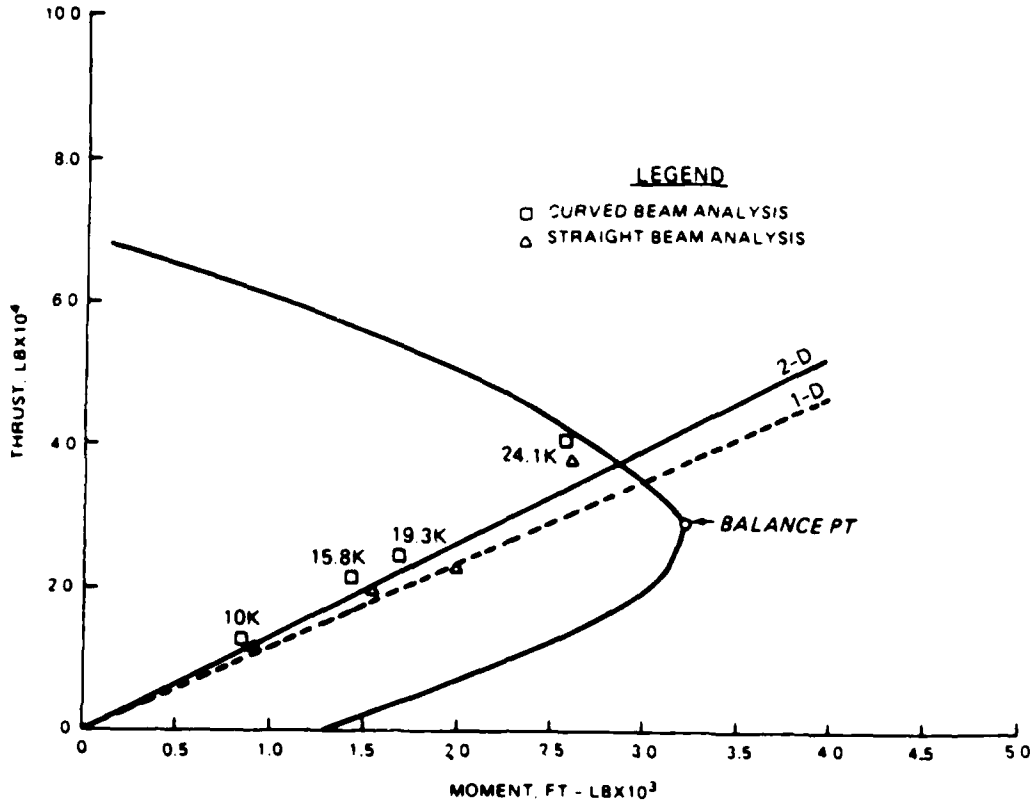

MODEL 5-2, CROWN

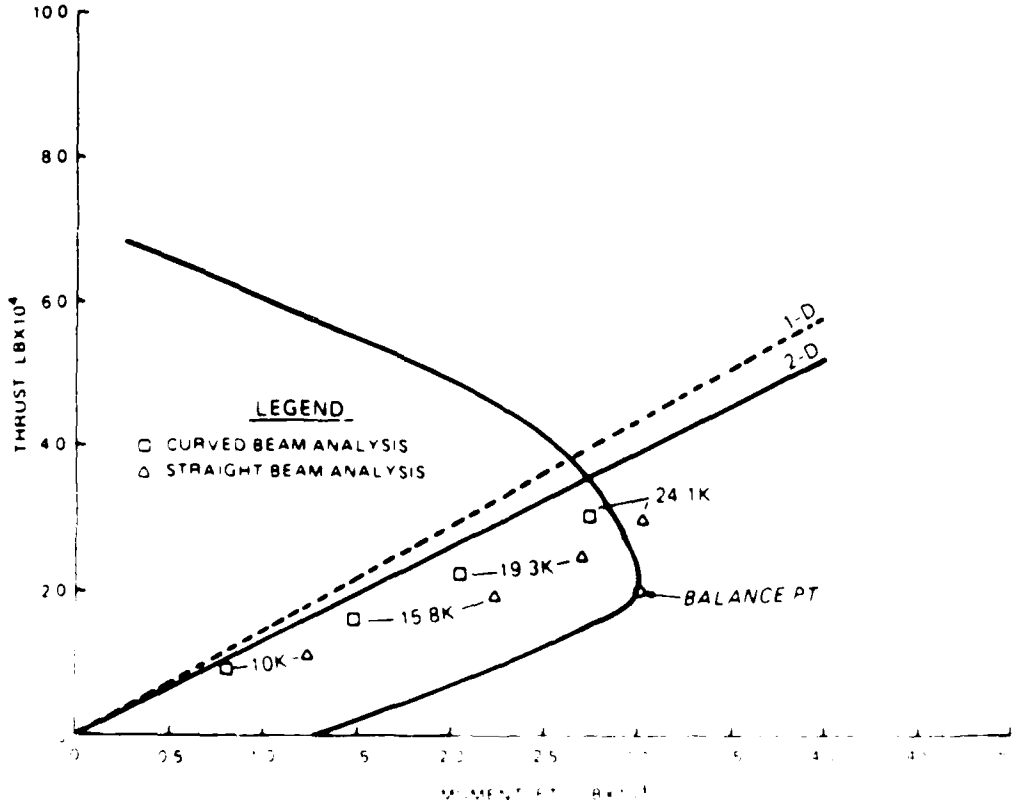

MODEL 5-2 SPRINGING LINE

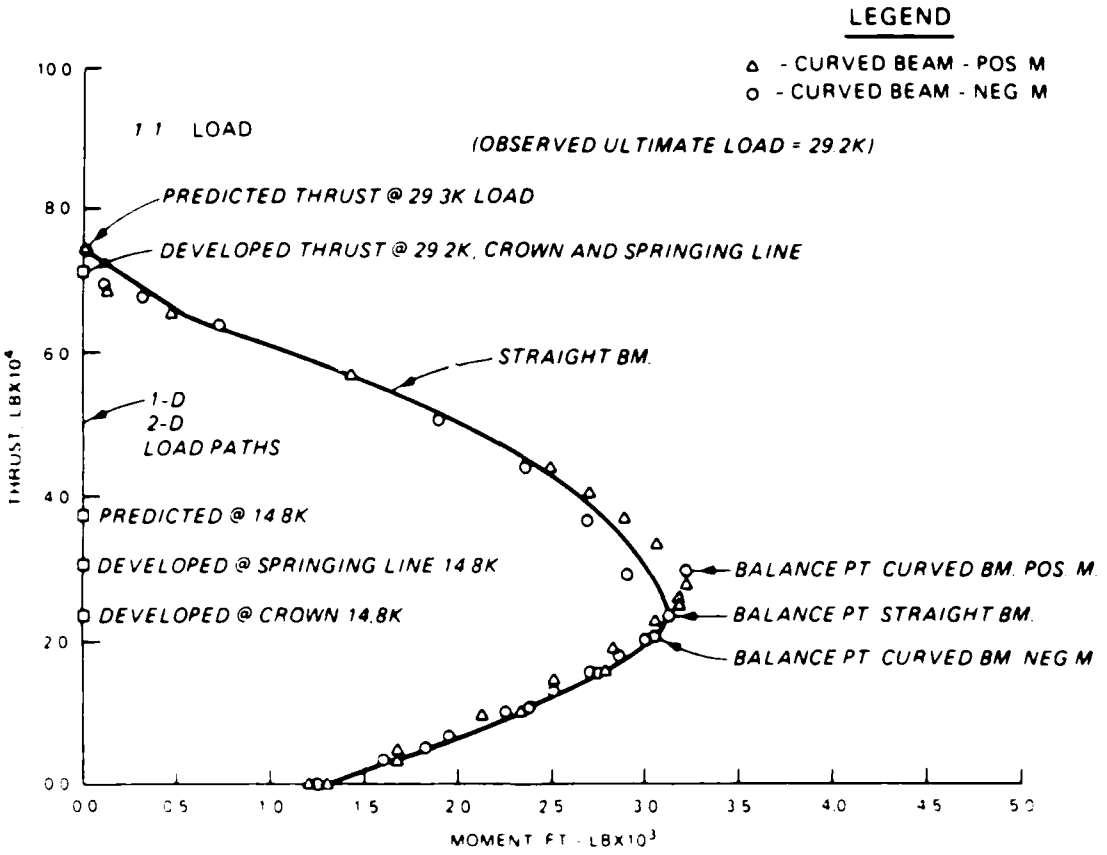
LEGEND
Δ - CURVED BEAM - POS M
o - CURVED BEAM - NEG M
1 1 LOAD
(OBSERVED ULTIMATE LOAD = 29.2K)
PREDICTED THRUST @ 29 3K LOAD
DEVELOPED THRUST @ 29 2K, CROWN AND SPRINGING LINE
STRAIGHT BM.
1-D
2-D
LOAD PATHS
PREDICTED @ 14 8K
DEVELOPED @ SPRINGING LINE 14 8K
DEVELOPED @ CROWN 14.8K
BALANCE PT CURVED BM. POS. M.
BALANCE PT STRAIGHT BM.
BALANCE PT CURVED BM NEG M
THRUST LBX10⁴
MOMENT FT - LBX10³
100
80
60
40
20
00
00
05
10
15
20
25
30
35
40
45
50

MODEL C5-3

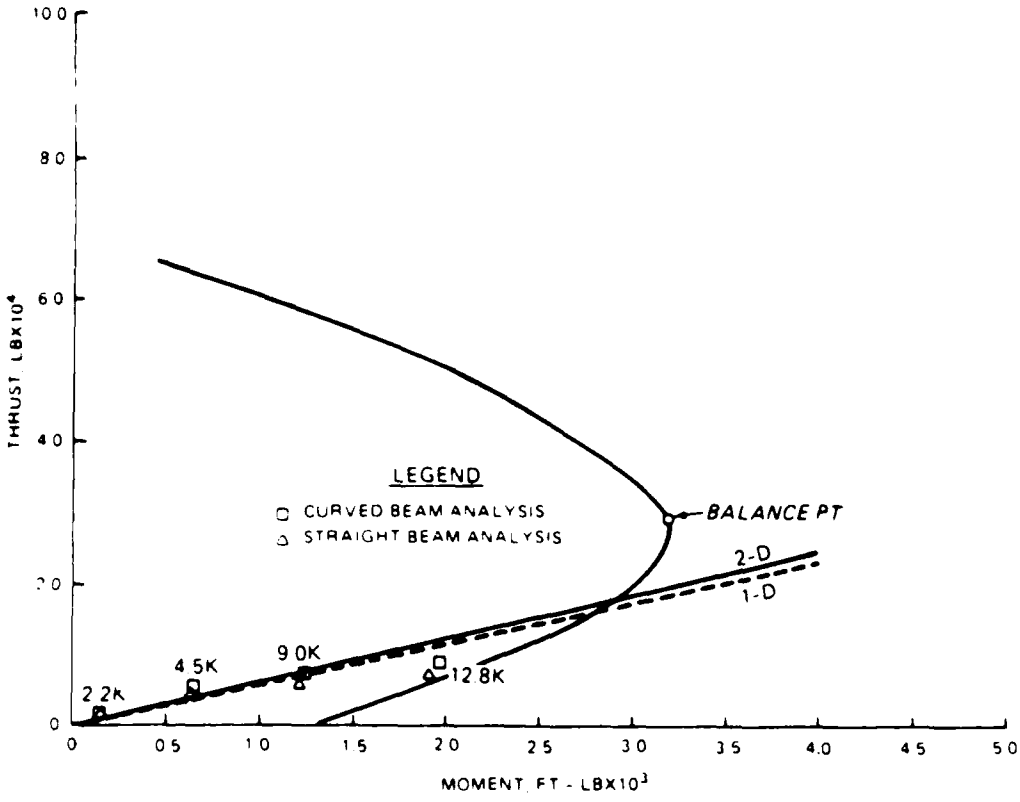

MODEL 5-4, CROWN

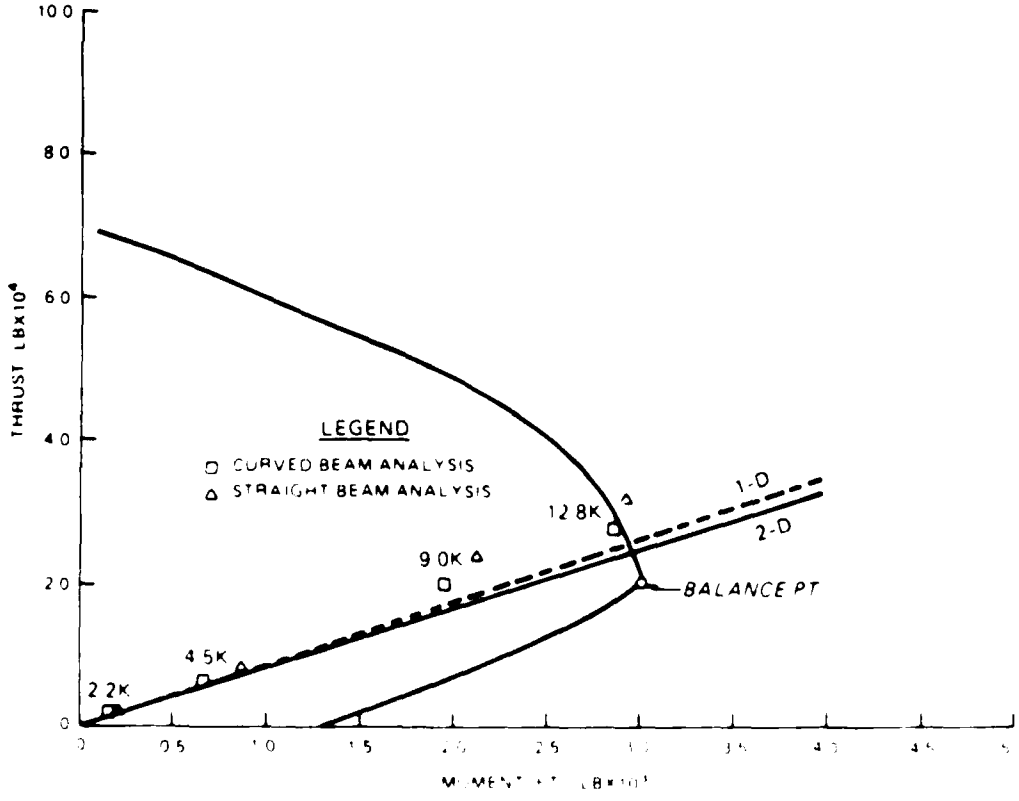

MODEL 5-4 SPRINGING LINE

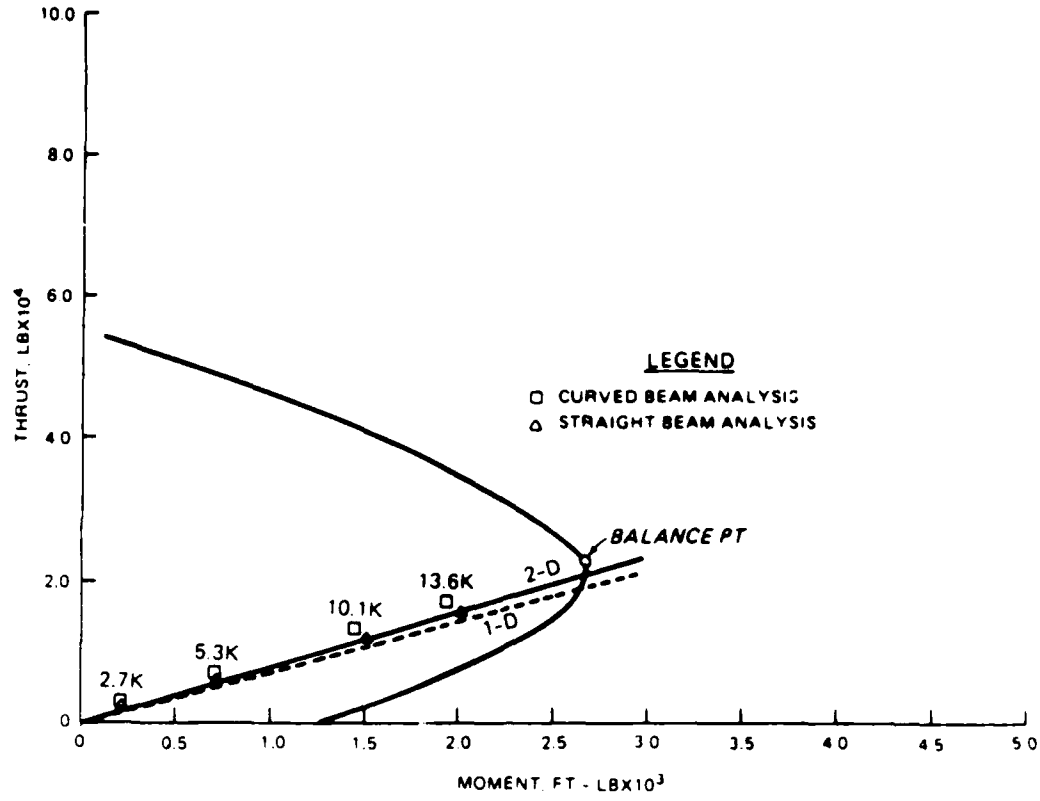

MODEL 6-1, CROWN

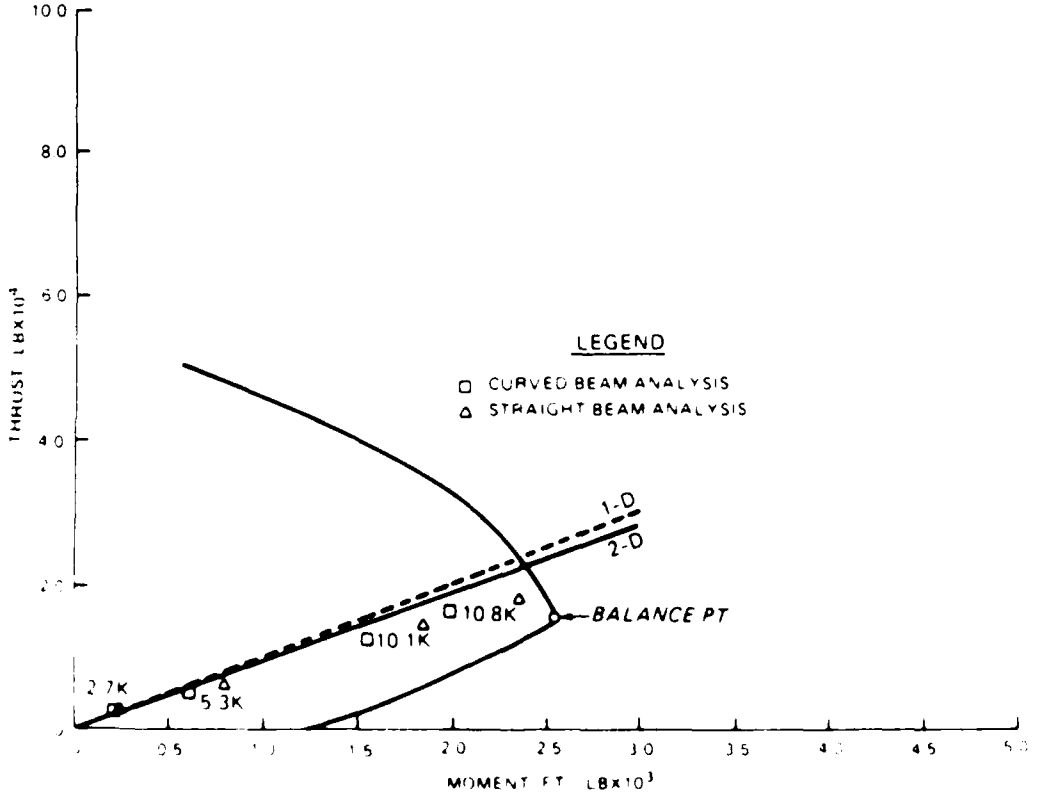

MODEL 6-1, SPRINGING LINE

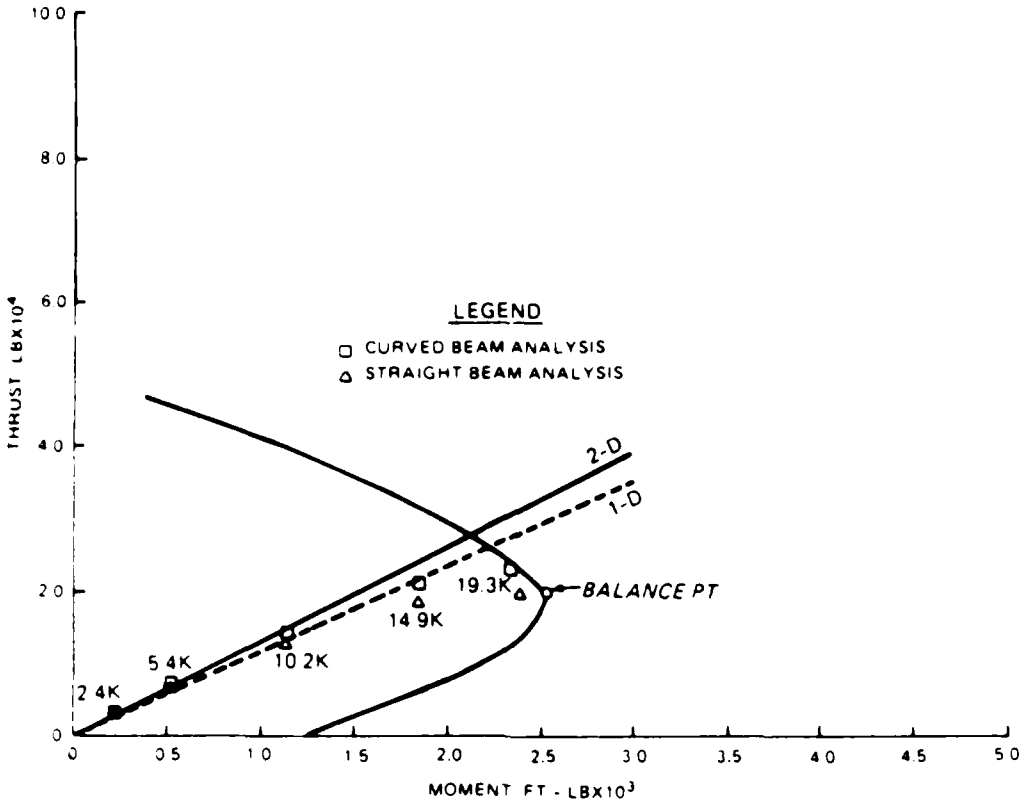

MODEL 6-2, CROWN

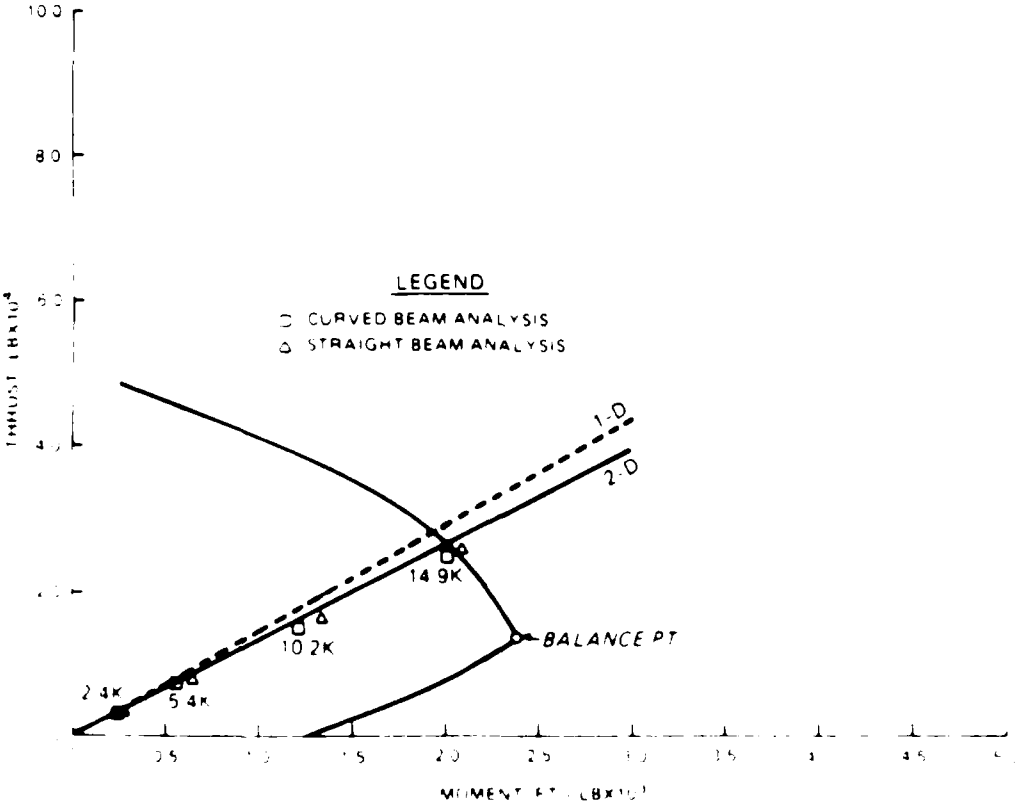

MODEL 6-2, SPRINGING LINE

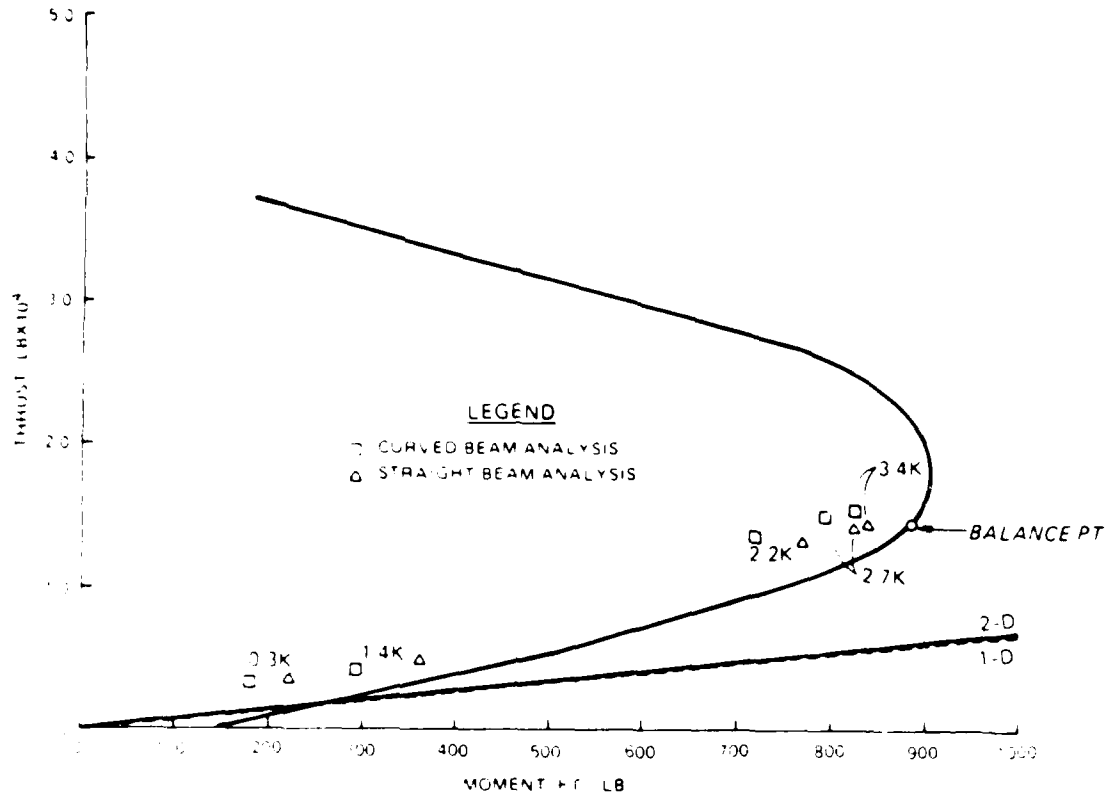

MODEL 7-1, CROWN

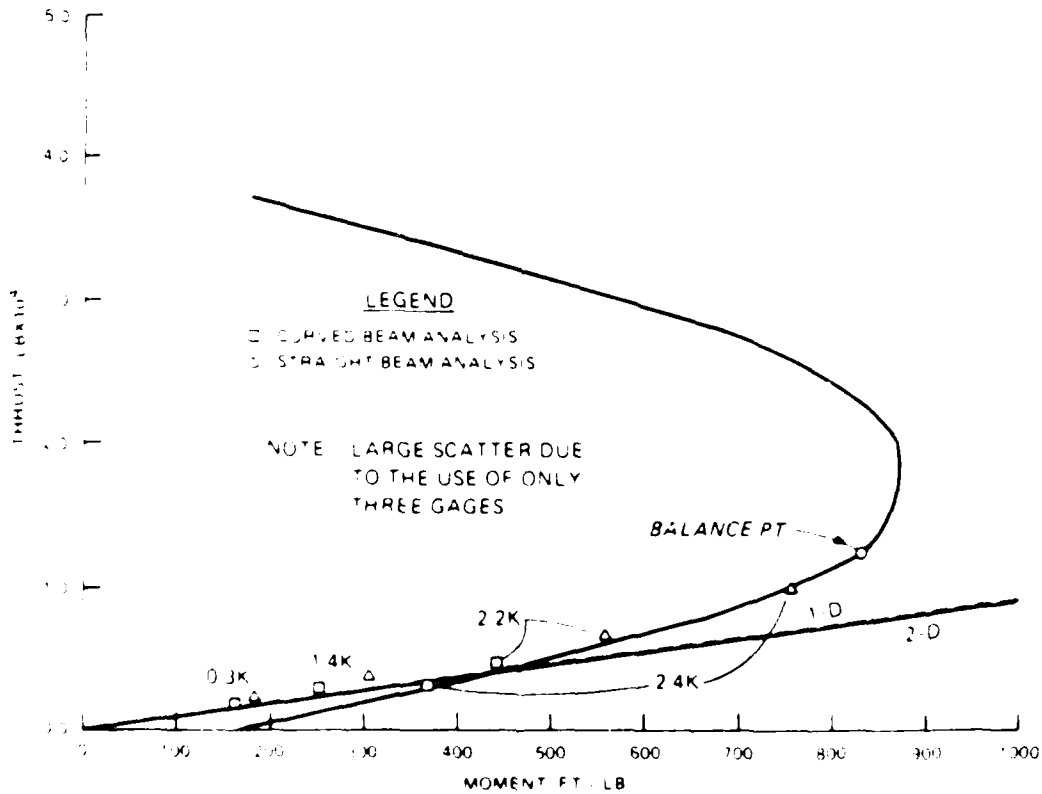

MODEL 7-1 SPRINGING LINE

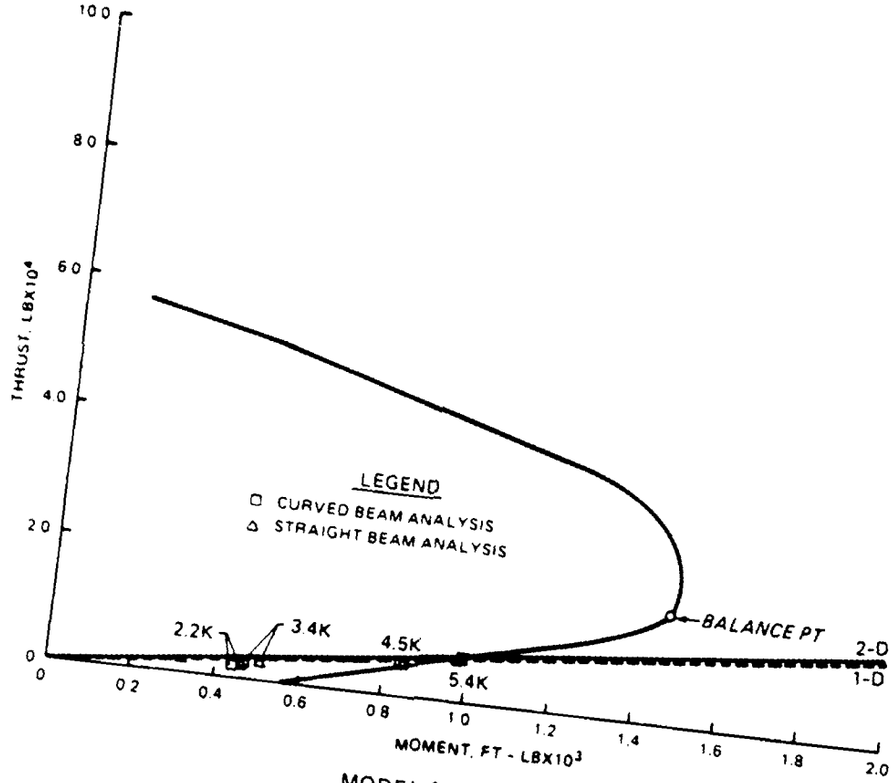

MODEL 8-1, CROWN

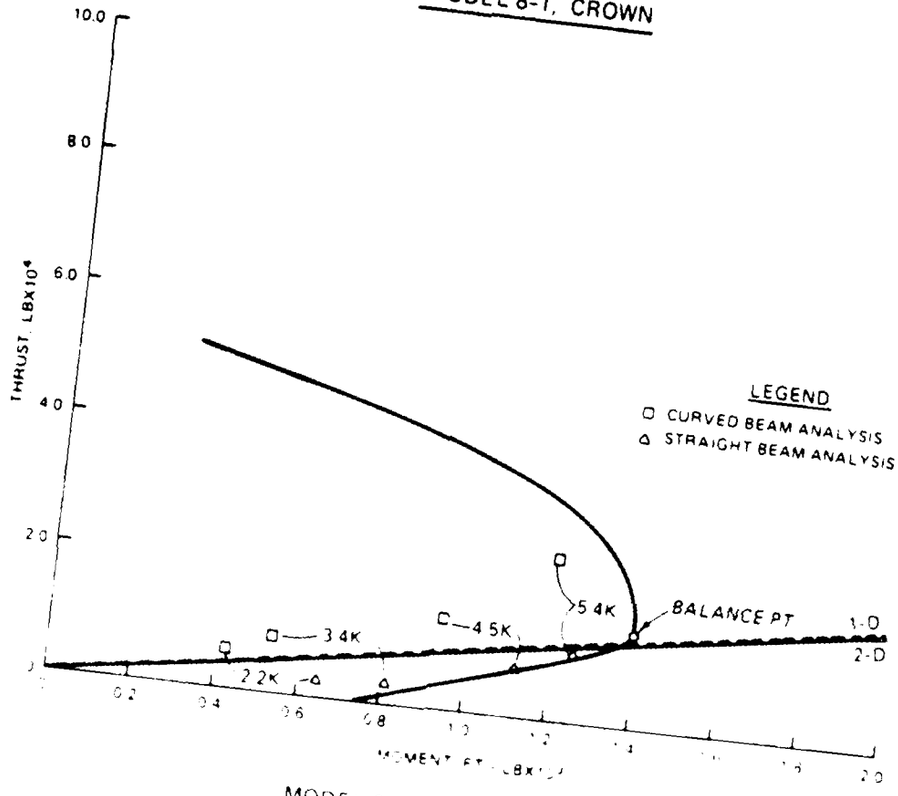

MODEL 8-1, SPRINGING LINE

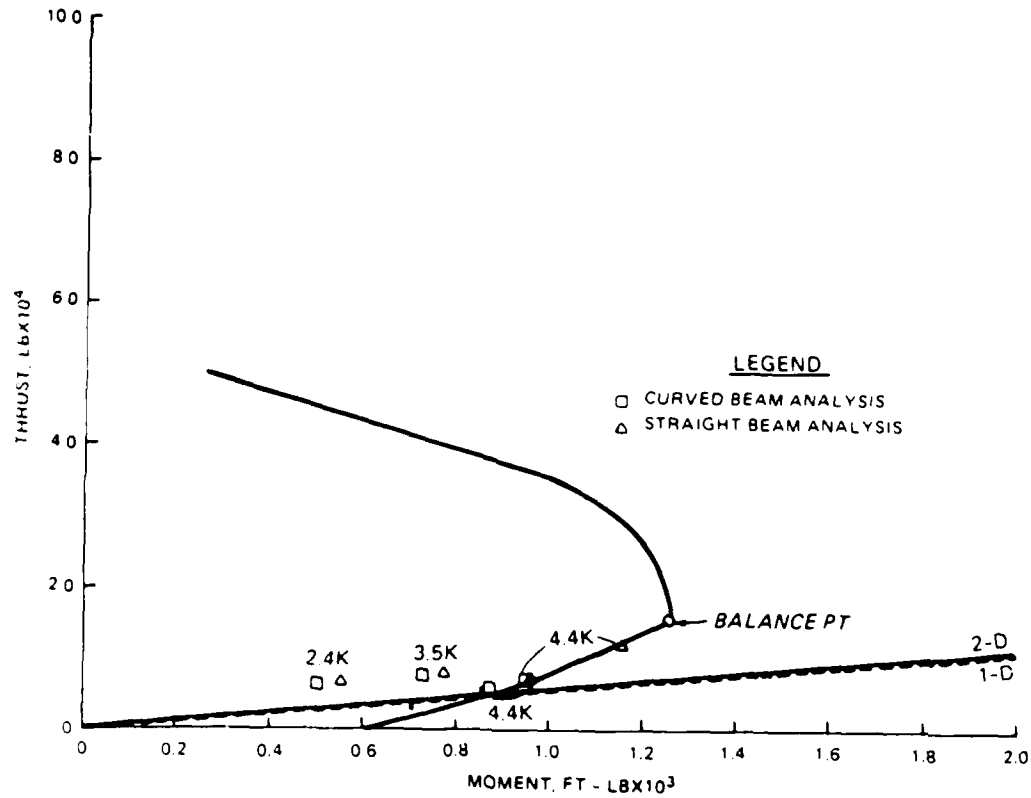

MODEL 8-2, CROWN

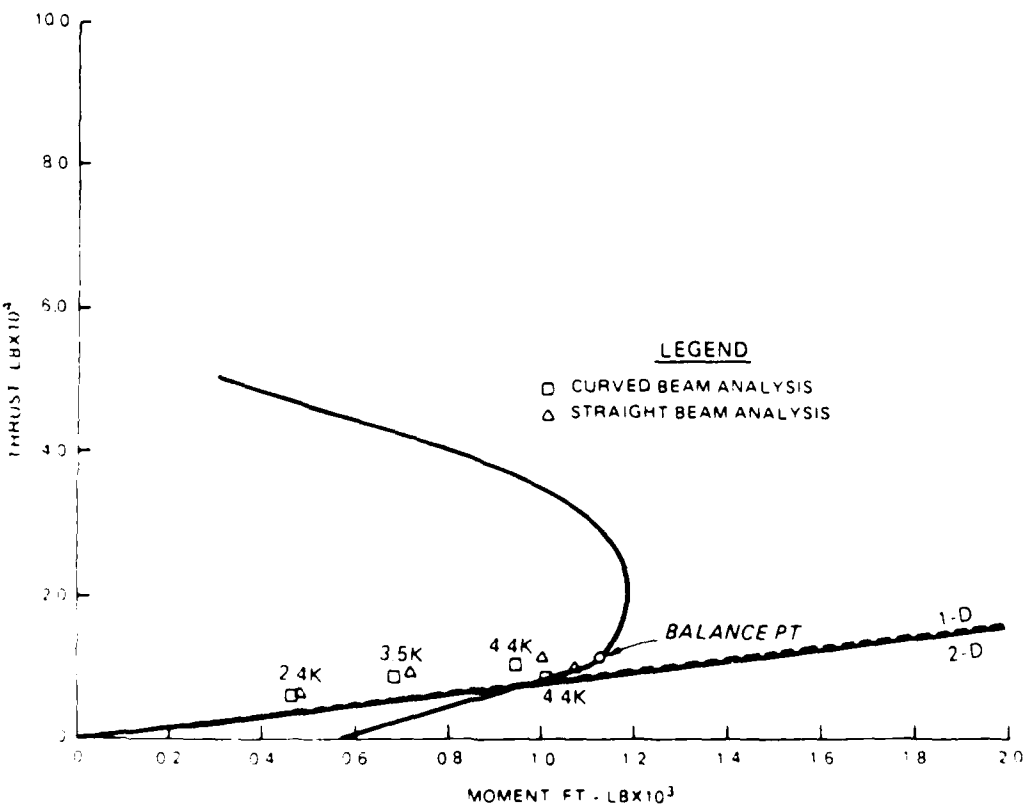

MODEL 8-2, SPRINGING LINE

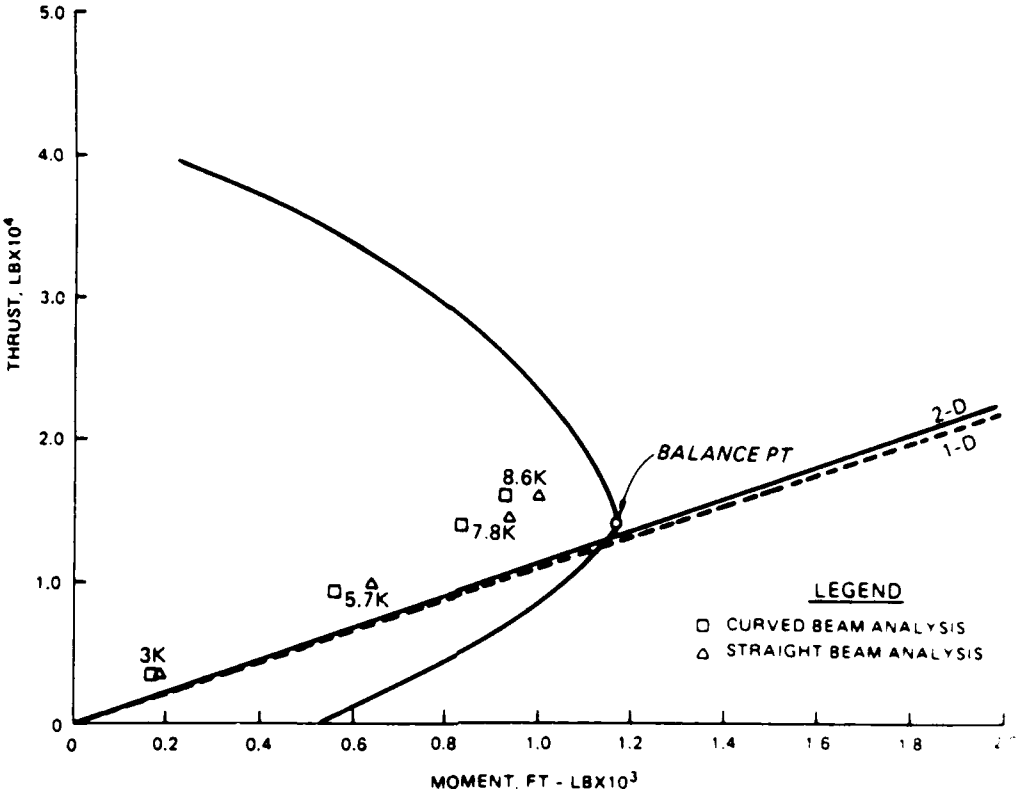

MODEL 8-3, CROWN

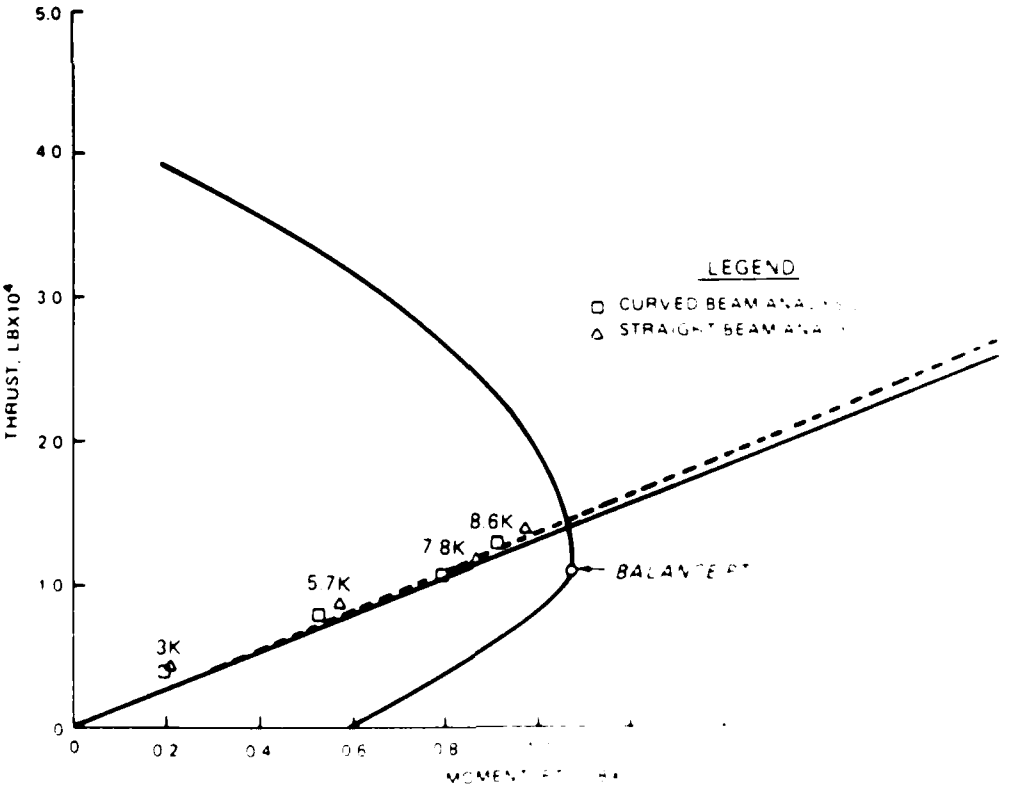

MODEL 8-3, SPR[illegible]

AD-A182 451 STRENGTH DESIGN OF REINFORCED CONCRETE HYDRAULIC STRUCTURES REPORT 5 EXPE (U) ARMY ENGINEER WATERWAYS EXPERIMENT STATION VICKSBURG MS STRUC 3/3

UNCLASSIFIED R S WRIGHT ET AL APR 87 WES/TR/SL-80-4/5 F/G 13/3 NL

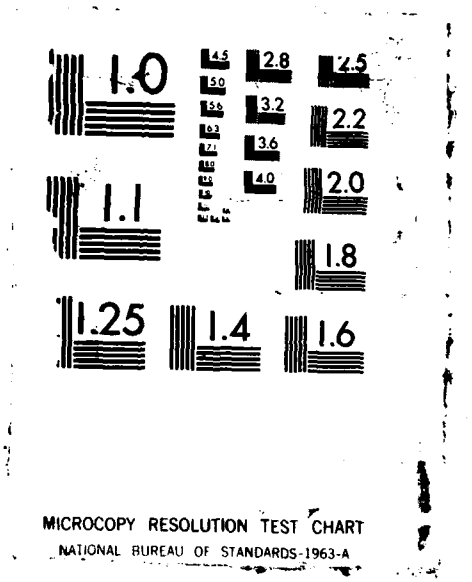
1.0
1.1
1.25
1.4
1.6
1.8
2.0
2.2
2.5
2.8
3.2
3.6
4.0
4.5
5.0
5.6
6.3
7.1
MICROCOPY RESOLUTION TEST CHART
NATIONAL BUREAU OF STANDARDS-1963-A

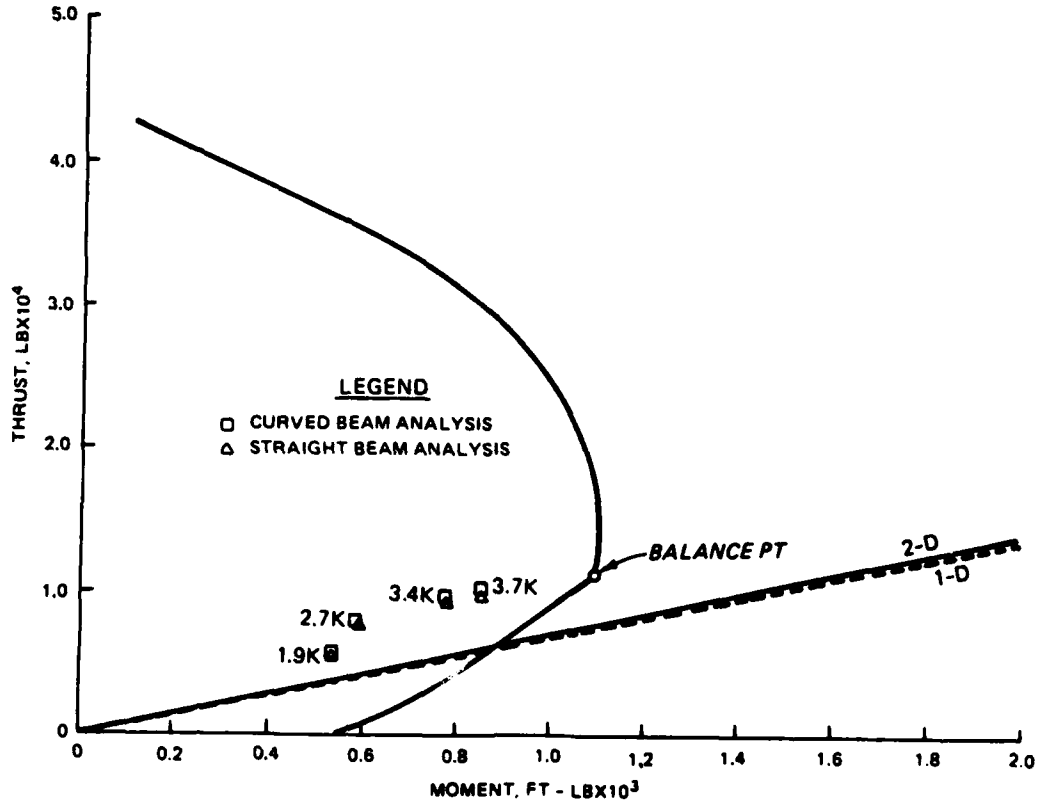

MODEL 9-1, CROWN

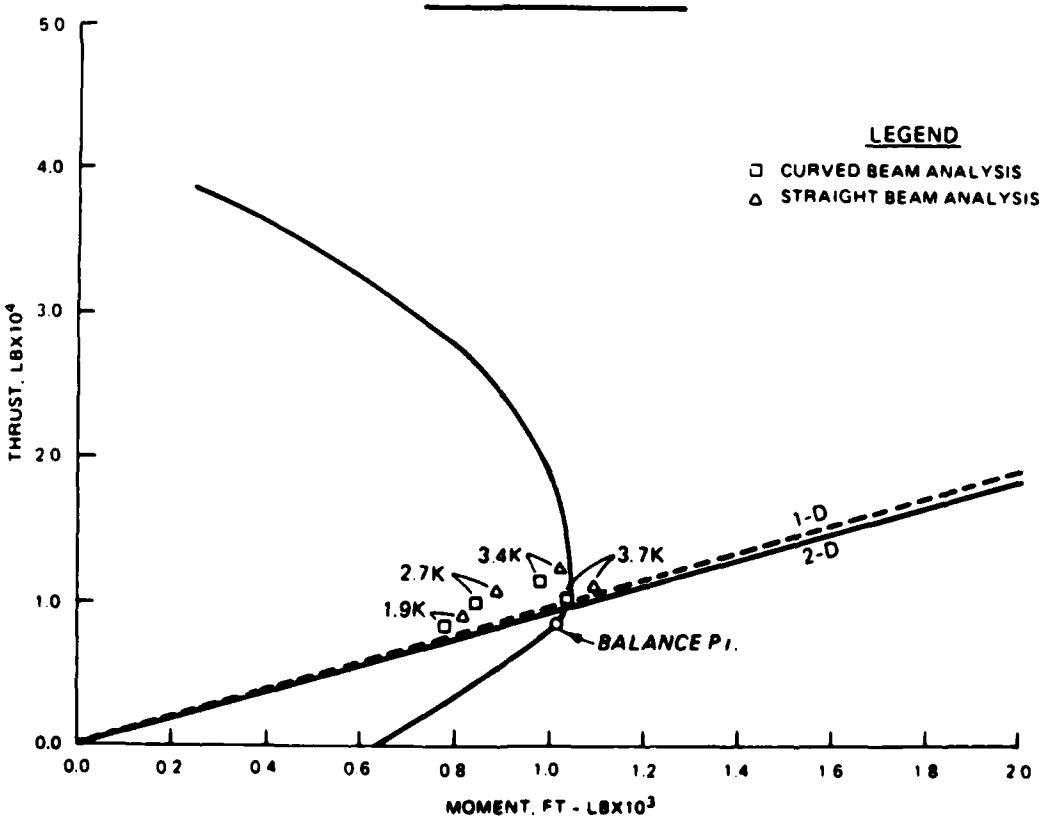

MODEL 9-1, SPRINGING LINE

APPENDIX H

NOTATION

a_1	Factor that is a function of location on ring and ratio of load at crown to load at springing line as defined in Equation 1, Part IV
a_2	Factor that is a function of ratio of load at crown to load and springing line as defined in Equation 2, Part IV
a_3	Factor that is a function of inner and outer radius of ring, location on ring, and ratio of load at crown to load at springing line as defined in Equation 4, Part IV
B	Width of section
c	Depth of section in compression
c/h	Ratio of depth of section in compression to overall depth of section
C	Crown
d	Distance from intrados to outer reinforcing steel as shown in Figure 1 (distance from extreme compression on fiber to centroid of tension reinforcement at springing line or negative moment sections)
d'	Distance from intrados to inner reinforcing steel as shown in Figure 1 (distance from extreme compression fiber to centroid of compression reinforcement at springing line or negative moment)
e_i	Error term in strain distribution fit
E_c	Initial elastic concrete modulus
E_s	Modulus of elasticity of steel
f'_c	28-day uniaxial compressive strength of concrete
f_y	Yield strength of reinforcing steel
h	Overall depth of section
K_1, K_2, K_3, K_4, K_5	Factors used in Airy stress analysis of thrust as defined in Equation 4, Part IV for purpose of simplifying and shortening lengthy equations
N	Number of data pairs for strain distribution fits as defined in Appendix F
p	Varying pressure component magnitude
P	Observed failure load
P_{cr}	Predicted failure load
P_{im}	Implosion pressure
q	Uniform pressure component magnitude
r^2	Correlation coefficient squared as defined in Appendix F

R	Radius of initial curvature to middepth of section
R/C	Reinforced concrete
R_i	Inner radius
R_o	Outer radius
R/h	Ratio of radius to height
S	Distance from center of reinforcing steel to nearest side as shown in Figure 1
SL	Springing line
T	Resultant thrust on section
t/D_o	Ratio of wall thickness to outside diameter
W	Distributed normal loading
y	Distance from the neutral axis
y'	Distance from the intrados at the positive moment section or distance from the extrados at the negative moment section
α	Maximum compressive strain
β	Location of neutral axis
γ_c	Unit weight of concrete
ε	Strain
ε_i	Measured value of strain
ε_i'	Predicted value of strain
ε_u	Maximum compressive strain
$\bar{\varepsilon}_i$	Average of measured values
θ	Angle measured from springing line
λ	Factor used in Airy stress analysis of thrust as defined in Equation 4, Part IV for purpose of simplifying lengthy equations
ν	Poisson's ratio, day of test
ρg	Total steel ratio = area of total steel divided by width and overall depth of section

END

8-87

DTIC